LE GOUVERNEMENT
DU GRAND-DUCHÉ DE LUXEMBOURG
Ministère de l'Agriculture, de la Viticulture
et du Développement rural

Institut viti-vinicole

LUXEMBOURG
INSTITUTE OF SCIENCE
AND TECHNOLOGY

LIST

# Tätigkeitsbericht 2020

## BioViM

Schaderreger-Monitoring und Ableitung ökologischer und umwelt-schonender Rebschutzstrategien im Weinbau

**https://www.list.lu/en/research/project/biovim/**

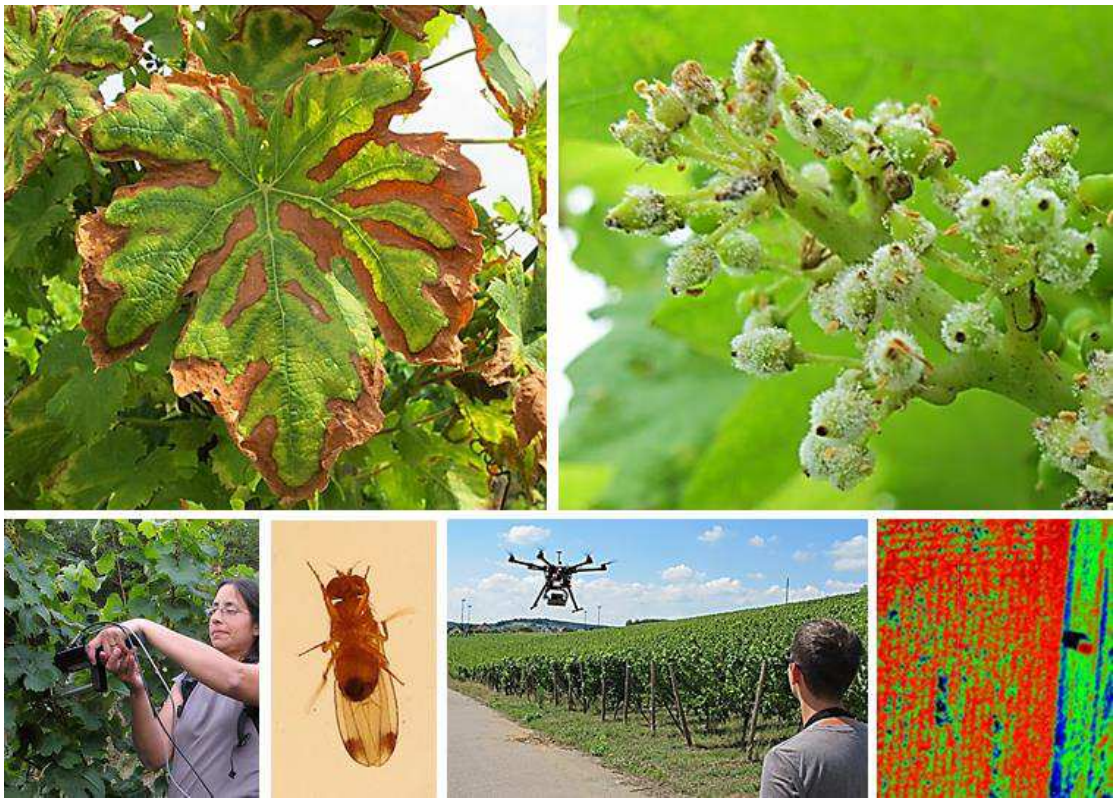

Berichtszeitraum: 1. Januar 2020 – 31. Dezember 2020

Mit Beiträgen von Daniel Molitor, Miriam Machwitz, Doriane Dam, Christian Bossung, Jürgen Junk und Marco Beyer

Unter Mitwirkung von Franz Ronellenfitsch, Christopher Simon, Mareike Schultz, Robert Mannes, Marine Pallez-Barthel und Katrin Scherer

# Inhaltsverzeichnis

**1 EINLEITUNG 1**

**2 MATERIAL UND METHODEN 2**

**2.1 Versuchsflächen 2**

**2.2 Pflanzenschutzmittel und sonstige Testsubstanzen 3**

**2.3 Versuchsaufbau 3**
2.3.1 Versuch L Monitoring *Scaphoideus titanus* 4
2.3.2 Versuch R Monitoring *Drosophila suzukii* 4
2.3.3 *Drosophila suzukii* – maintien d'une population dans un incubateur et expérimentations 6
*2.3.4* Versuch T Bekämpfung *Drosophila suzukii* 8
2.3.5 Versuch W Schnittsysteme 9
2.3.6 Versuch X Oidium 9
2.3.7 Versuch Y Fernerkundliche Erkennung der Peronospora 10
2.3.8 Versuch AA Erfassung symptomatischer Esca-Stöcke 14
2.3.9 Erfassung des Bestandsklima mittels mikro-meteorologischer Messungen mit dem Schwerpunkt Blattnässe 14

**2.4 Auswertung 16**
2.4.1 Traubenstruktur 16
2.4.2 Befallsverlauf *Botrytis cinerea* 16
2.4.3 Ertragserfassung und Mostanalysen 16
2.4.4 Monitoring *S. titanus* 17
2.4.5 Befallsbonituren Echter Mehltau und Falscher Mehltau 17
2.4.6 Erfassung des Fluges und der Eiablage durch *Drosophila suzukii* 17
2.4.7 Bonituren in den Freilandversuchen zur Bekämpfung der Kirschessigfliege 18
2.4.8 Fernerkundliche Verfahren zur Befallsdifferenzierung im Versuch Y 19
2.4.9 Monitoring der Esca-symptomatischen Stöcke im Versuch AA 26

**3 ERGEBNISSE UND DISKUSSION 26**

**3.1 Versuch L Monitoring *Scaphoideus titanus* 26**
3.1.1 Fangzahlen 26

**3.2 Surveillance des activités de vol et de ponte de *Drosophila suzukii* 27**

**3.3 Expériences de lutte contre *Drosophila suzukii* 29**
3.3.1 Essais de produits naturels contre *D. suzukii* au vignoble 29
3.3.2 Essais de produits naturels contre *D. suzukii* en laboratoire 31

**3.4 Versuch W Schnittsysteme 32**
3.4.1 Traubenstruktur und -gesundheit 32

3.4.2 Ernteparameter 33

**3.5 Versuch X Oidium-Bekämpfung 34**
3.5.1 Befallsstärken an den Blättern 34

**3.6 Versuch Y Fernerkundliche Erkennung der Peronospora 35**
3.6.1 Befallsstärken an den Blättern 35
3.6.2 Ergebnisse der fernerkundlichen Untersuchungen 36

**3.7 Versuch AA Monitoring symptomatischer Esca-Stöcke 44**
3.7.1 Ergebnisse der Erfassung symptomatischer Esca-Stöcke 44

**3.8 Bestandsklima in den verschiedenen Erziehungssystemen 46**

**4 ZWISCHENFAZIT 46**

**5 DANKSAGUNG 49**

**6 LITERATURVERZEICHNIS 50**

**7 ANHANG 51**

**7.1 Phänologische Entwicklung 2020 51**

**7.2 Tageswitterungsbedingungen in der Vegetationsperiode 2020 52**

**7.3 Veröffentlichungen 53**
7.3.1 Veröffentlichungen in wissenschaftlichen Journalen (2020) 53

**7.4 Pressemeldungen 54**

**7.5 Teilnahme an sonstigen Veranstaltungen 55**

# 1 Einleitung

Das Projekt BioViM2 (Suivi des ravageurs et développement de strategies de protection des cultures respectueuses de l'environnement en viticulture) ist eine Kooperation zwischen dem Weinbauinstitut (IVV) und dem Luxembourg Institute of Science and Technology (LIST) unter Einbindung der Winzer der Luxemburger Mosel. Das Projekt wird durch das IVV im Ministerium für Landwirtschaft, Weinbau und ländliche Entwicklung gefördert.

Die Produktion qualitativ hochwertiger Weine unter reduziertem Pflanzenschutzmitteleinsatz stellt eine besondere Herausforderung dar, weil viele andere Maßnahmen der Schaderregerbekämpfung, wie sie in der Landwirtschaft eingesetzt werden (beispielsweise Fruchtfolgen), aufgrund des dauerhaften Charakters der Weinkultur nicht eingesetzt werden können. Auch ein Wechsel der angebauten Sorten (weg von anfälligen Sorten hin zu Sorten mit höherer Resistenz gegenüber Schaderregern) ist im Weinbau weniger einfach umzusetzen, weil zahlreiche Konsumenten Rebsorten als Marke wahrnehmen und gezielt bekannte Sorten nachfragen.

Die EU-Direktive 2009/128 fordert im Rahmen der guten fachlichen Praxis im Pflanzenschutz alle Pflanzenschutzmaßnahmen standort-, kultur- und situationsbezogen durchzuführen und die Anwendung von Pflanzenschutzmitteln auf das notwendige Maß zu beschränken. Nationale Aktionspläne zur Reduzierung der PSM-Anwendung sollen erarbeitet werden. Das Projekt BioViM2 trägt insbesondere zur Umsetzung der Teile der Gesetze, Verordnungen und Pläne bei, die wissenschaftliche Methoden oder Konzepte erfordern. Hier werden folgende Ziele verfolgt:

1. Minimierung des Einsatzes von Pflanzenschutzmitteln im Weinbau;
2. Sicherung von Ertrag und Produktqualität;
3. Minimierung der Risiken für Mensch und Natur.

Im Folgenden werden die Untersuchungen des Versuchsjahres 2020 dargestellt. Das Jahr 2020 war durch die Maßnahmen zur Eindämmung des Virus Covid-19 geprägt. Zahlreiche Versammlungen sind ausgefallen oder wurden verschoben. Der Uni Trier war es größtenteils nicht gestattet, Dienstreisen ins Ausland zu machen, so dass die Datenakquise mit Drohnen fast ausschließlich in leicht geändertem Setting vom LIST durchgeführt wurde. Die Öffentlichkeitsarbeit fand im Jahr 2020 zur Vermeidung von Ansteckungen vorwiegend in Form von Schrift und Bild statt. Im Berichtszeitraum erschienene Veröffentlichungen sind im Anhang zu finden.

# 2 Material und Methoden

## 2.1 Versuchsflächen

Alle Versuche wurden auf Flächen des Institut Viti-Vinicole (IVV) (Tab. 1) in Remich oder in Weinbergen von Partnerwinzern (Monitoring *Scaphoideus titanus*; Monitoring *Drosophila suzukii*) entlang der luxemburgischen Mosel realisiert.

**Tab.1: Beschreibung der Versuchsflächen am IVV.**

| Versuch | Ort | Rebsorte | Unterlage | Pflanzjahr |
|---|---|---|---|---|
| W, Y | Remich | Pinot gris | SO4 | 1994 |
| W, X | Remich | Riesling | SO4 | 1994 |
| T | Remich | P. noir précoce | SO4 | 1999 |
| | | Cabaret noir | SO4 | 2014 |

Die Bewirtschaftung der Weinberge am IVV erfolgte – abgesehen von den Versuchsfragestellungen – in betriebsüblicher Weise. Eine Grundabdeckung gegenüber den weinbaulichen Hauptschaderregern *Plasmopara viticola* und *Erysiphe necator* erfolgte vom Boden in Form von Schlepper-gezogenen Sprühgeräten. Hierbei wurden überwiegend Pflanzenschutzmittel des ökologischen Anbaus verwendet. Zur Bekämpfung des Traubenwicklers kam in allen Versuchsparzellen die Pheromon-Verwirr-Methode zum Einsatz.

## 2.2 Pflanzenschutzmittel und sonstige Testsubstanzen

Folgende Pflanzenschutzmittel und sonstige Testsubstanzen kamen (außerhalb der Grundabdeckung) in den Versuchen zum Einsatz (Tab. 2):

**Tab. 2: Verwendete Pflanzenschutzmittel und sonstige Testsubstanzen.**

| Handelsname | Wirkstoff(e) / Zusammensetzung | Wirkstoffgehalt | Zulassungsinhaber / Vertrieb / Entwickler |
|---|---|---|---|
| Carboliq | Calcium Carbonat | 900 g/kg | Ets Monseu S.A. |
| Cutisan | Kaolin | Mind 990 g/kg | Biofa AG |
| Flint | Trifloxystrobin | 500 g/kg | Bayer Crop Science |
| Folpan 500 SC | Folpet | 500 g/l | ADAMA |
| Kocide Opti | Kupferhydroxid | 300 g/kg Kupfer | Spiess-Urania Chemicals GmbH |
| Kusabi | Pyriofenone | 300 g/l | Belchim Crop Protection |
| Luna Experience | Fluopyram<br>Tebuconazol | 200 g/l<br>200 g/l | Bayer Crop Science |
| Microthiol | Schwefel | 800 g/kg | UPL Europe Ltd. |
| Mildicut | Cyazofamid | 25 g/l | Belchim Crop Protection |
| Mycosin Vin | Schwefelsaure Tonerde | | Biofa AG |
| Nissodium | Cyflufenamid | 50 g/l | Certis Europe B.V. |
| Profiler | Fluopicolide<br>Fosetyl-Al | 44,4 g/kg<br>666,7 g/kg | Bayer Crop Science |
| Prüfmittel Fytosave | COS-OGA | 12,5 g/l | GOWAN |
| Prüfmittel Neu 1143 F | Pelargonsäure | 67,6 g/l | W. Neudorff GmbH KG |
| Sercadis | Fluxapyroxad | 300 g/l | BASF Agricultural Solutions |
| Teldor | Fenhexamid | 500 g/kg | Bayer CropScience AG |
| Topaz | Penconazol | 100 g/l | Syngenta Crop Protection NV |
| Veriphos | Kaliumphosphat | 755 g/l | Luxembourg Industries LTD |
| Vitisan | Kaliumhydrogen-carbonat | 994,9 g/kg | Biofa AG |
| Zorvec Zelavin | Oxathiapiprolin | 100 g/l | CORTEVA agriscience |

## 2.3 Versuchsaufbau

Die Versuche wurden als vollständig randomisierte Blockanlagen angelegt. Jedes Versuchsglied (VG) wurde vierfach wiederholt. Die Versuchsglieder in den einzelnen Versuchen sind den folgenden Tabellen zu entnehmen.

### 2.3.1 Versuch L Monitoring *Scaphoideus titanus*

Zur Überprüfung eines potentiellen Auftretens des Vektors der Flavescence dorée, *Scaphoideus titanus*, im Luxemburger Weinbau wurde während der Saison 2020, wie bereits 2013 bis 2019, ein Monitoring mit Gelbfallen an vier Standorten durchgeführt (Tab. 3).

**Tab. 3: Standorte des *S. titanus* Monitorings 2020.**

| Standort | Koordinaten |
|---|---|
| A Wellenstein | 49,528 N; 6,347 W |
| B Remich-IVV | 49,545 N; 6,354 W |
| C Ehnen | 49,602 N; 6,396 W |
| D Ahn | 49,628 N; 6,420 W |

Die Auswahl der Standorte erfolgte entweder aufgrund ihrer Position in klimatisch begünstigen Weinbergen (Standorte A, C, D), in der Nähe von Rebschulen (Standorte A, B) bzw. entlang einer Hauptverkehrsverbindung (Standort C).
Die Gelbfallen („Gelbtafel Profi PK“, Hermann Meyer KG, Rellingen, Deutschland) wurden am 13.07.2020 horizontal in der Höhe der Traubenzone installiert (Abb. 1)

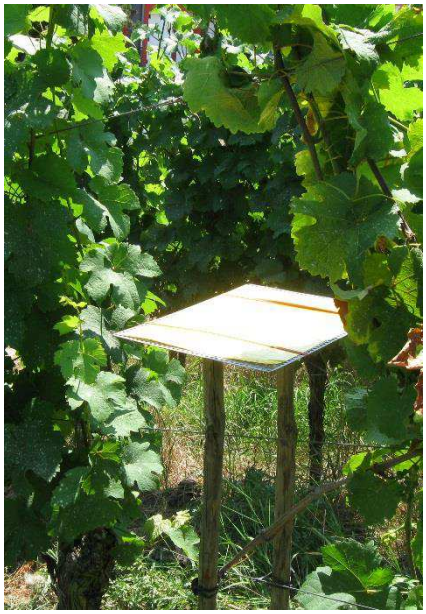

**Abbildung 1: Gelbfallen zur Überwachung des Fluges von *S. titanus*.**

### 2.3.2 Versuch R Monitoring *Drosophila suzukii*

Zur Überwachung des Flugs und der Eiablage durch die Kirchessigfliege, *Drosophila suzukii*, welche im Jahr 2014 erstmalig zu parzellenweise starken Schäden im Gebiet geführt hat, erfolgte im Jahr 2020 ein Monitoring in verschiedenen Rebsorten am Standort Remich (49,54 N; 6,35 W) (Tab. 4).

**Tab. 4: Parzellen im Monitoring zum Flug und zur Eiablage durch *Drosophila suzukii* im Jahr 2020.**

| Parzelle | Gemarkung (Koordinaten) | Standort/Sorte |
|---|---|---|
| **1** | **Remich** | **Pinotin** |
| **2** | **Remich** | **Efeu** |
| **3** | **Remich** | **Brombeeren** |
| **4** | **Remich** | **Pinot noir précoce** |
| **16** | **Remich** | **Pinot noir (130)** |
| **17** | **Remich** | **Pinot noir (109)** |
| **18** | **Remich** | **Cabaret noir** |

Zur Überwachung der Flugaktivität wurden Becherfallen der Firma Riga (Ellikon an der Thur, Schweiz) verwendet (Abb. 2).


**Abbildung 2: Riga-Becherfalle zur Überwachung der Flugaktivität von *Drosophila suzukii*.**

Während der Monate August und September wurden die Fallen wöchentlich ausgetauscht und die Fangzahlen erfasst.

### 2.3.3 *Drosophila suzukii* – maintien d'une population dans un incubateur et expérimentations

**Maintien d'une population dans un incubateur**

Les conditions de l'incubateur favorables à *Drosophila suzukii* sont 20 °C, 60 % d'humidité relative et 16:8 L:D.

Deux cages sont installées dans l'incubateur, une pour la population de *D. suzukii* et la seconde pour l'émergence des adultes (Abb. 3). Les mouches ont toujours à disposition de l'eau (par l'intermédiaire de papier absorbant), du pollen comme source de nourriture et des zones d'ombre pour se protéger de la lumière. Une fois par semaine, les cages sont nettoyées (collecte des individus morts), l'eau et le papier absorbant sont remplacés pour éviter le développement de microorganismes et du pollen est ajouté à la boite de Petri dédiée.

Les nouveaux adultes émergents sont placés dans une cage séparée pour s'assurer que d'autres espèces ne sont pas introduites dans la cage dédiée à *D. suzukii*. Les fruits donnés pour la ponte peuvent contenir des œufs d'autres espèces d'insecte ayant survécu à la congélation.


**Abbildung 3: Photographie de (gauche) l'arrangement des cages et boites à l'intérieur de l'incubateur et (droite) boite utilisée pour des stades œuf à adulte**

**Fruits pour la ponte d'œufs par *D. suzukii***

Pour permettre aux mouches de déposer leurs œufs, des fruits (raisins, framboises ou myrtilles) leur sont apportés 2 fois par semaine. Pour éviter que les fruits ne soient une source de contamination de la population, ils sont congelés à -20 °C au moins 3 jours et décongelés avant d'être donnés aux mouches. Pour éviter que les mouches ne se noient dans le jus des fruits, ils sont déposés sur du papier absorbant. Les mouches peuvent avoir des difficultés à pondre dans les raisins car leur peau est difficile à percer, par conséquent, une entaille est réalisée au scalpel pour offrir un accès à la chair du raisin.

**Gestion des stades œuf à adulte**

Les fruits dans lesquels ont été déposés les œufs sont installés dans un pot daté. Ce pot est installé dans la cage dédiée à l'émergence des adultes et y reste pour une durée de 1 mois pour s'assurer que tous les œufs ont pu éclore. Le fait que les mouches aient un plus grand espace, accès à de l'eau et de la nourriture facilement a augmenté le nombre d'adultes collectés.

Pour s'assurer que la population de mouches reste uniquement composée de *D. suzukii*, les nouveaux adultes qui émergent sont identifiés (*D. suzukii* femelle ou *D. suzukii* mâle ou autre espèce) à l'aide de la clé dichotomique (Vlach, 2013) avant d'être ajoutés à la cage contenant la population. L'identification des mouches est réalisée avec un intervalle d'au moins deux jours afin que les points sur les ailes des mâles aient le temps d'apparaitre.

**Manipulation des mouches**

Plusieurs méthodes sont utilisées pour la manipulation des mouches. S'il suffit de les déplacer, les mouches sont capturées à l'aide de l'exhausteur. A l'œil nu il est possible de distinguer les mâles et les femelles. Toutefois cette méthode demande un peu de dextérité pour ne pas que les mouches puissent s'échapper. Une autre méthode consiste à refroidir les mouches sur de la glace lorsqu'il faut par exemple identifier à quelle espèce elles appartiennent. Des pots sont mis sur de la glace et laissés refroidir au moins 5 mn. Les mouches sont collectées dans la cage à l'aide d'un exhausteur puis transvasées de l'exhausteur au pot refroidi. Le pot est maintenu fermé par un filet maintenu par un élastique. Il faut attendre quelques minutes que toutes les mouches ne bougent plus. Une fois les mouches endormies, elles peuvent être manipulées à l'aide d'un pinceau afin de les identifier au microscope ou les introduire dans une zone d'expérimentation. Il est important que les mouches ne restent pas trop longtemps refroidies sur la glace afin qu'elles puissent rapidement retrouver leurs esprits. Si elles restent refroidies trop longtemps, cela peut les tuer.

**Maintien de la diversité génétique**

Pour améliorer la diversité génétique, des mouches *D. suzukii* de l'extérieur ont été introduites dans la population. Des mûres et des raisins, sur lesquels des mouches similaires à *D. suzukii* ou des dégâts (trous de ponte, odeur de vinaigre) ont été observés, ont été récoltés et conservés dans des boites fermées par des filets. Les mouches émergeant de ces fruits sont identifiées et ajoutées à la cage dédiée.

### *2.3.4* Versuch T Bekämpfung *Drosophila suzukii*

Zur Bekämpfung der Kirschessigfliege wurden zwei Versuche in den Versuchsflächen des IVV angelegt.

In der Rebsorte Pinotin wurde ein Versuch zur repellenten Wirkung von Kaolin (zwei verschiedene Produkte) und Calcium Carbonat durchgeführt.

Folgende Versuchsglieder wurden realisiert (Tab. 5):

**Tab. 5: Versuchsglieder im Versuch T (Versuchsjahr 2020).**

| VG | Spritzfolge |
|---|---|
| 1 | unbehandelte Kontrolle |
| 2 | Kaolin Cutisan |
| 3 | Calcium Carbonat $CaCO_3$ |
| 4 | Kaolin Surround |

In den Versuchsgliedern 2 und 4 wurde am 19.08., 02.09. und 14.09. eine beidseitige Applikation der Prüfmittel durchgeführt. In der Versuchsgliedern 3 wurde am 19.08. und 02.09. appliziert. Die Applikation erfolgte mittels Akku-Rückenspritze der Firma Solo Kleinmotoren GmbH vom Typ Akku 416, ausgestattet mit Injektorflachstrahldüsen der Firma Agrotop (Typ Albuz AVI 80). Behandelt wurde die ganze Laubwand.

Die Anwendungskonzentrationen betrugen je 2%.

### 2.3.5 Versuch W Schnittsysteme

Im Versuch W wurden verschiedene Rebschnittsysteme hinsichtlich ihrer Effekte auf die Traubenstruktur und die Fäulnis-Epidemie untersucht.
Folgende Versuchsglieder wurden jeweils in den Rebsorten Riesling und Pinot gris angelegt (Tab. 6):

**Tab. 6: Versuchsglieder im Versuch W (Versuchsjahr 2020).**

| VG | Schnittssystem |
|---|---|
| 1 | Rebschnitt auf zahmes Holz |
| 2 | Rebschnitt auf wildes Holz |
| 3 | Sanfter Rebschnitt nach Simonit und Sirch |
| 4 | Doppelter Anschnitt; Entfernen zweite Bogrebe ca. 2 Wochen nach der Rebblüte |

In den Versuchsgliedern 1 bis 3 wurden jeweils pro Pflanze eine 12-äugige Bogrebe (Flachbogen) angeschnitten. In Versuchsglied 4 erfolgte ein Anschnitt auf zwei 12-äugige Bogreben; die zweite Bogrebe wurde hier jedoch ca. zwei Wochen nach der Rebblüte am 29.06. (Riesling: BBCH 73; Pinot gris: BBCH 73-75) entfernt. Der Arbeitszeitbedarf für diese Maßnahme betrug ca. 18 Arbeitskraftstunden pro Hektar.
Im Versuchsglied 1 wurden lediglich einjährige Triebe auf zweijährigem Holz angeschnitten, im VG 2 einjährige Triebe auf mehrjährigem Holz angeschnitten. Im VG 3 erfolgte der Rebschnitt nach dem Schnittsystem „Simonit und Sirch“, welches auch als „Sanfter Rebschnitt“ bezeichnet wird.

### 2.3.6 Versuch X Oidium

In Versuch X wurden verschiedene Strategien zur Kontrolle des Echten Mehltaus in der Rebsorte Riesling getestet. Es erfolgte mit Ausnahme der letzten sechs Spritzungen beim Prüfmittel Fytosave eine kontinuierliche Grundabdeckung gegen den Falschen Mehltau mittels Folpan (Tab. 7).

**Tab. 7: Versuchsglieder im Versuch X (Versuchsjahr 2020).**

| VG | Strategie | Erläuterung |
|---|---|---|
| 1 | unbehandelte Kontrolle | |
| 2 | Kontrolle | im Mehltaufenster unbehandelt |
| 3 | Flint (Strobilurin) | im Mehltaufenster |
| 4 | Luna Experience | im Mehltaufenster |
| 5 | Nissodium | im Mehltaufenster |
| 6 | Topas | letzte drei Spritzungen |
| 7 | Vitisan | Mehltaufenster + letzte drei Spritzungen |
| 8 | Fytosave | Mehltaufenster + letzte drei Spritzungen |
| 9 | Sercadis | im Mehltaufenster |
| 10 | Kusabi | im Mehltaufenster |

Folgende Pflanzenschutzmaßnahmen wurden im Versuchsjahr 2020 durchgeführt (Tab. 8):

**Tab. 8: Spritzplan Versuch X (Versuchsjahr 2020). Darstellung: Mannes, IVV.**

| | 1. Spritzung | 2. Spritzung | 3. Spritzung | 4. Spritzung | 5. Spritzung | 6. Spritzung | 7. Spritzung | 8.Spritzung | 9.Spritzung |
|---|---|---|---|---|---|---|---|---|---|
| | 5-Blatt | 7-Blatt | 9-Blatt | 12-Blatt | abgehende Blüte | Schrotkorngrösse | Erbsengrösse | Ende Traubenschluss | Ende Traubenschluss |
| | 04/05/2020 | 14/05/2020 | 20/05/2020 | 28/05/2020 | 09/06/2020 | 19/06/2020 | 01/07/2020 | 13/07/2020 | 24/07/2020 |
| 1 | Folpan WG 0,8 kg/ha | Folpan WG 0,8 kg/ha | Folpan WG 0,8 kg/ha | Folpan WG 0,8 kg/ha | Folpan WG 1,0 kg/ha | Folpan WG 1,2 kg/ha | Folpan WG 1,4 kg/ha | Folpan WG 1,6 kg/ha | Folpan WG 1,6 kg/ha |
| 2 | Folpan WG 0,8 kg/ha<br>Microthiol 4,5 kg/ha | Folpan WG 0,8 kg/ha<br>Microthiol 4,8 kg/ha | Folpan WG 0,8 kg/ha<br>Microthiol 6,0 kg/ha | Folpan WG 0,8 kg/ha | Folpan WG 1,0 kg/ha | Folpan WG 1,2 kg/ha | Folpan WG 1,4 kg/ha<br>Microthiol 6,0 kg/ha | Folpan WG 1,6 kg/ha<br>Microthiol 6,0 kg/ha | Folpan WG 1,6 kg/ha<br>Microthiol 6,0 kg/ha |
| 3 | Folpan WG 0,8 kg/ha<br>Microthiol 4,5 kg/ha | Folpan WG 0,8 kg/ha<br>Microthiol 4,8 kg/ha | Folpan WG 0,8 kg/ha<br>Microthiol 6,0 kg/ha | Folpan WG 0,8 kg/ha<br>Flint 50 WG 0,12 kg/ha | Folpan WG 1,0 kg/ha<br>Flint 50 WG 0,15 kg/ha | Folpan WG 1,2 kg/ha<br>Flint 50 WG 0,18 kg/ha | Folpan WG 1,4 kg/ha<br>Microthiol 6,0 kg/ha | Folpan WG 1,6 kg/ha<br>Microthiol 6,0 kg/ha | Folpan WG 1,6 kg/ha<br>Microthiol 6,0 kg/ha |
| 4 | Folpan WG 0,8 kg/ha<br>Microthiol 4,5 kg/ha | Folpan WG 0,8 kg/ha<br>Microthiol 4,8 kg/ha | Folpan WG 0,8 kg/ha<br>Microthiol 6,0 kg/ha | Folpan WG 0,8 kg/ha<br>Luna Exp. 250 ml/ha | Folpan WG 1,0 kg/ha<br>Luna Exp. 375 ml/ha | Folpan WG 1,2 kg/ha<br>Luna Exp. 0,5 L/ha | Folpan WG 1,4 kg/ha<br>Microthiol 6,0 kg/ha | Folpan WG 1,6 kg/ha<br>Microthiol 6,0 kg/ha | Folpan WG 1,6 kg/ha<br>Microthiol 6,0 kg/ha |
| 5 | Folpan WG 0,8 kg/ha<br>Microthiol 4,5 kg/ha | Folpan WG 0,8 kg/ha<br>Microthiol 4,8 kg/ha | Folpan WG 0,8 kg/ha<br>Microthiol 6,0 kg/ha | Folpan WG 0,8 kg/ha<br>Nissodium EW 240 ml/ | Folpan WG 1,0 kg/ha<br>Nissodium EW 360 ml/h | Folpan WG 1,2 kg/ha<br>Nissodium EW 0,5 L/ha | Folpan WG 1,4 kg/ha<br>Microthiol 6,0 kg/ha | Folpan WG 1,6 kg/ha<br>Microthiol 6,0 kg/ha | Folpan WG 1,6 kg/ha<br>Microthiol 6,0 kg/ha |
| 6 | Folpan WG 0,8 kg/ha<br>Microthiol 4,5 kg/ha | Folpan WG 0,8 kg/ha<br>Microthiol 4,8 kg/ha | Folpan WG 0,8 kg/ha<br>Microthiol 6,0 kg/ha | Folpan WG 0,8 kg/ha<br>Microthiol 5,0 kg/ha | Folpan WG 1,0 kg/ha<br>Microthiol 6,0 kg/ha | Folpan WG 1,2 kg/ha<br>Microthiol 6,0 kg/ha | Folpan WG 1,4 kg/ha<br>Topaz EC 0,28 L/ha | Folpan WG 1,6 kg/ha<br>Topaz EC 0,32 L/ha | Folpan WG 1,6 kg/ha<br>Topaz EC 0,32 L/ha |
| 7 | Folpan WG 0,8 kg/ha<br>Microthiol 4,5 kg/ha | Folpan WG 0,8 kg/ha<br>Microthiol 4,8 kg/ha | Folpan WG 0,8 kg/ha<br>Microthiol 6,0 kg/ha | Folpan WG 0,8 kg/ha<br>Vitisan 6,0 kg/ha | Folpan WG 1,0 kg/ha<br>Vitisan 7,0 kg/ha | Folpan WG 1,2 kg/ha<br>Vitisan 8,0 kg/ha | Folpan WG 1,4 kg/ha<br>Vitisan 8,0 kg/ha | Folpan WG 1,6 kg/ha<br>Vitisan 8,0 kg/ha | Folpan WG 1,6 kg/ha<br>Vitisan 8,0 kg/ha |
| 8 | Folpan WG 0,8 kg/ha<br>Microthiol 4,5 kg/ha | Folpan WG 0,8 kg/ha<br>Microthiol 4,8 kg/ha | Folpan WG 0,8 kg/ha<br>Microthiol 6,0 kg/ha | Fytosave 2,0 L/ha | Fytosave 2,0 L/ha | Fytosave 2,0 L/ha | Fytosave 2,0 L/ha | Fytosave 2,0 L/ha | Fytosave 2,0 L/ha |
| 9 | Folpan WG 0,8 kg/ha<br>Microthiol 4,5 kg/ha | Folpan WG 0,8 kg/ha<br>Microthiol 4,8 kg/ha | Folpan WG 0,8 kg/ha<br>Microthiol 6,0 kg/ha | Folpan WG 0,8 kg/ha<br>Sercadis SC 120 ml/ha | Folpan WG 1,0 kg/ha<br>Sercadis 180 ml/ha | Folpan WG 1,2 kg/ha<br>Sercadis 180 ml/ha | Folpan WG 1,4 kg/ha<br>Microthiol 6,0 kg/ha | Folpan WG 1,6 kg/ha<br>Microthiol 6,0 kg/ha | Folpan WG 1,6 kg/ha<br>Microthiol 6,0 kg/ha |
| 10 | Folpan WG 0,8 kg/ha<br>Microthiol 4,5 kg/ha | Folpan WG 0,8 kg/ha<br>Microthiol 4,8 kg/ha | Folpan WG 0,8 kg/ha<br>Microthiol 6,0 kg/ha | Folpan WG 0,8 kg/ha<br>Kusabi SC 150 ml/ha | Folpan WG 1,0 kg/ha<br>Kusabi SC 225 ml/ha | Folpan WG 1,2 kg/ha<br>Kusabi SC 225 ml/ha | Folpan WG 1,4 kg/ha<br>Microthiol 6,0 kg/ha | Folpan WG 1,6 kg/ha<br>Microthiol 6,0 kg/ha | Folpan WG 1,6 kg/ha<br>Microthiol 6,0 kg/ha |

Die Applikationen erfolgten mittels des Parzellenspritzgeräts des IVV.

### 2.3.7 Versuch Y Fernerkundliche Erkennung der Peronospora

In Versuch Y wurden (i) verschiedene Strategien zur Kontrolle des Falschen Mehltaus in der Rebsorte Pinot gris überprüft (Tab. 9), sowie (ii) fernerkundliche Verfahren zur Differenzierung des Befallsgrades am Reblaub getestet.

**Tab. 9: Versuchsglieder im Versuch Y (Versuchsjahr 2020).**

| VG | Strategie | |
|---|---|---|
| 1 | unbehandelte Kontrolle | ohne künstliche Inokulation |
| 2 | unbehandelte Kontrolle | künstliche Inokulation; 19.05.2020 |
| 3 | integriert | künstliche Inokulation; 19.05.2020 |
| 4 | Kupfer | künstliche Inokulation; 19.05.2020 |
| 5 | Phosphorige Säure | künstliche Inokulation; 19.05.2020 |
| 6 | Kupfer + Phosphorige S. | künstliche Inokulation; 19.05.2020 |
| 7 | Kupfer + Phosphorige S. bis BBCH 69 | künstliche Inokulation; 19.05.2020 |
| 8 | Kupfer + Prüfmittel Neu 1143F | künstliche Inokulation; 19.05.2020 |

Folgende Pflanzenschutzmaßnahmen wurden im Versuchsjahr 2020 durchgeführt (Tab. 10):

**Tab. 10: Spritzplan Versuch Y (Versuchsjahr 2020). Darstellung: Mannes, IVV.**

| | 1. Spritzung | 2. Spritzung | 3. Spritzung | 4. Spritzung | 5. Spritzung | 6. Spritzung | 7. Spritzung | 8. Spritzung |
|---|---|---|---|---|---|---|---|---|
| | 9-Blatt | 12-Blatt | abgehende Blüte | Schrotkorngrösse | Erbsengrösse | Traubenschluss | Ende Traubenschluss | |
| | 20/05/2020 | 29/05/2020 | 10/06/2020 | 19/06/2020 | 01/07/2020 | 13/07/2020 | 24/07/2020 | |
| 1 | *Microthiol 4,8 kg/ha* | *Microthiol 5,0 kg/ha* | *Microthiol 6,0 kg/ha* | *Microthiol 6,0 kg/ha* | *Microthiol 6,0 kg/ha* | *Microthiol 6,0 kg/ha* | *Microthiol 6,0 kg/ha* | |
| 2 | *Microthiol 4,8 kg/ha* | *Microthiol 5,0 kg/ha* | *Microthiol 6,0 kg/ha* | *Microthiol 6,0 kg/ha* | *Microthiol 6,0 kg/ha* | *Microthiol 6,0 kg/ha* | *Microthiol 6,0 kg/ha* | |
| 3 | *Microthiol 4,8 kg/ha*<br>*Folpan 0,8 kg/ha* | *Microthiol 5,0 kg/ha*<br>*Folpan 0,8 kg/ha* | *Microthiol 6,0 kg/ha*<br>*Zorvec Zelavin 240 ml/ha* | *Microthiol 6,0 kg/ha*<br>*Profiler WG 2,25 kg/ha* | *Microthiol 6,0 kg/ha*<br>*Mildicut SC 3,5 L/ha* | *Microthiol 6,0 kg/ha*<br>*Folpan 80 WG 1,6 kg/ha* | *Microthiol 6,0 kg/ha*<br>*Folpan 80 WG 1,6 kg/ha* | |
| 4 | *Microthiol 4,8 kg/ha*<br>*Kocide Opti 0,7 kg/ha* | *Microthiol 5,0 kg/ha*<br>*Kocide Opti 0,9 kg/ha* | *Microthiol 6,0 kg/ha*<br>Kocide Opti 1,2 kg/ha | *Microthiol 6,0 kg/ha*<br>*Kocide Opti 1,2 kg/ha* | *Microthiol 6,0 kg/ha*<br>*Kocide Opti 1,0 kg/ha* | *Microthiol 6,0 kg/ha*<br>*Kocide Opti 1,0 kg/ha* | *Microthiol 6,0 kg/ha*<br>*Kocide Opti 1,0 kg/ha* | |
| 5 | *Microthiol 4,8 kg/ha*<br>*Veriphos 2,0 L/ha* | *Microthiol 5,0 kg/ha*<br>*Veriphos 2,0 L/ha* | *Microthiol 6,0 kg/ha*<br>*Veriphos 3,0 L/ha* | *Microthiol 6,0 kg/ha*<br>*Veriphos 3,5 L/ha* | *Microthiol 6,0 kg/ha*<br>*Veriphos 3,5 L/ha* | *Microthiol 6,0 kg/ha*<br>*Veriphos 3,5 L/ha* | *Microthiol 6,0 kg/ha*<br>*Veriphos 3,5 L/ha* | |
| 6 | *Microthiol 4,8 kg/ha*<br>*Veriphos 2,0 L/ha*<br>*Kocide Opti 0,7 kg/ha* | *Microthiol 5,0 kg/ha*<br>*Veriphos 2,0 L/ha*<br>*Kocide Opti 0,9 kg/ha* | *Microthiol 6,0 kg/ha*<br>*Veriphos 3,0 L/ha*<br>Kocide Opti 1,2 kg/ha | *Microthiol 6,0 kg/ha*<br>*Veriphos 3,5 L/ha*<br>*Kocide Opti 1,2 kg/ha* | *Microthiol 6,0 kg/ha*<br>*Veriphos 3,5 L/ha*<br>*Kocide Opti 1,0 kg/ha* | *Microthiol 6,0 kg/ha*<br>*Veriphos 3,5 L/ha*<br>*Kocide Opti 1,0 kg/ha* | *Microthiol 6,0 kg/ha*<br>*Veriphos 3,5 L/ha*<br>*Kocide Opti 1,0 kg/ha* | |
| 7 | *Microthiol 4,8 kg/ha*<br>*Veriphos 2,0 L/ha*<br>*Kocide Opti 0,7 kg/ha* | *Microthiol 5,0 kg/ha*<br>*Veriphos 2,0 L/ha*<br>*Kocide Opti 0,9 kg/ha* | *Microthiol 6,0 kg/ha*<br>*Veriphos 3,0 L/ha*<br>Kocide Opti 1,2 kg/ha | *Microthiol 6,0 kg/ha*<br>*Kocide Opti 1,2 kg/ha* | *Microthiol 6,0 kg/ha*<br>*Kocide Opti 1,0 kg/ha* | *Microthiol 6,0 kg/ha*<br>*Kocide Opti 1,0 kg/ha* | *Microthiol 6,0 kg/ha*<br>*Kocide Opti 1,0 kg/ha* | |
| 8 | *Microthiol 4,8 kg/ha*<br>*Neu 1143 F 0,4 L/ha*<br>*Kocide Opti 0,7 kg/ha* | *Microthiol 5,0 kg/ha*<br>*Neu 1143 F 0,6 L/ha*<br>*Kocide Opti 0,9 kg/ha* | *Microthiol 6,0 kg/ha*<br>*Neu 1143 F 1,0 L/ha*<br>*Kocide Opti 1,2 kg/ha* | *Microthiol 6,0 kg/ha*<br>*Neu 1143 F 1,2 L/ha*<br>*Kocide Opti 1,0 kg/ha* | *Microthiol 6,0 kg/ha*<br>*Neu 1143 F 1,4 L/ha*<br>*Kocide Opti 1,0 kg/ha* | *Microthiol 6,0 kg/ha*<br>*Neu 1143 F 1,4 L/ha*<br>*Kocide Opti 1,0 kg/ha* | *Microthiol 6,0 kg/ha*<br>*Neu 1143 F 1,4 L/ha*<br>*Kocide Opti 1,0 kg/ha* | |

Die Aufzeichnungen der 8. Spritzung lagen bei Redaktionsschluss dieses Berichtes noch nicht vor.

Die künstliche Inokulation ($10^4$-$10^5$ Sporangien / ml) wurde am 19.05.2020 durchgeführt. Die Applikationen erfolgten mittels des Parzellenspritzgeräts des IVV.

Für eine Schätzung des Befallgrades waren zwei Kamerasysteme vorgesehen: (1) eine einfache multispektrale Kamera (Micasense RedEdge) mit fünf spektralen Bändern im Sichtbaren, RedEdge sowie nahen Infrarot. (2) eine Thermalkamera (Teax Thermal Capture Fusion Zoom). Die MicaSense Kamera gehört der Uni Trier, die diese auch betreibt. Aufgrund der unsicheren Covid-19 Situation wurde noch vor Beginn der Saison beschlossen, dass das LIST zusätzlich mit seinem eigenen hyperspektralen System (Headwall Nano) Daten erhebt, da die Einreisebeschränkungen für die Uni Trier nicht abschätzbar waren. Diese Annahme hatte sich im späteren Verlauf der Saison auch bestätigt, denn die Mitarbeiter der Uni Trier konnten sie lediglich zu drei Terminen Dienstreisen bewilligen lassen und alle weiteren Termine wurden ausschließlich mit den beiden Kameras vom LIST durchgeführt. Abbildung 4 zeigt eine Übersicht über die drei Kameras.


**Abbildung 4: Die drei eingesetzten Kameras im Vergleich. Links die Headwall Nano, Hyperspektralkamera, Mitte, die Teax Thermal Capture Fusion Zoom, Thermalkamera und rechts, die fünf-Band Kamera Micasense RedEdge**

Anders als in den vorangegangenen Jahren, wurde in der Saison 2020 nicht im festgelegten zweiwöchigen Rhythmus geflogen, sondern vielmehr bedarfsorientiert. Im Detail bedeutet das, dass es einen Flug vor der Innokulation gab und einen danach und im weiteren Verlauf entsprechend der Ausbreitung von Peronospora. Während keine Ausbreitung beobachtet werden konnte, fanden entsprechend keine Befliegungen statt. Hingegen, als sich Peronospora dann Ende Juni auszubreiten begann, wurden wöchentliche Flüge durchgeführt, um kleinere Änderungen gut erfassen zu können.

**Abbildung 5: Referenzmessungen der Panels**

Parallel zu jedem Flug fanden Referenzmessungen am Boden statt. Hierfür wurde ein Referenzpanel mit drei Graustufen, sowie ein weißes Spektralon installiert, das mit einem Spektrometer (Spectral Evolution) eingemessen wurde (Abb. 5). Zusätzlich wurden in diesem Jahr mit Alufolie überzogene Marker eingesetzt, die am Ende von jedem Versuchsplot, links, rechts und in der Mitte der Versuchsreihen ausgelegt wurden (Abb. 6). Insbesondere für die kontrastschwächeren Thermalaufnahmen dienen diese Marker zur besseren Orientierung und Plot-Erkennung im Bild.

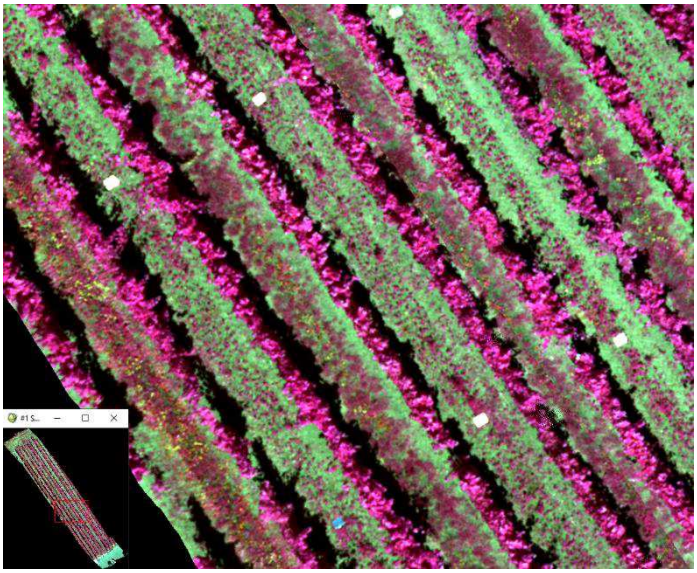

**Abbildung 6: Falschfarbenbild des Versuchs und in weiß dargestellt die Alu-Marker im Feld zur Ploterkennung**

**Abbildung 7: Livebild der Thermalaufnahmen mit sichtbaren Markern im Bild und Flug der LIST-Drohne mit der Headwall Nano Kamera über dem Versuch**

### 2.3.8 Versuch AA Erfassung symptomatischer Esca-Stöcke

Ziel des Versuchs AA ist die Erfassung symptomatischer Esca-Stöcke in den Weinbergen im Bereich „Berg“ des IVV in Remich. Hierzu erfolgt seit dem Jahr 2017 jährlich nach Reifebeginn eine Einzelstock-genaue Bonitur.

### 2.3.9 Erfassung des Bestandsklima mittels mikro-meteorologischer Messungen mit dem Schwerpunkt Blattnässe

Zur Erfassung des Bestandsklimas mit dem Schwerpunkt Blattnässe wurden zu Beginn des Jahres 2020 sechs meteorologische Stationen in den Versuchsfeldern installiert. In den verschiedenen Erziehungssystemen (E3 = Minimalschnitt im Spalier, E2 = Spaliererziehung, Entblätterung der Traubenzone, E1 = Spaliererziehung, ohne Entblätterung der Traubenzone) wurden jeweils zwei meteorologische Stationen installiert (Abbildung 8).

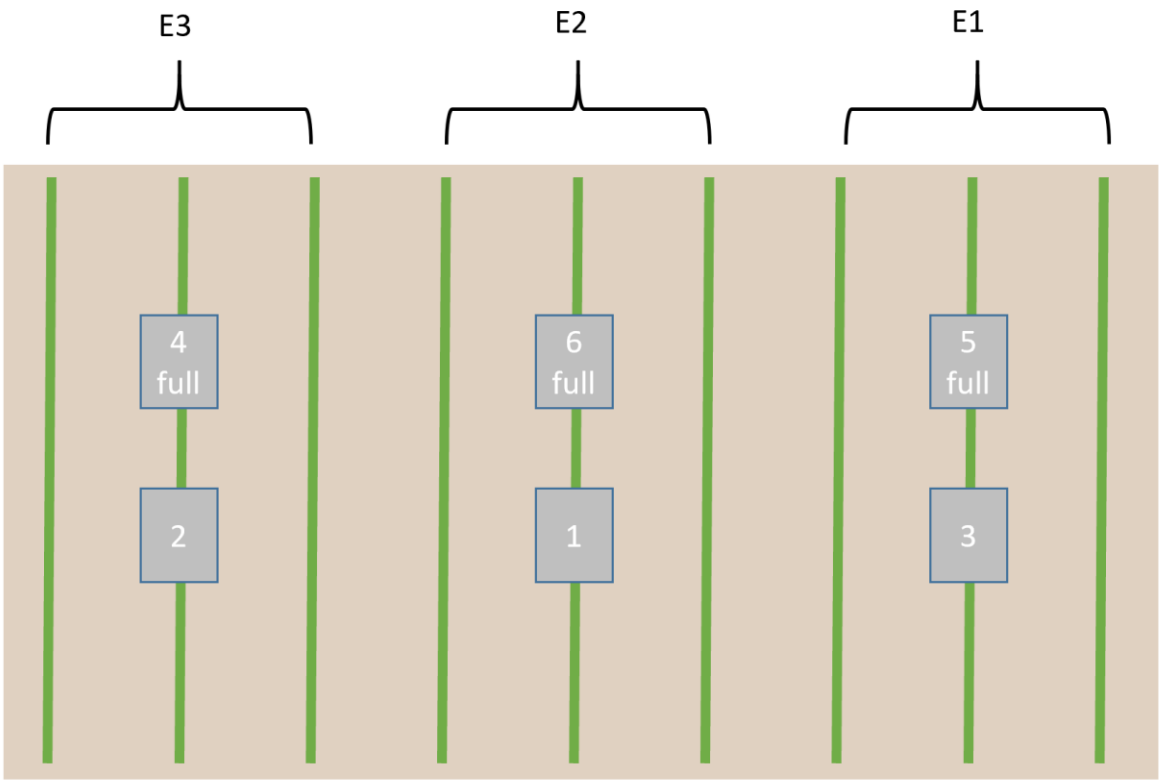


**Abbildung 8: Verteilung der meteorologischen Stationen in den verschiedenen Erziehungssystemen. Die mit „full“ gekennzeichneten Stationen erfassen zusätzlich zu der Blattnässe, Lufttemperatur und relativer Feuchte noch die Globalstrahlung im Bestand, sowie die Windrichtung und Geschwindigkeit über dem Bestand. E3 = Minimalschnitt im Spalier, E2 = Spaliererziehung, Entblätterung der Traubenzone, E1 = Spaliererziehung, ohne Entblätterung der Traubenzone.**

Pro Erziehungssystem gibt es eine Master Station, die die Parameter Lufttemperatur, relative Feuchte (im Bestand), Globalstrahlung (im Bestand), sowie Windrichtung und Geschwindigkeit (über dem Bestand) erfasst (Abbildung 9 links). Des Weiteren wurden in drei verschiedenen Höhen (unterhalb der Laubwand, in der Laubwand, sowie über dem Bestand) fünf Blattnässesensoren installiert. In den beiden unteren Messhöhen (unterhalb und in der Laubwand) wurde jeweils ein Blattnässesensor in Richtung der Laubwand und einer von der Laubwand weg gerichtet installiert. Über dem Bestand wurde nur ein einzelner Blassnässesensor pro Station installiert. Die Ausrichtung der Blattnässesensoren in Bezug auf Neigung wurde bei allen Stationen gleich vorgenommen. Die zweite Station in dem jeweiligen Erziehungssystem erfasst nur die Blattnässe (analoge Anordnung der fünf Sensoren), Lufttemperatur und relative Feuchte (Abbildung 9 rechts). Alle Stationen sind mit Datenloggern (CRX1000 der Firma Campbell Scientific) zur kontinuierlichen Datenaufzeichnung ausgestattet, die Stromversorgung erfolgt mittels Akkus. Die zeitliche Auflösung der Messwerte beträgt eine Minute.

**Abbildung 9: Voll ausgestattete Station (links) mit zusätzlichem Globalstrahlungsgeber und 2D Wind Sonic, sowie einfache Station (rechts) zur Erfassung der Blattnässe, Lufttemperatur und relativen Feuchte im Bestand.**

Bei der Auswahl der Blattnässesensoren wurde das gleiche Modell wie an der ASTA Station gewählt, um Unterschiede, die durch verschieden Sensoren und Messkonzepte entstehen, ausschlissen zu können. Es handelt sich um kapazitiv messende Fühler, die schwach auf relative Feuchte und stark auf kondensierende Nässe reagieren. Die Blattnässesensoren nach Hoffmann werden seit 1990 in verschiedenen Messnetzen wie z.B. DLR Rehinland Pfalz oder

LFL Bayern eingesetzt. Es handelt sich um neu angeschaffte Sensoren. Somit kann eine unterschiedliche Alterung weitgehend ausgeschlossen werden.

## 2.4 Auswertung

### 2.4.1 Traubenstruktur

Zur Beurteilung des Effektes der durchgeführten Maßnahmen auf die Traubenstruktur wurden im Versuch W jeweils 50 bzw. 100 Trauben pro Parzelle mit Hilfe der „Richtlinien zur Prüfung von Wachstumsregulatoren zur Auflockerung der Traubenstruktur und zur Vermeidung von Fäulnis an Trauben“ (Ipach et al., 2005) bewertet. Die Bewertungsskala innerhalb dieses Schemas bewegt sich zwischen „sehr lockerbeerige Traubenstruktur“ (Klasse 1) und „sehr kompakte Traubenstruktur“ (Klasse 5). Die Bonituren wurden vor Reifebeginn im BBCH-Entwicklungsstadium 79 (Ende des Traubenschlusses) am 04.08.2020 durchgeführt.

### 2.4.2 Befallsverlauf *Botrytis cinerea*

Die Befallsentwicklung von *Botrytis cinerea* wurde mit Hilfe eines Siebenklassen-Bonitur-Schemas (0%, 1 bis 5%, 6 bis 10%,11 bis 25%, 26 bis 50%, 51 bis 75%, 76 bis 100%) gemäß EPPO Richtlinie PP1/17(3) dokumentiert. Die Bonitur erfolgte im Versuch W regelmäßig ab dem Reifebeginn in ein- bis zweiwöchentlichem Abstand. Auf Gründen der Übersichtlichkeit werden in diesem Bericht lediglich die Ergebnisse der letzten Bonitur vor der Ernte angegeben. Pro Parzelle wurden jeweils 50 Trauben von beiden Zeilenseiten begutachtet.

### 2.4.3 Ertragserfassung und Mostanalysen

Zur Erfassung des Ertrags erfolgte im Versuch W eine parzellengenaue Versuchslese. Pro Variante und Wiederholung wurden vier Stöcke beerntet und aus den erfassten Gewichten der Durchschnittsertrag pro Stock errechnet.

Zur Erfassung der Mostinhaltstoffe wurden unmittelbar vor der Versuchslese aus jedem Versuchsglied und jeder Wiederholung ca. 10 Trauben entnommen. Um möglichst repräsentative Ergebnisse zu erhalten, wurden hierfür Trauben zu gleichen Teilen von der Sonnen- und Schattenseite bzw. von verschiedenen Positionen innerhalb der Laubwand ausgewählt. Zur Analysevorbereitung wurden die Trauben manuell gepresst und der Most zentrifugiert. Anschließend erfolgte die Bestimmung des Mostgewichtes, der Gesamtsäure, des NOPA-Wertes (hefeverfügbarer Stickstoff) sowie des Ammonium-Gehaltes mittels FTIR (FOSS Grapescan) im Wein-analytischen Labor des IVV.

### 2.4.4 Monitoring *S. titanus*

Die Gelbfallen wurden an allen Standorten im zweiwöchentlichen Abstand ersetzt und eine Bestimmung der gefangenen Arten durchgeführt (Abb. 10).

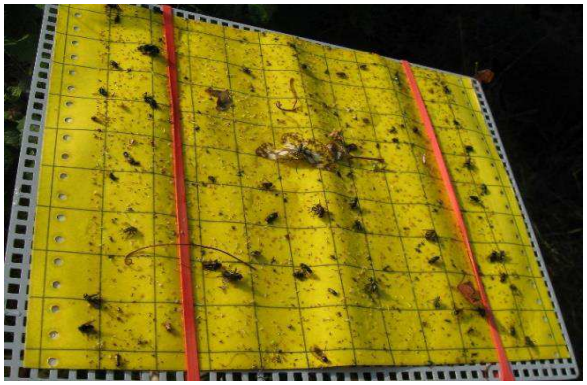

**Abbildung 10: Gelbfalle am Standort Wellenstein.**

### 2.4.5 Befallsbonituren Echter Mehltau und Falscher Mehltau

Bonituren zur Erfassung des Befalls durch Echten Mehltau bzw. Falschen Mehltau in den Versuchen X und Y erfolgte gemäß dem für *Botrytis cinerea* beschriebenen Siebenklassen-Bonitur-Schema zu verschiedenen Zeitpunkten im Laufe der Vegetationsperiode an Blättern sowie Trauben. In diesem Bericht werden lediglich die Ergebnisse der letzten Bonitur angegeben. Pro Parzelle wurden 100 Blätter bzw. Trauben begutachtet.

In Versuch Y erfolgte die Bonitur des Blattbefalls durch den Falschen Mehltau im etwa 7-tägigen Rhythmus (je nach Entwicklung des Befalls) jeweils am Termin der fernerkundlichen Messungen aus der Luft.

### 2.4.6 Erfassung des Fluges und der Eiablage durch *Drosophila suzukii*

Die Auswertung der Fallenfänge erfolgte getrennt nach männlichen und weiblichen Kirschessigfliegen mittels Binokular (Abb. 11).

**Abbildung 11: Männliche Kirschessigfliegen.**

Die Bonitur der Eiablage erfolgte an jeweils 50 Einzelbeeren pro Parzelle, welche aus ca. 15 im Weinberg entnommenen Traubenteilen stammten. Mittels Binokulars wurden die Einzelbeeren von allen Seiten untersucht und die Anzahl der abgelegten Kirschessigfliegen-Eier erfasst (Abb. 12).

**Abbildung 12: Bonituren der Eiablage und des Larvenbesatzes unter dem Binokular.**

### 2.4.7 Bonituren in den Freilandversuchen zur Bekämpfung der Kirschessigfliege

Pro Versuchsglied und Wiederholung wurde in beiden Versuchen eine Riga-Becherfalle in der Traubenzone befestigt und diese wöchentlich ausgezählt und ersetzt.
Weiterhin wurden in beiden Versuchen wöchentlich 15 Traubenteile entnommen und an 50 Beeren die Eiablage erfasst.
Die Auswertung der Fangzahlen und der Eiablage erfolgte wie in Kapitel 2.4.6 beschrieben.

### 2.4.8 Fernerkundliche Verfahren zur Befallsdifferenzierung im Versuch Y

Im Folgenden werden die erhobenen Fernerkundungsdaten und deren Vorprozessierung beschrieben.

#### 2.4.8.1 Drohnengestützte Messungen

Die Saison 2020 wurde aufgrund der Einreisebeschränkungen von COVID-19 an der Uni Trier fast ausschließlich mit den beiden Kameras des LIST durchgeführt. Beide Kameras haben aufgrund der Sensormechanik (Zeilenscanner) und durch Einschränkungen der Aufhängung nicht die Möglichkeit Schrägaufnahmen zu akquirieren. Folglich wurden fast ausschließlich Nadiraufnahmen (senkrechter Blick nach unten) aufgenommen. In den Vorjahren lieferten insbesondere in den trockenen Sommern, wie 2020, die Nadiraufnahmen die besseren Ergebnisse, da sie bei lichtem Bestand weniger anfällig für Hintergrundeinflüsse sind. Somit schätzen wir die Akquirierung von ausschließlich Nadiraufnahmen nicht als Einschränkung ein.

Die Definition der Wolkensituation wird in Tabelle 11 dargestellt. Die Wolkenbedingungen werden in fünf Klassen angegeben, um eventuelle Einflüsse der Wolkenbedingungen auf die Ergebnisse analysieren zu können.

**Tab. 11: Beschreibung der Wetterbedingungen zu den Flugterminen**

| Wetterbedingung | Beschreibung | Symbol |
|---|---|---|
| Sonnig | Himmel ist auch im grösseren Umfeld wolkenfrei, beste Flugbedingungen |  |
| Leicht bewölkt | Leichte oder dichtere Bewölkung im näheren Umfeld, Weinberg kann bei sonnigen Bedingungen beflogen werden, jedoch sind leichte Qualitätsverluste möglich |  |
| Bewölkt | Schwere und dichte Bewölkung in und um das Untersuchungsgebiet, Datenqualität wird nachteilig beeinflusst, |  |
| Leichte Cirrus | Schwache Cirrus-Wolken im Umfeld des Weinbergs, nur geringer Einfluss auf Datenqualität zu erwarten. |  |
| Dichte Cirrus | Viele und dichte Cirrus-Wolken, auch sichtbar während des Überfluges, Datenqualität beeinträchtigt. |  |

Die folgende Tabelle 12 gibt einen Überblick über alle Befliegungen der 4 Versuchsjahre und die Einstrahlungsbedingungen während der Flüge:

**Tab. 12: Flugtage, Wetterbedingungen, Wachstumsstadien der Pflanzen und Krankheitsklassen von Peronospora in den Jahren 2017, 2018, 2019 und 2020**

| YYYYMMDD | Tag | Wetter | Boden | BBCH | Symptomklasse | | | | | | |
|---|---|---|---|---|---|---|---|---|---|---|---|
| | | | | | 0 | 5 | 10 | 25 | 50 | 75 | 100 |
| 2017 | | | | | | | | | | | |
| 20170601 | T1 | | | 58 | | | | | | | |
| 20170613 | T2 | | | 69 | | | | | | | |
| 20170626 | T3 | | | 73-75 | | | | | | | |
| 20170713 | T4 | | | 79 | | | | | | | |
| 20170726 | T5 | | | 79 | | | | | | | |
| 20170807 | T6 | | trocken | 81 | | | | | | | |
| 20170822 | T7 | | feucht | 85 | | | | | | | |
| 2018 | | | | | | | | | | | |
| 20180530 | T0 | | | | | | | | | | |
| 20180606 | T1 | | trocken | 68 | | | | | | | |
| 20180620 | T2 | | trocken | | | | | | | | |
| 20180703 | T3 | | trocken | 77 | | | | | | | |
| 20180716 | T4 | | trocken | 79 | | | | | | | |
| 20180730 | T5 | | trocken | | | | | | | | |
| 2019 | | | | | | | | | | | |
| 20190605 (obl+nad) | T0 | | | | | | | | | | |
| 20190618 (obl+nad) | T1 | | trocken | 61 | | | | | | | |
| 20190626 (obl+nad) | T2 | | trocken | 71-73 | | | | | | | |
| 20190709 (obl+nad) | T3 | | trocken | 75 | | | | | few | | |
| 20190723 (obl+nad) (only flight) | T4 | | trocken | | | | | | | | |
| 20190730 (only LC) | T4 | | | 79-81 | | | | | few | few | |
| 20190808 Headwall nad., no Gamaya | T5 | | trocken | | | | | | | | |
| 20190903 (all drones, no LC) | T6 | | trocken | | | | | | | | |

**Tab. 12 (fortgesetzt)**

| YYYYMMDD | Tag | Wetter | Boden | BBCH | Symptomklasse | | | | | | |
|---|---|---|---|---|---|---|---|---|---|---|---|
| 2020 | | | | | 0 | 5 | 10 | 25 | 50 | 75 | 100 |
| 20200514 (nad, Nano+Teax) | T0 | | | | | | | | | | |
| 20200526 (nad, Nano+Teax) | T1 | | trocken | 55-57 | | | | | | | |
| 20200608 (nad, Nano+Teax) | T2 | | trocken | 65 | | | | | | | |
| 20200624 (nad,Nano+Teax+MicaSense) | T3 | | trocken | 75 | | | | | | | |
| 20200701 (nad, Nano+Teax) | T4 | | | | | | | | | | |
| 20200707 (nad, Nano+Teax+ MicaSense) | T5 | | trocken | | | | | | | | |
| 20200722 (nad, Nano+Teax+ MicaSense) | T6 | | | 79 | | | | | | | |
| 20200730 (nad, Nano+Teax) | T7 | | trocken | | | | | | | | |
| 20200812 (nad, Nano+Teax) | T8 | | trocken | | | | | | | | |

Trotz des jeweiligen Zeitfensters von einer Woche und des trockenen Sommers in 2020 war es nicht immer möglich, Daten unter optimalen Strahlungsbedingungen zu akquirieren (Tabelle 12). Für eine optimale Datengrundlage spielt neben dem Aufnahmewinkel auch die Sonneneinstrahlung eine wesentliche Rolle, um maximale Energie und minimalen Schatteneinfluss zu gewährleisten. Folglich wurden jeweils die Befliegungen pro Feldtag jeweils bei maximalem Sonnenstand gegen 13.00 Uhr MESZ im Nadir-Modus und Thermaldaten bei möglichst hohen Temperaturen und maximale Kontraste zu bekommen. Wobei hierbei immer ein Kompromiss zwischen der Wettervorhersage bzw. der vorhergesagten Wolkenentwicklung und dem Sonnenstand gefunden werden musste. Wie bereits erläutert, wurden während der Befliegungen Referenzmessungen am Boden durchgeführt. Atmosphärische Einflüsse und verschiedenen Sonnenstände lassen sich dadurch teilweise korrigieren.

### 2.4.8.2 Datenverarbeitung und Analysen

**Headwall – Nano Daten:**

Die Headwall – Nano ist ein Zeilenscanner, der Bilddaten nicht zentral-perspektivisch aufnimmt, sondern kontinuierlich in Flugrichtung das Untersuchungsgebiet zeilenweise aufnimmt. Diese Daten müssen einer umfangreichen Vorprozessierung unterzogen werden,

damit sie geometrisch und radiometrisch ausgewertet werden können. Der erste Schritt ist das Zusammenfügen der einzelnen Bilder zu Flugstreifen und die Flugstreifen zu einem Mosaik. Dieser Schritt erforderte einige genaue Anpassung, da die geometrische Kalibrierung nicht optimal und die Lagegenauigkeit einige Probleme im Bild zeigt. Eine manuelle Nachprozessierung brachte gute Ergebnisse.

Danach wurden die Daten radiometrisch mittels der am Boden gemessenen Spektren der Referenzpanele mit einer sog. *Empirical Line Correction* korrigiert. Dabei wurden immer die *in situ* Messungen vom 30. Juli 2020 in Kombination den im jeweiligen Bild extrahierten Panels verwendet, um alle Zeitpunkte auf eine Referenz zu kalibrieren und keine Sprünge zwischen den Zeitpunkten zu haben. Dies gewährleistet eine kombinierte Auswertung und Modellbildung von mehreren Zeitpunkten.

Im nächsten Schritt mussten die Reben von Hintergrund getrennt werden. Hierfür wurde eine *Maximum Likelihood* Klassifikation für die Trennung der vier dominanten Klassen durchgeführt: Reben, Schatten, Boden, Gras/Bodenvegetation. Dafür wurden zunächst bildbasiert Trainingsdaten erhoben. Das erstellte Klassifikationsergebnis diente im Anschluss als Maske. Aufgrund der zunehmenden Blattmasse und Bestandsbreite im Laufe der Saison sowie des Rebschnitts musste dieser Schritt für jeden Zeitpunkt individuell durchgeführt werden.

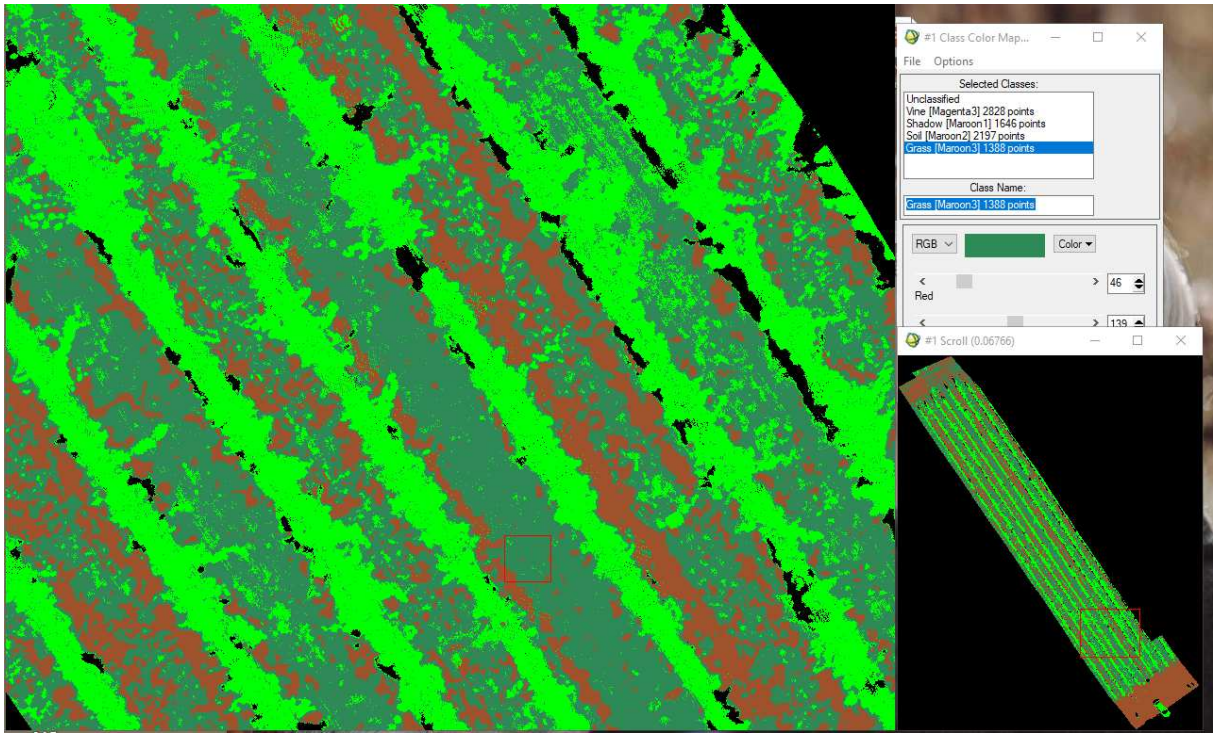


**Abbildung 13: Beispiel einer Klassifikation, um die Reben (hellgrün) vom Hintergrund (Schatten=schwarz, Boden= braun, Gras= dunkelgrün) zu trennen bzw. um den Hintergrund auszumaskieren.**

Die bereits beschriebenen, ausgelegten Marker waren gut im Bild sichtbar und konnten die Plotextraktion dadurch erheblich vereinfachen und die Genauigkeit erhöhen. Die Plots im Bild wurden digitalisiert und extrahiert, um sie im Anschluss auszuwerten. Das Ergebnis der angewandten Maske und die Extraktion der Plots ist in Abbildung 13 und Abbildung 14 am Beispiel des Datensatzes vom 07. Juli 2020 veranschaulicht. Das gleiche Verfahren wurde analog für alle Bilddaten/Zeitpunkte durchgeführt.

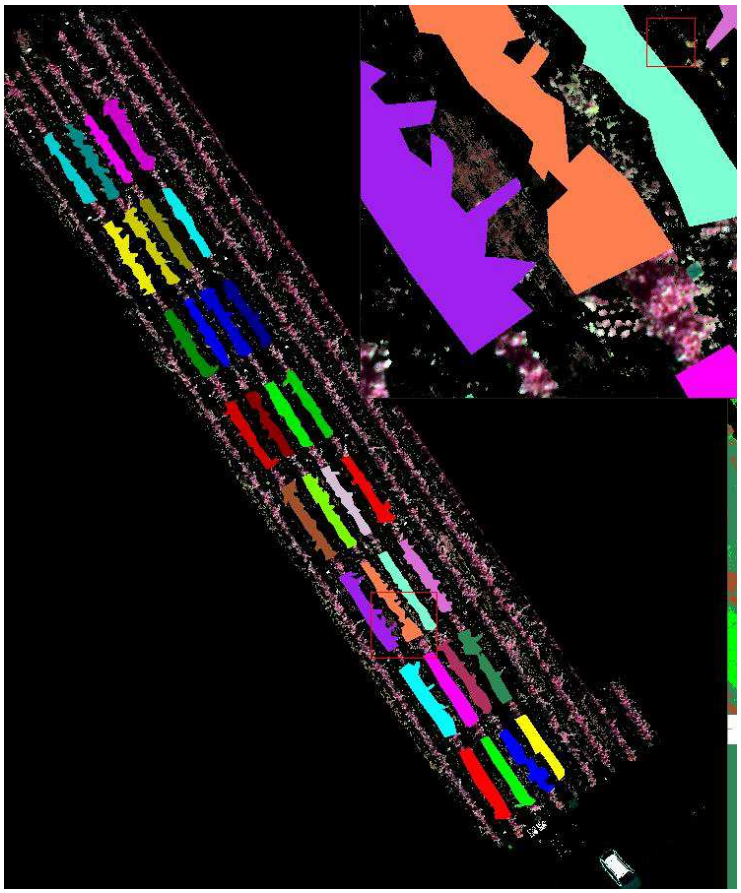

**Abbildung 14: Digitalisierung der Plots (Falschfarbendarstellung).**

**Teax - Daten**

Thermaldaten wurden immer am selben Tag wie die Hyperspektraldaten mit Hilfe der Teax Thermal Capture Fusion Zoom aufgenommen. Thermaldaten sind im Vergleich zu Daten aus dem sichtbaren oder Infrarot-Bereich deutlich kontrastärmer und wirken unscharf. Daher ist auch ihre Vorverarbeitung deutlich aufwendiger. Dennoch konnten erste Orthofotos auch den Flugstreifen erstellt werden und erste Datensätze ausgewertet werden. Allerdings ist dieser Teil noch nicht vollständig abgeschlossen, da aufgrund der ausgefallenen Befliegungen durch die Uni Trier wegen der Covid-19 Situation deutlich mehr Hyperspektradaten aufgenommen und ausgewertet wurden und der Schwerpunkt darauf gelegt wurde. Abbildung 15 zeigt ein

Orthomosaik der Thermaldaten vom 30. Juli 2020. In Rot sind hier die wärmeren Bereiche, wie Boden und die Straße dargestellt und in blau die niedrigeren Temperaturen. Das Mosaik besteht aus mehreren Flugstreifen, die mit Hilfe der Software Agisoft Metashape zusammengefügt wurden. Dieser Schritt ist wie bereits angedeutet aufgrund der geringen Kontraste relativ schwierig und zeitaufwändig.

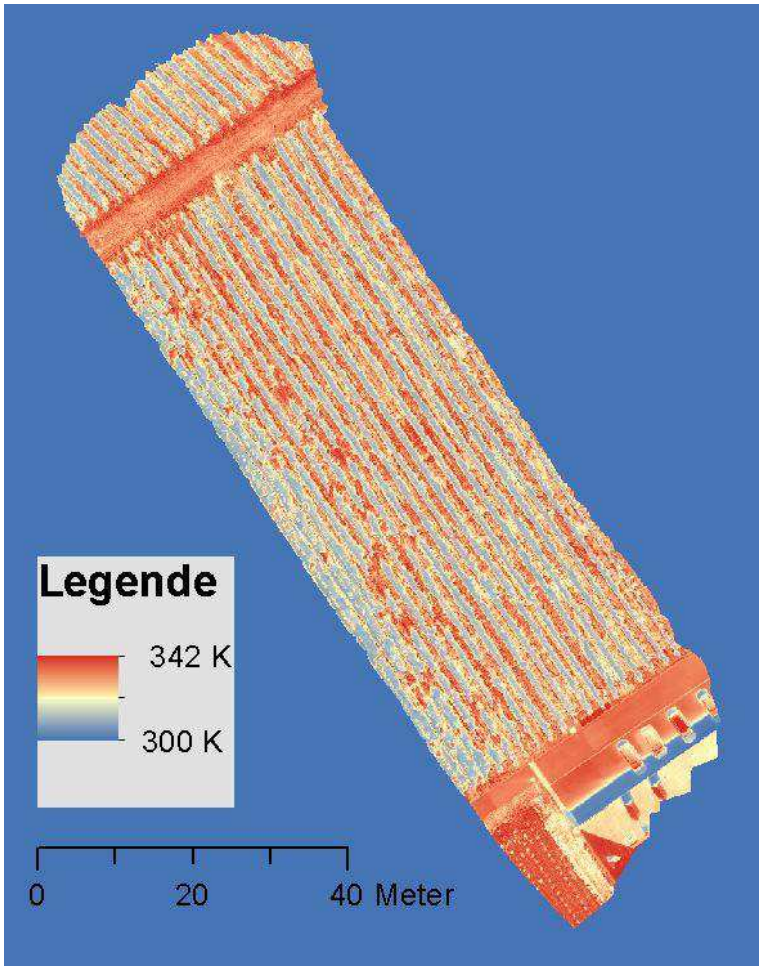


**Abbildung 15: Visualisierung der Thermalinformationen vom 30. Juli 2020**

**Methoden zur Auswertung der Befallstärke**

**PLSR:**

Die PLSR (Partial Least Squared Regression) ist ein multivariates statistisches Verfahren, das eine große Anzahl von co-linearen Variablen auf wenige nicht korrelierte unabhängige latente Variablen reduziert und die Varianz zwischen den beiden Matrizen X und Y dabei maximiert (Wold et al. 2001). In der vorliegenden Studie repräsentiert die latente Variable die Strukturinformationen, die in den Reflextionsmessungen (X) enthalten sind, um die abhängige Variable (Y) bzw den Befallsgrad vorhezusagen. Der Vorteil der PLSR ist die Reduktion eines großen Merkmalsraums auf wenige latente Faktoren (Udelhoven et al. 2013), was

insbesondere bei Hyperspektraldaten mit einem hohen Grad an Autokorrelation einen wesentlichen Vorteil bietet.

**Vegetationsindices:**

Wie auch in den vergangenen Jahren wurden eine Reihe etablierter Vegetationsindices berechnet und für die Schätzung der Befallsstärke getestet. Die Auswahl der Indizes berücksichtigt zwei Merkmale. Es wurden zum einen Indizes gewählt, die besonders sensitiv auf Pigmentveränderungen und andere biochemische Prozesse im Blatt reagieren. Hierzu zählt beispielsweise der PRI, der sensitiv für photosynthetische Aktivität bzw. die Lichtnutzungseffizient ist oder auch der Chlorophyll Index. Diese Indizes sind besonders für ein frühes Stadium der Krankheit geeignet, wenn erste Symptome in Form von Chlorosen und anderen Pigmentänderungen auftreten. Zum anderen wurden auch Indizes berücksichtigt, die insbesondere für die Blattmasse, den LAI (Leaf Area Index), sensitiv sind. Diese Indizes sind v.a. für einen stärkeren Befalls geeignet, wenn die Reben aufgrund von Peronospora Blätter verlieren. Hierzu zählen z.B der NDVI oder der NDRE2. Bei Auswertungen der letzten Jahre hatte sich bereits bestätigt, dass diese Indizes für einen hohe Befall gut geeignet sind.

**Tab. 13: Auswahl bereits publizierter Indizes, die zur Erfassung von Peronospora nützlich sein könnten**

| Index | Gleichung | Anwendung/Referenz |
|---|---|---|
| NDVI -Normalized difference vegetation index (Rouse et al. 1973.) | $\mathbf{NDVI} = (\mathbf{R_{800}} - \mathbf{R_{670}})/(\mathbf{R_{800}} + \mathbf{R_{670}})$ | Erkennung von grüner Vegetation aufgrund der Reflexionseigenschaften von Chlorophyll und Mesophyll |
| Chlorophyll index (Rouse et al., 1973) red edge | $\mathbf{Cl_{red\ edge}} = (\mathbf{R_{780}} / \mathbf{R_{710}}) - \mathbf{1}$ | Quantifizierung des Chlorophylls (Gitelson et al., 2003) |
| Red edge inflection point | $\mathbf{REIP} = \mathbf{700} + \mathbf{40}\big((\mathbf{R_{670}} + \mathbf{R_{780}})/\mathbf{2} - \mathbf{R_{700}}\big)/(\mathbf{R_{740}} - \mathbf{R_{700}}))$ | Bestimmung des Maximums des sog. Red Edge Inflection points, der sensitiv für den Chlorophyllgehalt ist (Herrmann et al., 2010) |
| Chl -Chlorophyll index | $\mathbf{Chl} = (\mathbf{R_{570}} - \mathbf{R_{700}})/(\mathbf{R_{515}} - \mathbf{R_{700}})$ | Quantifizierung des Chlorophylls (Yu et al., 2014) |
| PRI -Photochemical reflection index | $\mathbf{PRI} = (\mathbf{R_{531}} - \mathbf{R_{570}})/(\mathbf{R_{531}} + \mathbf{R_{570}})$ | Photosynthetische Aktivität und Lichtnutzungseffizienz basierend auf dem Xanthophyllgehalt (Gamon et al., 1992) |
| NDRE 2 | $\boldsymbol{NDRE2} = (\boldsymbol{R_{740}} - \boldsymbol{R_{665}})/(\boldsymbol{R_{740}} + \boldsymbol{R_{665}})$ | Ähnlich zu NDVI, aber unter Berücksichtigung des RedEdge (Barnes et al. 2000) |
| Downy mildew index 1 | $\mathbf{DMI_1} = (\mathbf{R_{682}}) / (\mathbf{R_{800}})$ | Kontrolliertes Experiment zur Entwicklung verschiedener Indizes zur Bestimmung von frühem Peronospora Befall (Oerke et al., 2016) |
| Downy mildew index 2 | $\mathbf{DMI_2} = (\mathbf{R_{550}} - \mathbf{R_{680}}) / (\mathbf{R_{550}} + \mathbf{R_{680}})$ | |

### 2.4.9 Monitoring der Esca-symptomatischen Stöcke im Versuch AA

Im September 2020 wurden die Weinberge im Bereich „Berg“ hinsichtlich (i) Symptomen durch den Esca-Komplex sowie (ii) Fehlstöcken visuell bonitiert und kartographisch dokumentiert. Es erfolgte eine Differenzierung der symptomatischen Stöcke in folgende Befallsklassen:

1 Apoplexie (plötzliches Absterben)
2 Blattsymptome (Tigerstreifen)
  a) leichte Symptome
  b) mittlere Symptome
  c) starke Symptome
3 Beerensymptome („black measels“)
  a) leichte Symptome
  b) mittlere Symptome
  c) starke Symptome
4 Blatt- und Beerensymptome
X Fehlstock

Die fernerkundliche Auswertung der Versuchsfläche erfolgt im Projekt “MonESCA”.

# 3 Ergebnisse und Diskussion

## 3.1 Versuch L Monitoring *Scaphoideus titanus*

### 3.1.1 Fangzahlen

**Tab. 14: Fangzahlen von *S. titanus* im Rahmen des Monitorings entlang der Luxemburger Mosel im Jahr 2020.**

| Standort | 27.07. | 10.08. | 24.08. | 07.09. | 21.09. |
|---|---|---|---|---|---|
| A Wellenstein | 0 | 0 | 0 | 0 | 0 |
| B Remich-IVV | 0 | 0 | 0 | 0 | 0 |
| C Ehnen | 0 | 0 | 0 | 0 | 0 |
| D Ahn | 0 | 0 | 0 | 0 | 0 |

Im Jahr 2020 konnte, wie in den sieben vorangegangenen Jahren, an keinem der Monitoring-Standorte das Auftreten des Vektors der Flavescence dorée beobachtet werden (Tab. 14). Eine am 13.07.2020 an allen Standorten durchgeführte Bonitur auf Larven-Besatz an den stammnahen Blättern lieferte ebenfalls keinen Hinweis auf *S. titanus*.

## 3.2 Surveillance des activités de vol et de ponte de *Drosophila suzukii*

La surveillance de activités de vol et de ponte de *D. suzukii* ont commencé mi-août 2020. La surveillance se concentre sur une variété à maturation précoce (Pinot noir) et deux à maturation plus tardive (Pinotin et Cabaret noir) ainsi que des plantes hôtes non cultivées telles que le lierre et un mûrier. Les premiers pièges ont été installés dans le vignoble en août. Dès la première date d'observation, des mouches ont été piégées dans toutes les variétés étudiées. Concernant les parcelles de vigne, une augmentation de l'activité de *D. suzukii* a été observée les 3 premières semaines avec un pic le 09.09 avant une légère diminution la semaine du 09.09 au 16.09. Pour les variétés Pinotin et Cabaret noir un nouveau pic, légèrement plus faible que le premier, est observé la semaine du 16.09 au 24.09. Puis lors de la dernière semaine de piégeage, les mouches n'étaient présentes qu'en très faible nombre. Concernant le piège situé dans le lierre, il suit les mêmes évolutions que ceux dans les vignes avec un nombre de mouches comptées largement plus important. Enfin, dans le mûrier, une augmentation du nombre de mouches est observée de la première semaine jusqu'à la semaine du 09.09 au 16.09 avant une nette diminution jusqu'à la dernière semaine d'observations (Tab. 15).
Concernant l'activité de ponte, des œufs ont été trouvés seulement dans les variétés les plus tardives. La variété Pinotin présentait des œufs dans les 3 dernières semaines d'observation notamment la semaine du 16.09 au 24.09 avec 9 œufs comptés. La variété Cabaret noir présentait un oeuf la semaine du 02.09 au 09.09 (Tab. 15). Les autres variétés de vigne étudiées n'ont pas subi d'activité de ponte, ceci peut être lié à leur précocité, en effet, elles ont été récoltées début septembre soit avant la période de forte présence de *D. suzukii* au vignoble.

**Tab. 15 : Nombre de mouches *D. suzukii* capturées dans les pièges (Ds. Fem pour les femelles et Ds. Male pour les males), nombre d'œufs dénombrés dans 50 baies individuelles et degré de maturité des baies pour les différents sites de surveillance en 2020.**

| Localité | Variété | 19.08.20 - 26.08.20 | | | | 26.08.20 - 02.09.20 | | | | 02.09.20 - 09.09.20 | | | |
|---|---|---|---|---|---|---|---|---|---|---|---|---|---|
| | | Ds. Fem | Ds. Male | #Oeufs | °Oe | Ds. Fem | Ds. Male | #Oeufs | °Oe | Ds. Fem | Ds. Male | #Oeufs | °Oe |
| Remich | Pinotin | 8 | 1 | 0 | 67 | 8 | 3 | 0 | 68 | 31 | 12 | 0 | 69 |
| Remich | Lierre | 9 | 1 | x | x | 4 | 0 | x | x | 181 | 53 | x | x |
| Remich | Mûrier | 24 | 24 | x | x | 10 | 21 | x | x | 114 | 95 | x | x |
| Remich | Pinot noir précoce | 3 | 0 | 0 | 97 | 0 | 0 | 0 | 93 | 25 | 8 | x | x |
| Remich | Pinot noir (130) | 4 | 0 | 0 | 77 | 6 | 1 | 0 | 80 | 45 | 23 | x | x |
| Remich | Pinot noir (109) | 3 | 1 | 0 | 72 | 13 | 0 | 0 | 91 | 33 | 18 | x | x |
| Remich | Cabaret noir | 3 | 2 | 0 | 67 | 7 | 2 | 0 | 72 | 42 | 9 | 1 | 79 |

| Localité | Variété | 09.09.20 - 16.09.20 | | | | 16.09.20 - 24.09.20 | | | | 24.09.20 - 30.09.20 | | | |
|---|---|---|---|---|---|---|---|---|---|---|---|---|---|
| | | Ds. Fem | Ds. Male | #Oeufs | °Oe | Ds. Fem | Ds. Male | #Oeufs | °Oe | Ds. Fem | Ds. Male | #Oeufs | °Oe |
| Remich | Pinotin | 19 | 10 | 2 | 80 | 22 | 22 | 9 | 83 | 1 | 1 | 1 | 80 |
| Remich | Lierre | 64 | 38 | x | x | 58 | 55 | x | x | 1 | 2 | x | x |
| Remich | Mûrier | 169 | 181 | x | x | 66 | 71 | x | x | 1 | 0 | x | x |
| Remich | Pinot noir précoce | 18 | 2 | x | x | x | x | x | x | x | x | x | x |
| Remich | Pinot noir (130) | 47 | 6 | x | x | x | x | x | x | x | x | x | x |
| Remich | Pinot noir (109) | 26 | 5 | x | x | x | x | x | x | x | x | x | x |
| Remich | Cabaret noir | 27 | 5 | 0 | 87 | 29 | 9 | x | x | 3 | 0 | x | x |

## 3.3 Expériences de lutte contre *Drosophila suzukii*

### 3.3.1 Essais de produits naturels contre *D. suzukii* au vignoble

Dès la première observation, des mouches *D. suzukii* ont été identifiées dans les pièges. L'activité la plus importante a été observée dès la seconde observation avant de diminuer puis ré-augmenter. La dernière semaine d'observation montre une très faible activité de vol des mouches (Tab. 16). Afin de déterminer l'effet du traitement sur la présence de *D. suzukii* dans le vignoble, des analyses de variances ont été effectuées (ANOVA à 1 et 2 facteurs). Les effets de la date et du traitement sont significatifs (respectivement, p-value < 2.2e-6 et p-value = 1.367e-7). L'effet de la date est logique dans la mesure où les conditions météorologiques influent sur l'évolution de la population de *D. suzukii*, on s'intéresse donc à l'effet des traitements pour chaque date individuellement. Pour les dates 02.09, 24.09 et 30.09, le nombre de mouches piégées est comparable entre tous les traitements. Pour le 09.09, significativement plus de *D. suzukii* ont été piégées dans la modalité $CaCO_3$ que dans les deux traitements au kaolin. Le contrôle non traité est aussi significativement différent du produit Surround. A la date du 16.09, le traitement $CaCO_3$ présente un nombre de mouches piégées comparable au contrôle non traité et au produit Cutisan mais supérieur à celui du produit Surround (Abb. 16). Après cet essai, on peut conclure que le produit Surround a un effet répulsif contre *D. suzukii* lorsque la population de mouche est importante mais cet effet est moins visible en cas d'infestation faible. Le produit Cutisan présente un faible effet répulsif avec en moyenne moins de mouches piégées que dans le contrôle mais cet effet n'est pas significatif. Enfin, le produit $CaCO_3$ n'a pas d'effet sur *D. suzukii* avec une activité de vol comparable à celle du contrôle.

**Tab. 16: Nombre d'individus de *D. suzukii* piégés dans l'expérience T. Moyennes de 4 répétitions.**

| ID | Stratégie | Nombre de mouches *D. suzukii* capturées par piège | | | | |
|---|---|---|---|---|---|---|
| | | 26.08. - 02.09.2020 | 02.09. - 09.09.2020 | 09.09. - 16.09.2020 | 16.09. - 24.09.2020 | 24.09. - 30.09.2020 |
| **1** | **Contrôle non traité** | 5.25 | 42.5 | 19 | 27.25 | 2 |
| **2** | **Kaolin Cutisan 2%** | 5.25 | 31.25 | 18 | 10.5 | 1.5 |
| **3** | **$CaCO_3$ 2%** | 10.75 | 52.5 | 22.75 | NA | NA |
| **4** | **Kaolin Surround 2%** | 4.25 | 29.5 | 10.75 | 14 | 0.75 |

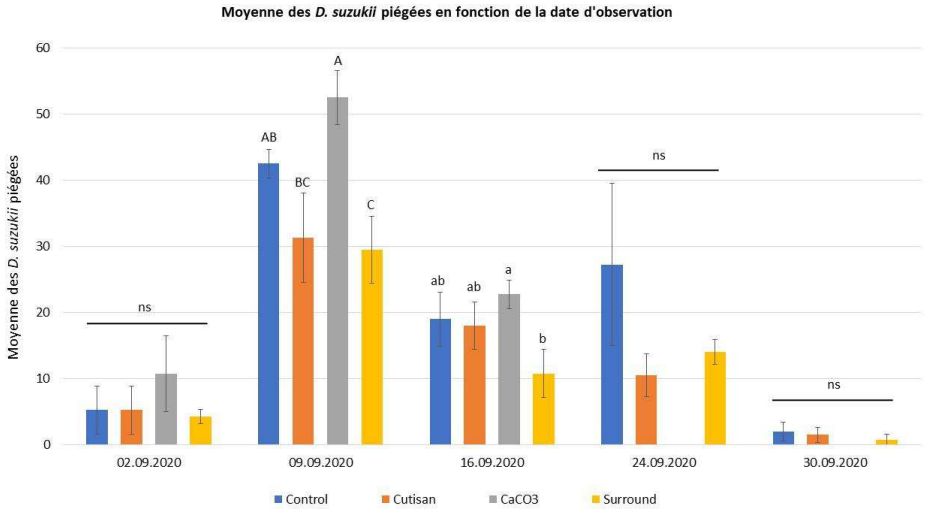


**Abbildung 16: Histogramme de la moyenne des *D. suzukii* piégées en fonction de la date d'observation et du traitement.**

Les barres verticales représentent d'écart type. Des lettres différentes montrent une différence statistiquement significative. Les lettres majuscules s'appliquent pour les 09.09.2020 et les lettres minuscules pour le 16.09.2020. "ns" signifie "non significatif".

Concernant l'activité de pontes des mouches *D. suzukii*, des œufs ont été observés dans tous les traitements. Dans le contrôle, les premiers œufs ont été trouvés le 09.09 puis chaque semaine jusqu'à la récolte avec la valeur la plus élevée le 24.09. Pour le produit Cutisan, des œufs ont été observés le 09.09 et le 30.09 seulement. Concernant le $CaCO_3$, des pontes ont été observées aux 2 dates étudiées. Enfin pour le produit Surround, des œufs ont seulement été dénombrés le 09.09 (Tab. 17). Statistiquement, les traitements n'ont eu pas d'effet sur l'activité de ponte (ANOVA non paramétrique (Kruskal-Wallis) avec des p-value de 0.34 ; 0.34 et 0.33 pour le 09.09, le 16.09 et le 30.09 respectivement). Pour le 24.09, l'analyse de variance indiquait un effet du traitement (p-value = 0.03) toutefois l'analyse complémentaire (Wilcoxon pairwise comparison) n'a pas permis d'identifier de différence significative. Ainsi, on peut conclure que les produits testés n'ont pas permis de diminuer l'activité de ponte.

**Tab. 17: Nombre d'œufs dénombrés dans 50 baies dans l'expérience T . Moyennes de 4 répétitions.**

| ID | Stratégie | Nombre d'oeufs de *D. suzukii* comptés dans 50 baies | | | | |
|---|---|---|---|---|---|---|
| | | 26.08. - 02.09.2020 | 02.09. - 09.09.2020 | 09.09. - 16.09.2020 | 16.09. - 24.09.2020 | 24.09. - 30.09.2020 |
| **1** | **Contrôle non traité** | 0 | 0.5 | 1 | 3 | 0.75 |
| **2** | **Kaolin Cutisan 2%** | NA | 0.5 | 0 | 0 | 0.5 |
| **3** | **$CaCO_3$ 2%** | NA | 2 | 2.75 | NA | NA |
| **4** | **Kaolin Surround 2%** | NA | 0.25 | 0 | 0 | 0 |

### 3.3.2 Essais de produits naturels contre *D. suzukii* en laboratoire

**Contexte et protocoles**

Pour répondre à une demande croissante de produits de lutte contre *D. suzukii*, la toxicité et l'effet sur la ponte de produits naturels ont été évalués à l'aide de fruits traités.

Des essais sur le produit Surround, à base de kaolin ont été menés en conditions de choix. Des fruits traités (Surround 2%) et non traités sont disposés dans un T-tube avec des solutions de sucrose 10%, 20 femelles et 10 mâles sont introduits dans le système pour 24h (Abb. 17). Une fois l'expérimentation terminée, la position et la mortalité des mouches est observée et le nombre d'œufs pondus dans les fruits sont dénombrés. Afin d'améliorer le recouvrement des fruits par le kaolin, le produit est pulvérisé à l'aide d'un pulvérisateur à main, ce traitement est réalisé 3 fois avec une période de séchage sous hotte aspirante d'1h entre chaque traitement puis de 2h avant le début de l'expérience. Les essais ont été répliqués 9 fois (3 replicats à 3 dates différentes.

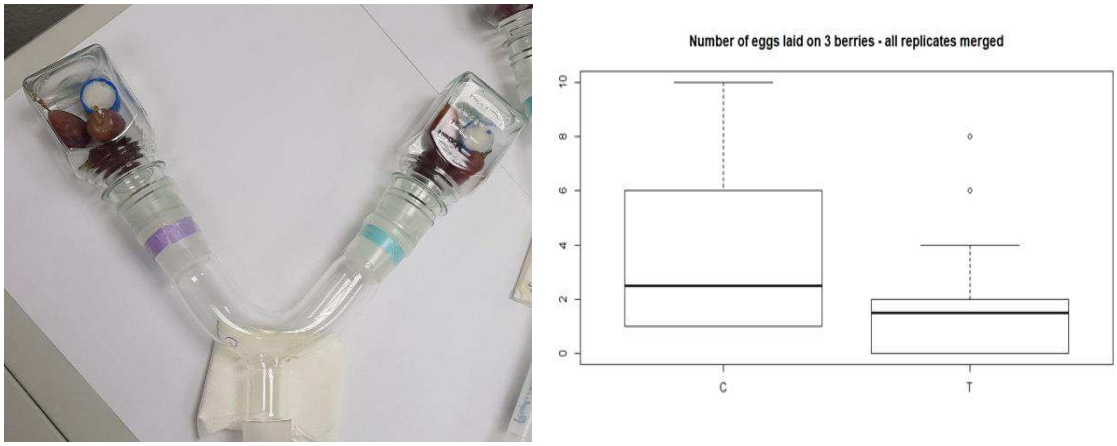


**Abbildung 17: (Gauche) Photographie du système de T-test : avec l'anneau violet les fruits traités et avec le bleu, les fruits non traités. (Droite) Boxplot : nombre d'œufs pondus par fruit en fonction du traitement (c= Contrôle négatif T= Surround 2%)**

**Conclusions**

Une analyse de variance a été réalisée pour comprendre l'effet du produit Surround sur la posiiton des mouches en fonction de leur sexe. Les mâles et les femelles répondent de la même manière au produit Surround (p-value = 0.94) et leur position n'est pas influencée par le traitement des fruits (p-value = 0.07 pour les femelles et p-value = 0.70 pour les males). Le produit Surround réduit de manière significative le nombre d'œufs pondus dans des fruits traités comparé à ceux dans des fruits non traités (Wilcoxon test p-value = 0.029), une réduction de 50.8% a été observée (Abb. 17).

## 3.4 Versuch W Schnittsysteme

### 3.4.1 Traubenstruktur und -gesundheit

**Tab. 18: Biegeindex-Werte (04.08.2020 sowie Befallsstärken (in %) *Botrytis cinerea* in den Rebsorten Pinot gris und Riesling (05.10.2020) im Versuch W im Jahr 2020.**

| VG | Versuchsglied | Biegeindex | Befallsstärke (%) |
|---|---|---|---|
| **Pinot gris** | | | |
| 1 | Rebschnitt auf zahmes Holz | 3,63 | 6,09 |
| 2 | Rebschnitt auf wildes Holz | 3,72 | 4,74 |
| 3 | Sanfter Rebschnitt nach Simonit und Sirch | 3,57 | 4,37 |
| 4 | Entfernen 2. Bogrebe nach Rebblüte | 3,49 | 2,29 |
| **Riesling** | | | |
| 1 | Rebschnitt auf zahmes Holz | 3,51 | 5,74 |
| 2 | Rebschnitt auf wildes Holz | 3,46 | 7,76 |
| 3 | Sanfter Rebschnitt nach Simonit und Sirch | 3,27 | 3,70 |
| 4 | Entfernen 2. Bogrebe nach Rebblüte | 2,82 | 0,92 |

Wie in den Vorjahren wurde beim Riesling der niedrigste Biegeindex-Wert im VG 4 (Entfernen der 2. Bogreben nach der Rebblüte) ermittelt. Auch beim Pinot gris wies das VG 4 in diesem Jahr den niedrigsten Biegeindex-Wert auf.

Bei niedrigem Befallsniveau im Jahr 2020 zeigten sich in beiden Rebsorten, wie in den Vorjahren, die geringsten Befallsstärken in der Versuchsvariante mit einem Entfernen der zweiten Bogrebe nach der Rebblüte. Die Wirkungsgrade im Vergleich zu einem Rebschnitt auf zahmes Holz lagen beim Pinot gris bei 22 (VG 2), 28 (VG 3) bzw. 62% (VG 4) und beim Riesling bei –35 (VG 2), 36 (VG 3) bzw. 84% (VG 4) (Tab. 18).

### 3.4.2 Ernteparameter

**Tab. 19: Stockerträge sowie Mostgewichte und Gesamtsäure-Gehalte bei Pinot gris und Riesling (08.10.2020) im Versuch W im Jahr 2020.**

| VG | Variante | Stockertrag (kg) | Mostgewicht (°Oe) | Gesamtsäure (g/l) |
|---|---|---|---|---|
| **Pinot gris** | | | | |
| 1 | Rebschnitt auf zahmes Holz | 5,25 | 86,5 | 6,5 |
| 2 | Rebschnitt auf wildes Holz | 4,92 | 84,0 | 6,4 |
| 3 | Sanfter Rebschnitt nach Simonit und Sirch | 4,77 | 86,1 | 6,1 |
| 4 | Entfernen 2. Bogrebe nach Rebblüte | 4,37 | 85,6 | 6,1 |
| **Riesling** | | | | |
| 1 | Rebschnitt auf zahmes Holz | 5,37 | 80,2 | 10,3 |
| 2 | Rebschnitt auf wildes Holz | 4,97 | 79,9 | 10,2 |
| 3 | Sanfter Rebschnitt nach Simonit und Sirch | 5,19 | 79,4 | 10,6 |
| 4 | Entfernen 2. Bogrebe nach Rebblüte | 3,18 | 82,3 | 10,2 |

Die Erträge im Versuchsjahr 2020 lagen aufgrund von Spätfrostschäden im Vorjahr auf einem hohen Niveau.

In beiden Rebsorten wurden die höchsten Stockerträge im Versuchsglied 1 (Rebschnitt auf zahmes Holz) ermittelt. Die niedrigsten Stockerträge wurden ebenfalls in beiden Rebsorten im VG 4 (Entfernen 2. Bogrebe) erzielt.

Die Erntemostgewichte im Pinot gris lagen in allen Versuchsgliedern auf vergleichbarem Niveau bewegten. Im Riesling deuten sich leicht erhöhte Mostgewichte im VG 4 im Vergleich zu den anderen Versuchsgliedern an, zwischen welchen keine deutlichen Mostgewichtsunterschiede festgestellt wurden.

Die Gesamtsäure-Gehalte lagen in beiden Rebsorten in allen Versuchsgliedern auf vergleichbarem Niveau (Tab. 19).

## 3.5 Versuch X Oidium-Bekämpfung

### 3.5.1 Befallsstärken an den Blättern

**Tab. 20: Befallsstärken (in %) des Echten Mehltaus an den Trauben am 18.08.2020 im Versuch X im Jahr 2020.**

| VG | Strategie | Erläuterung | Befallsstärke (%) |
|---|---|---|---|
| 1 | unbehandelte Kontrolle | | 1,40 |
| 2 | Kontrolle | im Mehltaufenster unbehandelt | 0,16 |
| 3 | Flint (Strobilurin) | im Mehltaufenster | 1,35 |
| 4 | Luna Experience | im Mehltaufenster | 0,00 |
| 5 | Nissodium | im Mehltaufenster | 0,19 |
| 6 | Topas | letzte drei Spritzungen | 0,07 |
| 7 | Vitisan | Mehltaufenster + letzte drei Spritzungen | 0,17 |
| 8 | Fytosave | Mehltaufenster + letzte drei Spritzungen | 0,08 |
| 9 | Sercadis | im Mehltaufenster | 0,01 |
| 10 | Kusabi | im Mehltaufenster | 0,07 |

Im Versuchsjahr 2020 trat, wie in den Vorjahren, kein bonitierbarer Oidium-Befall an Blättern auf.

Es wurde lediglich drei Bonituren des Traubenbefalls durchgeführt. Die Ergebnisse der letzten Bonitur am 18.08.2020 sind obenstehend durchgeführt. Das Befallsniveau war sehr gering und wurde in Form weniger Befallsherde beobachtet. Aufgrund des geringen Befalls und der hohen Streuung zwischen den Wiederholungen war eine exakte Differenzierung zwischen den Versuchsgliedern im Jahr 2020 nicht möglich. Es deutet sich jedoch an, dass

- die Wirksamkeit der Strobilurin-Präparates Flint in der Versuchsanlage nicht mehr ausreichend ist
- die beiden SDHI-Fungizide Luna Experience und Sercadis zur Zeit sehr starke Präparate zur Oidium-Bekämpfung darstellen (Tab. 20).

## 3.6 Versuch Y Fernerkundliche Erkennung der Peronospora

### 3.6.1 Befallsstärken an den Blättern

**Tab. 21: Befallsstärken (in %) des Falschen Mehltaus im Verlauf des Jahres im Versuch Y im Jahr 2020.**

| VG | Strategie | Infektionstyp | 09.06. | 24.06. | 01.07. | 07.07. | 23.07. | 30.07. | 12.08. |
|---|---|---|---|---|---|---|---|---|---|
| 1 | unbehandelte Kontrolle | ohne künstliche Inok | 0,00 | 0,27 | 2,06 | 5,90 | 11,48 | 14,82 | 13,70 |
| 2 | unbehandelte Kontrolle | künstliche Inok | 0,00 | 0,77 | 4,42 | 10,60 | 17,22 | 23,55 | 17,36 |
| 3 | integriert | künstliche Inok | 0,00 | 0,00 | 0,10 | 0,18 | 0,32 | 0,31 | 0,37 |
| 4 | Kupfer | künstliche Inok | 0,00 | 0,26 | 1,97 | 6,06 | 7,99 | 8,34 | 5,73 |
| 5 | Phosphorige Säure | künstliche Inok | 0,00 | 0,03 | 0,20 | 0,28 | 2,38 | 3,79 | 4,25 |
| 6 | Kupfer + Phosphorige Säure | künstliche Inok | 0,00 | 0,13 | 0,84 | 0,77 | 3,39 | 4,33 | 4,14 |
| 7 | Kupfer + Phosphorige S. bis BBCH 69 | künstliche Inok | 0,00 | 0,08 | 0,74 | 1,44 | 4,37 | 3,56 | 3,40 |
| 8 | Kupfer + Prüfmittel Neu 1143F | künstliche Inok | 0,00 | 0,31 | 2,09 | 5,08 | 7,94 | 10,57 | 6,89 |

Erste Blattsymptome wurden am 24.06 beobachtet. In der Folge kam es zu einem kontinuierlichen Befallsanstieg. Am letzten Boniturtermin wurden Befallsstärken am Blatt zwischen 0.37 (VG 3) und 17,36 (VG 2) erfasst (Tab. 21).

Am letzten Boniturtermin (12.08.2020) wurden folgende Wirkungsgrade in Bezug auf das Versuchsglied 2 erzielt: 97 (VG 3), 67 (VG 4), 76 (VG 5), 76 (VG 6), 80 (VG 7) und 60 % (VG 8). D.h. die Variante des integrierten Weinbaus zeigte, im Gegensatz zum Vorjahr, sehr gute Wirkungsgrade. Auch die Varianten mit Phosphoriger Säure zeigten im Jahr 2020 gute Wirkungsgrade, während die Varianten ohne Phosphorige Säure hinsichtlich des Wirkungsgrades etwas abfielen (Tab. 25).
Die angestrebte Variabilität innerhalb des Versuchsfeldes stellte sich im Jahr 2020 ein. Am letzten Boniturtermin wurden in den 32 Plots Befallsstärken zwischen 0,26 und 22,85% erfasst.

### 3.6.2 Ergebnisse der fernerkundlichen Untersuchungen

Ergebnisse der PLSR Modellierung mit Daten der Headwall-Nano:

Die PLSR Modelle wurden basierend auf 216 Spektralbändern (499 nm – 978 nm) der Headwall Nano aufgebaut. Die Spektralbänder zwischen 399 – 498 nm (45 Spektralkanäle), genauso wie die Bänder zwischen 979 – 1000 nm (10 Bänder) wurden aufgrund ihres hohen Signal-to-Noise Verhältnis nicht in die Analyse miteinbezogen.
Die PLSR – Modelle, die sich auf ein einzelnes Datum beschränken, sind einer Leave-One-Out Kreuzvalidierung (LOO-CV) unterzogen. Für eine mögliche Vorhersage wurde ein Modell basierend auf mehreren Zeitpunkten T6 – T7 erstellt. Mit diesem Modell wurde Zeitpunkt T8 vorhergesagt und es fand eine unabhängige Validierung statt.
Ein nennenswerter Befall trat erst bei den Zeitpunkten T3 und T4 auf. Zum Zeitpunkt T4 wurden zwar Bilddaten akquiriert, aufgrund der schlechten Wetterbedingungen mit einer dichten und uneinheitlichen Wolkenbedeckung ließen sich diese allerdings nicht zufriedenstellend korrigieren. Die Referenzmessungen zeigten aufgrund der wechselnden Bewölkung während des Flugs Schwankungen der Einstrahlung von ca. 30 % im Verlauf des Fluges. Die Erkennung von Reflexionsänderungen aufgrund von Peronospora wird bei so starken Schwankungen der Einstrahlung leider verhindert.

PLSR Modelle wurden zu den jeweiligen Zeitpunkten erstellt. Zum einen gingen alle Plots einzeln (n=32) in die Modellerstellung ein. Zum anderen wurden über die vier Wiederholungen A-D gemittelten Befallsgrade jedes Treatments erstellt und die zugehörigen gemittelten Spektren zur Berechnung der PLSR genutzt (n=8). Beide Ergebnisse für den jeweiligen Untersuchungstag sind in Abbildung 18 dargestellt.

| Date | Treatment einzeln (n = 32) | Treatment Mittelwerte (A-D, n = 8) |
|---|---|---|
| T3 | 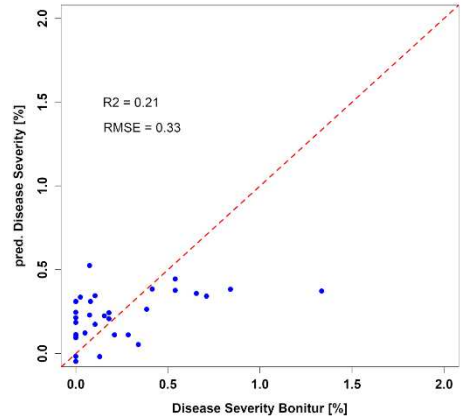 | 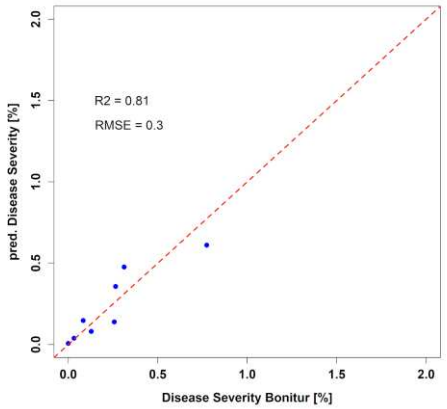 |
| T5 | 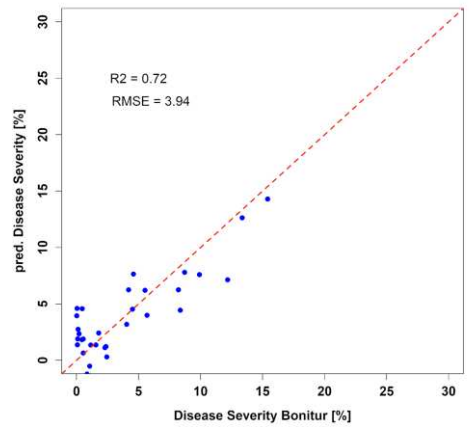 | 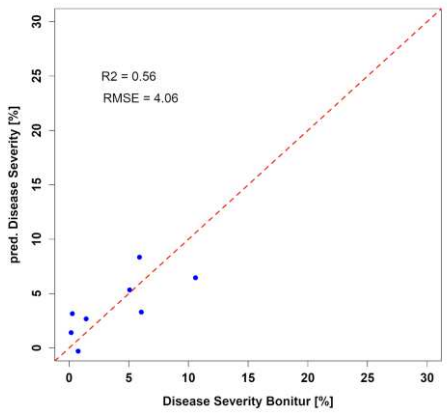 |
| T6 | 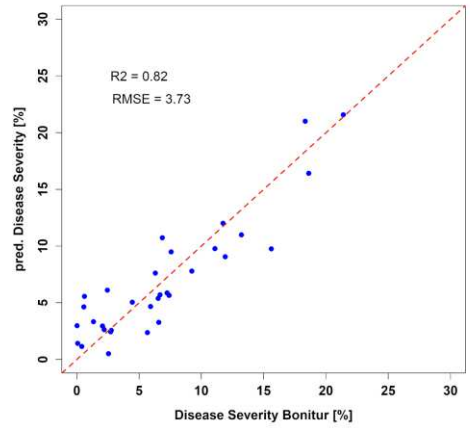 | 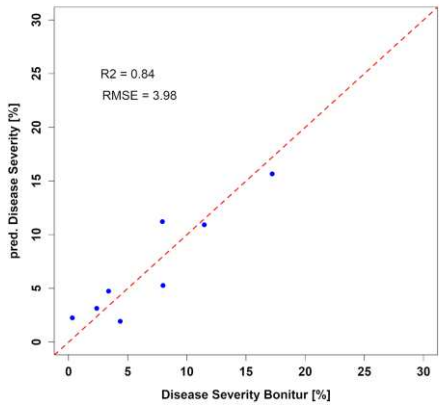 |
| T7 | 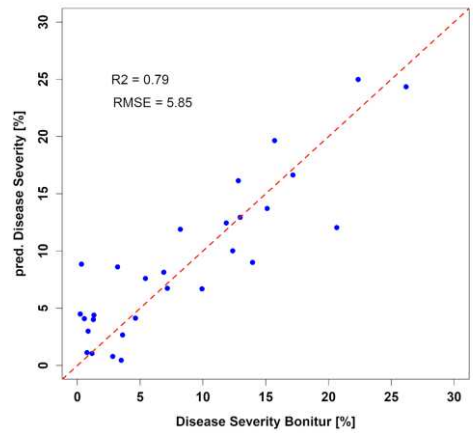 | 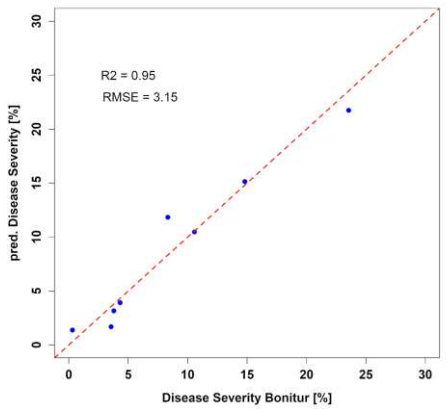 |

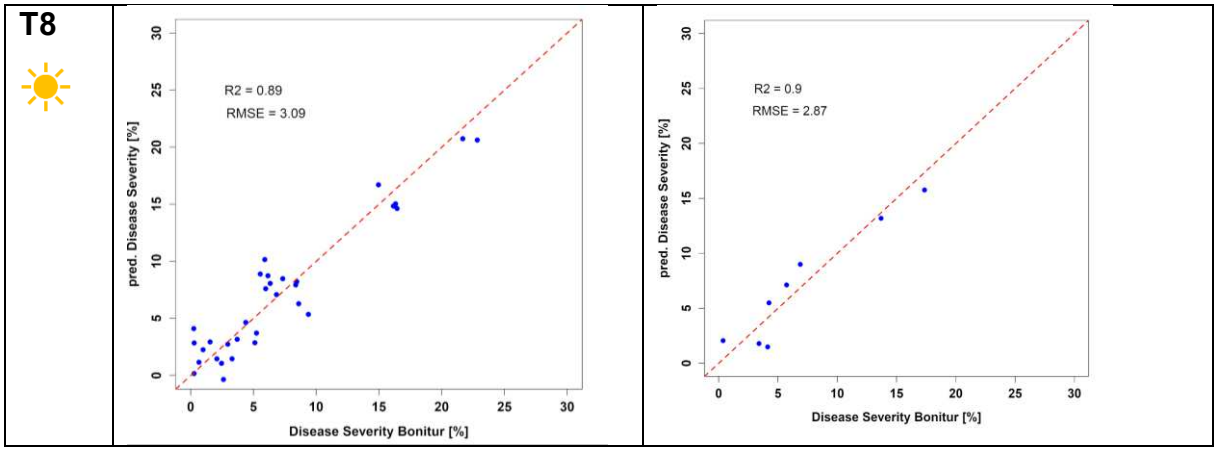


**Abbildung 18: Übersicht der PLSR-Modelle bezogen auf den Befliegungstermin und den dort auftretenden Befallsgrad. Links sind die Modelle der einzelnen Plots dargestellt, auf der rechten Seite finden sich die Mittelwerte der vier Wiederholungen (A-D) der Treatments.**

Die PLSR Modelle der Zeitpunkte T5 bis T8 zeigen einen sehr guten Zusammenhang innerhalb der einzelnen Flugtage mit einem $R^2$ von 0,79-0,89. Die Mittelung der vier Wiederholungen konnte eine leichte Verbesserung der Ergebnisse bewirken. Bei T5 konnte diese Verbesserung nicht festgestellt werden, bzw. es kam zu einer Verschlechterung der Ergebnisse. Warum T5 eher einen schwächeren Zusammenhang zeigt, kann nicht vollständig geklärt werden. Wir können nur mutmaßen, dass der eher geringe Befall und die zufällige Wahl der Blätter hier keinen sehr guten Zusammenhang zuließ. Es kann auch gemutmaßt werden, dass Symptome vielleicht verstärkt im unteren Teil der Laubwand auftraten und dadurch bei einer zu diesem Zeitpunkt schon stark ausgeprägten und dichten Laubwand schwerer fernerkundlich zu detektieren waren. Oder auch die Erstellung der Maske kann hier zu Problemen geführt haben.

Bei dem Befliegungszeitpunkt T3 mit dem niedrigsten Peronospera Befall unter 1,5% konnten die PLSR Modelle basierend auf dem Mittelwert der Wiederholungen A-D die Zusammenhänge deutlich stabilisieren und erhöhen. Die Einzelwerte der Plots zeigten hier noch eine starke Streuung und nur ein $R^2$ von 0,21 wurde erzielt. Die Mittelung der Werte konnte diesen Zusammenhang auf 0,81 erhöhen. Dieses Ergebnis ist bemerkenswert und wird in den kommenden Monaten noch mit anderen Methoden genauer analysiert.

In einem nächsten Schritt wurde das Potential zur Vorhersage analysiert. Um das Prognosepotential der PLSR abschätzen zu können wurde ein Modell aus den Befliegungen T6 und T7 kalibriert und damit der mittlere Befallsgrad von T8 geschätzt. In ersten Tests wurde ein Modell mit allen vorhanden Zeitpunkten (T3 + T5-T7) erstellt. Es zeigte sich aber als nicht besonders hilfreich, die lange (bis zu sechs Wochen) zurückliegenden Zeitpunkte mit einem anderen phänologischen Stadium und deutlich geringeren Befallsgraden miteinzubeziehen.

Erfolgreiche Prognosen wurden daher mit den späteren Zeitpunkten T6 und T7 mit höheren Befallsklassen für die Modellerstellung durchgeführt. Basierend auf diesem Modell konnte der Befall zum Zeitpunkt T8 mit einem RMSE von 4,97% und einer relativ nahen Verteilung entlang der 1x1 Linie prognostiziert werden (Abbildung 19).

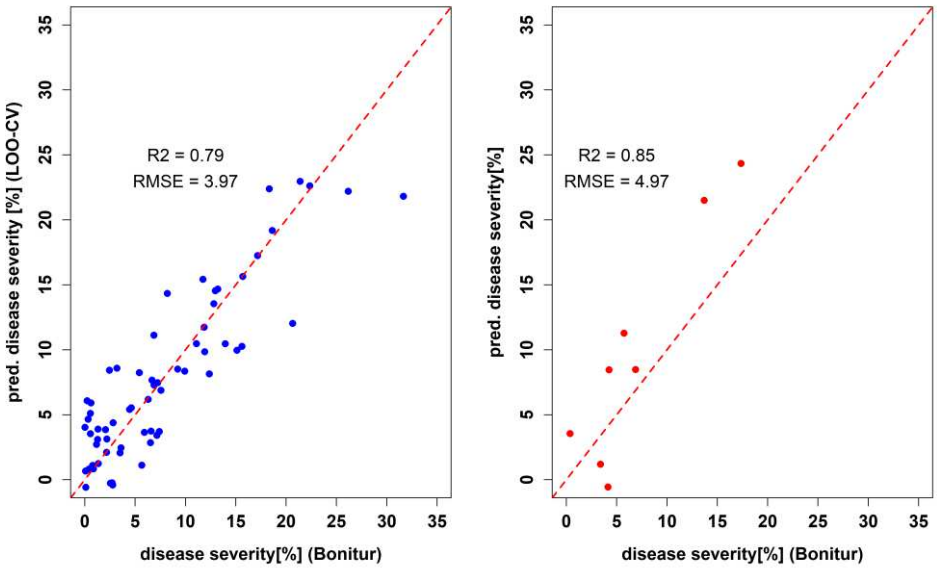


**Abbildung 19: Darstellung des PLSR-Modells zur Schätzung der Mittelwerte der vier Wiederholungen (A-D) zum Zeitpunkt T8 (rechts). Dabei ist zu beachten, dass die Kalibrierung (links) auf den Einzelwerten der Zeitpunkte T6 und T7 (n=64) erfolgte.**

Ergebnisse der Vegetationsindizes mit Daten der Headwall-Nano

Im Folgenden werden nur die Ergebnisse der vier Vegetationsindizes genauer beschrieben, die die besten Ergebnisse gezeigt hatten. Dies waren (1) der NDVI, der eher für Bestandstruktur sensitiv ist, (2) der PRI, der schon in den vergangenen Jahren insbesondere bei den Leaf Clip Messungen gut abgeschnitten hatte und eher die photosynthetische Aktivität berücksichtigt, (3) der NDRE, der den RedEdge Bereich berücksichtigt, der sowohl sensitiv für Chlorophyll ist, aber auch von der Bestandsstruktur beeinflusst wird und (4) der Chl, ein Chlorophyll-Index, der insbesondere die Chlorophyllpigmente in Relation zum Infrarotplateau (700 nm) berücksichtigt, und somit auch Bestandsinformation integriert.

**Tab. 22: Überblick der den R2 zwischen den verschiedenen Indizes und dem Befallsgrad berechnet auf Einzelwerten sowie dem RMSE zwischen den geschätzten Werten basierend auf einem linearen Modell des Index und dem gemessenen Befallsgrad**

| | T3 | | T5 | | T6 | | T7 | | T8 | |
|---|---|---|---|---|---|---|---|---|---|---|
| **Index** | **R2** | **RMSE** | **R2** | **RMSE** | **R2** | **RMSE** | **R2** | **RMSE** | **R2** | **RMSE** |
| **NDVI** | 0.03 | 0.30 | 0.02 | 4.21 | 0.33 | 4.67 | 0.44 | 6.17 | 0.28 | 5.11 |
| **Chl** | 0.00 | 0.31 | **0.26** | **3.68** | **0.41** | **4.39** | **0.62** | **5.06** | 0.70 | 3.31 |
| **PRI** | **0.18** | **0.28** | 0.04 | 4.17 | 0.09 | 5.43 | 0.46 | 6.07 | **0.74** | **3.09** |
| **NDRE2** | 0.03 | 0.30 | 0.05 | 4.16 | 0.38 | 4.50 | 0.52 | 5.72 | 0.36 | 4.83 |

| Einzelwerte (n=32) | Aggr. Befallsgrade (A-D) |
|---|---|
| 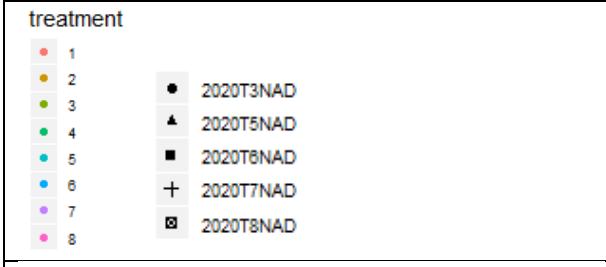 | |
| 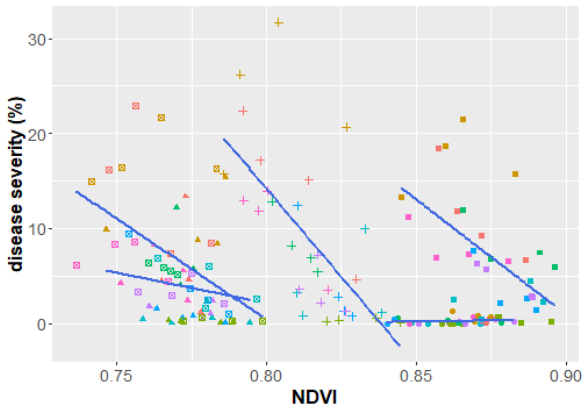 | 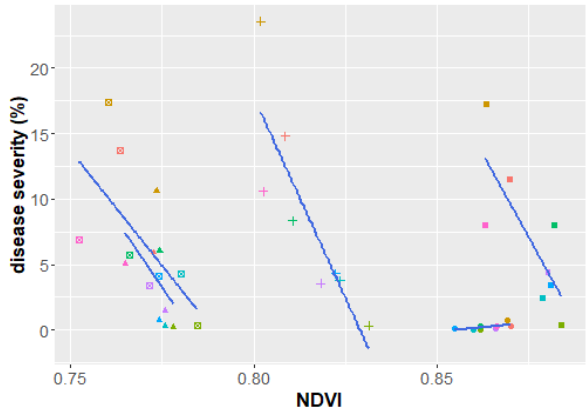 |
| 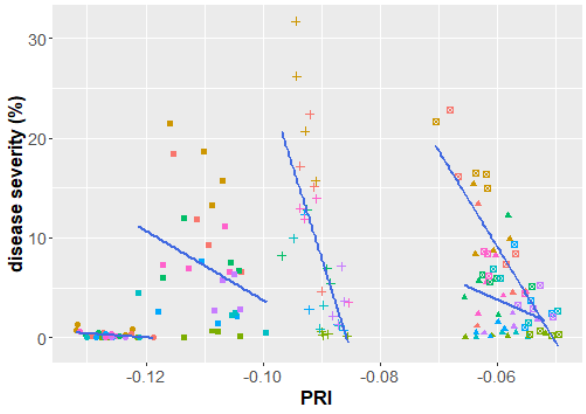 | 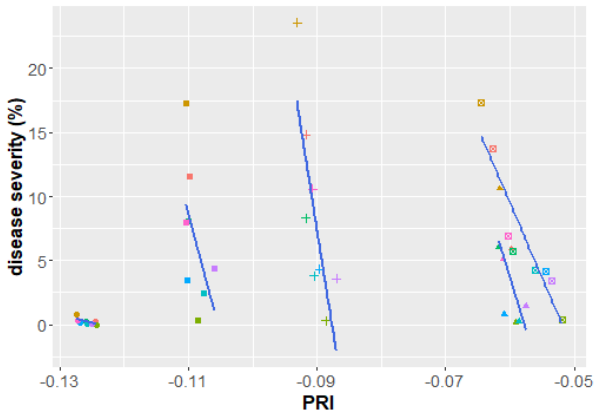 |
| 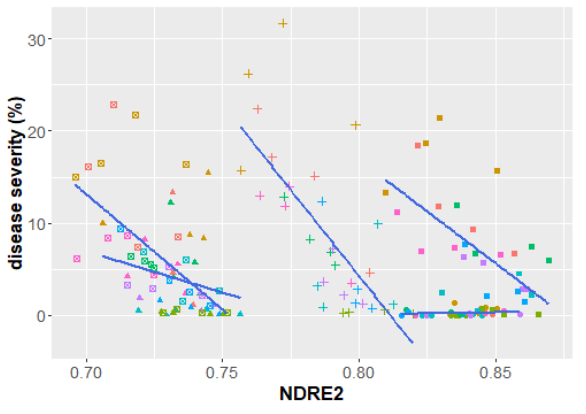 | 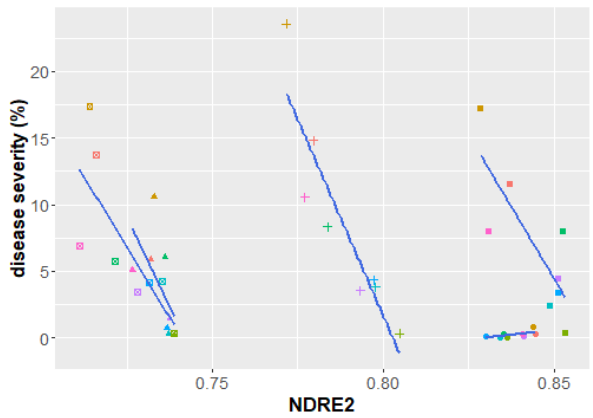 |

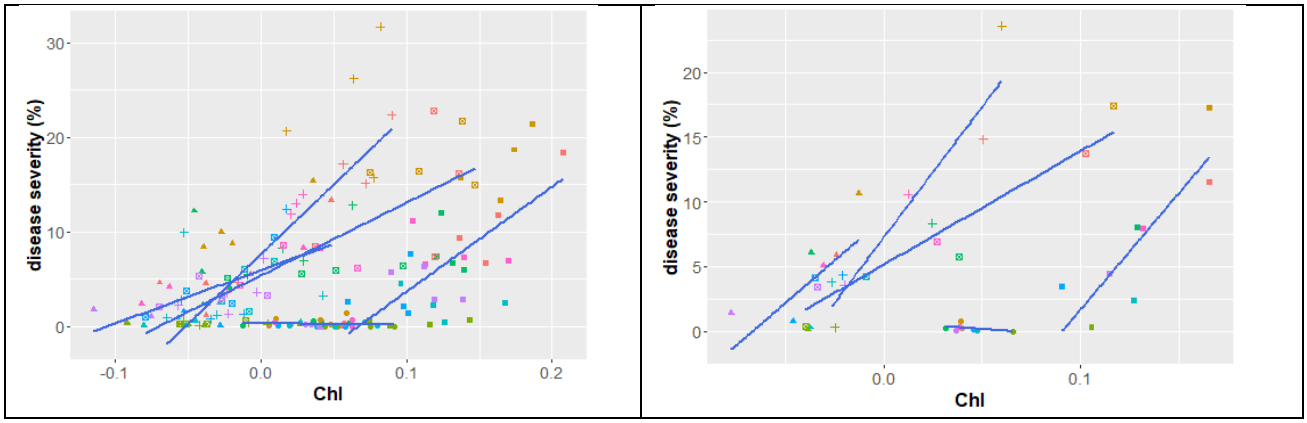


**Abbildung 20: Übersicht des Zusammenhanges der jeweiligen Indizes zu jedem Befliegungszeitpunkt basierend auf den Einzelwerten (links) und den über die Wiederholungen A-D gemittelten Werten (rechts)**

Alle Indizes zeigen sehr deutliche Unterschiede zwischen den verschiedenen Zeitpunkten trotz einer einheitlichen radiometrischen Korrektur (Abbildung 20). Entweder ließen sich die Beleuchtungsunterschiede nicht ausreichend korrigieren oder die Phänologie hat einen so starken Einfluss auf die Indizes, dass es zu den dargestellten Sprüngen kommt. Auch die Ausmaskierung des Hintergrunds könnte eine Rolle spielen, da die Maske für jeden Zeitpunkt einzeln erstellt wird. Falls bei einem Zeitpunkt weniger Hintergrund ausmaskiert wird als bei einem anderen, kommt es zu Einflüssen auf die spektrale Signatur. Besonders auffällig ist hierbei, dass für alle Indizes T5 im Wertebereich rausfällt, was diese Aussage unterstützt. Dies muss in weiteren Analysen noch genauer untersucht werden. Da die PLSR besser mit den unterschiedlichen Zeitpunkten umgehen konnte, könnten auch die einfachen Vegetationsindizes für die Analyse mehrerer Zeitpunkte schlichtweg nicht geeignet sein.

Für alle Indizes konnte für den ersten Zeitpunkt T3 mit den nur sehr geringen Symptomen und unter 1,5% Befall kein guter Zusammenhang hergestellt werden. Einen leichten Zusammenhang kann man beim PRI für die gemittelten Werte erkennen. Einen relativ guten Zusammenhang zeigt der PRI insbesondere für T8. Der NDVI war insbesondere für die stärkeren Befälle (T7) sensitiv, was zu den Beobachtungen der letzten Jahre passt und mit dem Einfluss von Peronospora auf die Laubdichte bei stärkerem Befall erklärt werden kann. Der NDRE2, der sowohl photochemische als auch bestandsabhängige Wellenlängen berücksichtigt, zeigt entsprechend für alle Zeitpunkte ähnliche Zusammenhänge. Vergleichbar sind die Ergebnisse des Chl, der ähnlich wie der NDRE2 auch photochemische und Bestandsinformationen einbezieht.

Analog zu den Ergebnissen der PLSR, wurden aus dem Befliegungszeitpunkt T7 ein lineares Modell aus dem besten Index (Chl) erstellt um T8 zu schätzen. Da T6 und T7, wie oben beschrieben, nicht gut zusammengefasst werden konnten, diente nur ein Zeitpunkt (T7) zur Vorhersage. Wie auch bei der PLSR, wurde das Modell mit Hilfe der Einzelwerte (n=32) aufgebaut und die aggregierten Wiederholungen wurden geschätzt (n=8). Das Ergebnis streut etwas mehr als das der PLSR (Abbildung 21). Dennoch ist die Vorhersage akzeptabel mit einem RMSE von 5,3% und einer guten 1x1 Beziehung. Weitere Analysen sind hier geplant.

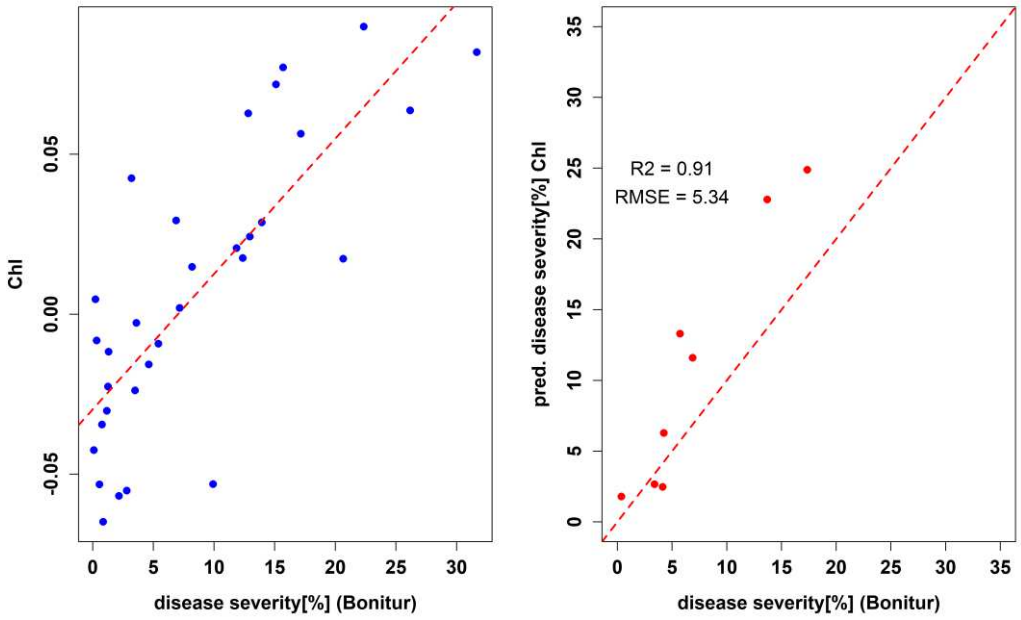


**Abbildung 21: Darstellung des Chl basierten Modells von T7 (links) und der Schätzung des Befallsgrades für T8 (rechts).**

### Erste Ergebnisse der Thermaldaten

Die Thermaldaten befinden sich aktuell noch im Stadium der Vorprozessierung. Basierend auf den Daten des Zeitpunkts T7 (30. Juli 2020) konnten erste Analysen durchgeführt werden. Zunächst wurde die mittlere Temperatur pro Plot erstellt und wiederum die vier Wiederholungen (A-D) gemittelt. Dann wurde der Zusammenhang zu den Befallsgraden betrachtet. Abbildung 22 zeigt einen leichten Zusammenhang der Temperatur mit dem Befall und einem $R^2$ von 0,54.

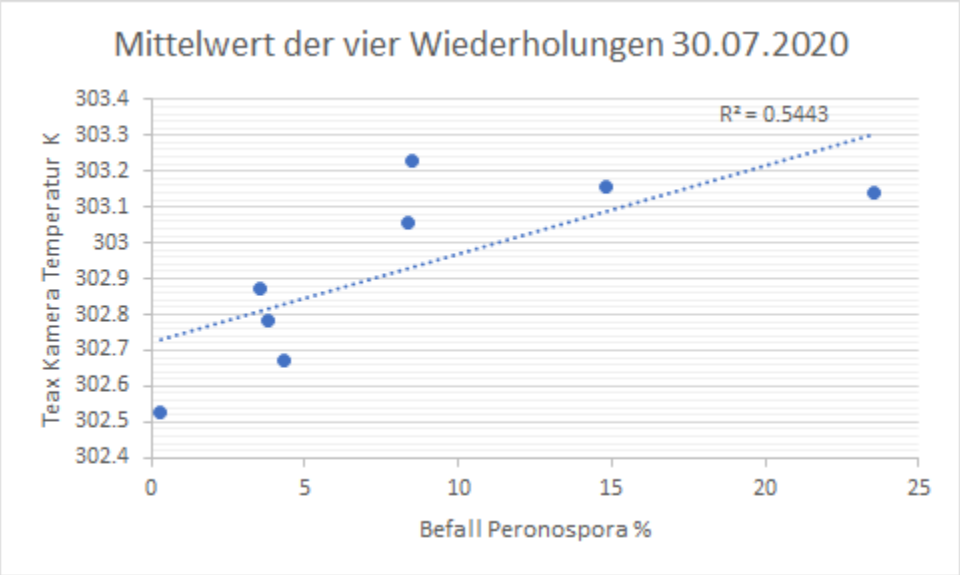


**Abbildung 22: Zusammenhang zwischen der Temperatur basierend auf den drohnenbasierten Aufnahmen und des Befallsgrades**

Um die räumliche Struktur zu analysieren und zu verstehen wurden die Thermaldaten pixelweise und für alle Plots dargestellt und der Bonitur gegenübergestellt. Eine Betrachtung der besonders hohen und besonders niedrigen Befallsgraden lässt sich auch in eher hohen und eher niedrigen Temperaturen erkennen (Abbildung 23). Hier müssen aber im Laufe der nächsten Monate noch detaillierte weitere Analysen durchgeführt werden.

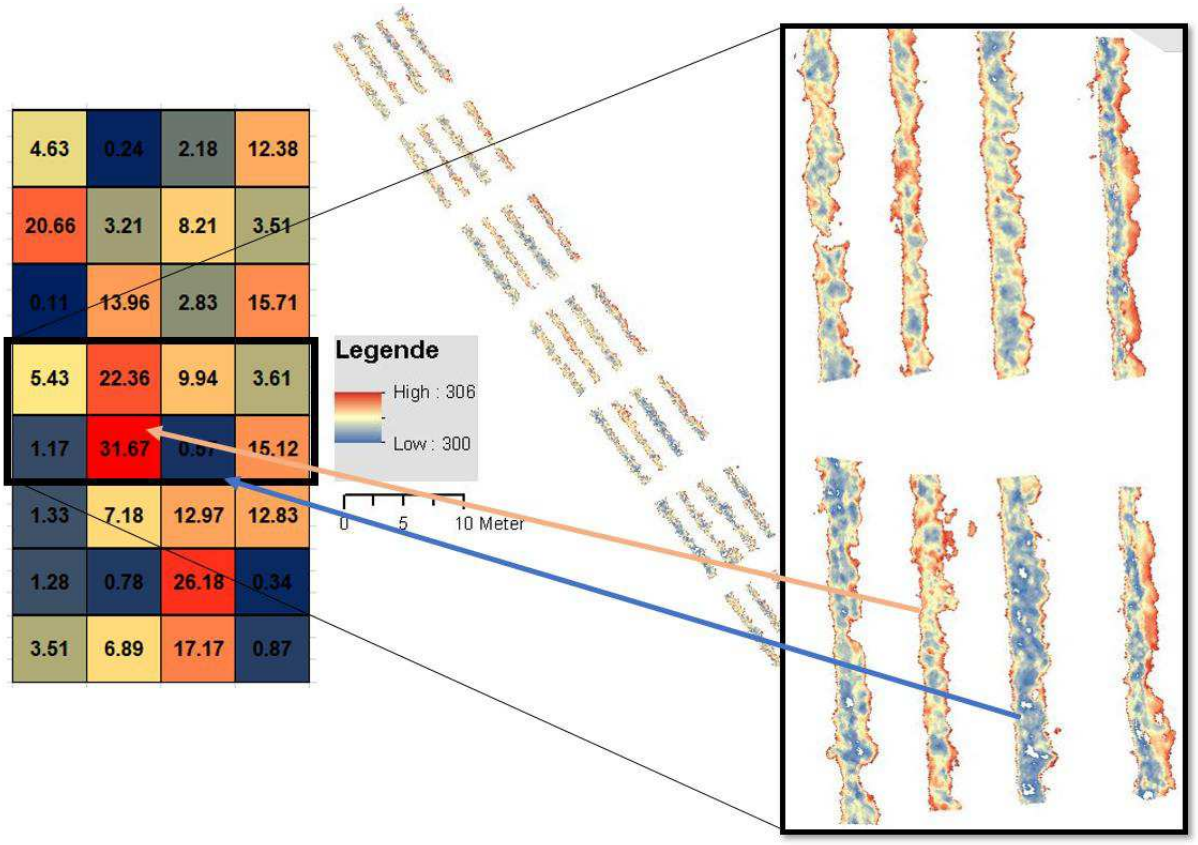


**Abbildung 23: Thermaldaten vom 30. Juli 2020 dargestellt für die Plots und links die entsprechende Bonitur. Mit dem roten und blauen Pfeil wird jeweils ein hoher und ein geringer Befallsgrad im Zoom zum Vergleich hervorgehoben.**

## 3.7 Versuch AA Monitoring symptomatischer Esca-Stöcke

### 3.7.1 Ergebnisse der Erfassung symptomatischer Esca-Stöcke

Die Bonitur auf Symptome des Esca-Komplexes erfolgte auf 01.09.2020.

Insgesamt wurden 7505 Rebstöcke erfasst. Von diesen zeigten 72% (5420) keine Symptome des Esca-Komplexes, 19% (1423) waren abgestorben oder nicht mehr existent und 9% (662) waren symptomatisch. Von diesen symptomatischen Stöcken zeigten 3% eine Apoplexie, 75% Blattsymptome und 69% Beerensymptome.

Die räumliche Verteilung ist aus Abbildung 24 ersichtlich.

| | |
|---|---|
| 0 | Ertragsstock |
| 1 | Apoplexie |
| 2a | Blatt leicht |
| 2b | Blatt mittel |
| 2c | Blatt stark |
| 3a | Trauben leicht |
| 3b | Traube mittel |
| 3c | Traube stark |
| x | Fehlstock |

**Abbildung 24: Räumliche Verteilung der Rebstöcke mit Blattsymptomen des Esca-Komplexes und Fehlstöcken (rot) in der Rebanlage „Berg“ des IVV. Erfassung am 01.09.2020.**

Die vergleichenden Analysen Entwicklung der symptomatischen Stöcke in den Jahren 2017 bis 2020 ist gegenwärtig noch nicht abgeschlossen. Diese Ergebnisse sowie der Ergebnisse fernerkundlicher Untersuchungen zur Erfassung des Esca-Befalls werden im Rahmen des Projektes MonESCA kommuniziert.

## 3.8 Bestandsklima in den verschiedenen Erziehungssystemen

Die Auswertung der im Projekt erfassten Daten zum Bestandsklima des ersten Untersuchungsjahres 2020 dauern gegenwärtig an. Die Ergebnisse werden im nächsten Jahresbericht erscheinen.

# 4 Zwischenfazit

Das seit 2013 durchgeführte ***Scaphoideus titanus*-Monitoring** lieferte keinerlei Hinweise auf das Vorkommen des Vektors der Flavescence dorée im Luxemburger Weinbaugebiet. Um die Voraussetzungen zur Beantragung einer Flavescence dorée-Schutzzone für Luxemburg zu erfüllen, wird das Monitoring in den Folgejahren fortgeführt.

Le **monitoring** de D. suzukii a montré une activité de vol importante en septembre 2020 et des pontes concentrées sur les variétés tardives et plus particulièrement Pinotin. Concernant les essais de lutte contre *D. suzukii* avec des produits naturels, des experimentations ont été menées en laboratoire et dans le vignoble. Au laboratoire, les produits Surround et Cutisan ont permis la diminution de l'activité de ponte mais n'ont pas eu d'effet répulsif. Le produit $CaCO_3$ n'a pas aucun effet sur *D. suzukii*. Au vignoble, aucun produit testé n'a eu d'effet sur l'activité de ponte. Concernant l'activité de vol, Surround a un effet répulsif significatif, Cutisan un léger effet répulsif et le $CaCO_3$ un effet légèrement attractif.

Die Untersuchungen zu den Effekten des **Schnittsystem**s auf die Fäulnisanfälligkeit zeigten in den Versuchsjahren 2016 bis 2020 einen reduzierten Fäulnisbefall bei einem Entfernen der zweiten Bogrebe nach der Rebblüte. In jedem Jahr und jeder der beiden Rebsorten lag die Befallsstärke am letzten Boniturtermin unter der der Kontrolle mit Rebschnitt auf zahmes Holz, Es wird vermutet, dass dieser Effekt durch eine geringere Befruchtungsrate während der Rebblüte aufgrund der erhöhten Gescheinsanzahl pro Rebe beim Anschnitt auf zwei Bogreben, welche um die zur Verfügung stehenden Assimilate konkurrieren, zu erklären ist. Dies lässt eine aufgelockerte Traubenstruktur und damit eine reduzierte Fäulnisneigung

erwarten. Bei den Erträgen sowie den Mostgewichten und sonstigen Inhaltsstoffen liegt bisher kein klares Bild zu den Effekten des Schnittsystems vor. Eine exakte statistischen Analyse der vorliegende Daten aus den fünf Versuchsjahren soll die vorliegenden Erkenntnis absichern. Ein wissenschaftliche Paper hierzu ist in Arbeit.

Das Befallsniveau im **Oidium**-Versuch war in allen Versuchsjahren am Standort Remich sehr gering, so dass eine klare Differenzierung zwischen den Versuchsgliedern nicht möglich war. Es deutet sich jedoch an, dass die beiden SDHI-Fungizide Luna Experience und Sercadis zur Zeit sehr starke Präparate zur Oidium-Bekämpfung darstellen. Dies würde Beobachtungen verschiedener Versuche an anderen Standorten sowie Beobachtungen aus der Praxis bestätigen. Weiterhin deutet das aktuelle Versuchsjahr 2020 an, dass auf diesem Standort die Wirksamkeit des Strobilurinpräparates Flint bei hohem Befallsdruck nicht ausreichend sein könnte. Zur Absicherung soll der Versuch im Folgejahr fortgeführt werden.

Im Versuch zur **fernerkundlichen Erkennung des Peronospora**-Befalls wurde im Versuchsjahr 2020 ein mittleres Befallsniveau erreicht. Hierbei zeigte die Variante des integrierten Weinbaus, im Gegensatz zum Vorjahr, sehr gute Wirkungsgrade.
Wie 2017 und 2018 stellte sich die angestrebte Variabilität innerhalb des Versuchsfeldes ein, so dass die Grundlage für die Kalibrierung eines Befallsstärken-Modells anhand der fernerkundlichen Daten gegeben war.
Mithilfe der hyperspektralen Nano-Daten und einem multivariaten statistischen Verfahren, der PLSR, konnten sehr gute Zusammenhänge für die einzelnen Versuchstage zwischen den Fernerkundungsdaten und dem Befallsgrad beobachtet werden. Wie auch die letzten Jahre waren insbesondere die sehr niedrigen Werte eher schwierig und zeigten eine starke Streuung. Allerdings konnte erstmals ein sehr guter Zusammenhang und 1x1 Beziehung zwischen geschätzten und gemessenen Daten bei Befallsgraden unter 1,5 % für die Mittelung der vier Wiederholungen erzielt werden. Für die höheren Befallsgrade gelang es auch eine gute Vorhersage in die Zukunft zu treffen. Diese Möglichkeit wir in den kommenden Wochen noch detaillierter untersucht.
Die Ergebnisse für die Vegetationsindizes schneiden im Vergleich etwas schwächer ab. Es konnten die Einzeltage mit einer teilweise guten Genauigkeit und einem Zusammenhang zwischen Index und Befall von $R^2$=0,62-0,74 bestimmt werden. Der RMSE der Schätzung lag bei ca. 3-6%. Eine gute Vorhersage für die hohen Befallsgrade konnte mit dem Vegetationsindex Chl getroffen werden mit einem RMSE von 5,3%. Weitere Analysen sowie eine Veröffentlichung der Ergebnisse sind geplant.
Mit den Thermaldaten konnten erst wenige Analysen durchgeführt werden. Es zeigen sich Zusammenhänge und räumliche Muster für starke Unterschiede im Befall. Inwiefern sich auch

geringe Befallsgrade in den Thermaldaten erkennen lassen muss noch untersucht werden. Durch die geringen Kontrastunterschiede und dem Einfluss von Luftbewegungen sind diese Daten schwierig zu analysieren und können vermutlich eher als Ergänzung zu den Hyperspektraldaten gesehen werden als eine alleinstehende Datengrundlage.

Zusammenfassend kann festgestellt werden, dass die Nano Daten eine hohe spektrale Qualität zeigen und gute Ergebnisse für die Schätzung von Peronospora erzielt werden konnten. Eine Reduzierung auf Nadiraufnahmen stellte eine ausreichende Datengrundlage dar. Da 2020 ein trockenes Jahr war und die Laubwand eine eher geringe Dichte aufwies, sind Nadirdaten in der Regel die bessere Wahl. Vergangene Untersuchungen hatten gezeigt, dass eine dünne Laubwand bei den Schrägaufnahmen für erhebliche Probleme sorgt, da der Hintergrund, der häufig aus trockenem Gras besteht, ein sehr ähnliches Signal zu Peronosorasymptomen aufweist. Die multivariaten Analysen der Nadirdaten scheinen gut für unsere Fragestellung geeignet zu sein.

Die Erfassung der **Esca**-symptomatischen Rebstöcke im Weinberg „Berg“ des IVV zeigte, dass deren Anzahl relativ hoch ist und über alle Sorten hinweg durchschnittlich 9% (2020) erreicht. Weiterhin ist zu vermuten, dass ein großer Anteil der „Fehlstöcke“, welche 19% (2020) der Gesamtpflanzenzahl ausmachen, in den letzten Jahren an den Folgen des Esca-Komplexes abgestorben ist. Zwischen den Erfassungen 2017 und 2020 ist der Anteil abgestorbener Reben von 14 auf 19% angestiegen. Generell wurden starke Rebsortenunterschiede deutlich. Die vergleichenden Analysen der symptomatischen Stöcke in den Jahren 2017, 2018 und 2019 ist gegenwärtig noch nicht abgeschlossen. Die Ergebnisse werden im Rahmen des Projektes MonESCA kommuniziert.

In den nächsten Jahren soll dieser Weinberg im Rahmen des MonESCA Projektes weiterhin intensiv untersucht werden, um eine weitere Ausweitung des Anteils symptomatischer Reben sowie spontane Genesungen zu erfassen und mögliche Befallsmuster zu erkennen.

Die Erfassung des Bestandsklimas mittels mikrometeorologischer Messungen wird in 2021 fortgesetzt. Des Weiteren erfolgt der Vergleich der Blattnässemessungen im Bestand mit den Messwerten der ASTA Station am IVV mit dem Ziel eine Transferfunktion zu erstellen. Diese ermöglicht eine realistischere Darstellung des Eingangsparameters Blattnässe in verschiedenen Schadmodellen für z.B. Pilzinfektionen.

# 5 Danksagung

Die Autoren bedanken sich beim Institut Viti-Vinicole für die finanzielle Unterstützung, die Bereitstellung der Versuchsflächen sowie die Mithilfe bei der Durchführung der Untersuchungen im Weinberg, im Labor und im Keller. Weiterhin gilt ein besonderer Dank Mareike Schultz, Christopher Simon, Robert Mannes, Serge Fischer, Serge Garidel, Jeff Lafleur, Joelle Koch, Heidi Litjens, Doriane Dam und Marine Pallez-Barthel für die Mitarbeit bei der Durchführung und Auswertung der Versuche sowie bei der Versuchslese. Michael Eickermann sei für die Unterstützung der entomologischen Bestimmungen im Rahmen des *S. titanus* Monitorings sowie für die Beratung bei der Methoden-Entwicklung für das Kirschessigfliegen-Monitoring und die -Bekämpfungsversuche gedankt. Weiterhin danken wir allen Winzern, die ihre Weinberge für die Monitoring-Programme zur Verfügung gestellt haben.

# 6 Literaturverzeichnis


BELLAMY, D. E., SISTERSON, M. S. & WALSE, S. S. 2013. Quantifying host potentials: indexing postharvest fresh fruits for spotted wing drosophila, *Drosophila suzukii*. *PLoS ONE,* 8**,** e61227.

GAMON, J. A., PEÑUELAS, J. & FIELD, C. B. 1992. A narrow-waveband spectral index that tracks diurnal changes in photosynthetic efficiency. *Remote Sensing of Environment,* https://doi.org/10.1016/0034-4257(92)90059-S.

GITELSON, A. A., GRITZ, Y. & MERZLYAK, M. N. 2003. Relationships between leaf chlorophyll content and spectral reflectance and algorithms for non-destructive chlorophyll assessment in higher plant leaves. *Journal of Plant Physiology,* 160**,** 271-282.

HERRMANN, I., PIMSTEIN, A., KARNIELI, A., COHEN, Y., ALCHANATIS, V. & BONFIL, D. J. 2010. Assessment of leaf area index by the red-edge inflection point derived from venus bands. *Hyperspectral 2010 Workshop*.

IPACH, R., HUBER, B., HOFMANN, H. & BAUS, O. 2005. *Richtlinie zur Prüfung von Wachstumsregulatoren zur Auflockerung der Traubenstruktur und zur Vermeidung von Fäulnis an Trauben. Outline for an EPPO-guideline*.

LORENZ, D. H., EICHHORN, K. W., BLEIHOLDER, H., KLOSE, R., MEIER, U. & WEBER, E. 1995. Phenological growth stages of the grapevine, *Vitis vinifera* L. ssp. *vinifera*. Codes and descriptions according to the extended BBCH scale. *Australian Journal of Grape and Wine Research,* 1**,** 100-103.

OERKE, E.-C., HERZOG, K. & TÖPFER, R. 2016. Hyperspectral phenotyping of the reaction of grapevine genotypes to *Plasmopara viticola*. *Journal of Experimental Botany,* doi:10.1093/jxb/erw318.

RETZLAFF, R., MOLITOR, D., BEHR, M., BOSSUNG, C., ROCK, G., HOFFMANN, L., EVERS, D. & UDELHOVEN, T. 2015. UAS-based multi-angular remote sensing of the effects of soil management strategies on grapevine. *Journal International des Sciences de la Vigne et du Vin,* 49**,** 85-102.

ROUSE, J. W., HASS, R. H., SCHELL, J. A. & DEERING, D. W. 1973. Monitoring vegetation systems in the great plains with ERTS. *Third Earth Resources Technology Satellite (ERTS) Symposium,* 1**,** 309-317.

UDELHOVEN, T., DELFOSSE, P., BOSSUNG, C., RONELLENFITSCH, F., MAYER, F., SCHLERF, M., MACHWITZ, M. & HOFFMANN, L. 2013. Retrieving the Bioenergy Potential from Maize Crops Using Hyperspectral Remote Sensing. *Remote Sensing 5(1):254–73*.

VLACH, J. 2013. Identifying *Drosophila suzukii*. *https://www.oregon.gov/ODA/shared/Documents/Publications/IPPM/SpottedWingDrosophilaIDKey.pdf*.

WOLD, S., SJÖSTRÖM, M., ERIKSSON, L. 2001. PLS-Regression: A Basic Tool of Chemometrics. *Chemometrics and Intelligent Laboratory Systems*, 58, 109-130

YU, K., LENZ-WIEDEMANN, V., CHEN, X. & BARETH, G. 2014. Estimating leaf chlorophyll of barley at different growth stages using spectral indices to reduce soil background and canopy structure effects. *ISPRS Journal of Photogrammetry and Remote Sensing,* 97**,** 58-77.

# 7 Anhang

## 7.1 Phänologische Entwicklung 2020

**Tab A1: Daten des Erreichens der phänologischen Entwicklungsstadien gemäß BBCH-Code (Lorenz et al., 1995) in den Versuchsflächen im Jahr 2020.**

| BBCH | Riesling Klon 3 | Rivaner Klon 22 | Elbling Zeile 77 | Gewürz-traminer Klon 312 | Pinot blanc Klon 54 | Auxerrois Klon 7 | S. blanc Klon 376 | Pinot gris Klon 7 | Chardonnay Klon Colmar 96 | Merlot | Pinot noir Klon Freiburg L13 |
|---|---|---|---|---|---|---|---|---|---|---|---|
| 01 | 24-Mar | 19-Mar | 22-Mar | 24-Mar | 22-Mar | 31-Mar | 4-Apr | 19-Mar | 17-Mar | 28-Mar | 18-Mar |
| 03 | 6-Apr | 4-Apr | 1-Apr | 5-Apr | 5-Apr | 7-Apr | 9-Apr | 5-Apr | 27-Mar | 5-Apr | 5-Apr |
| 5 | 9-Apr | 7-Apr | 6-Apr | 8-Apr | 8-Apr | 10-Apr | 11-Apr | 8-Apr | 4-Apr | 8-Apr | 8-Apr |
| 07 | 11-Apr | 10-Apr | 10-Apr | 10-Apr | 11-Apr | 12-Apr | 13-Apr | 10-Apr | 8-Apr | 11-Apr | 10-Apr |
| 09 | 13-Apr | 12-Apr | 11-Apr | 12-Apr | 13-Apr | 14-Apr | 15-Apr | 12-Apr | 10-Apr | 13-Apr | 12-Apr |
| 11 | 16-Apr | 15-Apr | 13-Apr | 15-Apr | 15-Apr | 17-Apr | 17-Apr | 15-Apr | 13-Apr | 16-Apr | 15-Apr |
| 12 | 19-Apr | 17-Apr | 15-Apr | 17-Apr | 18-Apr | 20-Apr | 19-Apr | 17-Apr | 16-Apr | 18-Apr | 18-Apr |
| 13 | 21-Apr | 20-Apr | 18-Apr | 20-Apr | 21-Apr | 22-Apr | 23-Apr | 20-Apr | 19-Apr | 20-Apr | 21-Apr |
| 14 | 24-Apr | 23-Apr | 20-Apr | 23-Apr | 24-Apr | 25-Apr | 26-Apr | 23-Apr | 22-Apr | 23-Apr | 23-Apr |
| 15 | 26-Apr | 25-Apr | 23-Apr | 26-Apr | 26-Apr | 27-Apr | 28-Apr | 26-Apr | 24-Apr | 27-Apr | 26-Apr |
| 16 | 29-Apr | 27-Apr | 25-Apr | 29-Apr | 30-Apr | 30-Apr | 4-May | 29-Apr | 26-Apr | 30-Apr | 29-Apr |
| 17 | 8-May | 6-May | 27-Apr | 6-May | 9-May | 10-May | 10-May | 8-May | 28-Apr | 10-May | 9-May |
| 18 | 16-May | 10-May | 29-Apr | 10-May | 16-May | 16-May | 18-May | 14-May | 9-May | 16-May | 14-May |
| 19 | 18-May | 16-May | 9-May | 16-May | 18-May | 18-May | 20-May | 18-May | 12-May | 19-May | 18-May |
| 53 | 27-Apr | 27-Apr | 24-Apr | 24-Apr | 27-Apr | 27-Apr | 30-Apr | 27-Apr | 24-Apr | 28-Apr | 27-Apr |
| 55 | 12-May | 10-May | 30-Apr | 10-May | 12-May | 12-May | 14-May | 10-May | 9-May | 12-May | 10-May |
| 57 | 24-May | 23-May | 24-May | 25-May | 24-May | 25-May | 28-May | 23-May | 21-May | 26-May | 23-May |
| 61 | 2-Jun | 1-Jun | 1-Jun | 2-Jun | 31-May | 1-Jun | 3-Jun | 31-May | 29-May | 1-Jun | 31-May |
| 63 | 4-Jun | 3-Jun | 3-Jun | 3-Jun | 1-Jun | 3-Jun | 8-Jun | 1-Jun | 31-May | 3-Jun | 1-Jun |
| 65 | 9-Jun | 7-Jun | 7-Jun | 8-Jun | 4-Jun | 7-Jun | 10-Jun | 3-Jun | 2-Jun | 7-Jun | 3-Jun |
| 68 | 11-Jun | 9-Jun | 9-Jun | 10-Jun | 9-Jun | 10-Jun | 10-Jun | 7-Jun | 7-Jun | 9-Jun | 8-Jun |
| 69 | 12-Jun | 11-Jun | 11-Jun | 12-Jun | 11-Jun | 12-Jun | 12-Jun | 9-Jun | 8-Jun | 11-Jun | 10-Jun |
| 71 | 14-Jun | 13-Jun | 13-Jun | 14-Jun | 13-Jun | 14-Jun | 14-Jun | 11-Jun | 10-Jun | 14-Jun | 12-Jun |
| 73 | 18-Jun | 17-Jun | 16-Jun | 18-Jun | 16-Jun | 19-Jun | 23-Jun | 15-Jun | 14-Jun | 18-Jun | 15-Jun |
| 75 | 30-Jun | 25-Jun | 2-Jul | 1-Jul | 25-Jun | 2-Jul | 30-Jun | 24-Jun | 25-Jun | 24-Jun | 25-Jun |
| 77 | 2-Jul | 13-Jul | 6-Jul | 4-Jul | 3-Jul | 6-Jul | 4-Jul | 1-Jul | 3-Jul | 20-Jul | 11-Jul |
| 79 | 13-Jul | 31-Jul | 15-Jul | 16-Jul | 13-Jul | 18-Jul | 17-Jul | 12-Jul | 16-Jul | 12-Aug | 3-Aug |
| 81 | 14-Aug | 1-Aug | 11-Aug | 5-Aug | 8-Aug | 5-Aug | 8-Aug | 4-Aug | 8-Aug | 13-Aug | 7-Aug |
| 83 | 17-Aug | 4-Aug | 15-Aug | 8-Aug | 11-Aug | 8-Aug | 12-Aug | 8-Aug | 12-Aug | 18-Aug | 11-Aug |
| 85 | 20-Aug | 7-Aug | 17-Aug | 13-Aug | 14-Aug | 11-Aug | 15-Aug | 12-Aug | 14-Aug | 21-Aug | 14-Aug |

## 7.2 Tageswitterungsbedingungen in der Vegetationsperiode 2020

**Tab. A2: Tagesmitteltemperaturen ($t_m$) sowie Tagesniederschläge (N) im Zeitraum 01. April bis 30. September 2020 an der Wetterstation Remich (Quelle: agrimeteo.lu).**

| Tag | Monat | | | | | | | | | | | |
|---|---|---|---|---|---|---|---|---|---|---|---|---|
| | April | | Mai | | Juni | | Juli | | August | | September | |
| | $t_m$(°C) | N (mm) | $t_m$ (°C) | N (mm) | $t_m$(°C) | N (mm) | $t_m$ (°C) | N (mm) | $t_m$(°C) | N (mm) | $t_m$ (°C) | N (mm) |
| 1 | 4,70 | ,00 | 9,28 | 25,72 | 19,49 | ,00 | 19,39 | ,01 | 24,42 | 6,10 | 15,70 | ,00 |
| 2 | 5,48 | ,00 | 8,40 | ,93 | 20,35 | ,00 | 18,52 | ,07 | 21,44 | ,28 | 15,85 | ,12 |
| 3 | 6,27 | ,00 | 9,84 | ,08 | 19,16 | 7,73 | 16,66 | ,00 | 17,04 | ,00 | 16,85 | ,00 |
| 4 | 7,99 | ,00 | 12,58 | ,00 | 14,02 | 7,15 | 18,33 | ,00 | 17,58 | ,00 | 22,72 | ,00 |
| 5 | 13,49 | ,00 | 10,73 | ,00 | 10,56 | 2,26 | 20,75 | ,34 | 19,88 | ,00 | 16,61 | ,00 |
| 6 | 14,11 | ,00 | 11,20 | ,00 | 12,41 | 3,67 | 15,33 | ,38 | 22,84 | ,00 | 13,19 | ,00 |
| 7 | 15,26 | ,00 | 12,98 | ,00 | 12,49 | ,00 | 15,18 | ,00 | 25,52 | ,00 | 14,86 | ,00 |
| 8 | 15,53 | ,00 | 16,05 | ,00 | 13,96 | ,81 | 16,44 | ,00 | 27,15 | ,00 | 16,43 | ,00 |
| 9 | 15,07 | ,00 | 14,72 | 4,76 | 13,97 | 1,54 | 21,67 | ,00 | 27,12 | ,00 | 17,23 | ,00 |
| 10 | 16,58 | ,00 | 16,03 | 14,52 | 15,39 | ,86 | 18,69 | ,00 | 27,66 | ,00 | 19,00 | ,00 |
| 11 | 15,88 | ,00 | 7,82 | 5,11 | 16,11 | ,00 | 16,18 | ,00 | 27,70 | ,00 | 17,78 | ,00 |
| 12 | 14,84 | ,00 | 7,81 | ,00 | 18,07 | 6,73 | 17,75 | ,00 | 25,72 | ,22 | 18,19 | ,00 |
| 13 | 10,11 | ,01 | 9,77 | ,00 | 17,89 | 2,18 | 19,48 | ,00 | 23,88 | ,00 | 18,48 | ,00 |
| 14 | 5,95 | ,00 | 10,02 | ,00 | 16,94 | ,72 | 17,44 | 1,68 | 21,92 | 1,96 | 20,93 | ,00 |
| 15 | 10,41 | ,00 | 11,37 | ,00 | 17,01 | ,04 | 16,78 | 4,95 | 22,75 | ,03 | 22,59 | ,00 |
| 16 | 13,47 | ,00 | 12,34 | ,00 | 17,35 | ,00 | 15,37 | 1,80 | 23,87 | 2,17 | 21,08 | ,41 |
| 17 | 15,92 | ,00 | 12,87 | ,00 | 15,10 | 28,77 | 17,96 | ,00 | 20,78 | 2,11 | 18,86 | ,00 |
| 18 | 15,38 | ,08 | 15,54 | ,00 | 16,46 | ,00 | 20,54 | ,00 | 18,49 | 1,96 | 18,74 | ,00 |
| 19 | 13,68 | ,06 | 17,62 | ,00 | 16,48 | ,00 | 21,82 | ,00 | 20,00 | ,23 | 19,71 | ,00 |
| 20 | 14,23 | ,00 | 19,04 | ,00 | 16,26 | ,06 | 20,60 | ,00 | 26,26 | ,15 | 18,66 | ,00 |
| 21 | 15,57 | ,00 | 19,53 | ,00 | 18,35 | ,01 | 19,04 | ,00 | 25,89 | ,12 | 16,97 | ,00 |
| 22 | 16,39 | ,00 | 19,68 | ,02 | 17,95 | ,00 | 18,81 | ,00 | 21,64 | ,00 | 17,09 | ,00 |
| 23 | 15,58 | ,00 | 12,01 | 10,44 | 20,64 | ,00 | 19,60 | ,00 | 19,08 | ,00 | 17,41 | 3,70 |
| 24 | 14,34 | ,00 | 12,25 | ,04 | 22,52 | ,00 | 19,02 | ,61 | 17,83 | ,00 | 15,03 | 6,32 |
| 25 | 12,03 | ,00 | 14,03 | ,04 | 26,22 | ,00 | 20,25 | ,00 | 19,18 | ,00 | 10,05 | 2,31 |
| 26 | 12,40 | ,00 | 16,04 | ,00 | 20,94 | 23,28 | 20,30 | ,42 | 19,68 | ,00 | 9,79 | 5,99 |
| 27 | 13,27 | ,00 | 17,22 | ,00 | 20,90 | 8,96 | 22,42 | ,00 | 17,41 | ,12 | 10,02 | 18,32 |
| 28 | 12,83 | 2,28 | 17,48 | ,00 | 18,20 | ,00 | 20,79 | ,00 | 17,17 | 3,39 | 9,26 | 5,77 |
| 29 | 12,53 | 1,93 | 16,32 | ,00 | 16,99 | ,58 | 17,79 | ,00 | 15,91 | ,06 | 12,76 | 4,35 |
| 30 | 10,55 | 12,21 | 16,79 | ,00 | 16,00 | ,00 | 21,72 | ,00 | 15,41 | ,70 | 14,40 | ,32 |
| 31 | | | 16,05 | ,00 | | | 26,10 | ,00 | 15,28 | 4,93 | | |

## 7.3 Veröffentlichungen

### 7.3.1 Veröffentlichungen in wissenschaftlichen Journalen (2020)

Molitor D., Fraga H., Junk J. (2020): UniPhen–a unified high resolution model approach to simulate the phenological development of a broad range of grape cultivars as well as a potential new bioclimatic indicator. Agricultural and Forest Meteorology 291, 108024. DOI: 10.1016/j.agrformet.2020.108024.

Leolini L., Costafreda-Aumedes S., Santos J.A., Menz C., Fraga H., Molitor D., Merante P., Junk J., Kartschall T., Destrac-Irvine A., van Leeuwen C., Malheiro A.C., Eiras-Dias J., Silvestre J., Dibari C., Bindi M., Moriondo M. (2020): Phenological model intercomparison for estimating grapevine budbreak date (*Vitis vinifera* L.) in Europe. Applied Sciences 10, 3800. DOI: 10.3390/app10113800.

Molitor D., Baus O., Didry Y., Junk J., Hoffmann L., Beyer M., (2020): BotRisk: simulating the annual bunch rot risk on grapevines (*Vitis vinifera* L. cv. Riesling) based on meteorological data. International Journal of Biometeorology. DOI: 10.1007/s00484-020-01938-5.

Santos J.A., Fraga H., Malheiro A.C., Moutinho-Pereia J., Dinis L.-T., Correia C., Moriondo M., Leolini L., Dibari C., Costafreda-Aumedes S., Kartschall T., Menz C., Molitor D., Junk J., Beyer M., Schultz H.R. (2020): A review of the potential climate change impacts and adaptation options for European viticulture. Applied Sciences 10, 3092. DOI: 10.3390/app10093092

Fraga H., Molitor D., Leolini L., Santos J.A. (2020): What is the impact of heatwaves on European viticulture? A modelling assessment. Applied Sciences 10: 3030. DOI: 10.3390/app10093030

Parker A.K., Garcia de Cortazar-Atauri I., Gény L., Spring J.-L., Destac A., Schultz H.R., Molitor D., Lacombe T., Graça A., Monamy C., Stoll M., Storchi P., Trought M., Hofmann R., van Leeuwen C. (2020): Temperature-based grapevine sugar ripeness modelling for a wide range of *Vitis vinifera* L. cultivars. Agricultural and Forest Meteorology 285-286: 107902.

Veröffentlichungen hängen diesem Bericht an.

## 7.4 Pressemeldungen

**[LIST Press article]**

### 12. Lëtzebuerger Wäibaudag

***De Letzeburger Bauer, 28/02/20:***

Vierter Teil unseres Berichts.- Am 5. Februar fand der 12. Weinbautag im Wormeldinger Kulturzentrum statt. Nachdem wir in der letzten Nummer auf die Klimawandelthematik eingegangen sind, geht es im nachfolgenden vierten Teil um Drohnen im Weinbau, eine weintouristische Imagekampagne sowie Alkoholreduzierung.

**Drohneneinsatz zur Krankheitserkennung**

Dem Einsatz drohnenbasierter Aufnahmen von Krankheiten im Weinbau war der Vortrag von Dr. Myriam Machwitz vom Luxembourg Institute of Science and Technology (LIST) gewidmet. Die Wissenschaftlerin erklärte, dass es sich bei den Forschungsarbeiten um eine Gemeinschaftsarbeit von verschiedenen Einrichtungen handelt. Zwei Projekte mit Drohnenfernerkundung werden derzeit bearbeitet: Monesca (ESCA) und Biovim (Peronospora). Beim Projekt Biovim wird das Laub bei verschiedenen Befallsstärken von Peronospora am IVV spektrometrisch untersucht. Zwecks Datengewinnung wird u.a. Peronospora-Befall künstlich induziert. Welche spektrometrischen Auffälligkeiten sind zu beobachten: Das Infrarot-Spektrum ändert sich in Form und Höhe der Kurve je nach Befallsstärke. Die Expertin vom LIST führte hierzu aus, dass bei der Auswertung die Befallsstärke mit verschiedenen Farben visualisiert wird, von grün (befallsfrei) bis rot (stark befallen).

2017 ergab sich ein hoher Befall von bis zu 50% und die Schätzung des Schadens war mit 95% Wahrscheinlichkeit besonders gut. Schrägaufnahmen von der Seite erwiesen sich 2017 als nützlicher, während in den dünnen Beständen des Jahres 2018 die Aufnahmen direkt von oben die besten Ergebnisse brachten. 2018 handelte es sich um einen mittleren Befall mit maximal 15% und die Schadensschätzung mittels Drohne war noch recht genau. Dies war im letzten Jahr gänzlich anders. Der Befall lag unter 5% und nur in einem Beispiel war eine brauchbare Schätzung möglich.

Monesca wurde 2019 gestartet. Dieses dient einem ESCA-Monitoring an der Luxemburger Mosel durch Fernerkundung. Der tatsächliche Zustand auf den Praxisflächen wird automatisch erfasst. Daraus soll auch abgeleitet werden, wie groß die ökonomische Bedeutung der Krankheit ist, welche sich immer stärker ausbreitet.

Über die Möglichkeiten eines digitalen Einzelstockinventars im Rahmen von Monesca referierte im Anschluss Gilles Rock von Geocoptix. Diese ist nur machbar mit einer hochaufgelösten Drohnenfernerkundung, wo große Flächen binnen kurzer Zeit abgeflogen werden können. Im Sommer kann man auf Aufnahmen die Einzelstöcke mitunter nicht erkennen und für Winteraufnahmen muss eine eigene Methodik entwickelt werden, um die Daten für die Vegetationszeit abzuleiten. Ein weiterer Punkt ist die Spektralerfassung auf Einzelstockebene, um sehen zu können, ob der Stock unter Stress leidet. Der Experte zeigte eine Aufnahme aus Niederdonven und erläuterte, dass man daraus ablesen kann, wo sich gesunde Stöcke befinden, wo die Fotosynthese bereits geringer ist und wo es Fehlstellen gibt.

## 7.5 Teilnahme an sonstigen Veranstaltungen

Wäibaudag 2020

Am 5. Februar 2020 fand im Kulturzentrum zu Wormeldange der **12. Lëtzebuerger Wäibaudag** statt. Das LIST war mit einer Präsentation von Miriam Machwitz (oben) zu Möglichkeiten und Grenzen der Erkennung von Peronospora mittel Fernerkundung und mit zwei Teilnehmern (Jürgen Junk und Daniel Molitor, unteres Bild, rechts) an der Prodiumsdiskussion mit dem Titel „Klimawandel – Wie können wir uns anpassen?“ vertreten.

# *BotRisk: simulating the annual bunch rot risk on grapevines (*Vitis vinifera *L. cv. Riesling) based on meteorological data*

**Daniel Molitor, Ottmar Baus, Yoanne Didry, Jürgen Junk, Lucien Hoffmann & Marco Beyer**


**International Journal of Biometeorology**

ISSN 0020-7128

Int J Biometeorol
DOI 10.1007/s00484-020-01938-5

Springer

International Journal of Biometeorology
https://doi.org/10.1007/s00484-020-01938-5

ORIGINAL PAPER

# BotRisk: simulating the annual bunch rot risk on grapevines (*Vitis vinifera* L. cv. Riesling) based on meteorological data

Daniel Molitor[1] · Ottmar Baus[2] · Yoanne Didry[1] · Jürgen Junk[1] · Lucien Hoffmann[1] · Marco Beyer[1]

Received: 19 April 2019 / Revised: 14 April 2020 / Accepted: 9 May 2020


## Abstract

The aim of the present investigations was to simulate the annual risk of bunch rot (*Botrytis cinerea*) on *Vitis vinifera* L. cv. Riesling grapes based on three long-term ($n = 3 \times 7 = 21$ cases) assessment data sets originating from three Central European grape-growing regions. Periods when meteorological parameters were significantly ($p < 0.01$) correlated with the cumulative degree day ($CDD_{7;18;24}$) reaching 5% disease severity were determined by Window Pane analysis. Analyses revealed five critical weather constellations ("events") influencing annual epidemics: relatively low temperatures after bud break, dry conditions during flowering, high temperatures after flowering, and low temperatures and high precipitation sums during/after veraison were all associated with thermal-temporal early epidemics. Meteorological data in each of the five events served as input for the bunch rot risk model "BotRisk." The multiple linear regression model resulted in an adjusted coefficient of determination ($R^2_{adj.}$) of 0.63. BotRisk enables (i) the simulation of the thermal-temporal position of the annual epidemic and, based on this, (ii) the classification of the annual bunch rot risk into three classes: low, medium, or high risk. According to leave-one-out cross-validation, 11 of 21 case studies were correctly classified. No systematic bias caused by location was observed, indicating that the transfer of the model into other locations with comparable climatic conditions could be possible. BotRisk (i) represents a novel viticultural decision support tool for crop cultural and chemical measures against bunch rot and (ii) enables an estimation of the bunch rot risk under changing environmental conditions.

**Keywords** *Botrytis cinerea* · Bunch rot risk · Climate change · Decision support tool · Cumulative degree days · Epidemiology · Window Pane analysis

## Introduction

Grape bunch rot caused by *Botrytis cinerea* is a major fungal disease on grapevines (*Vitis vinifera* L.) worldwide, threatening both grape yield and wine quality (Kassemeyer and Berkelmann-Löhnertz 2009; Smart and Robinson 1991). Under the climatic conditions of many traditional grape-growing regions, grape bunch rot appears virtually every season (Molitor et al. 2016).

Recent statistical investigations into the epidemics of *B. cinerea* in the *Vitis vinifera* cultivar Riesling recorded in Geisenheim/Germany enabled (i) the simulation of the epidemic disease progress and (ii) the identification of weather conditions with predictive value for annual grape bunch rot epidemics (Molitor et al. 2016). Here, the annual disease progress as a function of thermal time (summation of the physiologically effective temperature (Trudgill et al. 2005) reflecting the phenological development) turned out to be well described by sigmoidal curves ($0.97 < R^2$) with comparable slope factors in all years, while the thermal-temporal position of the epidemic strongly varied (Molitor et al. 2016). Window Pane analysis carried out according to Coakley and Line (1982) showed that annual weather conditions greatly affected the timing of the annual bunch rot epidemic, which is linked to the potential wine quality (Molitor et al. 2016).

**Electronic supplementary material** The online version of this article (https://doi.org/10.1007/s00484-020-01938-5) contains supplementary material, which is available to authorized users.

✉ Daniel Molitor
daniel.molitor@list.lu

[1] Environmental Research and Innovation (ERIN) Department, LIST – Luxembourg Institute of Science and Technology, 41, rue du Brill, L-4422 Belvaux, Luxembourg

[2] Hochschule Geisenheim University, Institute of Phytomedicine, Von-Lade-Str. 1, D-65366 Geisenheim, Germany

Published online: 20 May 2020

Grape bunch rot models have already been developed under different climatic conditions in the past, such as in the models of Broome et al. (1995), Nair and Allen (1993), and the "Bacchus" model (Agnew et al. 2004). Common to all of them is that they advise botryticide applications based on the interactions between temperature and wetness duration. All three models assume that the effects of temperature-dependent wetness durations on the infection level are constant during berry development. However, recent results (Molitor et al. 2016) demonstrated that wetness-based models might not be suitable to guide botryticide treatments in the case of the cultivar Riesling and in cool climate viticulture conditions.

The significant links established between annual weather conditions in specific periods of grape development and the seasonal bunch rot risk (Molitor et al. 2016) provide an excellent starting point to model the annual thermal-temporal position of the bunch rot epidemic (i) to quantify the annual bunch rot risk and (ii) to potentially support grape growers' decisions concerning bunch rot control measures.

To broaden the database for such a bunch rot risk model and make it more robust for local conditions or effects, in the present investigations, we analyzed a data set of 21 cases of annual bunch rot assessment series originating from three Central European grape-growing regions and their corresponding daily meteorological records.

The investigation aimed to (i) develop a bunch rot risk model simulating the annual risk in terms of the annual position of the bunch rot epidemic on the cultivar Riesling based on the output of Window Pane analysis and (ii) validate the model output to test its general suitability as a decision support tool for practical viticulture.

## Materials and methods

### Assessment and meteorological data

The progress of the grape bunch rot disease on the white *Vitis vinifera* L. cultivar Riesling was monitored between 2007 and 2013 (Geisenheim, Germany) and between 2010 and 2016 (Remich, Luxembourg; Deidesheim, Germany) at weekly to bi-weekly intervals between veraison and harvest. The Riesling vineyards under observation were trained in a vertical shoot positioning system and are described in detail in Table 1. No fungicides with known activity against *B. cinerea* (botryticides) were applied.

In the case of Geisenheim and Remich, visually observed disease severities were classified into seven classes (0%; 1–5%; 6–10%; 11–25%; 26–50%; 51–75%; 76–100%) following the EPPO guideline PP1/17. In Deidesheim, visually observed disease severities were classified into four classes (0%, 0.1–5%, 5.1–25%, 25.1–100%). One hundred randomly selected clusters were assessed in three (Deidesheim) or four (Geisenheim, Remich) replicated plots of the experimental vineyards. Average disease severities per plot were generally calculated by summing up the number of observations per class multiplied by the arithmetic mean of the class interval and dividing this sum by the total number of observations ($n$ = 100). Overall averages (whole observation vineyard) are the averages of the three or four plots, respectively.

For all locations, the daily average air temperatures (measured 2 m above the ground) and precipitation sums (measured 1 m above the ground) of the closest weather station were used. Distances between experimental vineyards and respective weather stations are given in Table 1. In the case of Deidesheim, weather data originated from Neustadt-Mussbach (Table 1). Key meteorological data from the three locations in the respective observation years are shown in Table 2.

### Disease progress curves

Sigmoidal curves have been demonstrated to be well adapted to the annual bunch rot epidemic under Central European conditions (Molitor et al. 2015, 2016, 2017, 2018, 2019; Porsche et al. 2018). Such sigmoidal curves were fitted to the disease severity data of each year and for each location plotted against the thermal time (summation of the physiologically effective temperature (Trudgill et al. 2005)) reflecting the phenological development using SigmaPlot 13 (Systat Software Inc., San Jose, CA, USA). This thermal time is expressed as the cumulative degree days $CDD_{7;18;24}$ after BBCH 65 (Molitor et al. 2016; Molitor et al. 2014b) using Eq. (1) following Molitor et al. (2016):

$$y = \frac{100}{1 + e^{-((x-x_0)/a)}} \quad (1)$$

where $y$ is the disease severity, $x$ the cumulative degree day $CDD_{7;18;24}$, $x_0$ the inflection point of the curve, and $a$ the slope factor of the curve in the inflection point.

For each of the year-location combination, parameters describing the disease progress curve were determined. Coefficients of determination ($R^2$) and significance levels ($p$) were determined to quantify the adaptation of the fitted curves to the observation data.

Based on Eq. (1), the cumulative degree day $CDD_{7;18;24}$, reaching a disease severity of 5% ($x_{5\%}$), was computed for every season. The threshold of 5% was selected following Beresford et al. (2006) and Evers et al. (2010).

### Window Pane analysis

To detect critical periods during the season (relative to the date of BBCH 65), when environmental variables were related

**Table 1** Features of the experimental vineyards

| Location | Geisenheim, Germany | Remich, Luxembourg | Deidesheim, Germany |
|---|---|---|---|
| Coordinates | 49.98 N, 7.95 E | 49.54 N, 6.35 E | 49.42 N, 8.19 E |
| Year of plantation | 1982 | 1994 | 1980 |
| Cultivar | Riesling | Riesling | Riesling |
| Clone | Gm 239 | unknown | N 90 |
| Rootstock | 5C | SO4 | 5C |
| Weather station | Geisenheim | Remich | Neustadt-Mussbach |
| Distance to weather station (km) | 0.1 | 0.1 | 5.1 |
| Observation years | 7 (2007–2013) | 7 (2010–2016) | 7 (2010–2016) |

with the thermal-temporal position of the epidemic, Window Pane analysis was conducted following the approach of Coakley and Line (1982), as described by Kriss et al. (2010). Window Pane analyses determine the length and the starting time of temporal windows during which average values of environmental variables are significantly correlated with plant disease levels at a specific time point (target) such as at the end of a season (Kriss et al. 2010; Molitor et al. 2016). In the present study, the impact of the environmental variables, i.e., the daily average air temperature and daily precipitation sum, on the cumulative degree day $CDD_{7;18;24}$ reaching a disease severity of 5%, was examined based on all 21 cases. Linear correlations between the summary environmental variables (average values of environmental variables in the different time windows) and the cumulative degree day $CDD_{7;18;24}$ reaching a disease severity of 5% (target) were calculated for the window widths 5, 10, 20, 30, 50, and 100 days. Pearson correlation coefficients ($r$ values) and significance levels ($p$ values) were determined for each summary environmental variable. Significant correlations were declared when individual $p$ values were below 0.05 and highly significant correlations when $p < 0.01$.

**Table 2** Key annual and growing season (April–October) meteorological variables in the three observation locations

| Location | Year | Mean annual temperature (°C) | Mean growing season temperature (°C) | Annual precipitation sum (mm) | Growing season precipitation sum (mm) |
|---|---|---|---|---|---|
| Geisenheim | 2007 | 11.5 | 15.7 | 509 | 274 |
| | 2008 | 10.9 | 15.2 | 535 | 339 |
| | 2009 | 10.8 | 16.1 | 583 | 311 |
| | 2010 | 9.7 | 14.9 | 658 | 426 |
| | 2011 | 11.3 | 16.0 | 469 | 305 |
| | 2012 | 10.8 | 15.3 | 531 | 330 |
| | 2013 | 10.4 | 15.5 | 557 | 397 |
| | Average | 10.8 | 15.5 | 549 | 340 |
| Remich | 2010 | 10.0 | 15.0 | 695 | 388 |
| | 2011 | 11.4 | 15.5 | 533 | 287 |
| | 2012 | 10.3 | 14.4 | 700 | 449 |
| | 2013 | 9.9 | 14.7 | 813 | 576 |
| | 2014 | 11.8 | 15.9 | 722 | 444 |
| | 2015 | 11.5 | 15.6 | 540 | 347 |
| | 2016 | 10.9 | 15.9 | 760 | 462 |
| | Average | 10.8 | 15.3 | 680 | 422 |
| Deidesheim | 2010 | 10.1 | 15.3 | 742 | 462 |
| | 2011 | 11.7 | 16.4 | 566 | 379 |
| | 2012 | 11.3 | 15.9 | 593 | 377 |
| | 2013 | 10.4 | 15.6 | 644 | 465 |
| | 2014 | 12.2 | 16.4 | 524 | 350 |
| | 2015 | 11.8 | 16.2 | 400 | 216 |
| | 2016 | 11.3 | 16.1 | 582 | 383 |
| | Average | 11.3 | 16.0 | 578 | 376 |

### Model development and validation

Window Pane analysis identified five critical meteorological constellations, hereafter referred to as "events," with highly significant correlations between the summary environmental variables and the $CDD_{7;18;24}$ values when reaching 5% disease severity ($x_{5\%}$). A multiple linear regression model based on one summary environmental variable in each of the five events was developed to simulate the $x_{5\%}$ value using the open access software tool R. The selection of potential input variables for the novel bunch rot risk model—hereafter referred to as "BotRisk"—took place in the following order:

1. Summary environmental variables causing a local maximum of the absolute $r$ values in a series of highly significant Pearson correlation coefficients ($p < 0.01$) in Window Pane analysis were selected in the different window widths.
2. Of these selected potential input variables, one summary environmental variable per event was included in the multiple linear regression model. The best model was selected based on the highest adjusted $R^2$ value of the model.

According to their calculated $CDD_{7;18;24}$ values, annual bunch rot risk classes were declared as follows:

– Class 1—"low" annual bunch rot risk:

predicted $CDD_{7;18;24}$ values reaching 5% disease severity > 1000

– Class 2—"medium" annual bunch rot risk:

predicted $CDD_{7;18;24}$ values reaching 5% disease severity > 900 and < = 1000

– Class 3—"high" annual bunch rot risk:

predicted $CDD_{7;18;24}$ values reaching 5% disease severity were < = 900.

Class ranges were defined to achieve (i) approximately equal numbers of observed cases in each of the three classes as well as (ii) class boundaries that were as round as possible for practical applications.

The predictive value was tested by leave-one-out cross-validation according to Ladenbruch and Mickey (1968). Predicted $CDD_{7;18;24}$ values reaching 5% disease severity values (as simulated by BotRisk) were calculated by averaging all but one (n - 1) data sets and compared with observed $CDD_{7;18;24}$ values (retrieved from disease progress curves). Coefficients of determination ($R^2_{adj.}$), mean bias errors (MBE), and mean absolute errors (MAE) of the cross-validated model were calculated. The validation of correct risk classification in the cross-validated model took place based on observed and predicted $CDD_{7;18;24}$ values reaching 5% disease severity.

## Results

### Disease progress as a function of thermal time

Disease severities at the different assessment dates and locations are shown in Table 3.

Sigmoidal curves of the type $y = \frac{100}{1+e^{-((x-x_0)/a)}}$ fitted the disease progress curves precisely ($r^2 \geq 0.87$, $p \leq 0.069$) (Supplementary Table 1; Fig. 1).

Disease severities of 5% were reached between 781 (Geisenheim 2010) and 1112 (Deidesheim 2012) cumulative degree days $CDD_{7;18;24}$.The average $CDD_{7;18;24}$ reaching 5% disease severity were 972 (Geisenheim), 931 (Remich), and 961 (Deidesheim) with no significant differences between locations according to the analysis of variance ($p = 0.05$) (Supplementary Table 1).

### Impact of environmental conditions

Supplementary Figs. 1 and Fig. 2 show the results of Window Pane analysis for the summary environmental variables' daily average temperatures and daily precipitation sum using all six tested window widths (5, 10, 20, 30, 50, 100 days). Pearson correlation coefficients as result of the Window Pane analysis are (as defined by Kriss et al. (2010)) generally depicted at the end of the respective summary period.

The following summary environmental variables were highly significantly ($p \leq 0.01$) and positively (high value ➔ late epidemic) correlated with the thermal-temporal position of the epidemic ($x_{5\%}$ value):

- Summary environmental variable daily average air temperature

- Bbetween − -42 and − -39, between 72 and 76 days as well as 91 days after BBCH 65 (D65) (window width:, 5 days),
- Bbetween − -39 and − -35 as well as between 75 and 80 D65 (window width:, 10 days),
- Bbetween − -30 and − -28 as well as between 75 and 90 D65 (window width,: 20 days),
- aAt − -19 and − -18, between 73 and 85 as well as between 88 and 99 D65 (window width:, 30 days),
- Bbetween 88 and 108 D65 (window width,: 50 days)

**Table 3** *Botrytis cinerea* disease severities at the different assessment dates in the different observation years in Geisenheim, Remich, and Deidesheim

| | Year | Date | DOY * | $D_{65}$ | $CDD_{7;18;24}$ after BBCH 65 | Disease severity |
|---|---|---|---|---|---|---|
| Geisenheim | 2007 | 22.08. | 234 | 86 | 850.9 | 0.4 |
| | 2007 | 28.08. | 240 | 92 | 914.4 | 0.6 |
| | 2007 | 04.09. | 247 | 99 | 975.5 | 3.3 |
| | 2007 | 24.09. | 267 | 119 | 1120.5 | 9.6 |
| | 2007 | 09.10. | 282 | 134 | 1211.5 | 44.4 |
| | 2008 | 27.08. | 239 | 81 | 829.9 | 0.2 |
| | 2008 | 10.09. | 253 | 95 | 967.9 | 1.7 |
| | 2008 | 09.10. | 282 | 124 | 1111 | 32.3 |
| | 2009 | 15.09. | 258 | 98 | 999.4 | 0.5 |
| | 2009 | 22.09. | 265 | 105 | 1074.4 | 6.7 |
| | 2009 | 01.10. | 274 | 114 | 1149.6 | 12.1 |
| | 2009 | 08.10. | 281 | 121 | 1200 | 38.0 |
| | 2010 | 31.08. | 243 | 70 | 724.2 | 2.2 |
| | 2010 | 10.09. | 253 | 80 | 801 | 4.1 |
| | 2010 | 14.09. | 257 | 84 | 836.4 | 18.6 |
| | 2010 | 23.09. | 266 | 93 | 894.1 | 41.7 |
| | 2010 | 29.09. | 272 | 99 | 921.4 | 48.2 |
| | 2010 | 07.10. | 280 | 107 | 980.5 | 80.8 |
| | 2010 | 14.10. | 287 | 114 | 1009.5 | 92.4 |
| | 2011 | 29.08. | 241 | 89 | 884.5 | 7.7 |
| | 2011 | 05.09. | 248 | 96 | 952.9 | 19.2 |
| | 2011 | 13.09. | 256 | 104 | 1034.4 | 60.7 |
| | 2011 | 19.09. | 262 | 110 | 1077.1 | 82.3 |
| | 2012 | 05.09. | 248 | 83 | 862.2 | 0.8 |
| | 2012 | 12.09. | 255 | 90 | 929.1 | 1.0 |
| | 2012 | 18.09. | 261 | 96 | 973.6 | 2.7 |
| | 2012 | 25.09. | 268 | 103 | 1012.7 | 6.8 |
| | 2012 | 02.10. | 275 | 110 | 1048.6 | 11.9 |
| | 2012 | 08.10. | 281 | 116 | 1080.2 | 20.9 |
| | 2012 | 12.10. | 285 | 120 | 1090.5 | 25.0 |
| | 2013 | 09.09. | 252 | 77 | 791.9 | 0.2 |
| | 2013 | 16.09. | 259 | 84 | 842.4 | 0.7 |
| | 2013 | 23.09. | 266 | 91 | 886.1 | 2.9 |
| | 2013 | 30.09. | 273 | 98 | 932 | 7.1 |
| | 2013 | 08.10. | 281 | 106 | 975 | 13.1 |
| | 2013 | 14.10. | 287 | 112 | 988.7 | 37.0 |
| | 2013 | 21.10. | 294 | 119 | 1029.1 | 65.7 |
| Remich | 2010 | 09.09. | 252 | 74 | 743.8 | 0.6 |
| | 2010 | 21.09. | 264 | 86 | 830.0 | 1.4 |
| | 2010 | 28.09. | 271 | 93 | 869.9 | 2.9 |
| | 2010 | 06.10. | 279 | 101 | 935.9 | 12.3 |
| | 2010 | 13.10. | 286 | 108 | 980.2 | 30.9 |
| | 2011 | 10.08. | 222 | 67 | 623.1 | 0.0 |
| | 2011 | 24.08. | 236 | 81 | 775.4 | 0.1 |
| | 2011 | 06.09. | 249 | 94 | 890.8 | 1.6 |
| | 2011 | 14.09. | 257 | 102 | 965.5 | 3.1 |
| | 2011 | 22.09. | 265 | 110 | 1020.4 | 7.7 |
| | 2011 | 28.09. | 271 | 116 | 1075.9 | 13.1 |
| | 2012 | 17.09. | 260 | 88 | 865.7 | 0.0 |

**Table 3** (continued)

| | Year | Date | DOY * | $D_{65}$ | $CDD_{7;18;24}$ after BBCH 65 | Disease severity |
|---|---|---|---|---|---|---|
| | 2012 | 01.10. | 274 | 102 | 929.1 | 0.4 |
| | 2012 | 08.10. | 281 | 109 | 959.5 | 2.3 |
| | 2012 | 15.10. | 288 | 116 | 974.6 | 5.8 |
| | 2012 | 24.10. | 297 | 125 | 1038.8 | 20.4 |
| | 2013 | 17.09. | 260 | 75 | 726.1 | 0.5 |
| | 2013 | 01.10. | 274 | 89 | 816.2 | 4.9 |
| | 2013 | 08.10. | 281 | 96 | 858.4 | 7.0 |
| | 2013 | 14.10. | 287 | 102 | 869.5 | 14.7 |
| | 2014 | 01.09. | 244 | 79 | 779.0 | 1.1 |
| | 2014 | 16.09. | 259 | 94 | 928.4 | 3.1 |
| | 2014 | 22.09. | 265 | 100 | 988.9 | 5.1 |
| | 2014 | 30.09. | 273 | 108 | 1047.1 | 10.3 |
| | 2014 | 07.10. | 280 | 115 | 1105.2 | 22.8 |
| | 2015 | 31.08. | 243 | 76 | 738.1 | 0.0 |
| | 2015 | 17.09. | 260 | 93 | 871.5 | 5.5 |
| | 2015 | 23.09. | 266 | 99 | 910.8 | 23.6 |
| | 2015 | 30.09. | 273 | 106 | 956.3 | 38.8 |
| | 2016 | 05.09. | 248 | 71 | 733.2 | 0.4 |
| | 2016 | 19.09. | 262 | 85 | 879.1 | 0.6 |
| | 2016 | 28.09. | 271 | 94 | 956.0 | 2.8 |
| | 2016 | 05.10. | 278 | 101 | 1000.4 | 5.9 |
| | 2016 | 12.10. | 285 | 108 | 1017.0 | 17.1 |
| | 2016 | 18.10. | 291 | 114 | 1039.6 | 22.1 |
| Deidesheim** | 2010 | 16.09. | 259 | 92 | 907.1 | 2.3 |
| | 2010 | 23.09. | 266 | 99 | 950.8 | 4.7 |
| | 2010 | 01.10. | 274 | 107 | 990.6 | 8.6 |
| | 2011 | 05.09. | 248 | 99 | 1001.9 | 9.7 |
| | 2011 | 12.09. | 255 | 106 | 1075.1 | 20.0 |
| | 2012 | 03.09. | 246 | 82 | 862.9 | 0.0 |
| | 2012 | 10.09. | 253 | 89 | 937.0 | 0.1 |
| | 2012 | 17.09. | 260 | 96 | 993.2 | 0.4 |
| | 2012 | 24.09. | 267 | 103 | 1041.1 | 1.1 |
| | 2012 | 01.10. | 274 | 110 | 1078.8 | 2.4 |
| | 2013 | 26.08. | 238 | 60 | 629.8 | 0.2 |
| | 2013 | 02.09. | 245 | 67 | 703.2 | 0.4 |
| | 2013 | 09.09. | 252 | 74 | 777.3 | 0.4 |
| | 2013 | 16.09. | 259 | 81 | 827.4 | 1.1 |
| | 2013 | 23.09. | 266 | 88 | 871.8 | 6.2 |
| | 2013 | 30.09. | 273 | 95 | 918.4 | 13.3 |
| | 2013 | 07.10. | 280 | 102 | 949.6 | 24.6 |
| | 2014 | 18.08. | 230 | 71 | 746.9 | 0.0 |
| | 2014 | 25.08. | 237 | 78 | 801.0 | 0.4 |
| | 2014 | 01.09. | 244 | 85 | 869.5 | 1.5 |
| | 2014 | 08.09. | 251 | 92 | 942.4 | 3.2 |
| | 2014 | 15.09. | 258 | 99 | 1004.9 | 7.1 |
| | 2014 | 22.09. | 265 | 106 | 1072.5 | 13.5 |
| | 2015 | 17.08. | 229 | 69 | 676.5 | 0.0 |
| | 2015 | 24.08. | 236 | 76 | 748.4 | 0.1 |
| | 2015 | 31.08. | 243 | 83 | 819.3 | 0.9 |

**Table 3** (continued)

| Year | Date | DOY * | $D_{65}$ | $CDD_{7;18;24}$ after BBCH 65 | Disease severity |
|---|---|---|---|---|---|
| 2015 | 07.09. | 250 | 90 | 876.9 | 8.6 |
| 2015 | 14.09. | 257 | 97 | 938.6 | 14.0 |
| 2016 | 22.08. | 234 | 71 | 740.8 | 0.0 |
| 2016 | 29.08. | 241 | 78 | 813.7 | 0.0 |
| 2016 | 05.09. | 248 | 85 | 890.7 | 0.7 |
| 2016 | 12.09. | 255 | 92 | 967.6 | 2.3 |
| 2016 | 19.09. | 262 | 99 | 1038.3 | 7.9 |
| 2016 | 26.09. | 269 | 106 | 1093.3 | 12.4 |

DOY, day of the year; $D_{65}$, days after BBCH 65; $CDD_{7;18;24}$, cumulative degree days according to Molitor et al. (2016). Assessment data from Geisenheim were originally published in Molitor et al. (2016)

*29 February was not considered in leap years

**Assessment data from Deidesheim were kindly provided by DLR Rheinpfalz, Neustadt/Weinstraße

- Summary environmental variable daily precipitation sum

- At 4 $D_{65}$ (window width, 5 days)
- Between 6 and 8 $D_{65}$ (window width, 10 days)
- At 17 $D_{65}$ (window width, 20 days)
- At 38, 47 as well as between 41 and 44 $D_{65}$ (window width, 50 days)

On the other hand, the following summary environmental variables were significantly and negatively (low value ➔ late epidemic) correlated with the thermal-temporal position of the epidemic ($x_{5\%}$ value):

- Summary environmental variable daily average air temperature

- Between 32 and 34 $D_{65}$ (window width, 5 days)
- Between 38 and 40 $D_{65}$ (window width, 50 days)

- Summary environmental variable daily precipitation sum

- At 77 as well as between 80 and 87 $D_{65}$ (window width, 20 days)
- Between 81 and 87 $D_{65}$ (window width, 30 days)
- Between 100 and 108 as well as between 110 and 123 $D_{65}$ (window width, 50 days) (Supplementary Fig. 1, Fig. 2)

Analyses revealed five critical meteorological "events" where summary environmental variables were highly significantly ($p \leq 0.01$) correlated with the thermal-temporal position of the epidemic ($x_{5\%}$ value) in different window widths:

– Temperatures around 40 days prior to flowering (event 1)
– Temperatures around 30 days after flowering (event 2)
– Temperatures around 70 days after flowering (event 3)
– Precipitation around flowering (event 4)
– Precipitation around 70 days after flowering (precipitation) (event 5)

## BotRisk model to simulate the position of the annual bunch rot (*Botrytis cinerea*) epidemic

Multiple linear regression kept the following input variables for the BotRisk model:

– Event 1: summary environmental variable temperature on day − 38 $D_{65}$ (window width, 10 days) = variable a

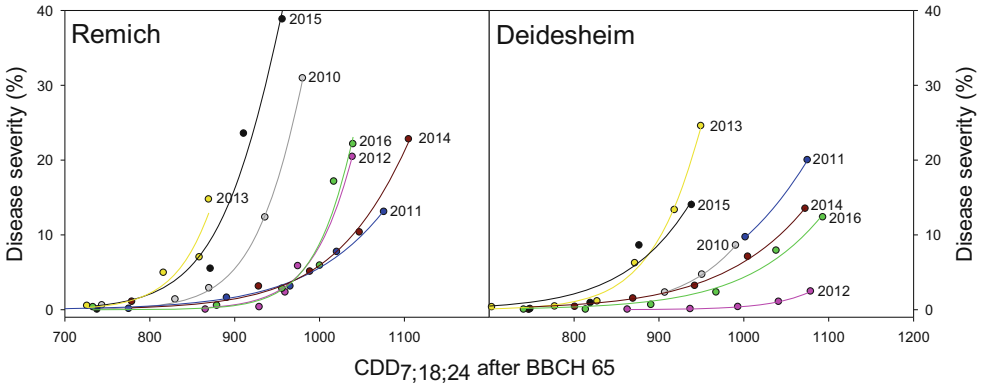


**Fig. 1** Disease progress curves in Remich and Deidesheim in the different seasons as functions of the thermal time ($CDD_{7;18;24}$ after BBCH 65). Disease progress curves of Geisenheim are illustrated in Molitor et al. (2016)

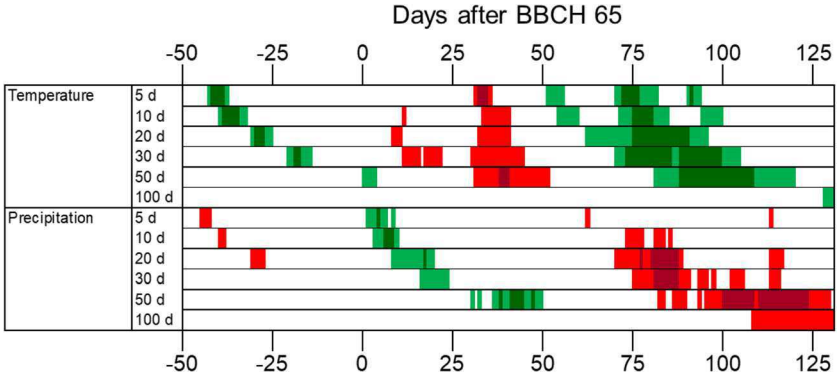


**Fig. 2** Significant (significance level: $p \leq 0.05$) positive (green), highly significant ($p \leq 0.01$) positive (dark green), significant ($p \leq 0.05$) negative (red), or highly significant ($p \leq 0.01$) negative (dark red) correlations between the summary environmental variables of daily average temperatures (temperature) and daily precipitation sums (precipitation) and the cumulative degree days $CDD_{7;18;24}$ reaching a disease severity of 5%) depending on (i) the starting date of a window (relative to the date of BBCH 65) and (ii) the window width according to Window Pane analysis. Correlation coefficients are depicted on the last day of each temporal window

- Event 2: summary environmental variable temperature on day 33 $D_{65}$ (window width, 5 days) = variable b
- Event 3: summary environmental variable temperature on day 74 $D_{65}$ (window width, 5 days) = variable c
- Event 4: summary environmental variable precipitation on day 17 $D_{65}$ (window width, 20 days) = variable d
- Event 5: summary environmental variable precipitation on day 87 $D_{65}$ (window width, 30 days) = variable e

Based on this model, the $CDD_{7;18;24}$ reaching 5% disease severity can be calculated as follows:

951.476

+ 7.2173 * summary environmental variable temperature on day − 38 $D_{65}$ (window width, 10 days)

– 16.317 * summary environmental variable temperature on day 33 $D_{65}$ (window width, 5 days)

+ 10.793 * summary environmental variable temperature on day 74 $D_{65}$ (window width, 5 days)

+ 21.986 * summary environmental variable precipitation on day 17 $D_{65}$ (window width, 20 days)

+ 2.512 *summary environmental variable precipitation on day 87 $D_{65}$ (window width, 30 days)

$R^2$ of the model is 0.7244, $R^2_{adj.}$ (model accuracy) 0.6325, and the $p$ value of the model 0.0008.

Leave-one-out cross-validation resulted in a coefficient of determination ($R^2_{cv}$) of 0.51. The mean bias errors (MBE) in the leave-one-out cross-validation were − 10.8 $CDD_{7;18;24}$ for Geisenheim, − 1.5 $CDD_{7;18;24}$ for Remich, and 14.4 $CDD_{7;18;24}$ for Deidesheim (overall average MBE, 0.7 $CDD_{7;18;24}$) with mean absolute errors (MAE) of 61.5 (Geisenheim), 45.6 (Remich), and 54.6 $CDD_{7;18;24}$ (Deidesheim) (overall average MAE, 53.9 $CDD_{7;18;24}$). The leave-one-out cross-validation of the classification of annual bunch rot risk classes demonstrated that in 11 of 21 cases, the predicted classification matched the observed classification. In four cases, observed classes were one class higher than the predicted classes and in six cases, one class lower than the predicted classes. No cases were observed in which the prediction indicated a high risk, but a low risk was observed in practice and vice versa (Fig. 3, Table 4).

## Discussion

### Impact of meteorological conditions on the annual epidemic

Window Pane analysis demonstrated that the annual thermal-temporal position of the bunch rot epidemic was independent

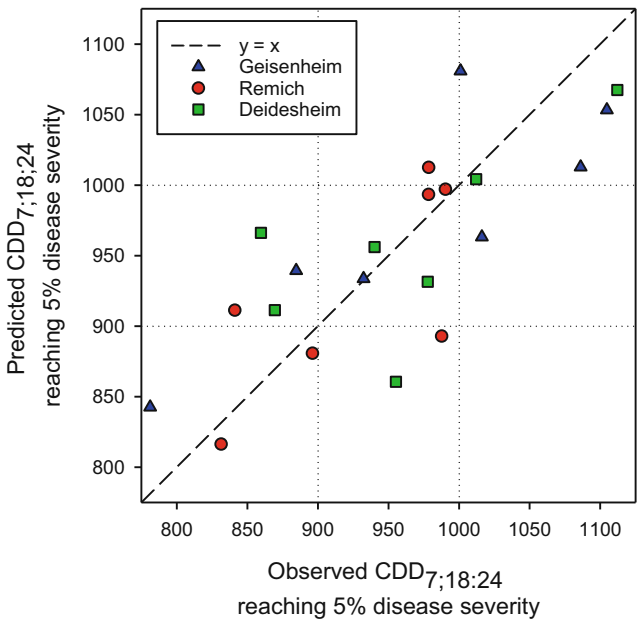


**Fig. 3** Leave-one-out cross-validation: Predicted plotted versus the observed cumulative degree days $CDD_{7;18;24}$ after BBCH 65 reaching a disease severity of 5% in Geisenheim (blue triangles), Remich (red circles), and Deidesheim (green squares). The dashed line represents the 1:1 relationship. The dotted lines represent the frontiers of the risk classes according to the bunch rot risk model BotRisk

**Table 4** Cross-validation of the classification of annual bunch rot risk classes

| | | Observed | | | |
|---|---|---|---|---|---|
| | | Class 3 "high risk" | Class 2 "medium risk" | Class 1 "low risk" | Sum |
| Predicted | Class 1 "low risk" | 0 | 2 | 4 | 6 |
| | Class 2 "medium risk" | 4 | 4 | 2 | 10 |
| | Class 3 "high risk" | 3 | 2 | 0 | 5 |
| | Sum | 7 | 8 | 6 | 21 |

The predicted number of cases according to leave-one-out cross-validation in classes 1 to 3 is plotted against the observed number of cases in the respective classes. Class 1, "low" annual bunch rot risk: predicted CDD7;18;24 values reaching 5% disease severity > 1000; class 2, "medium" annual bunch rot risk: predicted CDD7;18;24 values reaching 5% diseases severity > 900 and < = 1000; class 3, "high" annual bunch rot risk: predicted CDD7;18;24 values reaching 5% diseases severity were < = 900

of the location and significantly correlated with the meteorological conditions in specific periods of grape phenology.

Five distinct periods (referred to as critical "events") were identified when meteorological conditions were of high prognostic value for the annual thermal-temporal position of the epidemic:

Event 1: Post-bud break period (temperatures)

Obviously, high temperatures in the period around − 40 days $D_{65}$ are linked to a thermal-temporal late annual bunch rot epidemic. For the years 1993 to 2015, BBCH 63 was reached in Luxembourg on average 56 days after BBCH 09 (bud break) (Molitor and Keller 2016). Hence, the critical event identified here represents the period of approximately 16 days after bud break. Warm conditions during the initial shoot development and flower formation period in spring are leading to increased flower sizes (Keller 2015). Interestingly, studies with the cultivar Sauvignon blanc in 2010 showed that the elongation effects of gibberellic acid applications on the cluster stem length were most pronounced where the treatment was applied 14 to 36 days after budburst (Molitor et al. 2012b), which indicates that this period might be the most crucial period for inflorescence stem growth. Potentially, the effect of warm post-bud break temperatures on the epidemic might be explained by an elongation of the cluster stems leading to a looser cluster structure. The latter has been demonstrated several times to be strongly correlated with a lower predisposition to bunch rot (e.g., Molitor et al. (2012a, 2015); Hed et al. (2009); Intrigliolo et al. (2014); Tello and Ibanez (2017)).

Event 2: Post-flowering period (temperatures)

The present investigation demonstrated that high temperatures in a period of approximately 30 days after flowering were significantly correlated with an early epidemic. We suppose that this effect might be explained by intensified cell division and cell expansion processes under warm conditions in this period (Keller 2015), leading to more compact grape clusters.

Events 3 and 5: Period between veraison and harvest (temperatures + precipitation)

While the effects of meteorological conditions on the annual bunch rot epidemic in events 1 and 2 can supposedly be explained by indirect effects on the cluster structure, the link between high precipitation sums between veraison and harvest and the thermal-temporal position of the epidemic might be caused by the following direct effect of moist conditions on the epidemiology of the disease:

(i) The availability of water promotes the development of fungal pathogens.
(ii) High post-veraison water availability facilitates the water uptake into the berries, resulting in larger berries, compact clusters, and a high risk of the fruit cracking (Keller et al. 2003).
(iii) Rain events after veraison re-activate latent *B. cinerea* infections, which often lead to direct infections of ripening berries (Evans and Emmett 2011).

Most likely, the inverse influence of air temperature and precipitation between veraison and harvest on bunch rot epidemics is related to the frequently observed negative association between precipitation and temperature during the summer months under Central European conditions.

However, especially under changing environmental conditions, extreme events such as severe rain events in combination with high air temperatures or combinations of both are becoming more likely (IPCC 2012), and those conditions are highly favorable for fungal infections. Consequently, to keep the model robust against those non-steady environmental factors, both variables remained in the model even though some collinearity between them exists.

Event 4: Flowering period (precipitation)

Furthermore, there was a strong link between the amount of precipitation during the flowering process and the thermal-temporal position of the annual epidemic. As described before

(Molitor et al. 2016), wet weather conditions around grape bloom are associated with a (thermal-temporal) late annual bunch rot epidemic. This supports the hypothesis that during grape flowering, in particular, adverse weather conditions are reducing the degree of the fruit set—as described by Kliewer (1977), Nesbitt et al. (2016), and Mosedale et al. (2015)—and, consequently, are loosening the bunch structure and reducing the predisposition to bunch rot.

The observed phenomena demonstrated that the same environmental factor can have both, a positive or a negative effect on the thermal-temporal position of the epidemic depending on the phenological stage of the host plants.

## The bunch rot risk model BotRisk

Based on the highly significant correlations between the meteorological conditions and the $CDD_{7;18;24}$ reaching a disease severity of 5% in the five critical events identified above, the novel bunch rot risk model BotRisk was developed using a multiple linear regression approach with five input variables.

Model validation showed that the model did not markedly over- or underestimate the time point reaching 5% disease severity in any of the three locations. On average, the overall mean absolute error (MAE) of the cross-validated model was 53.9 $CDD_{7;18;24}$, which reflects a time frame of 6 days (assuming an average daily temperature of 16.0 °C; average (2000–2009) September temperatures in Geisenheim/Germany, 15.6 °C, in Remich/Luxembourg, 15.6 °C).

Observed adjusted coefficients of determination show an adequate level of goodness of fit for the model to simulate the cumulative degree days reaching 5% disease severity ($R^2_{adj.}$ = 0.633). Obviously, there are other factors besides air temperature and precipitation that influence the thermal-temporal position of the epidemic. Potentially, unexplained variance between the different years might be due to crop cultural practices changing from year to year: e.g., the moment of first shoot topping has been demonstrated to influence the annual epidemic in a significant manner (Molitor et al. 2015).

Furthermore, the annual epidemic might have been influenced by grape pests, such as the grape berry moth (*Lobesia botrana* (Denis & Schiffermüller), *Eupoecilia ambiguella* (Hübner)), or fungal diseases, such as powdery mildew (*Erysiphe necator* Schwein.), which are able to wound berry skin and create entry points for *Botrytis cinerea*. Furthermore, frequently observed fluctuations in the annual yield level (Molitor and Keller 2016) and, in consequence, differences in the pace of grape maturation after veraison might have influenced the epidemic.

Interestingly, in the present model, the influence of the location (potentially including differences in soil type, soil fertility or soil management, fertilization, grape vigor, age of plants, rootstock, clone, planting density, canopy management regime) turned out to be of minor importance. This is demonstrated by the fact that the differences in the mean bias errors of the model caused by the location are negligible (MBE, − 10.8 to 14.4 $CDD_{7;18;24}$ = − 1.2 to 1.6 days (assuming a daily average temperature of 16 °C)). Potential location differences caused by generally higher or generally lower temperatures at specific sites may have been adjusted for during the calculation of the $CDD_{7;18;24}$. Furthermore, validation indicates that model transfer to other locations with comparable climatic conditions might be possible. However, keeping in mind that Geisenheim, Remich, and Deidesheim are located in cool climate viticulture regions with comparable climatic conditions, the present model should not be directly transferred to regions with markedly deviating climatic conditions without previous validation with local data sets.

The predicted risk class differed by a maximum of one class compared with the observation class. I.e., in none of the 21 studied cases did the model predict a low bunch rot risk while a high bunch rot risk was observed or vice versa.

## Potential BotRisk applications

BotRisk enables a simulation of the thermal-temporal position of the annual bunch rot epidemic in the Riesling cultivar in the past or (based on climate projections) in the future even if only the basic, most frequently recorded environmental variables, temperatures, and precipitation, are available. Here, the calculated $CDD_{7;18;24}$ reaching a disease severity of 5% functions as the annual risk indicator. The lower the simulated annual value of the $CDD_{7;18;24}$ reaching a disease severity of 5%, the higher the annual risk for an early bunch rot epidemic. Based on this, three bunch rot risk classes have been defined indicating years with low, medium, or high bunch rot risk.

Founded on observation data from the three first critical events coupled with long-term average data for the two missing critical events 3 and 5 in the period between veraison and harvest, an estimation of the annual bunch rot risk of the present season can be realized around 1 month after flowering, and this information can then be integrated into the bunch rot control strategy. This might, under practical conditions, support the decisions, if botryticide applications (e.g., at bunch closure or veraison) or crop cultural measures are necessary or (monetarily as well as environmentally) meaningful. In the past, practical bunch rot control strategies were mainly based on routine fungicide applications (Shtienberg 2007). However, excessive chemical bunch rot control measures are becoming increasingly criticized and restricted (Elmer and Michailides 2007; Shtienberg 2007). Consequently, the classification of the annual bunch rot risk might be efficiently implemented in the fungicide regime as a measure of Integrated Pest Management enabling either (i) a reduction of the number of botryticide applications and thus a reduction in pesticide use in years with a lower bunch rot risk or (ii) a

higher bunch rot control efficiency due to the targeted application of botryticides in years with a high bunch rot risk.

The annual thermal-temporal position of the epidemic has been demonstrated to be significantly correlated with annual wine quality (Molitor et al. 2016) as the presence of *B. cinerea* at early (unripe) stages of berry development negatively affects wine composition (because of berry decay) and hinders further grape maturation (Molitor et al. 2012a). BotRisk might be combined with phenological models (Molitor et al. 2014b, 2016, 2020) as well as regional or local climate change projections (Molitor et al. 2014a; Molitor and Junk 2019) aiming for a simulation of the bunch rot disease progress in relation to the progress of the grape phenology/maturity. This study might reveal if the risk of vintages with an early bunch rot epidemic at stages of incomplete grape maturity (leading to low potential wine quality) is supposed to increase or decrease in the future and if specific adaptation strategies might become necessary.

## Conclusions

The annual meteorological conditions during specific periods of grape development are significantly correlated with the thermal-temporal position of the bunch rot epidemic on *Vitis vinifera* L. cv. Riesling. Based on periods of highly significant correlations between meteorological data and the thermal-temporal position of the epidemic, the bunch rot risk model BotRisk was developed based on a multiple linear regression approach. BotRisk allows for a simulation of the annual thermal-temporal position of the bunch rot epidemic in Riesling based on temperature and precipitation records in different periods of grape development with an accuracy ($R^2_{adj.}$) of 0.63 and classifies the annual bunch rot risk in three risk classes. The observed minor influence of the location on model robustness indicates that a transfer into other locations of comparable climatic conditions might be possible. Presently, BotRisk represents a bunch rot risk model for the grape cultivar Riesling. However, the approach of BotRisk is open for parameterization for other cultivars based on respective long-term observation data sets.

**Acknowledgments** The authors thank A. Ehlig (Hochschule Geisenheim University, Geisenheim, Germany); R. Mannes and S. Fischer (Institut Viti-Vinicole, Remich, Luxembourg) for providing weather data; B. Ziegler and U. Schäfer (DLR Rheinpfalz, Neustadt/Weinstrasse, Germany) for bunch rot assessment data from Deidesheim; M. Keller (Washington State University, Prosser, Washington, USA), C. Bossung, O. Parisot, P. Bruneau, and B. Otjacques (LIST, Belvaux, Luxembourg) for fruitful discussion; L. Auguin (LIST) for language editing; O. Faber (LIST) for his support in GIS; and the Institut Viti-Vinicole for financial support in the framework of the research projects "ProVino – pesticide reduction in viticulture" and "TerroirFuture - Impact of climate change on viticulture and wine typicity in the AOP region 'Moselle Luxembourgeoise' – risk assessment and potential adaptation strategies," as well as the European Union for supporting the project "Clim4Vitis - climate change impact mitigation for European viticulture: knowledge transfer for an integrated approach" (grant agreement No 810176).

## References

Agnew RH, Mundy DC, Balasubramaniam R (2004) Effects of spraying strategies based on monitored disease risk on grape disease control and fungicide usage in Marlborough. N Z Plant Protect 57:30–36

Beresford RM, Evans KJ, Wood PN, Mundy DC (2006) Disease assessment and epidemic monitoring methodology for bunch rot (*Botrytis cinerea)* in grapevines. N Z Plant Protect 59:355–360

Broome JC, English JT, Marois JJ, Latorre BA, Aviles JC (1995) Development of an infection model for Botrytis bunch rot of grapes based on wetness duration and temperature. Phytopathology 85:97–102

Coakley SM, Line RF (1982) Prediction of stripe rust epidemics on winter wheat using statistical models. Phytopathology 72:1006

Elmer PAG, Michailides TJ (2007) Epidemiology of *Botrytis cinerea* in orchards and vine crops. In: Elad Y, Williamson K, Tudzynski P, Delen N (eds) *Botrytis*: biology, pathology and control. Springer, Dordrecht, pp 243–272

Evans KJ, Emmett RW (2011) Botrytis. Questions and answers. Grape and Wine Research and Development Corporation + Innovators network

Evers D, Molitor D, Rothmeier M, Behr M, Fischer S, Hoffmann L (2010) Efficiency of different strategies for the control of grey mold on grapes including gibberellic acid (Gibb3), leaf removal and/or botryticide treatments. J Int Sci Vigne Vin 44:151–159

Hed B, Ngugi HK, Travis JW (2009) Relationship between cluster compactness and bunch rot in Vignoles grapes. Plant Dis 93:1195–1201

Intrigliolo DS, Llacer E, Revert J, Esteve MD, Climent MD, Palau D, Gomez I (2014) Early defoliation reduces cluster compactness and improves grape composition in Mandó, an autochthonous cultivar of *Vitis vinifera* from southeastern Spain. Sci Hortic 167:71–75

IPCC (2012) Managing the risks of extreme events and disasters to advance climate change adaptation. In: Field CB et al (eds) A special report of working groups I and II of the Intergovernmental Panel on Climate Change. Cambridge University Press, Cambrige and New York, p 582

Kassemeyer H-H, Berkelmann-Löhnertz B (2009) Fungi of grapes. In: König H, Unden G, Fröhlich J (eds) Biology of microorganisms on grapes, in must and in wine. Springer-Verlag, Berlin, Heidelberg, pp 61–87

Keller M (2015) The science of grapevines. Anatomy and physiology, 2nd edn. Elsevier Academic Press, London

Keller M, Viret O, Cole FM (2003) *Botrytis cinerea* infection in grape flowers: defense reaction, latency, and disease expression. Phytopathology 93:316–322

Kliewer WM (1977) Effect of high temperatures during the bloom-set period on fruit-set, ovule fertility, and berry growth of several grape cultivars. Am J Enol Viticult 28:215–222

Kriss AB, Paul PA, Madden LV (2010) Relationship between yearly fluctuations in Fusarium Head Blight intensity and environmental variables: a window-pane analysis. Phytopathology 100:784–797

Ladenbruch PA, Mickey MR (1968) Estimation of error rates in discriminant analysis. Technometrics 10:1–11

Molitor D, Junk J (2019) Climate change is implicating a two-fold impact on air temperature increase in the ripening period under the conditions of the Luxembourgish grapegrowing region. Oeno One 53:409–422

Molitor D, Keller M (2016) Yield of Müller-Thurgau and Riesling grapevines is altered by meteorological conditions in the current and the previous growing seasons. Oeno One 50:245–258

Molitor D, Behr M, Hoffmann L, Evers D (2012a) Impact of grape cluster division on cluster morphology and bunch rot epidemic. Am J Enol Viticult 63:508–514

Molitor D, Behr M, Hoffmann L, Evers D (2012b) Research note: benefits and drawbacks of pre-bloom applications of gibberellic acid (GA3) for stem elongation in sauvignon blanc. S Afric J Enol Vitic 33:198–202

Molitor D, Caffarra A, Sinigoj P, Pertot I, Hoffmann L, Junk J (2014a) Late frost damage risk for viticulture under future climate conditions: a case study for the Luxembourgish winegrowing region. Austr J Grape Wine R 20:160–168

Molitor D, Junk J, Evers D, Hoffmann L, Beyer M (2014b) A high resolution cumulative degree day based model to simulate phenological development of grapevine. Am J Enol Viticult 65:72–80

Molitor D, Baron N, Sauerwein T, Kicherer A, Döring J, André C, Stoll M, Beyer M, Hoffmann L, Evers D (2015) Postponing first shoot topping reduces grape cluster compactness and delays bunch rot epidemic. Am J Enol Viticult 66:164–176

Molitor D, Baus O, Hoffmann L, Beyer M (2016) Meteorological conditions determine the thermal-temporal position of the annual Botrytis bunch rot epidemic on *Vitis vinifera* L. cv. Riesling grapes. Oeno One 50:231–244

Molitor D, Hoffmann L, Beyer M (2017) Overall efficacies of combined measures for controlling grape bunch rot can be estimated by multiplicative consideration of individual effects. Oeno One 51:387–393

Molitor D, Biewers B, Junglen M, Schultz M, Clementi P, Permesang G, Regnery D, Porten M, Herzog K, Hoffmann L, Beyer M, Berkelmann-Löhnertz B (2018) Multi-annual comparisons demonstrate differences in the bunch rot susceptibility of nine *Vitis vinifera* L. cv. Riesling clones. Vitis 57:17–25

Molitor D, Schultz M, Mannes R, Pallez-Barthel M, Hoffmann L, Beyer M (2019) Semi-minimal pruned hedge: a potential climate change adaptation strategy in viticulture. Agronomy 9:173

Molitor D, Fraga H, Junk J (2020) UniPhen – a unified model approach to simulate the phenological development of grape cultivars under cool climate conditions. Agric For Meteorol (in review)

Mosedale JR, Wilson RJ, Maclean IMD (2015) Climate change and crop exposure to adverse weather: changes to frost risk and grapevine flowering conditions. PLoS One 10:e0141218

Nair NG, Allen RN (1993) Infection of grape flowers and berries by *Botrytis cinerea* as a function of time and temperature. Mycol Res 97:1012–1014

Nesbitt A, Kemp B, Steele C, Lovet A, Dorling S (2016) Impact of recent climate change and weather variability on the viability of UK viticulture – combining weather and climate records with producers' perspectives. Austr J Grape Wine R 22:324–335

Porsche F, Molitor D, Beyer M, Charton S, André C, Kollar A (2018) Antifungal activity of saponins from the fruit pericarp of *Sapindus mukorossi* against *Venturia inaequalis* and *Botrytis cinerea*. Plant Dis 102:991–1000

Shtienberg D (2007) Rational management of *Botrytis*-incited diseases: integration of control measures and use of warning systems. In: Elad Y, Williamson K, Tudzynski P, Delen N (eds) *Botrytis*: biology, pathology and control. Springer, Dordrecht, pp 335–347

Smart R, Robinson M (1991) Sunlight into wine. A handbook for winegrape canopy management. Winetitles, Adelaide

Tello J, Ibanez J (2017) What do we know about grapevine bunch compactness? A state-of-the-art review. Austr J Grape Wine Res 24:6–23. https://doi.org/10.1111/ajgw.12310

Trudgill DL, Honek A, Li D, Van Straalen NM (2005) Thermal time - concepts and utility. Ann Appl Biol 146:1–14

Agricultural and Forest Meteorology 285–286 (2020) 107902

Contents lists available at ScienceDirect

Agricultural and Forest Meteorology

journal homepage: www.elsevier.com/locate/agrformet

# Temperature-based grapevine sugar ripeness modelling for a wide range of *Vitis vinifera* L. cultivars

Amber K. Parker[a,*], Iñaki García de Cortázar-Atauri[b], Laurence Gény[c], Jean-Laurent Spring[d], Agnès Destrac[e], Hans Schultz[f], Daniel Molitor[g], Thierry Lacombe[h], Antonio Graça[i], Christine Monamy[j], Manfred Stoll[f], Paolo Storchi[k], Mike C.T. Trought[a,l], Rainer W. Hofmann[a], Cornelis van Leeuwen[e]

[a] *Department of Wine, Food and Molecular Biosciences, Faculty of Agriculture and Life Sciences, Lincoln University, PO Box 85084, Lincoln 7647, Christchurch, New Zealand*
[b] *L'institut national de recherche pour l'agriculture, l'alimentation et l'environnement (INRAE) US 1116 AGROCLIM, F-84914 Avignon, France*
[c] *ISSV, University Bordeaux, Unité de Recherche Œnologie EA 4577-USC 1366 INRAE, Chemin de Leysotte, 33883 Villenave d'Ornon, France*
[d] *Agroscope, Avenue de Rochettaz 21, 1009 Pully, Switzerland*
[e] *EGFV, Bordeaux Sciences Agro, INRAE, Univ. Bordeaux, ISVV, Chemin de Leysotte, 33883 Villenave d'Ornon, France*
[f] *Hochschule, Giesenheim University, Von-Lade-Straße 1, D-65366 Geisenheim*
[g] *Environmental Research and Innovation (ERIN) Department 41, Luxembourg Institute of Science and Technology (LIST), rue du Brill, L-4422 Belvaux, Luxembourg*
[h] *Institut National de la Recherche Agronomique (INRAE), AGAP, University Montpellier, CIRAD, INRAE, Montpellier SupAgro, 2 place Viala, F-34060 Montpellier, France*
[i] *Sogrape Vinhos S.A., Rua 5 de Outubro 4527, 4430-852 Avintes, Portugal*
[j] *Bureau Interprofessionnel des Vins de Bourgogne – BIVB, 12 boulevard Bretonnière, 21200 Beaune, France*
[k] *CREA – Centro di ricerca Viticoltura ed Enologia, Viale S.Margherita, 80, 52100 Arezzo, Italy*
[l] *The New Zealand Institute for Plant and Food Research Limited, Blenheim 7240, New Zealand*

ARTICLE INFO

*Keywords:*
Grape
Phenology modelling
Sugar
Cultivars
Climate change

ABSTRACT

Increasing temperatures due to climate change are leading to advances in grapevine phenology and sugar accumulation in grape berries. This study aims to (i) determine if a temperature-based model can predict the time to target sugar concentrations from 170 to 220 g/L for *Vitis vinifera* L., (ii) use the best model to characterise the time to the specified target sugar concentrations for a wide range of cultivars with statistical evaluation of each cultivar's parameterisation, and (iii) establish cultivar classifications based on these thermal times to the specified target sugar concentrations.

The Day of the Year (DOY) to reach the specified target sugar concentrations (170, 180, 190, 200, 210 and 220 g/L) was determined from time series of sugar concentrations collected from research institutes, extension services and private companies. Models were fitted for the species *Vitis vinifera* L. The two best-fit models for the DOY to reach the target sugar concentrations were selected using the Akaike Criterion (*AIC*) (evaluates model complexity and goodness of fit within one criterion) and assessed for model efficiency (*EF*) and error of prediction (*RMSE*, root means squared error) followed by a sensitivity analysis and model validation. The models were then parameterised for individual cultivars.

The best model across all target sugar concentrations was the non-linear best Sigmoid model "best SIG"' model (parameters: start date ($t_0$) = 86, $d = -0.1294$, $e = 14.87$). The best linear (Growing Degree Days) model was also selected which represents the model that required the least parameters and therefore the simplest in application for winegrowers. This model was termed the "Grapevine Sugar Ripeness" model (GSR) (parameters: base temperature ($Tb$) = 0 °C, start date ($t_0$) = 91 or 1 April, Northern Hemisphere). Both models performed better than the Winkler and Huglin growing degree day models.

Sixty-five cultivars were classified for the thermal time to one or more of the six sugar targets using these two models. Fifty percent of all combinations of cultivar and time to target sugar concentrations had *EF* values greater than 0.5 and *RMSE* values less than seven days. Confidence intervals were calculated for cultivars where there was sufficient data for the thermal time to target sugar concentrations. The classifications generated from both models provides the opportunity to implement either model to support cultivar choice in response to

* Corresponding author.
*E-mail address:* amber.parker@lincoln.ac.nz (A.K. Parker).

https://doi.org/10.1016/j.agrformet.2020.107902
Received 1 September 2019; Received in revised form 24 December 2019; Accepted 10 January 2020

concerns of climate change and may provide cultivar solutions to issues of harvesting grapes at high sugar concentrations with resultant higher alcohol wines.

## 1. Introduction

Air temperature is a key environmental factor that can determine ripening and the timing of grape harvest (Cook and Wolkovich, 2016; Garcia de Cortazar Atauri et al., 2017; Gladstones, 1992; Jones, 2006; Jones and Alves, 2012; Jones and Davis, 2000; Jones et al., 2005; Webb et al., 2007; Winkler et al., 1962). It has been demonstrated that climate, notably temperature, had a bigger impact on vine development and berry composition compared with soil or variety (van Leeuwen et al., 2004), and that the length of the growing season for each variety is directly related to growing season mean temperature (Jones, 2006).

Sugar concentration (which determines the alcohol concentration in the final wine) is a key quality component in grapes and is regularly monitored by the proxy of soluble solids throughout the ripening phase, to make harvest decisions. Increased temperatures from climate change have resulted in increased sugar concentrations at harvest (Dûchene and Schneider, 2005; Hall et al., 2016; Jones, 2006; Jones and Davis, 2000; Jones et al., 2005; Petrie and Sadras, 2008; van Leeuwen and Darriet, 2016; Webb et al., 2007, 2012). Advances in sugar accumulation raises the question of whether the climate of a region will still provide optimum ripening conditions for currently planted cultivars in future climate conditions. In grape and wine production, it is important to ensure that cultivars do not ripen too early in the season because ripening in the hottest part of the summer results in unbalanced wines that can be high in alcohol, lacking acidity, freshness and aroma expression (Duchêne et al., 2010; van Leeuwen and Seguin, 2006). Furthermore, the risk of rot may increase in areas with intermittent rainfall combined with high temperatures. The optimal timing for the ripening period can be achieved by choosing early ripening cultivars in cool climates (where obtaining full ripeness is a challenge) and late ripening cultivars in warm climates (where too early ripening may be an issue). Having precise knowledge about the timing of ripeness, in particular the time to target sugar concentrations, of a wide range of cultivars in relation to temperature is highly important to achieve this goal.

Process-based phenological models that use temperature as a driving climate factor can be used to investigate objectively whether temperatures during the growing season can be used to predict the time to target sugar concentrations of *V.vinifera* L. and the cultivars of this species. These models have been successfully used to characterise key phenological stages of the grapevine: budburst, flowering, and veraison (Caffarra and Eccel, 2010; Caffarra and Eccel 2011; Cuccia et al., 2014; Duchêne et al., 2010; García de Cortázar-Atauri et al., 2009; Hall et al., 2016; Molitor et al., 2014; Nendel, 2010; Parker et al., 2011, 2013), and in some cases to simulate phenophases (Costa et al., 2019; García de Cortázar-Atauri et al., 2010ab; Molitor et al., 2014; Verdugo-Vásquez et al., 2017). These models have also been used to characterise differences between cultivars: for example, the Grapevine Flowering Veraison (GFV) model (Parker et al., 2011) characterised the thermal time of 95 and 104 grapevine cultivars for flowering and veraison respectively (Parker et al., 2013). Alternatively, historical records of harvest dates have been used to evaluate past climate dynamics (Chuine et al., 2004; Cook and Wolkovich, 2016; García de Cortázar-Atauri et al., 2010b; Molitor et al., 2016) and could be considered for studies of climate change impacts on cultivar suitability. However, such long-term harvest records (more than 50 years) only exist for some cultivars in their specific production areas (Daux et al., 2012; Jones and Davis, 2000; Molitor et al., 2016; Tomasi et al., 2011). Furthermore, although “Harvest, Berries ripe” represents stage 38 on the modified Eichhorn and Lorenz scale of phenology (Coombe, 1995) (stage 89 in the BBCH scale), there is no one universal definition of “berry ripe”. Vineyard management (training system, disease management etc.) may change over the long-term while in the short-term berry composition parameters may vary at harvest and therefore harvest are not a true reflection of growth or phenological stage. Harvest date can also be influenced by (i) region and end use (for example sparkling versus still wine), (ii) balancing logistic requirements at the winery and target composition, and (iii) other exogenous factors such as disease pressure (García de Cortázar-Atauri et al., 2010b).

The cultivated grapevine (*Vitis vinifera* L.) shows considerable phenotypic diversity with over 1100 different cultivars planted today (Wolkovich et al., 2017); understanding differences in maturity among cultivars in response to temperatures represents a significant opportunity to adapt to future climate change. This relationship can be investigated using temperature-based models to predict the trait of “temperature requirements to sugar ripeness” for the grapevine as one proxy for “maturity”. Previous research has implemented a temperature-based approach to predict sugar concentrations of different cultivars. Huglin (1978) classified growing regions and developed a classification of cultivars into nine groups based on their thermal time to reach 200 g/L sugar using the “Huglin model”. However, the classification largely reflects the historic distribution of cultivars and is imprecise, grouping some mid-ripening cultivars like Sémillon and Merlot in the same group as the late ripening cultivar Cabernet-Sauvignon. The classification was also limited in that the groupings provide little differentiation between cultivars and only 26 cultivars were classified, including some marginally cultivated ones. Other classifications include that of Gladstones (2011) who classified a wide range of cultivars for the timing of ripeness, and Jones (2006) who produced a classification of maturity groupings of cultivars based on average growing season temperatures. Although the classifications of Huglin (1978) and Jones (2006) demonstrate a relationship between growing season temperatures and maturity, none of these classifications directly investigated whether a temperature-based model can predict the time to target sugar concentrations using modelling approaches and statistical methods of assessment. No one to date has tested if a process-based phenological model can be used to predict the thermal time to target sugar concentrations across a wider range of cultivars, sites and years.

Chuine et al. (2013) summarized a wide range of phenological models currently available that were developed for different plant species. Testing these models and the various physiological assumptions they represent is an important first step before defining a temperature-based model to predict target sugar concentrations for grapevine cultivars. Using a temporally and spatially diverse dataset to test these models can potentially result in them being subsequently applied in a wide range of environments and for a wide range of cultivars. The Metropolis algorithm of Chuine et al. (1998) implemented in the Phenological Modelling Platform (PMP v5.4 in Chuine et al., 2013) also makes it possible to test a full range of parameter values and avoid fitting to local minima values (Chuine et al., 1998). Finally, appropriate methodological steps of model calibration with statistical evaluation, sensitivity analysis, and validation provides an objective framework to evaluate model performance. This approach has already been used successfully to develop a phenological model for grapevine flowering and veraison at the species level (Parker et al., 2011).`

Although temperatures over longer periods of time (growing season) may be able to predict the time to target sugar concentrations (Huglin, 1978) or maturity (Jones, 2006), changes in sugar concentration at the mechanistic berry level are the product of water and sugar flux (Dai et al., 2010; Dai et al., 2011; Zhu et al., 2018).

Furthermore, water status (Dai et al., 2010, 2011; Martinez-Lüscher et al., 2016; Ojeda et al., 2001; van Leeuwen et al., 2009), $CO_2$ concentrations (Martinez-Lüscher et al., 2015, 2016), UV-B (Martinez-Lüscher et al., 2015), yield (Petrie and Clingeleffer, 2006; Parker et al., 2014ab, 2015), nitrogen status (Choné et al., 2001) and leaf area to fruit mass (LA: FM) ratio (Ollat and Gaudillere, 1998; Parker et al., 2014ab, 2015; Poni et al., 2006; Poni and Giachino, 2000), and within vineyard variability (Verdugo-Vásaquez et al. 2019) all influence the rate of sugar accumulation post-veraison.

One option may be to implement the most current physiological models of berry ripening (Dai et al., 2009) in the context of understanding changes in berry composition due to climate change. More accurate predictions between sugar accumulation and days rather than temperature have been demonstrated for these models which are based on mechanistic changes in carbon partitioning and sugar accumulation (Dai et al., 2009; Ollat and Gaudillere, 1998). However, there are currently limitations to apply these models to understand cultivar differences. Firstly, the berry physiology models often consider the time from fruitset or veraison rather than integrating the time to a sugar target over the full season; this has limited application when trying to study the consequence of increasing temperatures on advances in development and berry composition in the context of climate change and comparing timing to sugar targets for a wide range of cultivars. Secondly, these berry physiological models are often too complex to be scaled up to describe cultivar differences in sugar concentrations in response to increasing temperatures. The final limitation is that these models are often tested for one or a few cultivars and/or in one location, makes it difficult to extrapolate results to other cultivars, regions, or climates.

An objective approach to predicting the time to reach target sugar concentrations for different cultivars using temperature-driven models may provide a quantifiable means of anticipating the influence of climate change on grape cultivar sugar concentrations.

The present study aims to (i) determine if a temperature-based model developed a temporally and spatially diverse data set can predict varying time to target sugar concentrations from 170 to 220 g/L for *Vitis vinifera* L., (ii) use a robust and thorough modelling development process to determine the best temperature-based model (calibration testing the most widely available suite of relevant phenological models to date including models with temperature cap/considering upper temperature limits followed by sensitivity analysis and model validation), (iii) characterise the time to the specified target sugar concentrations for a wide range of cultivars with statistical evaluation of each cultivars parameterisation, and (iv) establish cultivar classifications based on these thermal times to the specified target sugar concentrations.

## 2. Methods

### 2.1. Database of target sugar concentrations

Time series of sugar concentrations (g/L or conversion to g/L of other sugar scales or measurements such as soluble solids where applicable) were collected from research institutes, extension services and private companies from various European countries (Table S1). Each time series was assessed using the criterion that sugar continues to accumulate with time with the possibility of reaching a concentration plateau (plateau identified as three consecutive similar sugar concentrations) representing the maximum concentration for that cultivar. Sugar concentration increases will occur either where the rate of sugar accumulation is greater than water or through water loss characterised by a concomitant decrease in berry weight. To avoid using data where sugar concentrations were suspected to be the result of dehydration rather than physiological ripening, data points were excluded when

**Table 1**
Models tested for calibration to target sugar concentrations (170, 180, 190, 200, 210 and 220 g/L).

| Model | Reference | Equation[a] | Variations |
|---|---|---|---|
| Growing degree days (GDD) | de Reamur (1735) in Wang (1960) | $R_f(x_t) = GDD(x_t) = \begin{cases} 0, \text{ if } x_t \le Tb \\ x_t - Tb, \text{ if } x_t > Tb \end{cases}$ | **GDD 1** – all parameters fitted<br>**GDD 2** – $t_o$ = 1 (1 January), base temperature fitted ($Tb$)<br>**GDD 3** – $t_o$ = 1 (1 January), $Tb$ = 10 °C<br>**GDD 4** – the Grapevine Flowering Veraison model (GFV) (Parker et al., 2011) $t_o$ = 60, $Tb$ = 0 °C<br>**GDD5** – Winkler model parameterisation (1962), $t_o$ = 90, $T_b$ = 10 °C |
| Sigmoid model | Chuine et al. (1999) | $R_f(x_t) = \begin{cases} 0, \text{ if } x_t < 0 \\ \frac{1}{1+e^{d(x_t-e)}}, \text{ if } x_t \ge 0 \end{cases}$ | **SIG 1** – all parameters fitted<br>**SIG 2** – $t_o$ = 1, all other parameters fitted |
| Chuine model | Chuine et al. (1999) | $R_f(x_t) = \frac{1}{1+e^{(a(x-c))^2+b(x-c)}}$ | **CHU 1** – all parameters fitted<br>**CHU 2** – $t_o$ = 1, all other parameters fitted |
| Richardson model | Richardson et al. (1974) | $R_f(x_t) = \begin{cases} x_t - Tlow \text{ if } x_t < Thigh \\ Thigh \text{ if } x_t \ge Thigh \\ 0 \text{ if } x_t < Tlow \end{cases}$ | **RIC 1** – all parameters fitted<br>**RIC 2** – $t_o$ = 1, $T_{low}$ and $T_{high}$ fitted<br>**RIC 3** – $t_o$ fitted, $T_{low}$ = 0 °C, $T_{high}$ = 40 °C<br>**RIC 4** – $t_o$ and $T_{high}$ fitted, $T_{low}$ = 0 °C<br>**RIC 5** – $t_o$ = 1, $T_{low}$ = 0 °C, $T_{high}$ fitted<br>**RIC 6** – $t_o$ = 1, $T_{low}$ = 0 °C, $T_{high}$ = 40 °C |
| Wang and Engel (WE) model | Wang and Engel (1998) | $R_f(x_t) = \begin{cases} \frac{2(x_t - T_{min})^{\alpha}(T_{opt} - T_{min})^{\alpha} - (x_t - T_{min})^{2\alpha}}{(T_{opt} - T_{min})^{2\alpha}}, \text{ if } T_{min} \le x_t \le T_{max} \\ 0, \text{ if } x_t = Tmin \text{ or } x_t = Tmax \end{cases}$<br>where α is defined as $\propto = \frac{log2}{log\left[\frac{(T_{max} - T_{min})}{T_{opt} - T_{min}}\right]}$ | **WE 1** – all parameters fitted<br>**WE 2** – $t_o$ = 1, all other parameters fitted<br>**WE 3** – $t_o$ = 1, $T_{min}$ = 0 °C, all other parameters fitted<br>**WE 4** – $t_o$ = 1, $T_{min}$ = 0 °C, $T_{max}$ = 40 °C, $T_{opt}$ fitted<br>**WE 5** – $T_{min}$ = 0 °C, all other parameters fitted<br>**WE 6** – $T_{min}$ = 0 °C, $T_{max}$ = 40 °C, all other parameters fitted |
| Huglin Index | Huglin (1978) | $R_f(x_t) = \begin{cases} \frac{(x_t - 10) + (\mathrm{T\,max} - 10)}{2} \cdot k \end{cases}$ | **HI** – $t_o$ = 90, $t_s$ = 274, $k$ = daylength coefficient ranging 1.02–1.06 for 40–50 degrees latitude *Tmax* = maximum temperature |

[a] $x_t$, daily mean temperature value. $R_f$, rate of forcing. $T_b$, base temperature. *a, b and c* are the parameters describing the Chuine structure, *d* and *e* are the parameters describing the Sigmoid structure. $T_{low}$ and $T_{high}$ are the low and high temperatures for Richardson function, the $T_{opt}$, $T_{min}$ and $T_{max}$ are respectively the optimal temperature, the minimum temperature and the maximum temperature parameter of the Wang and Engel model.

sugar concentration suddenly increased after a plateau of several days. Furthermore, if a measured sugar concentration on a given sample date decreased compared to preceding sample date in the time series, the time series was also eliminated from the first time point from which sugar concentration decreased. For the remaining time series, data was only included when sugar concentrations were measured on at least three different dates which corresponds to the minimum number required to evaluate an accumulation trend. For each time series (site x year x cultivar combination), the Day of the Year (DOY) to reach the specified target sugar concentration (170, 180, 190, 200, 210, 220 and 230 g/L) was determined by two-point linear interpolation of the two data points either side of the target sugar concentration. Once the dataset was established the database was randomly partitioned into two independent datasets. Each data point for the DOY to reach a target sugar concentration was randomly assigned to either the calibration or the validation dataset. Ninety percent of the data was randomly assigned to the calibration dataset and 10% of the data to the validation dataset (Table S1). Based on the poor performance of all models at 230 g/L (likely caused by the dominance of concentration effects), and the lack of data, this target sugar concentration was excluded from further analysis.

### 2.2. Temperature data

Daily minimum and maximum temperatures were collected from meteorological stations for each year for which sugar data was provided. The full year of data was obtained, and the arithmetic daily mean temperature was calculated for each day from the daily minimum and maximum temperatures. The temperature data had to meet the following requirements for the study (method established in Parker et al., 2011): the meteorological station where the temperature data was recorded was situated within the limits of a five kilometre distance and ±100 metre altitude range from the corresponding sugar data site, and the temperature data was deemed representative of the sugar data site by the data provider.

### 2.3. Model calibration and evaluation

The methodology described in Parker et al. (2011) was used to calibrate different models (Table 1). For each DOY to reach the target sugar concentrations of 170, 180, 190, 200, 210 and 220 g/L, all data from the calibration dataset (across all cultivars) was used to fit the most accurate model for the species. Five model types were tested: GDD model, Sigmoid model, Chuine model, Richardson model and Wang and Engel model (as outlined in Chuine et al., 2013). The Sigmoid (Chuine et al., 1999), Chuine (Chuine et al., 1999) and Richardson (Richardson et al., 1974) models include a temperature threshold, above which the rate of the development ceases to increase (also known as a temperature 'caps' or upper limit in the temperature response). The Wang and Engel model (1998) not only incorporates this upper limit, but it also incorporates the known effect of reduced rates of development at higher temperatures (Chuine et al., 2013). Twenty-one different variations of these model types (fixed and fitted parameter combinations) representing different assumptions of the plant response to the temperature were tested (Table 1).

All the models were fitted using the optimization algorithm of Metropolis following Chuine et al. (1998) and PMP v5.4 (Chuine et al., 2013). The model fitting process (Metropolis algorithm as in Chuine et al., 1998), does not constrain any model parameters unless specified, and the algorithm optimizes the parameter combination. The advantage of this approach is that the fitting process will objectively test all potential start dates, base temperatures, optimal temperatures, and thermal summations values (i.e. all model parameters for each model type) via a rigorous statistical method (Chuine et al., 1998). The fitting process avoids fitting local maxima and has been proven to be better than other methods (Downhill Simplex or Newton Methods; Chuine et al., 1998). This method enables the best possible start date and other model parameters to be determined based on the dataset used for calibration without pre-conceived bias/fixing of these parameters. Therefore, all models labelled 'all parameters fitted' had no parameters constrained. We also tested known models where parameters are fixed (for example, the GFV model with a start date of 60th day of the year and base temperature of 0 °C, Table 1).

The following temperature-based models already in the viticulture literature were also tested and compared with the best model(s) chosen: Growing Degrees Days base 10 °C model (GDD) starting at 1 January, the Grapevine Flowering Veraison model (GFV) (Parker et al., 2011), Winkler index parameters of GDD ($t_0$ = 90; $Tb$ = 10 °C) (Winkler et al., 1962); the start date of 1 January as proposed or tested by several preceding studies (Bindi et al., 1997a, Bindi et al., 1997b; Gutierrez et al., 1985; Nendel, 2010; Moncur et al., 1989; Oliveira, 1988; Riou, 1994) in combination with the widely used $Tb$ = 10 °C from Winkler et al. (1962), and the Huglin index (Huglin, 1978) (Table 1).

Each sugar by model combination was tested independently. For all models, the DOY to reach a target sugar concentration occurs at $t_s$ when the state of development has reached a critical threshold $F^*$

$$S_f(t_s) = \sum_{t_0}^{t_s} R_f(x_t) \geq F^* \quad (1)$$

where the state of development at $t$ is described as the daily sum of rates of development, $R_f$, from $t_0$ (DOY) until $t_s$ for the period for which $R_f$ is calculated.

Models were tested with different temperature data inputs ($x_t$) – the daily average temperature (arithmetic mean of daily minimum and maximum temperature, Tmean), the daily minimum temperature (Tmin), and the daily maximum temperatures (Tmax).

The best model was determined by the statistical criteria below. The best linear model (three parameter GDD model with a start date, base temperature, and thermal summation parameter) was also selected (here after called the "Grapevine Sugar Ripeness" (GSR) model) as it requires the least number of parameters and while it may not perform as well as other models (in terms of efficiency and parsimony), it may be easier to use by winegrowers and technical services.

A sensitivity analysis was performed to find the best $t_0$ and a single model parameter set that could be used for all DOY to sugar targets for each best model. If there were several $t_0$ values with equivalent average efficiencies ($EF$), then this range of $t_0$ values were retained and further tested via sensitivity analysis. The model with $t_0$ fixed was then tested for all DOY to reach each of the target sugar concentrations to determine the other model parameters. For the other model parameters, values that were retained were selected based on the best average efficiency across the range of DOY to reach target sugar concentrations. Once all parameters were fixed the performance of the best model parameterisation from the sensitivity analysis was compared with the performance of the original individually calibrated best models.

The two best models with final parameterisation resulting from the calibration and sensitivity analysis were validated with the validation dataset.

After model selection, calibration and validation datasets were combined to produce a single database with the maximum number of observations for each cultivar. An $F^*$ value for each cultivar was optimized (all other model parameters fixed to the values determined from calibration and sensitivity analysis) for each DOY to reach each sugar concentration. Associated confidence intervals (95% CI) for $F^*$ were calculated for each cultivar and DOY sugar target concentration combination (as proposed in Parker et al., 2013). Cultivar parameterisation required at least two observations in the database for the DOY to reach a target sugar concentration and CI characterisation required three observations or more. Where $F^*$ values were inconsistent (i.e. the thermal summation decreased relative to a preceding lower sugar

concentration for example), the $F^*$ values were eliminated from the classification based on the following criteria: (i) if the difference between the simulated and observed DOY was greater than 10 days for any point then this was eliminated, (ii) $F^*$ values for the larger of the two sugar concentrations (and subsequent higher sugar concentrations) were retained if the *EF* were greater at the larger concentrations, and (iii) if there were only 2—3 data points provided for the larger sugar concentration $F^*$ value then this was eliminated preferentially.

### 2.4. Statistical criteria and analysis

The best model(s) were selected for calibration of parameters based on *AIC* (Burnham and Anderson, 2002, Eq. (2)); this criterion deals with parsimony (model complexity) and goodness of fit reducing the risk of overfitting more complex models. The lowest *AIC* value is associated with the best model. The model efficiency i.e. percentage of variance explained (*EF*) (Eq. (3), *EF*, Nash and Sutcliffe, 1970) and goodness of fit was also determined (*RMSE*) (Eq. (4)) during the model choice stage, with *EF* being used for sensitivity analysis and validation of best models.

$$AIC = n \times \ln\left(\frac{\sum_{i=1}^{n}(S_i - O_i)^2}{n}\right) + 2k \quad (2)$$

$$EF = 1 - \left(\frac{\sum_{i=1}^{n}(S_i - O_i)^2}{\sum_{i=1}^{n}(O_i - \overline{O})^2}\right) \quad (3)$$

$$RMSE = \sqrt{\frac{\sum_{i=1}^{n}(S_i - O_i)^2}{n}} \quad (4)$$

where $O_i$ is the observed value, $S_i$ is the simulated value, $\bar{O}$ is the mean observed value for the data being modelled, $n$ is the number of observations, and $k$ is the number of parameters.

As per Eq. (3), *EF* reflects the model performance for simulated values relative to fitted values and the closer the value to 1, the better the fit (i.e. the closer the simulated value is to the observed value, as can be depicted by 1:1 plot of simulated and observed values, see Figures S1 and S2, Supplementary material). A negative value indicates that the model performs worse than the null model (mean of all observed dates where berries reached a target sugar concentration) and this would indicate that temperature cannot be used to predict the time to target sugar concentrations. A value greater than zero indicates the model explains more variance than the null model and temperature and can be used to predict the time to target sugar concentrations. *RMSE* is a common statistical criterion used to assess goodness of fit of models and this has been used to assess temperature-based model fits in grapevines elsewhere (Costa et al., 2019; Fila et al., 2014; Fraga et al., 2016; Garcia de Cortazar-Atauri et al., 2009; Parker et al., 2011, 2013; Verdugo-Vásquez et al., 2016, 2019), as well as other crops and species (some examples include: apricots in Andreini et al., 2014; boreal and temperate trees in Linkosalo and Hänninen, 2006; temperate trees in Vitasse et al., 2011; wheat in Xue and Baenziger, 2004). The *RMSE* value is a mean error of prediction in days. Therefore, both *EF* and *RMSE* were used in model choice, validation and cultivar parameterisation as they provided complementary information; *EF* describes the proportion of variance explained by the model (variance-based criterion) whereas *RMSE* characterises average differences between estimates and measurements (difference-based criterion). Ninety-five percent CIs were obtained using the optimization algorithm to randomly search the $F^*$ parameter space around the best parameter set found at the end of the optimization. The Fisher statistic was outputted for each parameter set obtained in this search. Parameter sets that provided a $p < 0.05$ of the Fisher statistic were retained and the corresponding 95% CI boundaries determined. Figures were plotted using Sigmaplot 12 (Systat Software, Inc., USA).

## 3. Results

### 3.1. Model calibration and evaluation

The best fitted models across all DOY to reach the 170–220 g/L target sugar concentrations occurred when all parameters were fitted for each of the five model categories (GDD which included the known parameterised models of Winkler and GFV, Sigmoid, Chuine, Richardson and Wang and Engel) (Table S2, *AIC* values, Supplementary material). For all three statistical criteria (*AIC, EF, RMSE*), models using Tmean temperature data outperformed models with Tmax and Tmin input temperature data for most DOY to target sugar concentrations and were selected for subsequent analysis (Table 2, Table S2, Supplementary material).

**Table 2**
Model efficiency (*EF*), Root Mean Squared Error (*RMSE*), and Akaike Information Criterion (*AIC*), for the day of the year to reach six target sugar concentrations(170, 180, 190, 200, 210 and 220 g/l) for five different models types using Tmean (average daily temperature), Tmin (minimum daily temperature) and Tmax (maximum daily temperature) and all parameters fitted.

| | | *EF* | | | | | | *RMSE* | | | | | | *AIC* | | | | | |
|---|---|---|---|---|---|---|---|---|---|---|---|---|---|---|---|---|---|---|---|
| Target sugar concentration (g/L) | | 170 | 180 | 190 | 200 | 210 | 220 | 170 | 180 | 190 | 200 | 210 | 220 | 170 | 180 | 190 | 200 | 210 | 220 |
| Model[a] | Temperature | | | | | | | | | | | | | | | | | | |
| GDD 1 | Tmean | 0.66 | 0.64 | 0.58 | 0.57 | 0.55 | 0.48 | 9.2 | 9.6 | 10.1 | 10.0 | 9.8 | 10.1 | 4450 | 4299 | 3740 | 3020 | 2080 | 1459 |
| | Tmin | 0.43 | 0.38 | 0.28 | 0.32 | 0.29 | 0.21 | 12.0 | 12.6 | 13.1 | 12.6 | 12.2 | 12.5 | 4973 | 4823 | 4164 | 3324 | 2283 | 1591 |
| | Tmax | 0.64 | 0.62 | 0.56 | 0.53 | 0.50 | 0.48 | 9.5 | 9.8 | 10.3 | 10.5 | 10.3 | 10.2 | 4518 | 4352 | 3778 | 3077 | 2130 | 1464 |
| SIG1 | Tmean | **0.67**[b] | **0.65** | **0.60** | **0.58** | **0.56** | **0.50** | **9.1** | **9.4** | **9.8** | **9.9** | **9.7** | **10.0** | **4432** | **4274** | **3702** | **3006** | **2071** | **1452** |
| | Tmin | 0.50 | 0.46 | 0.40 | 0.40 | 0.35 | 0.25 | 11.1 | 11.8 | 12.0 | 11.8 | 11.7 | 12.1 | 4830 | 4698 | 4026 | 3240 | 2248 | 1576 |
| | Tmax | 0.65 | 0.64 | 0.59 | 0.56 | 0.52 | **0.50** | 9.4 | 9.6 | 9.9 | 10.2 | 10.1 | **10.0** | 4485 | 4311 | 3711 | 3047 | 2110 | 1453 |
| CHU 1 | Tmean | **0.67** | **0.65** | **0.60** | **0.58** | **0.56** | **0.50** | **9.1** | **9.4** | **9.8** | **9.9** | **9.7** | **10.0** | 4434 | 4276 | 3704 | 3008 | 2073 | 1454 |
| | Tmin | 0.50 | 0.46 | 0.40 | 0.40 | 0.35 | 0.25 | 11.1 | 11.8 | 12.0 | 11.8 | 11.7 | 12.2 | 4832 | 4700 | 4029 | 3242 | 2250 | 1579 |
| | Tmax | 0.65 | 0.64 | 0.59 | 0.56 | 0.52 | **0.50** | 9.4 | 9.6 | 9.9 | 10.2 | 10.1 | **10.0** | 4487 | 4313 | 3713 | 3049 | 2112 | 1455 |
| RIC 1 | Tmean | **0.67** | **0.65** | 0.59 | **0.58** | **0.56** | 0.49 | **9.1** | **9.4** | 9.9 | 10.0 | **9.7** | **10.0** | 4434 | 4276 | 3710 | 3016 | 2075 | 1454 |
| | Tmin | 0.43 | 0.38 | 0.29 | 0.34 | 0.30 | 0.22 | 11.9 | 12.5 | 13 | 12.5 | 12.2 | 12.4 | 4966 | 4815 | 4159 | 3308 | 2285 | 1591 |
| | Tmax | 0.65 | 0.64 | 0.59 | 0.55 | 0.52 | 0.50 | 9.3 | 9.6 | 9.8 | 10.3 | 10.1 | **10.0** | 4478 | 4307 | 3708 | 3054 | 2114 | 1454 |
| WE 1 | Tmean | **0.67** | **0.65** | **0.60** | **0.58** | **0.56** | **0.50** | **9.1** | **9.4** | **9.8** | **9.9** | **9.7** | **10.0** | 4435 | 4275 | 3704 | 3010 | 2073 | 1454 |
| | Tmin | 0.50 | 0.46 | 0.40 | 0.40 | 0.35 | 0.25 | 11.1 | 11.8 | 12.0 | 11.9 | 11.7 | 12.2 | 4832 | 4699 | 4029 | 3244 | 2250 | 1579 |
| | Tmax | 0.64 | 0.62 | 0.58 | 0.52 | 0.46 | 0.44 | 9.5 | 9.8 | 10.0 | 10.6 | 10.7 | 10.6 | 4507 | 4351 | 3741 | 3102 | 2164 | 1491 |

[a] **GDD 1** – Growing degree days (GDD) model, all parameters fitted; **SIG 1** – Sigmoid model, all parameters fitted; **CHU 1** – Chuine model, all parameters fitted; **RIC 1** – Richardson model, all parameters fitted; **WE 1** – Wang and Engel (WE) model, all parameters fitted.

[b] Values **underlined and in bold** represent the best *EF, RMSE* or *AIC* obtained for day of the year to reach each sugar concentration.

SIG 1 and CHU 1 models (all parameters fitted) using the daily average temperature (Tmean) were the best fit models assessed by *AIC, EF* and *RMSE* (Table 2). The analysis of the parameters of the CHU 1 (Tmean) model showed that this model was the same as SIG 1 (Tmean) model (*a* parameter of CHU 1 model was 0 and other parameters were equivalent between both models, Table S3).

*EF* and *RMSE* values of WE 1 were close to the optimal statistical criteria obtained for SIG 1 and CHU 1 models. However, parameters of the WE model (WE 1 and WE 2) produced unrealistic $T_{min}$ parameter values (below 0 °C) (Table S3). When the $T_{min}$ parameter was fixed to 0 °C for the WE model (WE 3–6, Supplementary material Tables S2), the global quality of the model decreased compared to the original model fit for the DOY to different target sugar concentrations (Tables S2 Supplementary material). The RIC 1 model and the best fit WE model (WE with $T_{min} = 0$ °C) were eliminated from the best model selection because even though the *AIC* values were larger, *EF* and *RMSE* values similar to those of the SIG 1.

The best fit non-linear model, SIG 1, and the best fit linear model, GDD 1, were selected for further evaluation via sensitivity analysis and validation.

For GDD1 model, *Tb* sensitivity analysis was not necessary as *Tb* converged to 0 °C for all model fits (Table S3). Sensitivity analysis of the GDD1 model indicated that as $t_0$ increased, the *EF* increased and then stabilised for most DOY sugar targets with $Tb = 0$ °C (Fig. 1(a)). *EF* was less variable in response to changes in $t_0$ for the DOY to reach sugar concentrations 170–200 g/L compared with the DOY to reach sugar concentrations greater than 200 g/L. A non-linear regression fit of *EF* values across all DOY to reach sugar targets 170–220 g/L (average regression for DOY to reach target sugar concentrations of 170–220 g/L, $y = 0.5771 - 2.93(0.947)^x$, $R^2 = 0.30$, Fig. 1(a).) resulting in $t_0 = 85$ at the 95% of the upper asymptote value of the regression. When $t_0$ was rounded to 91 ($Tb = 0$ °C) which is the equivalent to 1 April representing a simple version transferable to winegrowers, there was no loss in model *EF* (DOY to reach 170–180 g/L sugar target) or minimal loss (up to 0.06 in *EF* for DOY to reach 190—220 g/L sugar targets) compared with $t_0 = 85$ ($Tb = 0$ °C) (Table S4). The best fit GDD model, with $t_0 = 91$ and $Tb = 0$ °C, performed better than existing models of GDD 3, 4, 5 for all DOY to sugar concentrations (Table 3); this model has been termed the "Grapevine Sugar Ripeness" (GSR) model.

Sensitivity analysis of SIG 1 model required three model parameters to be considered: $t_0$, *d*, and *e*. The model efficiency was stable as $t_0$ increased in the range 70–90, but *EF*s decreased above $t_0 = 90$ (Fig. 1(b)), therefore $t_0 = 70$, 80 and 90 were selected and tested in sensitivity analysis for *d* and *e*. $R_f(x_t)$ values that were not at 95% of maximum at 45 °C were assumed not to reflect the true response of plant growth and development to high temperatures (unrealistic mechanistically) and this defined the threshold of the $R_f(x_t)$ function for application in sensitivity analysis. When $R_f(x_t)$ responses exceeded 0.95 for any DOY to sugar concentration target for a temperature threshold of 45 °C, the corresponding parameter set was eliminated for *d* and *e* sensitivity analysis (Figure S3, Supplementary material). The average *d* and *e* values were calculated from the remaining $R_f(x_t)$ curves, DOY to reach sugar targets of 170, 180 and 190 g/L in combination with $t_0$ of 70, 80 and 90 (average $d = -0.1294$, $e = 14.87$). When $t_0$ was set to 70, 80 or 90 and *d* and *e* fixed at $-0.1294$ and 14.87 respectively, only small changes in *EF*s were observed (maximum decrease in $EF = 0.07$) compared to the original fitted parameters (Table S4). As the sensitivity analysis indicated that there was little difference if $t_0$ was 70, 80 or 90, the best fitted average $t_0 = 86$, from Fig. 1(b) was selected.

### 3.2. Model validation

The best SIG model ($t_0 = 86$, $d = -0.1294$, $e = 14.87$) performed only marginally better than the final GSR model ($t_0 = 91$, $Tb = 0$ °C) (differences of up to 0.03 in *EF*) for the validation dataset (Table S5, Supplementary material). *EF* values for best SIG model validation (Table S5) compared with SIG 1 calibration (Table 2) were within 0.1 difference for DOY to target sugar concentrations for 170–210 g/L. However, *EF* improved for 220 g/L with the validation dataset and the best SIG model (Table S5). *EF* values for the GSR model validation were greater than GDD 4 by 0.06–0.14 depending on the DOY target sugar concentration (Tables 2 and S5).

### 3.3. Characterisation of the time of year to reach target sugar concentrations for different cultivars of V. vinifera using the GSR and best SIG model

Sixty-five cultivars were characterised (Table 4), of which approximately 50% of all combinations of cultivar and DOY to target sugar concentrations had *EF* values greater than 0.50 (Table S6, Supplementary material), and *RMSE* values less than seven days (Table S7, Supplementary material). Thirty observations or more resulted in the greatest reductions in CIs (GSR model, Fig. 2, and best SIG model, Fig. S4, data for the number of observations in Table S8, Supplementary material). Some exceptions occurred when cultivars had greater than 15 observations. However, overall as the sugar concentration increased, so did the magnitude of the CI and often *EF*s decreased irrespective of the model used (GSR model, Fig. 2, and best SIG model, Fig. S4, Table S6). There were some differences between the GSR and best SIG model

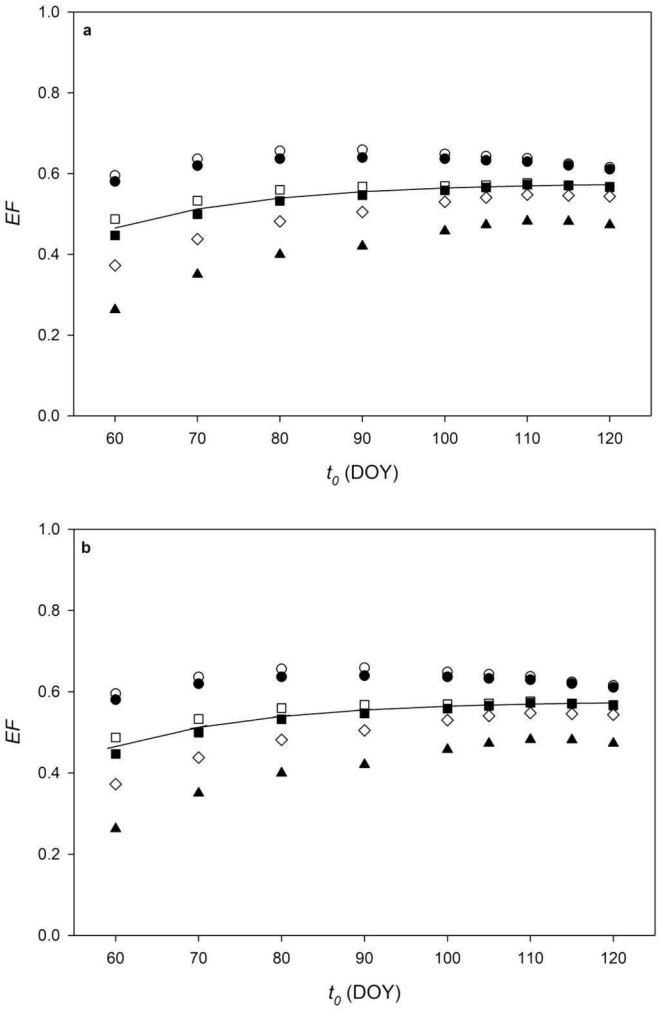


**Fig. 1.** (a) Sensitivity analysis for the start date, $t_0$, for the Growing Degrees Days (GDD) model with $Tb = 0$ °C. (b) Sensitivity analysis for the start date $t_0$ for the Sigmoid model (*d* and *e* fitted) for the Day Of the Year (DOY) to 170 g/l (○), 180 g/L (●), 190 g/L (□), 200 g/L (■), 210 g/L (◊) and 220 g/L (▲). *EF* = model efficiency.

**Table 3**
Comparison of model efficiency of the best SIG model ($t_0$ = 86, $d$ = −0.1294; $e$ = 14.87) and the Grapevine Sugar Ripeness (GSR) model ($t_0$ = 91, $Tb$ = 0 °C) with existing Growing Degree Days (GDD) based models: GDD 3 ($t_0$ = 1, $Tb$ = 10 °C) the Grapevine Flowering Veraison (GFV) model (GDD 4; $t_0$ = 60, $Tb$ = 0 °C), the Winkler model parameterisation (GDD 5; $t_0$ = 91, $Tb$ = 10 °C), the Huglin Index calibrated for the day of the year to reach sugar concentrations 170–220 g/l.

| | Target sugar concentration (g/L) | | | | | |
|---|---|---|---|---|---|---|
| Model | 170 | 180 | 190 | 200 | 210 | 220 |
| Best SIG model | 0.66 | 0.65 | 0.59 | 0.57 | 0.54 | 0.46 |
| Best GDD model (=GSR) | 0.66 | 0.64 | 0.57 | 0.55 | 0.51 | 0.42 |
| GDD 3 | −1.07 | −1.17 | −1.63 | −2.17 | −2.02 | −1.80 |
| GDD 4 (=GFV) | 0.60 | 0.58 | 0.49 | 0.45 | 0.37 | 0.26 |
| GDD 5 (=Winkler index) | −0.71 | −0.70 | −1.15 | −1.52 | −1.68 | −1.36 |
| Huglin | −0.15 | −0.20 | −0.44 | −0.71 | −1.03 | −1.11 |

in the order of cultivars presented, however these changes were minor and often occurred with overlapping CIs. As sugar increased, the number of cultivars that were classified decreased and there were few differences in the order of the cultivar classification between the GSR and Best SIG models (Figs. 2 and S4). The GSR model performed best for the following cultivars: Gamay at 170 g/L ($EF$ = 0.79), Gamay and Chardonnay at 180 g/L ($EF$ = 0.79), Sauvignon at 190 g/L ($EF$ = 0.81), Gamay at 200 g/L ($EF$ = 0.84), Merlot at 210 g/L ($EF$ = 0.61) and Garnacha tinta at 220 g/L ($EF$ = 0.60). The GSR model performed the worst for cultivars (negative $EF$s) with five or less datapoints (excluding Cot which had more) (Table S8) and corresponded to Encruzado, Portugais bleu, Mencia, Cot, Loureiro, Portan (Tables S6 and S8). Cultivar parameterisation using the GSR model performed slightly better overall than the best SIG model for the combined dataset (Table S6).

## 4. Discussion

Phenology and sugar accumulation of grapevines (*Vitis vinifera* L.) are advancing as a result of increased temperatures resulting from climate change (Costa et al., 2019; Duchene and Schneider, 2005; Fila et al., 2014; Fraga et al., 2016; Garcia de Cortazar Atauri et al. 2017; Hall et al., 2016; Jones et al., 2005; Petrie and Sadras 2008; Webb et al., 2007, 2012). Cultivar differences in phenology exhibited by *Vitis vinifera* L. (Boursiquot et al., 1995) provides an opportunity to select genotypes suitable for this changing environment, optimising yield and wine quality. Phenology modelling and understanding cultivar differences is central to understanding developmental responses enabling growers to rationally manage cultivar choice (Parker et al., 2013; van Leeuwen and Destrac, 2017).

To better quantify which cultivars can be adapted to future climatic conditions, two temperature-based models have been developed to predict the time to reach sugar targets in the range of 170–220 g/L for a range of *Vitis vinifera* L. cultivars: a linear model (GSR, $t_0$ = 91, $Tb$ = 0 °C), and a Sigmoid model (the best SIG, $t_0$ = 86, $d$ = −0.129, $e$ = 14.87).

### 4.1. Modelling results: two models to simulate target sugar concentrations

The $EF$ values for the model calibration and model validation clearly demonstrate that a temperature-based approach is useful for predicting sugar target concentrations as the $EF$ values were in the 0.5–0.6 range for most time to target sugar concentration by model (GSR or the best SIG) combinations. The values improved once the thermal summations were individually parameterized for each cultivar.

The sigmoidal nature of the best SIG model means that cooler temperatures and more extreme hot temperatures (which are known to slow fruit development) are not equally weighted to the mid-range (which is the case for a linear response) when calculating the time to reach a sugar target (Chuine et al., 2013). The best SIG model had overall the best fit regarding model efficiency, parsimony, and applicability under new conditions (as illustrated during model validation).

The GSR model is a more viticulturist-friendly model as there are less parameters required. It is easily calculated by adding daily average temperatures (as the base temperature was optimized at 0 °C) from the 91st DOY (Northern Hemisphere). It was less efficient, and the $AIC$ value indicated less parsimonious than the best SIG model during the model calibration phase but when the calibration and validation datasets were combined for the cultivar parameterisations, there were few differences between the GSR and best SIG, (up to 0.03 in $EF$) and often GSR performed just as well or better. Therefore, both models can be considered robust models for predicting the time to target sugar concentrations, indicating that both can be implemented and investigated in future climate change studies. GSR and the best SIG models converged to a similar start date ($t_0$), close to the time of budburst for many cultivars. This is similar to the start date ($t_0$) during calibration of the data to estimate veraison in the GFV model indicating some convergence at later stages of phenology even though when both flowering and veraison were considered, a $t_0$ of 60 days performed better in Parker et al. (2011).

The best SIG and GSR models gave better results than the Winker and Huglin indices (Winkler et al., 1962; Huglin, 1978; Winkler et al., 1962) which are currently used extensively in viticulture studies. Unlike the Winkler and Huglin models, which used a $Tb$ of 10 °C, the GSR model performed best with a $Tb$ of 0 °C, the same value determined for modelling flowering and veraison with the GFV model (Parker et al., 2011, 2013). The difference may be a result of the extensive geographic and seasonal database used here and in our previous papers (Parker et al., 2013). Thorough testing of temperature input data, testing a diverse range of model types, and using an extensive fit process, sensitivity analysis and validation provides robust phenological and in this case sugar target models applicable to a diverse range of sites, years or cultivars.

### 4.2. A new grapevine classification

The classification developed in this study provides an ordering of cultivars in relation to thermal time required to achieve sugar targets. To account for different target sugar concentrations at harvest, the current analysis uses a range of six sugar concentrations. This makes it possible for end users to consider the $F^*$ value appropriate for their cultivar's sugar target. The number of cultivars classified demonstrates an extraordinary phenotypic diversity for the trait “temperature requirements to sugar ripeness”.

The approach here uses an objective measure of sugar concentration for "ripeness", which has not always existed in preceding classifications (Gladstones, 2011; Jones, 2006). The inclusion of CIs for each cultivar thermal summation ($F^*$) provides uncertainty information about the models used to predict these thermal times to sugar targets. The cultivar classifications developed using these new models can be used to inform cultivar choice in different climates and regions in the context of increasing temperatures. These outcomes will potentially provide alternative solutions to harvesting grapes at high sugar concentrations which leads to higher alcohol wines.

The order of cultivars in classifications using the GSR model and the best SIG model are globally consistent with orders presented in previous classifications (Gladstones, 2011; Jones, 2006; Huglin, 1978; Winkler et al., 1962). Cultivars grown in cool climates (Pinot Meunier, Sauvignon, Gewürztraminer, Pinot noir and Chardonnay) need little thermal time to reach target sugar concentrations. Conversely, Cinsaut, Carignan, Monastrell and Xynomavro, which are grown in Mediterranean climates, had greater $F^*$ values reflecting the need for higher temperature sums during the growing seasons to reach similar sugar concentrations. The number of cultivars reported here is greater than any other studies reported to date (26 and 21 reported by Huglin, 1978

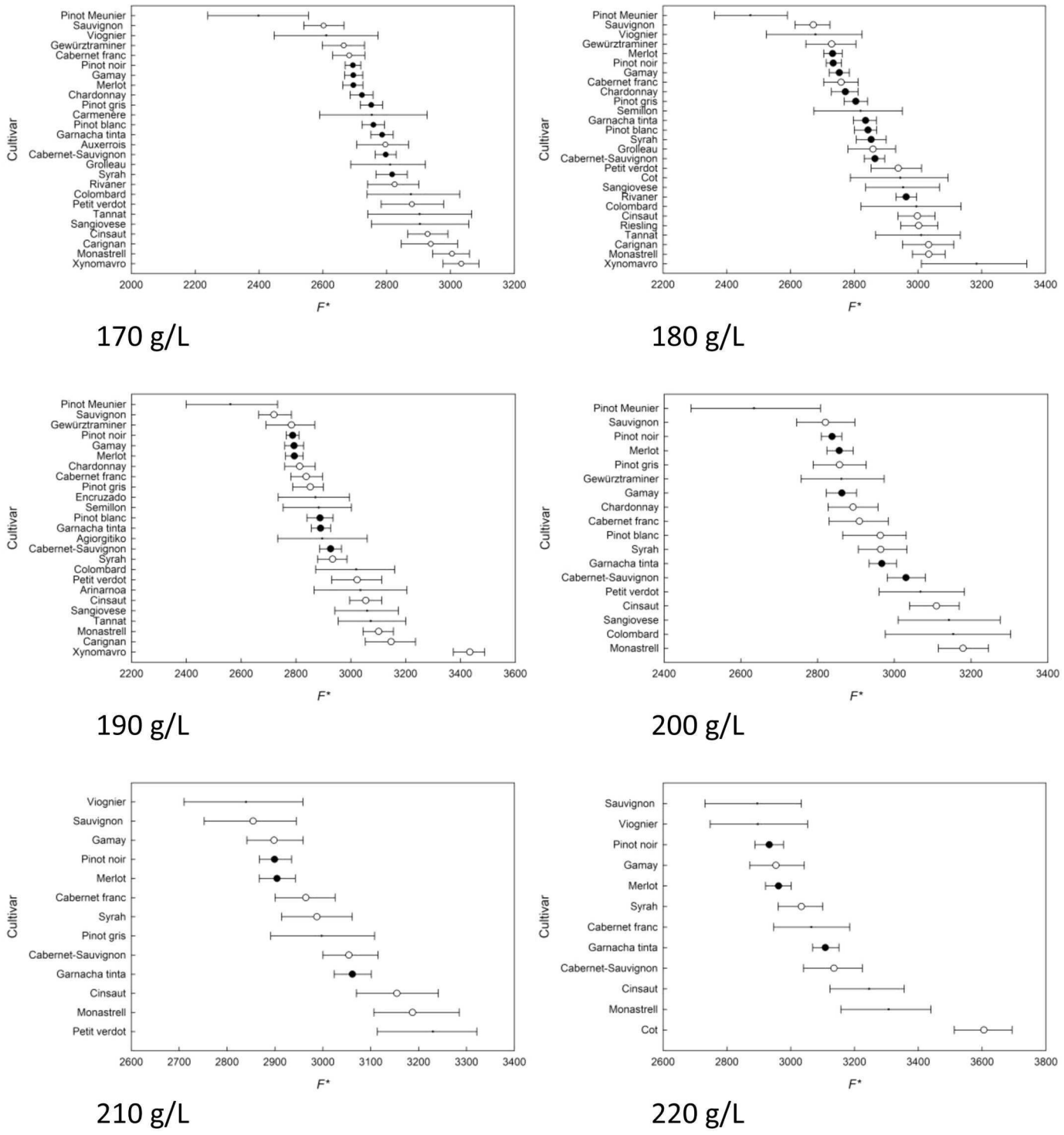


**Fig. 2.** Classification and confidence intervals (CI) of cultivars for the Day Of the Year (DOY) to reach sugar concentrations of 170, 180, 190, 200, 210 and 220 g/l for the Grapevine Sugar Ripeness (GSR) model. Closed circles correspond to parameterisations where CI <100, open circles correspond to CIs in the range 100–200 and no circle corresponds to CIs in the range of 201–350. Cultivar parameterisations with CIs > 350 or negative efficiencies are not depicted. $F^*$ = thermal summation using the GSR model.

and Jones, 2006, respectively).

While the database is extensive some cultivars are represented by limited data from few locations or years. However, the approach used to develop one model to work across all cultivars helped reduce this limitation; it includes many possible scenarios available and enables less well-known cultivars to still be characterised for which there is limited data. The number of observations on which the classification is based is variable by cultivar. In general, the greater number of observations resulted in smaller CIs similar to that reported in Parker et al. (2013). Therefore, cultivars such as Merlot, Cabernet franc, Cabernet-Sauvignon, Pinot noir, Chardonnay, and Syrah which were widely reported, provided the statistically most reliable estimates for both the GSR and Best Sig models. Irregular cultivar classification occurred with low data numbers or low spatial or temporal representation

**Table 4**
*F** values for each cultivar and each day of the year to a target sugar concentration for the Grapevine Sugar Ripeness (GSR) model and the best SIG model.

| Cultivar | GSR model[a] | | | | | | Best SIG model[a] | | | | | |
|---|---|---|---|---|---|---|---|---|---|---|---|---|
| Target sugar concentration (g/L) | 170 | 180 | 190 | 200 | 210 | 220 | 170 | 180 | 190 | 200 | 210 | 220 |
| Agiorgitiko | | | 2895 | 3055 | 3243 | 3271 | | | 96.6 | 100.1 | 106.1 | 106.8 |
| Alfrocheiro Preto | | 2733 | 2849 | 3019 | 3191 | | | 92.9 | 96 | 101.7 | 107 | |
| Alicante Bouschet | | | | 3012 | 3120 | 3216 | | | | 98.9 | 102.4 | 105.5 |
| Alvarinho | 2815 | 2857 | 2915 | | | | 95 | 95.9 | 98.3 | | | |
| Arinarnoa | | | 3035 | 3057 | 3152 | 3253 | | | 102.5 | 102.9 | 105.9 | 109.8 |
| Arneis | 2904 | 2982 | 3018 | 3039 | 3100 | | 96.7 | 99.5 | 100.9 | 101.6 | 103.1 | |
| Assyrtiko | 2981 | 3093 | | | | | 100.4 | 104 | | | | |
| Auxerrois | 2796 | | | | | | 94.5 | | | | | |
| Cabernet franc | 2683 | 2759 | 2837 | 2909 | 2964 | 3065 | 90.1 | 92.6 | 95.1 | 97.4 | 99.1 | 103 |
| Cabernet-Sauvignon | 2797 | 2865 | 2926 | 3031 | 3055 | 3136 | 94 | 96.2 | 98.2 | 101.4 | 101.9 | 104.5 |
| Carignan noir | 2938 | 3033 | 3147 | | | | 97.2 | 100.4 | 104.2 | | | |
| Carmenère | 2753 | 2878 | 2988 | 3071 | 3207 | 3333 | 92 | 96.4 | 98.5 | 101.7 | 106.3 | 109.1 |
| Chardonnay | 2723 | 2772 | 2813 | 2892 | | | 92.2 | 93.6 | 94.9 | 97.8 | | |
| Chenin | 2798 | 2875 | 2989 | 3055 | | | 93.7 | 96 | 99.9 | 102 | | |
| Cinsaut | 2928 | 2998 | 3055 | 3110 | 3155 | 3246 | 97 | 99.2 | 101.1 | 102.6 | 104.2 | 107.4 |
| Colombard | 2876 | 2995 | 3020 | 3154 | 3250 | | 96.2 | 100 | 101.1 | 105.2 | 108.7 | |
| Cornalin | 2751 | 2825 | 2882 | 2957 | | | 92.9 | 95.3 | 97.2 | 99.6 | | |
| Cortese | | 2982 | 3018 | 3039 | | | | 91.1 | 93.3 | 96.6 | | |
| Cot (=Malbec) | 2811 | 2945 | 3016 | 3189 | 3253 | 3606 | 94 | 98 | 101.2 | 105.8 | 107.9 | 117.8 |
| Encruzado | 2696 | 2764 | 2871 | 2915 | 3075 | | 91.1 | 93.5 | 96.5 | 98.3 | 103.1 | |
| Gamay | 2696 | 2753 | 2793 | 2863 | 2898 | 2954 | 91 | 92.9 | 94.3 | 96.6 | 97.7 | 99.2 |
| Gewürztraminer | 2666 | 2729 | 2783 | 2862 | | | 90.4 | 92.7 | 94.4 | 97.4 | | |
| Garnacha tinta (=Grenache) | 2786 | 2836 | 2890 | 2967 | 3062 | 3108 | 92.9 | 94.3 | 96.2 | 98.7 | 101.5 | 102.9 |
| Graciano (=Morrastrel) | 3240 | | | | | | 109 | | | | | |
| Grolleau | 2811 | 2859 | 2918 | | | | 95.1 | 96.4 | 98.4 | | | |
| Hibernal | 2792 | 2898 | 2999 | | | | 94 | 97.2 | 100.7 | | | |
| Liliorila | 2624 | 2699 | 2771 | 2872 | 2968 | | 88.7 | 91.2 | 93.5 | 97 | 100 | |
| Loureiro | 2999 | 3089 | | | | | 100.8 | 103.6 | | | | |
| Maccabeu | | 2889 | 3193 | | | | | 86 | 104.5 | | | |
| Marselan | 2760 | 2834 | 2971 | | | | 92.8 | 95 | 99.5 | | | |
| Melon | 2936 | | | | | | 98.6 | | | | | |
| Mencia | 2826 | 2913 | 3032 | | | | 94.6 | 98.1 | 101.2 | | | |
| Merlot | 2696 | 2732 | 2794 | 2856 | 2904 | 2962 | 90.8 | 92.1 | 93.9 | 96.1 | 97.4 | 99.2 |
| Monastrell (=Mourvèdre) | 3005 | 3034 | 3102 | 3179 | 3187 | 3307 | 99.6 | 100.5 | 102.5 | 105.2 | 105.4 | 108.9 |
| Muscadelle | 2926 | 3039 | | | | | 97.1 | 100.4 | | | | |
| Nebbiolo | | | 2855 | 2930 | 2974 | 3064 | | | 94.2 | 96.5 | 98.5 | 101.4 |
| Petit Verdot | 2879 | 2938 | 3023 | 3069 | 3230 | 3270 | 96.7 | 98.3 | 101.5 | 103 | 107.3 | 109 |
| Petite Arvine | 2769 | 2840 | 2844 | 2923 | 3005 | | 93.2 | 95.6 | 96 | 98.5 | 86 | |
| Pinot blanc | 2758 | 2843 | 2888 | 2964 | | | 93.6 | 96.2 | 97.8 | 99.9 | | |
| Pinot gris | 2752 | 2805 | 2852 | 2857 | 2998 | | 93.5 | 95 | 96.6 | 96.8 | 101.3 | |
| Pinot Meunier | 2398 | 2474 | 2561 | 2634 | 2660 | 2727 | 80.2 | 82.6 | 85.4 | 87.7 | 88.3 | 90.3 |
| Pinot noir | 2695 | 2734 | 2788 | 2838 | 2899 | 2933 | 91.2 | 92.7 | 94.4 | 95.9 | 97.9 | 98.7 |
| Portan | | | | 2565 | 2613 | | | | | 86.1 | 87.6 | |
| Portugais bleu | 2541 | | | | | | 84.5 | | | | | |
| Primitivo (=Zinfandel) | | 2943 | | | | | | 97.64 | | | | |
| Prunelard | 2868 | | | | | | 96.7 | | | | | |
| Riesling | 2893 | 3002 | 3069 | 3225 | | | 98.1 | 101.8 | 103.5 | 108.4 | | |
| Rivaner | 2825 | 2963 | 3105 | 3181 | | | 95.7 | 99.8 | 104.3 | 106.9 | | |
| Rkatsiteli | 3048 | 3013 | | | | | 102.1 | 101.4 | | | | |
| Roussanne | 2905 | 2981 | 2977 | 3138 | | | 97.1 | 99.2 | 99.3 | 104.5 | | |
| Sangiovese | 2904 | 2953 | 3060 | 3143 | | | 97 | 98.3 | 101.5 | 104.4 | | |
| Saperavi | 2606 | 2659 | 2711 | | | | 88 | 89.6 | 91.3 | | | |
| Sauvignon | 2602 | 2671 | 2719 | 2820 | 2854 | 2895 | 87.7 | 89.9 | 91.4 | 94.8 | 96.3 | 97.2 |
| Sciaccarello | 2986 | 3081 | 3068 | 3177 | 3303 | | 98.9 | 101.9 | 101.3 | 104.5 | 108.9 | |
| Semillon | 2833 | 2820 | 2883 | | | | 94.7 | 94.5 | 96.8 | | | |
| Sylvaner | 2682 | 2776 | 2913 | | | | 89.2 | 92.2 | 96.4 | | | |
| Syrah | 2817 | 2853 | 2934 | 2965 | 2987 | 3034 | 93.8 | 95 | 97.5 | 98.7 | 99.2 | 100.1 |
| Tannat | 2903 | 3010 | 3073 | 3128 | 3193 | 3230 | 97.3 | 100.8 | 103.3 | 105.2 | 107.2 | 107.6 |
| Tempranillo | 2794 | 2853 | 2889 | | | | 93.4 | 95 | 96.6 | | | |
| Tinto Cao | 3130 | | | | | | 105.4 | | | | | |
| Touriga Francesa | | | 3020 | 3136 | 3338 | 3535 | | | 99 | 102.2 | 108.6 | 114.3 |
| Touriga Nacional | 2836 | 3041 | 3075 | | | | 94.7 | 101.8 | 102.7 | | | |
| Trebbiano Toscano (=Ugni blanc) | 3108 | 3181 | | | | | 103.1 | 105.5 | | | | |
| Viognier | 2611 | 2678 | 2758 | 2833 | 2839 | 2897 | 87.8 | 89.7 | 92.2 | 94.7 | 94.8 | 96.9 |
| Xynmavro | 3034 | 3184 | 3434 | | | | 100.6 | 105.4 | 113.4 | | | |

[a] Blank cells are where there were zero or one observation or when computed *F** values were unrealistic (see methods).

in the database: for example, Semillon appears later than expected, but its classification was based on a limited data set (between five and nine data points depending on the sugar concentration), resulting in a large CI. CIs could not be determined for cultivars with two or less data points, but an initial characterization has been included for which more accurate *F** values and associated CIs could be developed in the future if more data become available.

Cultivars reach different maximum sugar concentrations, and when

observed in the same site, this can be due to different ripening rates and different sugar plateau concentrations (Sadras et al., 2008). For some cultivars in the database, for example Chasselas, Rivaner and Riesling, the maximum sugar concentrations plateau off around 170 and 180 g/L, respectively, in the data collected for our research, indicating a limited capacity to accumulate sugar. Subsequent increases in sugar were likely to be the result of berry dehydration, rather than further sugar accumulation (Dai et al., 2010; 2011). The rigorous database establishment method ensured that dehydration data was not modelled as data points were excluded when (i) sugar concentration suddenly increased after a plateau of several days, or (ii) if a measured sugar concentration on a given sample date decreased compared to preceding sample date in the time series. Due to low maximum sugar concentration and the concentration versus accumulation dynamics, Chasselas was omitted from the classification.

The historic classification of cultivars (e.g. 'early' or 'late') has been confounded by different harvesting aims. For example, Sauvignon blanc is considered an 'early' cultivar because it is often picked around a target sugar concentration of 200 g/L whereas Merlot is considered a 'mid' to 'late' cultivar because it is preferentially picked at a later target of 220—230 g/L. With lower temperatures and light intensity as the season progresses, the time taken to accumulate the final 20 to 30 g/L may be three to four weeks. Thus, while these cultivars have similar degrees days ($F^*$) for flowering and veraison (in Parker et al., 2013) and for the DOY to reach a target of sugar concentration of 200 g/L, the difference in historic classifications is probably a reflection of the different target sugar concentrations at harvest. The classification of both cultivars in our analysis was based on a large dataset from a wide range of locations, resulting in small CIs, and there is no reason to challenge their classification. Therefore, the classifications enable these comparisons to be made and to further critically evaluate whether cultivars are truly 'early' or 'late' in development or have been historically categorised this way based on differing harvest aims. This may also in part explain some of the cultivar inconsistencies observed in the prior classification of Huglin (1978). The classifications also indicate different orders depending on the target sugar concentrations, which suggests that cultivars may have different ripening rates (in g/d or g/°d). Future studies should consider investigating ripening rates, and this may include considering either models based on g/d or g/°d over the season as well as models that start from veraison.

### 4.3. Limits of the methodology and the classification

The start date converged to DOY 91 (Northern Hemisphere) indicating that temperature can predict sugar concentrations if the thermal summation is considered over the growing season. It is noted that the fitting process did not result in the start date corresponding to veraison, the start of the ripening window, and therefore sugar accumulation models from veraison to harvest may differ to the growing season thermal summation to the time of a target sugar concentration that is presented here. Other environmental factors such as vine water status, UVB, $CO_2$, as well as management factors (LA:FM ratio, yield, vine nitrogen status) are also known to influence sugar accumulation (Choné et al., 2001; Dai et al., 2010; 2011; Martinez-Lüscher et al., 2015, 2016; Ojeda et al., 2001; Ollat and Gaudillere, 1998; Parker et al., 2014a, Parker et al., 2014b, 2015; Petrie and Clingeleffer, 2006; Poni et al., 2006; Poni and Giachino, 2000; van Leeuwen et al., 2009; Zhu et al., 2018). The impacts of these factors are likely to be reflected in the CIs of this study, but extreme deviations may warrant a different approach to modelling target sugar concentrations, such as rates analysis during the ripening phase, and incorporation of these other factors into ripening models. For example, Petit Verdot, which is among the latest cultivars to reach veraison (Parker et al., 2013), is not among the latest to reach various target sugar concentrations (except at 210 g/L) because of quick ripening dynamics. In general, European vineyards are unirrigated and managed to a relatively high LA:FM ratio, particularly compared to other international areas where irrigation may be used (e.g. California, New Zealand, Australia). The understanding of cultivar versus environment and management effects on the duration of veraison to a given sugar concentration in berries needs to be investigated in future studies. Different clones may also influence observed sugar concentration variation for a given cultivar (Gonçalves et al., 2016; Laidig et al., 2009), although this is reported to account for a lesser percentage of variation than the environmental differences (Laidig et al., 2009).

All these factors often influence the ripening dynamics and may have contributed to reduced fits and increased variance of the models at higher sugar concentrations (210, 220 and 230 g/L). This indicates that integrating temperature influences over the season rather than just through the ripening period is important when applying temperature-based processed models for prediction of the thermal time to sugar targets. The thermal time to reach a given sugar concentration between the earliest cultivar and the latest cultivar in the classifications is greater than the number of days determined by the associated *RMSE* values. For example, the difference in thermal time between Pinot Meunier and Xynomavro determined by the GSR model for 190 g/L sugar target is 863 DD, which is approximately 43 days, when considering an average day temperature during grape ripening of 20 °C. However, the *RMSE* values are only $<2$ days for both cultivars for 190 g/L sugar target. This demonstrates clearly the distinction of early and late cultivars via the classification and statistical methods. Where there were large CIs associated with $F^*$ values despite the use of extensive spatial and temporal data datasets, it could be hypothesized that the other factors may play a more important role.

Recent research has investigated temporal within field variability of total soluble solids and demonstrated important differences at a site scale (Verdugo-Vásquez et al., 2016, Verdugo-Vásquez et al., 2018 2019). Verdugo-Vásquez et al. (2018) demonstrated that within block patterns of sugar variability are stable over time within a season and they can be used to project harvest sugar concentrations 40 days in advance within a season. Spatial modelling of phenology at a site scale is possible (Verdugo-Vásquez et al., 2019) to get higher resolution information of within vineyard variability in phenology, although the study by Verdugo-Vásquez et al., 2019 also demonstrated satisfactory performance when using the GFV model (Parker et al., 2011, 2013) to predict phenology. The approach in Verdugo-Vásquez et al. (2019) could be considered for time to target sugar concentrations in future studies, to continue to investigate the performance of temperature-based models at a site scale to capture this variability.

Finally, while sugar is one of the most important quality parameters to consider in the context of climate change, future studies will need to consider modelling other parameters that are important for ripening (e.g. phenolics, organic acids, colour, aroma compounds etc.) (Pons et al., 2017). Research also indicates decoupling (desynchronization) between sugar, acids, and polyphenol metabolism will impact berry composition at harvest in response to temperature changes (Rienth et al., 2016; Sadras and Moran, 2012; Torregrosa et al., 2017) so similar approaches could be developed for these compounds elsewhere.

### 4.4. Perspectives

Modelling the plateau sugar concentration for each cultivar may be the next step in increasing our understanding of grape berry ripening dynamics; Sadras et al. (2008) did this for 12 cultivars and this could be expanded. This would be highly complementary to our sugar target modelling approach in order to model specific harvest dates for each cultivar. Future modelling work could consider developing phenophase modelling approaches for cultivars with the aim to better predict the time between early phenological events (budburst, flowering and veraison) and the various sugar target concentrations. This would mean for each cultivar, an individual calibration is necessary, and they would no

longer be able to be compared within a classification; a temporally and spatially diverse dataset would also be required, and similar methods steps carried out to develop a robust cultivar model (calibration, sensitivity analysis, validation). Some examples of individual cultivar phenophase models already exist in the literature (Caffarra et al. 2010; García de Cortázar-Atauri et al. 2010a; Molitor et al., 2014a, Molitor et al., 2014b).

As this research has characterised the time to target sugar concentrations as a proxy for a phenological stage, future research should consider sugar accumulation rates and investigate the best way to account for these by testing different approaches. For example, research that has developed mechanistic models for sugar accumulation during the ripening phase at the berry level (Dai et al., 2009; Dai et al., 2011; Zhu et al., 2018) could be tested and developed for a wider range of cultivar and conditions. While these berry modelling approaches warrant further development, they are currently not tested on a diverse spatial and temporal scale, and they contain a measure of error that would need consolidating if they were to be applied at larger scale, such as the one adapted here. Future work should also consider comparing these mechanistic approaches with sugar ripening dynamic approaches based on g/d versus g/°d to determine the best way to account for cultivar differences in ripening dynamics.

Given that the results presented here have successfully used temperature only for prediction of time to various sugar targets for a wide range of cultivars for two models, the integrated nature of this output is useful for future application in new regions, sites, or under climate change scenarios.

## 5. Conclusions

This research demonstrated that a temperature-based model could be used to predict the time to varying target sugar concentrations (170 g/L to 220 g/L) for *V.vinifera* L. Moreover, two models, the best SIG and the GSR model, have been successfully developed (model efficiencies in the range of 0.5–0.6). These models were successfully used to characterise a wide range of cultivars for the time to the various sugar targets concentrations, producing the most extensive classifications to date of the thermal time to target sugar concentrations for the grapevine. Best performing cultivars as determined by GSR and CIs < 100 were Gamay at 170 g/L ($EF = 0.79$), Gamay and Chardonnay at 180 g/L ($EF = 0.79$), Sauvignon at 190 g/L ($EF = 0.81$), Gamay at 200 g/L ($EF = 0.84$), Merlot at 210 g/L ($EF = 0.61$) and Garnacha tinta at 220 g/L ($EF = 0.6$). The worst performing cultivars (negative *EF* values) generally had very few data points. Overall, results indicated that the grapevine (*Vitis vinifera* L.) shows an extraordinary phenotypic diversity for the trait "temperature requirements to sugar ripeness". The modelling approach resulted in six classifications based on the thermal time to target sugar concentrations for a wide range of cultivars using both the GSR and the best SIG model. The successful cultivar parameterisations by both models means that this provides options to test both models in future climate change studies. As the data used to develop these models were spatially and temporally diverse, the classifications can be used by growers cultivating grapes in widely diverse climatic conditions to select cultivars for which the timing of ripeness is ideal to produce high-quality wines. With temperatures increasing due to climate change, the knowledge of the thermal time to flowering, veraison and different target sugar concentrations for different cultivars will also be useful to adapt cultivars to future climatic conditions in winegrowing regions worldwide.

## Declaration of Competing Interest

The authors declare that they have no known competing financial interests or personal relationships that could have appeared to influence the work reported in this paper.

## Acknowledgments

The authors would like to acknowledge all those individuals and companies that contributed data. Individuals and companies that contributed at the time of the project (affiliations may have changed subsequently) include: Montse Torres Viñals and Xavier Sort Camañes (Torres, Spain), Jean-Michel Boursiquot (Montpellier SupAgro- INRA), the late Eric Lebon (INRA-Montpellier SupAgro), Gérard Barbeau (INRA Angers), Jean-Yves Cahurel (Institut Français de la Vigne et du Vin, Pôle Bourgogne- Beaujolais-Jura-Savoie), J-M. Chevet (INRA), Marion Claverie (IFVV/ AREDVI Pôle Rhône-Méditerranée), Betrand Daulny (SICAVAC), Lionel Le Duc (CRVI de Corse), Françoise Dijon (Inter-Rhone), Eric Duchêne (INRA Colmar), Thierry Dufourcq (IFVV, Pôle Sud-Ouest), Natacha Fontes (Sogrape Vinhos), Serge Fischer (IVV Remich), the late Guy Guimberteau, Olivier Jacquet (Chambre d'agriculture de Vaucluse), Stephanos Koundouras (University of Thessaloniki), Christophe Larrouquis (Cave Irouleguy), Sadrine Lalet (INRA "Vassal" grape collection), Rodrigo Laytte (château Kirwan), Robert Mannes (IVV Remich), Francis Mayeur (Château d'Yquem), Etienne Neethling (INRA), Hernan Ojeda (INRA – Unité Expérimentale de Pech Rouge), Jean-Christophe Payan (IFVV Rhone-Méditerranée), Begoña Rodriquez Lovelle (Syndicat Général des Vignerons des Côtes du Rhône), Gervais Ruton and Matthieu Bordes (Château Lagrange), Gilles Salva (CRVI de Corse), Christophe Schneider (INRA Colmar), Ivan Sivadon (CIRAME), Jean-Pierre Soyer (INRA), Marta Teixeira (Sogrape Vinhos), William Trambouze (Chambre d'agriculture de l'Hérault). The authors would like to thank Luna Centioni, Marco Meroni for collecting data. The authors would like to acknowledge The Agricultural and Marketing Research and Development Trust, New Zealand, for the scholarship to Dr Amber Parker, and Bordeaux Sciences Agro ISVV-UMR EGFV and Lincoln University for their cooperation with the project. The Experimental Unit UE 1442 Vigne Bordeaux is acknowledged for managing the VitAdapt experimental site at INRA Bordeaux, where data was collected for this project.

## Supplementary materials

Supplementary material associated with this article can be found, in the online version, at doi:10.1016/j.agrformet.2020.107902.

## References

Andreini, L., García de Cortázar-Atauri, I., Chuine, I., Viti, R., 2014. Understanding dormancy release in apricot flower buds (*Prunus armeniaca* L.) using several process-based phenological models. Agric. Meteorol. 184, 210–219.

Bindi, M., Miglietta, F., Gozzini, B., Orlandini, S., Seghi, L., 1997a. A simple model for simulation of growth and development in grapevine (*Vitis vinifera* L). 1. model description. Vitis 36, 67–71.

Bindi, M., Miglietta, F., Gozzini, B., Orlandini, S., Seghi, L., 1997b. A simple model for simulation of growth and development in grapevine (*Vitis vinifera* L). 2. model validation. Vitis 36, 73–76.

Boursiquot, J.M., Dessup, M., Rennes, C., 1995. Distribution of the main phenological, agronomical and technological characters of *vitis vinifera* l. Vitis 34, 31–35.

Burnham, K.P., Anderson, D.R., 2002. Model Selection and Multimodel Inference: A Practical Information – Theoretic Approach. Springer-Verlag, New York.

Caffarra, A., Eccel, E., 2010. Increasing the robustness of phenological models for *vitis vinifera* cv. chardonnay. Int. J. Biometeorol. 54, 255–267.

Caffarra, A., Eccel, E., 2011. Projecting the impacts of climate change on the phenology of grapevine in a mountain area. Aust. J. Grape Wine Res. 17, 52–61.

Choné, X., van Leeuwen, C., Chery, P., Ribereau-Gayon, P., 2001. Terroir influence on water status and nitrogen status of non irrigated cabernet-sauvignon (*Vitis vinifera*): vegetative development, must and wine composition. S. Afr. J. Enol. Vitic. 22, 8–15.

Chuine, I., Cour, P., Rousseau, D.D., 1998. Fitting models predicting dates of flowering of temperature-zone trees using simulated annealing. Plant Cell Environ. 21, 455–466.

Chuine, I., Cour, P., Rousseau, D.D., 1999. Selecting models to preodict the timing of flowering of temperate tress: implications for tree phenology modelling. Plant Cell Environ. 22, 1–13.

Chuine, I., García de Cortázar-Atauri, I., Kramer, K., Hänninen, H., 2013. Plant development models. In: Schwartz, M.D. (Ed.), Phenology: An Integrative Environmental Science. Springer, Dordrecht, pp. 275–293.

Chuine, I., Yiou, P., Viovy, N., Seguin, B., Daux, V., Ladurie, E.L., 2004. Historical phenology: grape ripening as a past climate indicator. Nature 432, 289–290.

Cook, B.I., Wolkovich, E.M., 2016. Climate change decouples drought from early wine

grape harvests in france. Nat. Clim. Chang. 6, 715–719.
Coombe, B.G., 1995. Adoption of a system for identifying grapevine growth stages. Aust. J. Grape Wine Res. 1, 104–110.
Costa, R., Fraga, H., Fonseca, A., García de Cortázar-Atauri, I., Val, M.C., Carlos, C., Reis, S., Santos, J.A., 2019. Grapevine phenology of cv. touriga franca and touriga nacional in the douro wine region: modelling and climate change projections. Agronomy 9, 210. https://doi.org/10.3390/agronomy9040210.
Cuccia, C., Bois, B., Richard, Y., Parker, A.K., García de Cortázar-Atauri, I., van Leeuwen, C., Castel, T., 2014. Phenological model performance to warmer conditions: application to pinot noir in burgundy. J. Int. Sci. Vigne Vin 48, 169–178.
Dai, Z.W., Ollat, N., Gomes, E., Decroocq, S., Tandonnet, J.P., Bordenave, L., Pieri, P., Hilbert, G., Kappel, C., van Leeuwen, C., Vivin, P., Delrot, S., 2011. Ecophysiological, genetic, and molecular causes of variation in grape berry weight and composition: a review. Am. J. Enol. Vitic. 62, 413–425.
Dai, Z.W., Vivin, P., Barrieu, F., Ollat, N., Delrot, S., 2010. Physiological and modelling approaches to understand water and carbon fluxes during grape berry growth and quality development: a review. Aust. J. Grape Wine Res. 16, 70–85.
Dai, Z.W., Vivin, P., Robert, T., Milin, S., Li, S.H., Genard, M., 2009. Model-based analysis of sugar accumulation in response to source-sink ratio and water supply in grape (*Vitis vinifera*) berries. Funct. Plant Biol. 36, 527–540.
Daux, V., García de Cortázar-Atauri, I., Yiou, P., Chuine, I., Garnier, E., Le Roy Ladurie, E., Mestre, O., Tardaguila, J., 2012. An open-access database of grape harvest dates for climate research: data description and quality assessment. Clim. Past 8, 1403–1418.
De Reaumur, R.A.F., 1735. Observations du thermomètre, faites à paris pendant l'année 1735, comparées avec celles qui ont été faites sous la ligne, à l'Isle de france, à alger et quelques unes de nos isles de l'Amérique. Mém. Acad. Sci. Paris 1735.
Duchêne, E., Huard, F., Dumas, V., Schneider, C., Merdinoglu, D., 2010. The challenge of adapting grapevine varieties to climate change. Clim. Res. 41, 193–204.
Duchêne, E., Schneider, C., 2005. Grapevine and climatic changes: a glance at the situation in alsace. Agron. Sustainable Dev. 25, 93–99.
Fila, G., Gardiman, M., Belvini, P., Meggio, F., Pitacco, A., 2014. A comparison of different modelling solutions for studying grapevine phenology under present and future climate scenarios. Agric. Meteorol. 195, 192–205.
Fraga, H., García de Cortázar-Atauri, I., Malheiro, A.C., Santos, J.A., 2016. Modelling climate change impacts on viticultural yield, phenology and stress conditions in europe. Glob. Chang Biol. 22, 3774–3788.
García de Cortázar-Atauri, I., Brisson, N., Gaudillere, J.P., 2009. Performance of several models for predicting budburst date of grapevine (*Vitis vinifera* L.). Int. J. Biometeorol. 53, 317–326.
García de Cortázar-Atauri, I., Chuine, I., Donatelli, M., Parker, A., van Leeuwen, C., 2010a. A curvilinear process-based phenological model to study impact of climatic change on grapevine (*Vitis vinifera* L.). In: Proceedings of Agro 2010: the Eleventh ESA Congress, pp. 907–908.
García de Cortázar-Atauri, I., Daux, V., Garnier, E., Yiou, P., Viovy, N., Seguin, B., Boursiquot, J.M., Parker, A.K., van Leeuwen, C., Chuine, I., 2010b. Climate reconstructions from grape harvest dates: methodology and uncertainties. Holocene 20, 599–608.
García de Cortázar-Atauri, I., Duchêne, E., Destrac-Irvine, A., Barbeau, G., de Resseguier, L., Lacombe, T., Parker, A.K., Saurin, N., van Leeuwen, C., 2017. Grapevine phenology in france: from past observations to future evolutions in the context of climate change. OENO One 51, 115–126.
Gladstones, J., 1992. Viticulture and Environment. Winetitles, Adelaide.
Gladstones, J., 2011. Wine, Terroir and Climate Change. Wakefield Press, Kent Town.
Gonçalves, E., Carrasquinho, I., Almeida, R., Pedroso, V., Martins, A., 2016. Genetic correlations in grapevine and their effects on selection. Aust. J. Grape Wine Res. 22, 52–63.
Gutierrez, A.P., Williams, D.W., Kido, H., 1985. A model of grape growth and development: the mathematical structure and biological considerations. Crop Sci. 25, 721–728.
Hall, A., Mathews, A.J., Holzapfel, B.P., 2016. Potential effect of atmospheric warming on graepvine phenology and post-harvest heat accumulation across a range of climates. Int. J. Biometeorol. 60, 1405–1422.
Huglin, P., 1978. Nouveau mode d'évaluation des possibilités héliothermiques d'un milieu viticole. Comptes rendus des Séances de l'Académie d'Agriculture de France 64, 1117–1126.
Jones, G., 2006. Climate and terroir: Impacts of Climate Variability and Change On wine. Fine Wine and Terroir—The Geoscience Perspective. In: Macqueen, R.W., Meinert, L.D. (Eds.), Geoscience Canada, St John's, pp. 1–14.
Jones, G.V., Alves, F., 2012. Impact of climate change on wine production: a global overview and regional assessment in the Douro valley of portugal. Int. J. Glob. Warm. 4, 383–406.
Jones, G.V., Davis, R.E., 2000. Climate influences on grapevine phenology, grape composition, and wine production and quality for bordeaux, france. Am. J. Enol. Vitic. 51, 249–261.
Jones, G.V., White, M.A., Cooper, O.R., Storchmann, K., 2005. Climate change and global wine quality. Clim. Change 73, 319–343.
Laidig, F., Piepho, H.P., Hofäcker, W., 2009. Statistical analysis of 'White riesling' (*Vitis vinifera* ssp. *sativa* L.) clonal performance at 16 locations in the rheinland-pfalz region of germany between 1971 and 2007. Vitis 48, 77–85.
Linkosalo, T., Hänninen, H., 2006. Models of spring phenology of boreal and temperate trees: is there something missing. Tree Physiol. 26, 1165–1172.
Martínez-Lüscher, J., Kizildeniz, T., Vučetić, V., Dai, Z., Luedeling, E., van Leeuwen, C., Gomès, E., Pascual, I., Irigoyen, J.J., Morales, F., Delrot, S., 2016. Sensitivity of grapevine phenology to water availability, temperature and $CO_2$ concentration. Front. Environ. Sci. 4. https://doi.org/10.3389/fenvs.2016.00048.
Martínez-Lüscher, J., Morales, F., Sánchez-Díaz, M., Delrot, S., Aguirreolea, J., Gomès, E., Pascual, I., 2015. Climate change conditions (Elevated $CO_2$ and temperature) and uv-b radiation affect grapevine (*Vitis vinifera* cv. tempranillo) leaf carbon assimilation, altering fruit ripening rates. Plant Sci. 236, 168–176.
Molitor, D., Caffarra, A., Sinigoj, P., Pertot, I., Hoffmann, L., Junk, J., 2014a. Late frost damage risk for viticulture under future climate conditions: a case study for the luxembourgish winegrowing region. Aust. J. Grape Wine Res. 19, 160–168.
Molitor, D., Junk, J., Evers, D., Hoffman, L., Beyer, M., 2014b. A high resolution cumulative degree day based model to simulate the phenological development of grapevine. Am. J. Enol. Vitic. 65, 72–80.
Molitor, D., Udelhoven, T., Ney, S., Hoffmann, L., Pfister, L., 2016. Historical vintage descriptions from Luxembourg- an indicator for the climate conditions in the past. Vitis 55, 23–30.
Moncur, M.W., Rattigan, K., Mackenzie, D.H., McIntyre, G.N., 1989. Base temperatures for budbreak and leaf appearance of grapevines. Am. J. Enol. Vitic. 40, 21–26.
Nash, J.E., Sutcliffe, J.V., 1970. River flow forecasting through conceptual models Part I A discussion of principles. J. Hydrol. (Amst) 10, 282–290.
Nendel, C., 2010. Grapevine bud break prediction for cool winter climates. Int. J. Biometeorol. 54, 231–241.
Ojeda, H., Deloire, A., Carbonneau, A., 2001. Influence of water deficits on grape berry growth. Vitis 40, 141–145.
Oliveira, M., 1998. Calculation of budbreak and flowering base temperatures for *vitis vinifera* cv. touriga francesa in the douro region of portugal. Am. J. Enol. Vitic. 49, 74–78.
Ollat, N., Gaudillere, J.P., 1998. The effect of limiting leaf area during stage i of berry growth on development and composition of berries of *vitis vinifera* L. cv. cabernet sauvignon. Am. J. Enol. Vitic. 49, 251–258.
Parker, A., García de Cortázar-Atauri, I., Chuine, I., Barbeau, G., Bois, B., Boursiquot, J.-M., Cahurel, J.-Y., Claverie, M., Dufourcq, T., Geny, L., Guimberteau, G., Hofmann, R., Jacquet, O., Lacombe, T., Monamy, C., Ojeda, H., Panigai, L., Payan, J.-C., Rodriquez-Lovelle, B., Rouchaud, E., Schneider, C., Spring, J.-L., Storchi, P., Tomasi, D., Trambouze, W., Trought, M., van Leeuwen, C., 2013. Classification of varieties for their timing of flowering and veraison using a modelling approach. a case study for the grapevine species *vitis vinifera* l. Agric Meteorol. 180, 249–264.
Parker, A., García de Cortázar-Atauri, I., van Leeuwen, C., Chuine, I., 2011. General phenological model to characterise the timing of flowering and veraison of *vitis vinifera* l. Aust. J. Grape Wine Res. 17, 206–216.
Parker, A.K., Hofmann, R.W., van Leeuwen, C., McLachlan, A.R.G., Trought, M.C.T., 2014a. Leaf area to fruit mass ratio determines the time of veraison in sauvignon blanc and pinot noir grapevines. Aust. J. Grape Wine Res. 20, 422–431.
Parker, A.K., Hofmann, R.W., van Leeuwen, C., McLachlan, A.R.G., Trought, M.C.T., 2015. Manipulating the leaf area to fruit mass ratio alters the synchrony of total soluble solids accumulation and titratable acidity of grapevines: implications for modelling fruit development. Aust. J. Grape Wine Res. 21, 266–276.
Parker, A.K., Trought, M.C.T., Hofmann, R.W., McLachlan, A.R.G., van Leeuwen, C., 2014b. The influence of two methods of crop removal at different leaf areas on maturation of sauvignon blanc (*Vitis vinifera* l. J. Int. Sci. Vigne Vin 48, 43–50.
Petrie, P.R., Clingeleffer, P.R., 2006. Crop thinning (hand versus mechanical), grape maturity and anthocyanin concentration: outcomes from irrigated cabernet sauvignon (*Vitis vinifera* L.) in a warm climate. Aust. J. Grape Wine Res. 12, 21–29.
Petrie, P.R., Sadras, V.O., 2008. Advancement of grapevine maturity in australia between 1993 and 2006: putative causes, magnitude of trends and viticultural consequences. Aust. J. Grape Wine Res. 14, 33–45.
Poni, S., Casalini, L., Bernizzoni, F., Civardi, S., Intrieri, C., 2006. Effects of early defoliation on shoot photosynthesis, yield components, and grape composition. Am. J. Enol. Vitic. 57, 397–407.
Poni, S., Giachino, E., 2000. Growth, photosynthesis and cropping of potted grapevines (*Vitis vinifera* L. cv. cabernet sauvignon) in relation to shoot trimming. Aust. J. Grape Wine Res. 6, 216–226.
Pons, A., Allamy, L., Scütler, A., Rauhut, D., Thibon, C., Darriet, P., 2017. What is the expected impact of climate change on wine aroma compounds and their precursors in grapes. OENO One 51, 141–146.
Richardson, E.A., Seeley, S.D., Walker, D.R., 1974. A model for estimating the completion of rest for 'Redhaven' and 'Elberta' peach trees. HortScience 9, 331–332.
Rienth, M., Torregrosa, L., Gautier, S., Ardisson, M., Brillouet, J.-M., Romieu, C., 2016. Temperature desynchronizes sugar and organic acid metabolism in ripening grapevine fruits and remodels their transcriptome. BMC Plant Biol. 16, 164–187.
Riou, C., 1994. The Effect of Climate on Grape Ripening: Application to the Zoning of Sugar Content in the European Community. Office des Publications Officielles des Communautés Européennes, Luxembourg.
Sadras, V.O., Collins, M., Soar, C.J., 2008. Modelling variety-dependent dynamics of soluble solids and water in berries of *vitis vinifera*. Aust. J. Grape Wine Res. 14, 250–259.
Sadras, V.O., Moran, M.A., 2012. Elevated temperature decouples anthocyanins and sugars in berries of shiraz and cabernet franc. Aust. J. Grape Wine Res. 18, 115–122.
Tomasi, D., Jones, G., Giust, M., Lovat, L., Gaiotti, F., 2011. Grapevine phenology and climate change: phenology and trends in the veneto region of italy for 1964 – 2009. Am. J. Enol. Vitic. 62, 329–339.
Torregrosa, L., Doligez, A., Lecourieux, D., Rienth, M., Luchaire, N., Pieri, P., Chatbanyong, R., Shahood, R., Farnos, M., Roux, C., Adiveze, A., Pillet, J., Sire, Y., Zumstein, E., Veyret, M., Le Cunff, L., Lecourieux, F., Saurin, N., Muller, B., Ojeda, H., Houel, C., Péros, J.-P., This, P., Pellegrino, A., Romieu, C., 2017. Developmental, molecular and genetic studies on the grapevine response to temperature open breeding strategies for adaptation to warming. OENO One 51, 155–165.
van Leeuwen, C., Darriet, P., 2016. The impact of climate change on viticulture and wine quality. J. Wine Econ. 11, 150–167.
van Leeuwen, C., Destrac, A., 2017. Modified grape composition under climate change

conditions requires adaptations in the vineyard. OENO One 51, 147–154.
van Leeuwen, C., Friant, P., Chone, X., Tregoat, O., Koundouras, S., Dubourdieu, D., 2004. Influence of climate, soil and cultivar on terroir. Am. J. Enol. Vitic. 55, 207–217.
van Leeuwen, C., Seguin, G., 2006. The concept of terroir in viticulture. J. Wine Res. 17, 1–10.
van Leeuwen, C., Tregoat, O., Choné, X., Bois, B., Pernet, D., Gaudillère, J.-P., 2009. Vine water status is a key factor in grape ripening and vintage quality for red bordeaux wine. how can it be assessed for vineyard management purposes. J. Int. Sci. Vigne Vin 43, 121–134.
Verdugo-Vásquez, N., Acevedo-Opazo, C., Valdés-Gómez, H., Araya-Alman, M., Ingram, B., García de Cortázar-Atauri, I., Tisseyre, B., 2016. Spatial variability of phenology in two irrigated grapevine cultivar growing under semi-arid conditions. Precis. Agr. 17, 218–245.
Verdugo-Vásquez, N., Acevedo-Opazo, C., Valdés-Gómez, H., Ingram, B., García de Cortázar-Atauri, I., Tisseyre, B., 2018. Temporal stability of within-field variability of total soluble solids of grapevine under semi-arid conditions: a first step towards a spatial model. OENO One 52, 15–30.
Verdugo-Vásquez, N., Acevedo-Opazo, C., Valdés-Gómez, H., Ingram, B., García de Cortázar-Atauri, I., Tisseyre, B., 2019. Towards an empirical model to estimate the spatial variability of grapevine phenology at the within field scale. Precis. Agr. https://doi.org/10.1007/s11119-019-09657-7.
Verdugo-Vásquez, N., Pañitrur-De la Fuente, C., Ortega-Farías, S., 2017. Model development to predict phenological scales of table grapes (cvs. thompson, crimson and superior seedless and red globe) using growing degree days. OENO One 51, 277–288.
Vitasse, Y., François, C., Delpierre, N., Dufrêne, E., Kremer, A., Chuine, I., Delzon, S., 2011. Assessing the effects of climate change on the phenology of european temperate trees. Agric Meteorol. 151, 969–980.
Wang, E., Engel, T., 1998. Simulation of phenolgical development of wheat crops. Agric Syst. 58, 1–24.
Wang, J.Y., 1960. A critique of the heat unit approach to plant response studies. Ecology 41, 785–789.
Webb, L.B., Whetton, P.H., Barlow, E.W.R., 2007. Modelled impact of future climate change on the phenology of winegrapes in australia. Aust. J. Grape Wine Res. 13, 165–175.
Webb, I.B., Whetton, P.H., Bhend, J., Darbyshire, R., Briggs, P.R., Barlow, W.R., 2012. Earlier wine-grape ripening driven by climate warming and drying and management practices. Nat. Clim. Chang 2l, 259–264.
Winkler, A.J., Cook, J.A., Kliewer, W.M., Lider, L.A., 1962. General Viticulture. University of California Press Berkeley and Los Angeles.
Wolkovich, E.M., Burge, D.O., Walker, M.A., Nicholas, K.A., 2017. Phenological diversity provides opportunities for climate change adaptation in winegrapes. J. Ecol. 105, 905–912.
Xue, Q., Baenziger, P.S., 2004. Predicting phenological development in winter wheat. Clim. Res. 25, 243–252.
Zhu, J., Génard, M., Poni, S., Gambetta, G.A., Vivin, P., Vercambre, G., Trought, M.C.T., Ollat, N., Delrot, S., Dai, Z., 2018. Modelling grape growth in relation to whole-plant carbon and water fluxes. J. Exp. Bot. 70, 2505–2521.

Agricultural and Forest Meteorology 291 (2020) 108024

Contents lists available at ScienceDirect

Agricultural and Forest Meteorology

journal homepage: www.elsevier.com/locate/agrformet

# UniPhen – a unified high resolution model approach to simulate the phenological development of a broad range of grape cultivars as well as a potential new bioclimatic indicator

Daniel Molitor[a,*], Helder Fraga[b], Jürgen Junk[a]

[a] Luxembourg Institute of Science and Technology (LIST), Environmental Research and Innovation (ERIN) Department,41, rue du Brill, L-4422 Belvaux, Luxembourg
[b] Centre for the Research and Technology of Agro-Environmental and Biological Sciences, Universidade de Trás-os-Montes e Alto Douro, Quinta de Prados, P-5000-801 Vila Real, Portugal

ARTICLE INFO

*Keywords:*
Cumulative degree days
Climate change
High resolution phenological model
Grapevine
Precocity
*Vitis vinifera* L

ABSTRACT

Present investigations aimed at developing a unified cumulative degree day based model approach allowing for (i) a precise simulation of grapevine phenological development of a broad range of cultivars and (ii) a classification of the cultivar specific relative precocity of different cultivars at different stages of grape development. Based on a long-term (7-year) data set of high-resolution phenological observations for 11 cool climate cultivars originating from Remich/Luxembourg, the unified phenological model (UniPhen) was developed using a cumulative degree day approach with three temperature thresholds (lower threshold: 10 °C; upper threshold: 20 °C; heat threshold: 30 °C). The average normalized standard deviation of UniPhen over all stages and cultivars was 5.26 corresponding to 5.26 days at 15 °C. In the cross-validated model, on average 53% of the observations were located in a range of ± 3 days and 82% in a range of ± 7 days (assuming daily mean temperatures of 15 °C) around the predicted date. The sequence of the cultivar-specific relative precocity was not stable over the different stages of phenological development. The model approach (i) enables a precise simulation of all 31 BBCH stages between beginning of the bud swell (01) and berries being ripe for harvest (89) for 11 cultivars grown in the climatic conditions of the Luxembourgish grapegrowing region and (ii) is open to being extended to other grape cultivars and re-calibrated under deviant climatic conditions. Due to their instability, a classification of the cultivars' relative precocity is only reasonable if it relates to a specific phenological stage. UniPhen represents a precise high-resolution phenological model approach and might be applied as a bioclimatic indicator describing the suitability of a location/region for the cultivation of specific cultivars.

## 1. Introduction

The phenological development of grapevines (*Vitis vinifera* L.) as well as of many other crops is mainly temperature-driven. Although other atmospheric variables (e.g. radiation, precipitation) may influence the growth and development of grape plants, air temperature is considered the main factor influencing phenological timings (e.g., Caffarra and Eccel, 2010; Duchene et al., 2010; Fraga et al., 2016; García de Cortázar-Atauri et al., 2009; Gladstones, 2011; Jones, 2013; Jones and Davis, 2000; Nendel, 2010; van Leeuwen et al., 2008; Webb et al., 2007). As a consequence, commonly used grape phenology models are usually based on air temperature data as an input parameter (e.g., Caffarra and Eccel, 2010; Cola et al., 2014; Garcia de Cortazar-Atauri et al., 2009; Hoppmann and Berkelmann-Loehnertz, 2000; Oliveira, 1998; Parker et al., 2011; Webb et al., 2007).

Many models take into account linear air temperature sums or cumulative degree days calculated by accumulating temperatures above a defined threshold (often referred to as 'base temperature') between a start date or prior phenological stage and the target phenological stage (Amerine and Winkler, 1944; Duchene et al., 2010; Nendel, 2010; Parker et al., 2011; Zapata et al., 2015). Such linear cumulative degree day-based phenology models assume that the effect of temperatures on phenological development is linear and unlimited. However, there is physiological evidence that above plant-specific threshold temperatures, the forcing effect of the temperature will not increase further or even tends to decrease (Bonhomme, 2000; Mariani et al., 2012; Molitor et al., 2014b; Wang and Engel, 1998; Yan and Hunt, 1999). Consequently, the analyses of Molitor et al. (2014b) demonstrated that the incorporation of (i) an upper threshold temperature, above which a further increase of the temperature will not accelerate plant

* Corresponding author.
*E-mail addresses:* daniel.molitor@list.lu (D. Molitor), hfraga@utad.pt (H. Fraga), juergen.junk@list.lu (J. Junk).

https://doi.org/10.1016/j.agrformet.2020.108024
Received 5 June 2019; Received in revised form 25 March 2020; Accepted 28 April 2020

development and (ii) a heat threshold, above which a further increase of the temperature leads to a development deceleration, significantly improved the model accuracy compared to the cumulative degree day approaches previously published. Generally, simple cumulative degree day approaches are easily understandable for the grapegrowers (Parker et al., 2020). While commonly used phenological models focus on selected key stages of grapevine development (e.g., budburst (Garcia de Cortazar-Atauri et al., 2009; Nendel, 2010) and/or flowering and veraison (Caffarra and Eccel, 2010; Duchene et al., 2010; Hoppmann and Berkelmann-Loehnertz, 2000; Parker et al., 2011; Zapata et al., 2017)), the high-resolution phenological model proposed by Molitor et al. (2014b) is the first model covering all phenological stages according to the BBCH (Biologische Bundesanstalt, Bundessortenamt und CHemiche Industrie) scale (Lorenz et al., 1995) from budburst to berries ripe for harvest. This high-resolution allows the simulation of phenophases, where e.g. environmental conditions or crop cultural measures have a distinct influence on, e.g., yield formation (Molitor and Keller, 2016), wine typicity (Molitor and Junk, 2019) or susceptibility towards pests or diseases (Molitor et al., 2016).

Recently, additional phenological models have been developed covering the 17 stages of the phenological scale modified by Coombe (1995) (Ortega-Farias and Riveros-Burgos, 2019; Verdugo-Vasquez et al., 2017).

Originally, the high-resolution phenological model of Molitor et al. (2014b) was calibrated for the Müller-Thurgau (syn. Rivaner) cultivar and has meanwhile been parameterized for the Riesling (Molitor et al., 2016) and Pinot noir cultivars (Molitor and Junk, 2019) with optimized upper, lower and heat thresholds specifically for these cultivars. However, due to the specific optimized thresholds, the temperature sums necessary to reach a specific phenological stage in different cultivars are difficult to compare directly with each other. To the best of our knowledge, a unified phenological model covering all BBCH stages from the beginning of bud swelling to berries ripe to harvest that is valid for all possible cultivars does not yet exist in the scientific literature. Such a high resolution is of specific interest for the classification of relative precocity in specific phenological stages or in analyses of the effects of meteorological conditions in specific phenophases (Molitor and Keller, 2016). Frequently, the relative precocity of grape cultivars is classified according to the relative temporal position of the maturation period (either fixed as the moment of veraison (Parker et al., 2013), maturity (Wolkovich et al., 2018) or reaching a specific sugar content in berries (Parker et al., 2020; Wolkovich et al., 2017)). However, a cultivar classification into “early” and “late” might (i) depend on the specific environmental conditions in the location/region of observation and (ii) not be true for all phenological stages. There is a practical interest in classifying the relative precocity of different cultivars in other stages, such as budburst, when thinking for example about relative susceptibility towards late frost damage.

Consequently, the aim of the present investigation is (i) to obtain a long-term dataset of high-resolution phenological observations for 11 cool climate cultivars in an experimental vineyard in Remich/Luxembourg, and (ii) to develop a unified cumulative degree day-based model using the same threshold triplet valid for all cultivars of observation (as well as being valid for other cultivars) allowing for (a) a precise simulation of the phenological development and (b) a classification of the relative precocity of different cultivars at all BCCH stages between beginning of bud swelling and berries ripe for harvest.

## 2. Materials and methods

### 2.1. Vineyard of observation

Systematic phenological assessments in the Riesling, Rivaner (syn. Müller-Thurgau), Elbling, Gewürztraminer, Pinot blanc, Auxerrois, Sauvignon blanc, Pinot gris, Chardonnay, Merlot and Pinot noir cultivars took place from 2012 to 2018 in the experimental vineyard of the Institut Viti-Vinicole in Remich/Luxembourg (lat. 49°32′N; long. 6°21′E, 207 m a.s.l.). All cultivars were cultivatedother in a cane-pruned vertical shoot positioning system (VSP). Plots of the different cultivars were in direct proximity to each other. Grapevines were grafted onto SO4 rootstocks (except Merlot, grafted on to 101–14 MG) and planted between 1991 (Chardonnay) and 2004 (Merlot). Exact information about the cultivars of investigation is given in Supplementary Table 1. The space per plant was 2.4 $m^2$ (2 m between rows, 1.2 m between vines) and the canopy height approximately 2 m. Retained number of buds per plant in winter pruning was approximately 10. Six plants were monitored per cultivar; plants of observation were the same in all seven years.

### 2.2. Assessment of phenological stages

All phenological growth stages according to the BBCH scheme as defined by Lorenz et al. (1995) (Supplementary Table 2) between BBCH 01 and BBCH 85 were recorded when 50% of the vines or shoots exhibited the respective stage. The assessment intervals ranged from two to three days. Records were taken in all years in all cultivars by the same person. The date of reaching a specific phenological stage was noted as day of the year (DOY).

Maturity control took place at weekly intervals between veraison (BBCH 81) and harvest by collecting 100 randomly selected berries (clusters from different positions of the canopy; berries from different positions in the cluster) per cultivar (avoiding berries with visible bunch rot symptoms). The date of BBCH 89 was defined as the DOY when 60° Oechsle (=14.17° brix) were reached or exceeded for the first time in the respective year. 60° Oechsle represents the legal minimum threshold of total soluble solids for the production of wines with the protected designation of origin in Luxembourg. Total soluble solids (TSS) of the extracted juice were determined by FT-IR (FOSS NIRSystems, Laurel, MD, USA). Annual yields were not systematically recorded but are estimated to range on average between 60 and 100 hl/ha.

### 2.3. Meteorological measurements

Weather information was recorded during the period of examination by an automatic weather station of the national agricultural administration ASTA (Administration des services techniques de l'agriculture) located in Remich/Luxembourg in direct proximity (distance < 200 m) of the experimental vineyard. Air temperatures at 2 m and precipitation at 1 m height were measured at 10 min resolution. Key meteorological data are given in Supplementary Table 3.

### 2.4. Development of the unified high resolution phenological model approach “UniPhen”

In the present study, the approach of the high-resolution cumulative degree day-based phenological model, as previously developed for the Rivaner cultivar (Molitor et al., 2014b) and parameterized for Riesling (Molitor et al., 2016) and Pinot noir (Molitor and Junk, 2019), was applied to all selected cultivars.

In this approach with lower, upper and heat temperature thresholds, degree days (DD) for a specific day are calculated based on the daily average air temperatures (derived from the 10 min values) calculated using the following conditions:

$$
\begin{aligned}
DD_{(a;b;c)} &= 0\ ^\circ C, && \text{if } t < a \text{ or if } c+(b\text{-}a) < t\\
&(t - a)\ ^\circ C, && \text{if } a < t < b\\
&(b - a)\ ^\circ C, && \text{if } b < t\\
&((b - a) - (t - c))\ ^\circ C, && \text{if } c < t
\end{aligned}
$$

where $a$ is the lower threshold temperature ( °C), $b$ is the upper threshold temperature ( °C), c is the heat threshold temperature ( °C)

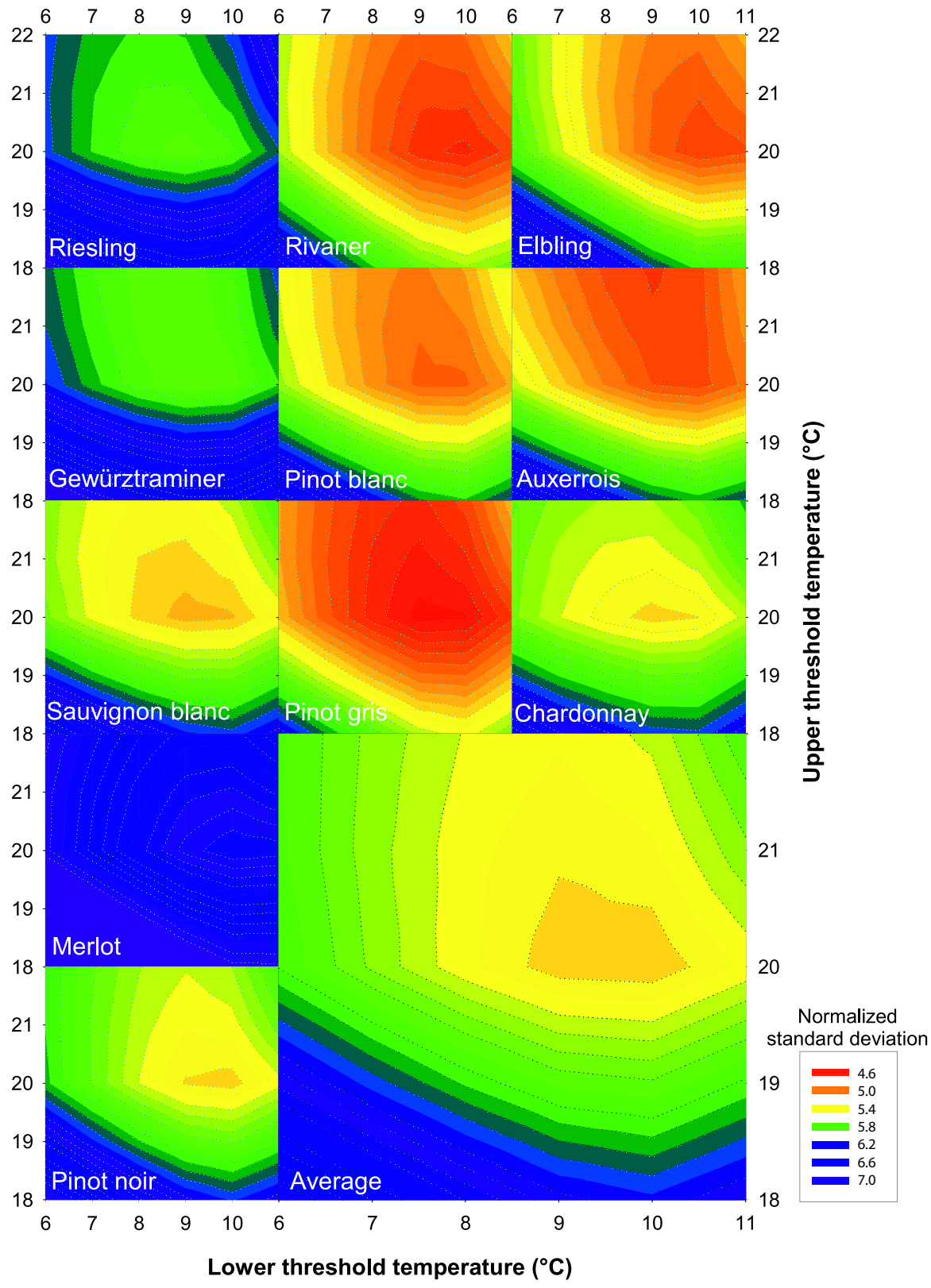


**Fig. 1.** Contour plots of normalized standard deviations $SD_{15°}$ depending on the lower and upper threshold temperatures for the 11 cultivars under observation, as well as the average for all cultivars.

and t the daily mean temperature (Supplementary Figure 1).

Degree days were calculated for every day for all integer temperature triplets between 6 and 11 °C as lower thresholds, 18 to 22 °C as the upper thresholds and 25 to 30 °C as the heat thresholds.

In the following, for every growth stage, degree days (DD) were summed up to cumulative degree days (CDDs). The reference date was the day of year (DOY) at which BBCH 09 was reached in Riesling (representing a standard cultivar in Central European viticulture).

**Table 1**
Cultivars of observation, as well as the respective lower, upper and heat threshold triplets leading to minimum average normalized standard deviations. $SD_{15°}$ = normalized standard deviation at 15 °C.

| Cultivar | Lower threshold | Upper threshold | Heat threshold | Average $SD_{20°}$ |
|---|---|---|---|---|
| Riesling | 9 | 20 | – | 5.76 |
| Rivaner | 10 | 20 | – | 4.74 |
| Elbling | 10 | 20 | – | 4.88 |
| Gewürztraminer | 9 | 20 | – | 5.66 |
| Pinot blanc | 9 | 20 | – | 4.98 |
| Auxerrois | 9 | 22 | – | 4.86 |
| Sauvignon blanc | 9 | 20 | – | 5.20 |
| Pinot gris | 9 | 20 | – | 4.56 |
| Chardonnay | 9 | 20 | – | 5.32 |
| Merlot | 9 | 20 | 23 | 6.14 |
| Pinot noir | 10 | 20 | – | 5.28 |
| | | | Average | 5.22 |

Cumulative degree days relative to the reference date were calculated using the Eq. (1):

$$CDD_{(a;b;c)} = \sum_{i=m+1}^{n} DD_{(a;b;c)} \quad (1)$$

where $CDD_{(a;b;c)}$ are the cumulative degree days relative to the date of BBCH 09 in Riesling; $DD_{(a;b;c)}$ the value of the degree day for the day *i;* *m* the DOY when BBCH 09 was observed in Riesling; and *n* the DOY when the target phenological stage was reached in the respective cultivar.

To determine general temperature thresholds to simulate all phenological stages between BBCH 01 and BBCH 89 in all cultivars, the following unified approach was applied. For all calculations, SPSS Statistics 19 (IBM, Chicago, IL, USA) was used:

a) For all tested threshold triplet combinations, standard deviations of the cumulative degree days were calculated for each phenological stage in each cultivar.
b) To normalize the relative value of the standard deviations caused by the daily DD values, standard deviations were divided by the theoretical DD at (15 °C (approximate growing season temperature in Remich in the period of observation (see Supplementary Table 3)) in the respective threshold triplet combinations.
c) Average normalized standard deviations per cultivar were calculated based on the normalized standard deviations of each of the stages BBCH 09 to BBCH 89. The lower the average normalized standard deviation, the better the adaptation of the model to the observation data. The temperature threshold triplet resulting in the minimum average normalized standard deviations was defined as the optimized temperature threshold for each cultivar.
d) Furthermore, the global average normalized standard deviation was calculated as the average value of all 11 cultivars. Based on the temperature threshold triplet resulting in the minimum average normalized standard deviations as an average of all cultivars, then the unified global optimized threshold temperature triplet was fixed.

Using the unified global optimized temperature thresholds of the best adapted approach, the average CDD values were calculated for each cultivar, relative to the date that BBCH 09 was reached in Riesling for each phenological stage between BBCH 01 and BBCH 89.

### 2.5. Data analysis

To assess the goodness of fit of the unified model approach, normalized standard deviations are given for all phenological stages and all cultivars. In fact, the normalized standard deviation represents the standard deviation in days assuming daily average temperatures of 15 °C.

Calculated CDD values based on the unified global optimized temperature threshold triplet in each phenological stage were analysed for the effect of the cultivar by one-way ANOVAs using SPSS Statistics 19 (IBM, Chicago, IL, USA). For each cultivars, years of observation were considered as replicates in statistical analyses. In cases where null-hypotheses were rejected ($P \leq 0.05$), pair-wise multiple comparisons according to Duncan's multiple comparison procedure were performed for cultivar effects.

Leave-one-out cross-validations according to Ladenbruch and Mickey (1968) were carried out to test the model precision. For each phenological stage and each cultivar, predicted CDD were calculated by averaging all but one (n - 1) data sets and the comparison with observed CDD. In order to assess the goodness of fit of the cross-validated model, mean absolute errors (MAE) were calculated for all phenological stages in each cultivar. The percentage of observations situated in a range of 15 or 35 CDD above or below the predicted cumulative degree days was calculated, with this range corresponding to ± 3 or 7 days around the observation date, at daily average temperatures of 15 °C.

## 3. Results

### 3.1. Phenological observation data

Supplementary Table 4 shows the days of the year (DOY) on which the phenological stages BBCH 01 to 89 were reached from 2012 to 2018 in the 11 cultivars of observation.

### 3.2. Optimized temperature thresholds triplets per cultivar

Normalized standard deviations are depicted in Fig. 1, depending on the lower and upper threshold temperature in the 11 cultivars of observations, as well as on the average of all cultivars.

The optimized temperature threshold per cultivar is given in Table 1.

Optimized lower threshold temperatures ranged between 9 and 10 °C, while upper thresholds were 20 °C in all cultivars except Auxerrois (22 °C).

The introduction of the heat threshold reduced the average normalized standard deviation only in the case of Merlot (6.14 instead of 6.32 in case of only two thresholds). In the other cultivars, the minimum average normalized standard deviations were achieved without heat threshold.

### 3.3. Unified global optimized temperature threshold triplet

The lowest global average normalized standard deviation on average of all 11 cultivars observed in case of the using 10 °C as the lower threshold temperature and 20 °C as the upper threshold temperature. The introduction of a heat threshold did not further decrease the global average normalized standard deviation. However, to avoid overlooking the verified decelerating effects of above optimum temperatures under warmer conditions, a heat threshold of 30 °C was defined for the unified phenological model, from now on referred to as “UniPhen”.

Global average normalized standard deviations using the unified optimized threshold triplet 10, 20 and 30 °C was 5.26, which corresponds to 5.26 days at daily average temperatures of 15 °C.

Average normalized standard deviations using optimized threshold triplets per cultivar differed only marginally from the average normalized standard deviations using the unified threshold triplet 10, 20 and 30 °C (Table 2).

### 3.4. The unified high-resolution phenological model uniphen

Table 3 presents the average $CDD_{10,20,30}$ values (average of all 7

**Table 2**
Average normalized standard deviations, using optimized threshold triplets per cultivar, compared with the average normalized standard deviations using the unified threshold triplet 10, 20 and 30 °C in the different cultivars. Δ= difference. $SD_{15°}$ = normalized standard deviation at 15 °C.

| Cultivar | Average $SD_{15°}$ using optimized threshold triplets per cultivar | Average $SD_{15°}$ using the unified threshold triplet 10, 20 and 30 °C | Δ |
|---|---|---|---|
| Riesling | 5.76 | 5.86 | 0.10 |
| Rivaner | 4.74 | 4.74 | 0.00 |
| Elbling | 4.88 | 4.88 | 0.00 |
| Gewürztraminer | 5.66 | 5.68 | 0.02 |
| Pinot blanc | 4.98 | 4.98 | 0.00 |
| Auxerrois | 4.86 | 4.92 | 0.06 |
| Sauvignon blanc | 5.20 | 5.22 | 0.02 |
| Pinot gris | 4.56 | 4.58 | 0.02 |
| Chardonnay | 5.32 | 5.36 | 0.04 |
| Merlot | 6.14 | 6.20 | 0.06 |
| Pinot noir | 5.28 | 5.28 | 0.00 |
| Global average | 5.22 | 5.24 | 0.04 |

seasons of observation) relative to BBCH 09 in Riesling until the respective BBCH stage was reached, according to UniPhen, as well as normalized standard deviations at 15 °C in the 11 cultivars.

On average of all the cultivars, the lowest average $SD_{20°}$ values were observed at BBCH 09 (1.6) and the highest at BBCH 89 (16.2). On average, for the stages BBCH 11 to 89, the lowest average $SD_{20°}$ values were observed in Pinot gris (4.6) and the highest in Merlot (6.2) (Table 3). On average for all the cultivars, the lowest average $SD_{15°}$ values of the stages BBCH 11 to 89 was 5.26 (Table 2, Table 3).

No significant differences were observed according to the Duncan test in the $CDD_{10,20,30}$ values ($P \leq 0.05$) between the 11 cultivars at stages 01, 03, 05, 07, 12, 53, 55 and 89. The earliest budburst (BBCH 09) was observed in Chardonnay and the latest in Riesling. Chardonnay and Elbling reached BBCH 09 significantly earlier than Riesling, while no significant differences were observed between the other cultivars. Flowering (BBCH 61) started significantly earlier in Chardonnay than in Riesling and Sauvignon blanc. Veraison (BBCH 81) was reached first by Rivaner and last by Merlot. In Rivaner, the $CDD_{10,20,30}$ values at veraison (BBCH 81) were significantly lower than in all other cultivars. BBCH 89 was observed first in Pinot noir and last in Elbling with no statistical differences between the cultivars of observation (Table 3, Table 4,

**Fig. 2** shows the heat map of the average $CDD_{10,20,30}$ values relative to BBCH 09 in Riesling until the respective BBCH stage was reached in the 11 cultivars of investigation. In each BBCH stage, the cultivar with the lowest $CDD_{10,20,30}$ value (= earliest development) is depicted in green and the cultivar with the highest $CDD_{10,20,30}$ value (= latest development) in red. Intermediate values are presented in graduated colours between green and red. Until bunch closure, Chardonnay showed the earliest development in most stages. Riesling was usually the cultivar with latest development in the early pre-flowering period stages while this was the case for Sauvignon blanc between the late pre-flowering stages and pea-size of the berries. Veraison and later stages were recorded in most cases earliest in Rivaner and latest in Merlot (Fig. 2).

### 3.5. Model validation

In the cross validated UniPhen model, average mean absolute errors (MAE) ranged from 7 (BBCH 09) to 70 $CDD_{10,20,30}$ (BBCH 89). On average, 53% of the observations were located in a range of ± 3 days and 82% of the observations in a range of ± 7 days (assuming daily mean temperatures of 15 °C) around the predicted cumulative degree day. Average mean absolute errors (MAE) per cultivar ranged between 19 in Pinot gris and 25 $CDD_{10,20,30}$ in Merlot (Supplementary Table 5).

## 4. Discussion

The present investigations confirmed the general suitability of the cumulative degree day approach using three threshold temperatures as proposed by Molitor et al. (2014b). Optimized lower threshold temperatures per cultivar were observed to be in a very narrow frame from 9 °C and 10 °C indicating the similar behaviour of all cultivars of investigation towards basic temperature requirements for phenological development. In comparison, lower threshold temperatures for grape development reported by other authors were e.g. 0 °C (Parker et al., 2011), 5 °C (Garcia de Cortazar-Atauri et al., 2009; Molitor et al., 2014b), 7 °C (Molitor et al., 2016), 8 °C (Alleweldt and Hofäcker, 1975), 10 °C (Amerine and Winkler, 1944; Schultz, 1992; Huglin, 1978) 13 °C (Hoppmann, 2010), and 15 °C (Peyer and Koblet, 1966).

Interestingly, besides Auxerrois, the optimized individual upper threshold temperatures of all cultivars, as well as the unified global optimized upper threshold, was determined to be 20 °C. This confirms additionally the upper threshold temperatures of 20 °C determined based on independent data sets for Müller-Thurgau (Molitor et al., 2014b) and Pinot noir (Molitor and Junk, 2019). Similarly, Gladstones (1992) demonstrated that the incorporation of an upper threshold temperature of 19 °C (in addition to the base temperature of 10 °C) improved the precision of the Winkler degree approach.

In present investigations, mathematically, the introduction of a heat threshold decreased the global average normalized standard deviation only in the case of Merlot. It might be discussed that the deviating reaction of Merlot might be influenced by the rootstock, which was 101–14 MG in Merlot and SO4 in all other cultivars.

Due to physiological evidence that the forcing effect of temperature decreases at above optimal temperatures (Mariani et al., 2012; Wang and Engel, 1998; Yan and Hunt, 1999), a heat threshold of 30 °C was defined for the unified model. Under present Central European climatic conditions, a heat threshold of 30 °C does not influence the model output since daily average temperatures above 30 °C are extremely unlikely. However, this heat threshold was nevertheless included in the model to avoid overlooking the verified decelerating effects of above optimum temperatures in warmer conditions (as expected in the area of investigation for the future (Molitor and Junk, 2019)). Additionally, given the future warming projected for many winemaking regions in the world (Fraga et al., 2019; Hannah et al., 2013; Jones et al., 2005), this threshold may become of importance in climate change impact studies. The selection of 30 °C as the heat threshold temperature takes into account practical reflections. Following the mathematically determined thresholds of 10 °C and 20 °C, the heat threshold of 30 °C was determined considering the high practical applicability of an approach using straight numbers. The unified phenological model using the threshold triplet 10, 20 and 30 °C is referred to as “UniPhen”.

Global average normalized standard deviations using the optimized threshold triplet correspond to 5.26 days (at 15 °C) demonstrating the high accuracy of the present unified model. The extremely low deviations between the average normalized standard deviations of the optimized threshold triplet per cultivar and the unified threshold triplet (corresponding to 0.04 days at 15 °C) are negligible in practical conditions and highlight the strong robustness of the unified model, independent of the cultivar.

In the present approach, the cumulative degree days until reaching a specific date are calculated relative to the date of reaching BBCH 09 in the Riesling cultivar. This starting date was selected since this stage can be determined relatively precisely in the field. In practical conditions, the start can either be fixed by observations or calculated using a budburst model (i) directly for the Riesling cultivar (Garcia de Cortazar-Atauri et al., 2009; Nendel, 2010) or (ii) indirectly via a model for any of the other cultivars of investigation, such as for Chardonnay (Caffarra and Eccel, 2010; Garcia de Cortazar-Atauri et al., 2009), Merlot, Pinot noir, Sauvignon blanc (Garcia de Cortazar-Atauri et al.,

**Table 3**
Average $CDD_{10,20,30}$ values relative to BBCH 09 in Riesling until reaching the respective BBCH stage, as well as normalized standard deviation at 15 °C in the 11 cultivars. Negative values indicate that the respective BBCH stage has been reached prior to BBCH 09 in Riesling. *Av* = Average. $SD_{15°}$ = normalized standard deviation at 15 °C. Average $SD_{15°}$ are the averages of the BBCH stages 11 to 89. $CDD_{10,20,30}$ = cumulative degree days using the optimized temperature threshold triplet 10, 20 and 30 °C.

| | Riesling | | Rivaner | | Elbling | | Gewürztraminer | | Pinot blanc | | Auxerrois | | Sauvignon blanc | | Pinot gris | | Chardonnay | | Merlot | | Pinot noir | | Average | |
|---|---|---|---|---|---|---|---|---|---|---|---|---|---|---|---|---|---|---|---|---|---|---|---|---|
| BBCH stage | *Av* | $SD_{15°}$ | *Av* | $SD_{15°}$ | *Av* | $SD_{15°}$ | *Av* | $SD_{15°}$ | *Av* | $SD_{15°}$ | *Av* | $SD_{15°}$ | *Av* | $SD_{15°}$ | *Av* | $SD_{15°}$ | *Av* | $SD_{15°}$ | *Av* | $SD_{15°}$ | *Av* | $SD_{15°}$ | *Av* | $SD_{15°}$ |
| 01 | −42.6 | 3.0 | −44.7 | 3.6 | −44.9 | 3.6 | −43.7 | 3.6 | −42.4 | 3.8 | −42.9 | 3.6 | −39.8 | 4.2 | −41.0 | 3.6 | −45.0 | 3.6 | −43.9 | 3.8 | −44.7 | 3.6 | −43.2 | 3.6 |
| 03 | −31.1 | 3.0 | −33.6 | 3.4 | −35.0 | 3.8 | −33.9 | 3.2 | −32.8 | 3.4 | −32.5 | 3.4 | −30.8 | 3.6 | −32.3 | 3.2 | −38.5 | 3.4 | −33.4 | 3.6 | −34.6 | 3.6 | −33.5 | 3.4 |
| 05 | −24.2 | 3.0 | −27.7 | 3.4 | −27.6 | 3.4 | −26.3 | 3.6 | −25.2 | 3.8 | −23.0 | 3.6 | −20.2 | 3.2 | −24.6 | 3.2 | −31.4 | 3.4 | −22.5 | 4.2 | −25.8 | 3.8 | −25.3 | 3.6 |
| 07 | −12.7 | 2.4 | −15.2 | 3.0 | −19.4 | 3.0 | −18.3 | 2.8 | −14.2 | 3.0 | −13.8 | 3.0 | −12.9 | 2.4 | −12.8 | 2.4 | −23.1 | 3.0 | −12.7 | 3.4 | −16.3 | 2.8 | −15.6 | 2.8 |
| 09 | 0.0 | 0.0 | −5.0 | 2.0 | −10.6 | 2.2 | −8.7 | 2.0 | −6.7 | 1.8 | −0.6 | 1.6 | −3.0 | 1.4 | −0.5 | 1.0 | −16.2 | 2.2 | −0.3 | 1.6 | −6.1 | 1.2 | −5.2 | 1.6 |
| 11 | 7.4 | 1.6 | 5.8 | 1.4 | −1.7 | 2.6 | 2.0 | 1.2 | 2.0 | 1.8 | 5.0 | 1.6 | 5.8 | 1.8 | 6.2 | 1.2 | −7.8 | 1.2 | 6.7 | 1.8 | 5.1 | 1.2 | 3.3 | 1.6 |
| 12 | 14.8 | 2.0 | 12.2 | 2.2 | 1.7 | 2.4 | 9.7 | 1.6 | 10.5 | 2.4 | 11.6 | 2.2 | 9.5 | 2.4 | 13.3 | 2.4 | 2.8 | 1.0 | 12.9 | 3.0 | 9.6 | 2.0 | 9.9 | 2.2 |
| 13 | 21.7 | 2.0 | 18.0 | 2.4 | 9.4 | 2.4 | 19.1 | 2.2 | 19.9 | 2.0 | 18.4 | 2.4 | 17.1 | 2.4 | 18.1 | 2.0 | 7.6 | 1.6 | 19.2 | 2.8 | 15.7 | 2.2 | 16.7 | 2.2 |
| 14 | 37.3 | 2.2 | 26.7 | 2.6 | 17.4 | 2.6 | 25.2 | 3.0 | 30.1 | 2.0 | 28.6 | 2.2 | 34.7 | 2.2 | 32.4 | 1.8 | 17.3 | 2.2 | 27.8 | 4.4 | 26.2 | 2.4 | 27.6 | 2.6 |
| 15 | 47.0 | 2.0 | 43.7 | 1.6 | 25.8 | 2.2 | 42.2 | 2.6 | 45.4 | 2.4 | 44.1 | 1.6 | 45.9 | 2.4 | 48.7 | 1.8 | 30.9 | 2.2 | 45.5 | 3.4 | 42.2 | 2.8 | 41.9 | 2.2 |
| 16 | 59.7 | 1.4 | 60.8 | 2.2 | 40.5 | 2.2 | 53.7 | 2.4 | 60.7 | 2.4 | 59.6 | 1.8 | 59.2 | 2.8 | 59.8 | 1.6 | 47.0 | 1.8 | 59.0 | 2.8 | 54.7 | 1.8 | 55.9 | 2.2 |
| 17 | 76.5 | 1.6 | 73.6 | 2.4 | 54.4 | 2.4 | 68.2 | 2.4 | 77.9 | 2.2 | 73.2 | 2.2 | 84.8 | 2.4 | 76.7 | 1.2 | 56.8 | 1.8 | 75.1 | 2.8 | 71.1 | 1.4 | 71.7 | 2.0 |
| 18 | 89.7 | 1.8 | 86.0 | 2.6 | 63.9 | 2.6 | 79.4 | 1.6 | 87.6 | 2.4 | 87.3 | 2.2 | 97.8 | 3.2 | 90.3 | 1.4 | 68.7 | 2.2 | 90.4 | 3.0 | 79.7 | 1.4 | 83.7 | 2.2 |
| 19 | 109.1 | 2.2 | 101.6 | 2.2 | 77.1 | 2.4 | 92.3 | 2.0 | 106.1 | 2.6 | 106.1 | 2.6 | 115.9 | 3.0 | 116.2 | 4.0 | 85.5 | 2.4 | 105.5 | 3.2 | 99.5 | 1.2 | 101.4 | 2.6 |
| 53 | 54.6 | 3.4 | 57.0 | 3.0 | 46.6 | 4.0 | 54.2 | 4.2 | 51.2 | 4.2 | 51.4 | 4.0 | 55.8 | 3.8 | 54.4 | 3.2 | 40.8 | 3.4 | 49.9 | 4.6 | 49.3 | 3.6 | 51.4 | 3.8 |
| 55 | 81.7 | 2.6 | 71.0 | 6.0 | 69.3 | 4.0 | 92.3 | 5.2 | 80.0 | 2.6 | 78.3 | 3.0 | 81.3 | 4.8 | 79.0 | 4.6 | 66.9 | 3.6 | 79.9 | 4.8 | 71.2 | 3.8 | 77.4 | 4.0 |
| 57 | 158.7 | 4.0 | 149.8 | 4.0 | 146.9 | 3.8 | 157.9 | 3.6 | 156.6 | 4.0 | 160.6 | 5.4 | 167.7 | 5.2 | 163.1 | 4.0 | 129.2 | 4.8 | 167.5 | 4.6 | 150.6 | 4.4 | 155.3 | 4.4 |
| 61 | 221.8 | 6.4 | 214.4 | 6.0 | 215.6 | 7.0 | 221.2 | 6.2 | 214.5 | 6.2 | 216.5 | 6.6 | 231.4 | 6.0 | 213.4 | 6.4 | 179.7 | 8.6 | 218.4 | 6.8 | 202.2 | 7.2 | 213.6 | 6.6 |
| 63 | 232.8 | 6.2 | 226.3 | 5.6 | 228.1 | 6.4 | 231.1 | 5.8 | 225.8 | 5.6 | 232.2 | 6.0 | 247.1 | 6.2 | 223.1 | 5.6 | 194.6 | 7.6 | 228.9 | 6.4 | 217.9 | 6.4 | 226.2 | 6.2 |
| 65 | 242.6 | 6.0 | 235.8 | 5.2 | 239.3 | 6.4 | 239.4 | 5.8 | 234.9 | 5.2 | 246.8 | 5.8 | 261.7 | 5.4 | 233.9 | 5.2 | 207.8 | 7.0 | 239.9 | 6.8 | 228.5 | 6.0 | 237.3 | 5.8 |
| 68 | 261.4 | 6.0 | 250.0 | 4.8 | 255.3 | 6.0 | 258.2 | 6.4 | 251.1 | 5.6 | 263.3 | 5.6 | 273.4 | 5.6 | 251.7 | 5.4 | 226.9 | 7.0 | 256.7 | 6.8 | 240.7 | 5.6 | 253.5 | 5.8 |
| 69 | 268.9 | 5.8 | 259.5 | 4.8 | 265.3 | 5.8 | 266.2 | 6.0 | 264.5 | 5.2 | 273.6 | 5.8 | 285.7 | 5.8 | 263.8 | 5.4 | 235.7 | 7.0 | 270.1 | 6.4 | 250.1 | 5.8 | 262.9 | 6.2 |
| 71 | 283.7 | 5.6 | 271.8 | 5.0 | 277.9 | 4.8 | 284.3 | 6.0 | 281.2 | 5.0 | 292.5 | 5.4 | 302.3 | 6.2 | 279.6 | 5.6 | 251.3 | 7.4 | 289.0 | 6.2 | 266.2 | 5.4 | 280.0 | 5.6 |
| 73 | 316.1 | 5.8 | 306.1 | 5.0 | 315.4 | 5.0 | 325.0 | 7.4 | 297.0 | 8.4 | 324.9 | 7.4 | 338.3 | 6.0 | 307.9 | 5.4 | 287.0 | 6.2 | 323.2 | 5.6 | 301.2 | 5.4 | 312.9 | 6.2 |
| 75 | 406.8 | 7.4 | 391.3 | 7.0 | 398.4 | 7.4 | 422.3 | 8.0 | 402.1 | 6.8 | 412.3 | 5.4 | 431.4 | 6.4 | 401.1 | 6.4 | 376.0 | 8.6 | 374.8 | 6.0 | 384.8 | 8.6 | 400.1 | 7.0 |
| 77 | 461.3 | 11.2 | 488.5 | 8.2 | 433.0 | 6.4 | 471.2 | 14.4 | 438.9 | 7.6 | 453.4 | 6.2 | 478.0 | 11.4 | 434.0 | 7.0 | 424.0 | 5.8 | 521.9 | 11.0 | 512.9 | 14.8 | 465.2 | 9.4 |
| 79 | 538.4 | 13.6 | 607.9 | 4.2 | 496.9 | 7.8 | 536.7 | 15.4 | 513.4 | 11.2 | 544.7 | 7.6 | 570.3 | 9.0 | 502.8 | 6.6 | 526.4 | 7.4 | 669.7 | 20.6 | 627.0 | 10.8 | 557.7 | 10.4 |
| 81 | 777.3 | 12.6 | 653.3 | 5.0 | 759.8 | 4.8 | 739.7 | 5.8 | 752.2 | 4.8 | 752.0 | 6.4 | 764.0 | 5.0 | 729.5 | 6.0 | 745.7 | 7.4 | 784.3 | 6.0 | 730.8 | 6.2 | 744.4 | 6.4 |
| 83 | 797.7 | 12.0 | 687.0 | 4.8 | 782.1 | 4.2 | 766.4 | 5.8 | 780.5 | 4.6 | 772.6 | 6.6 | 788.2 | 5.0 | 765.9 | 3.8 | 769.1 | 6.2 | 800.0 | 9.6 | 762.7 | 5.2 | 770.2 | 6.2 |
| 85 | 819.9 | 12.2 | 719.0 | 6.4 | 801.3 | 5.6 | 792.2 | 6.8 | 803.7 | 6.2 | 791.7 | 6.4 | 807.9 | 6.0 | 791.9 | 3.8 | 788.2 | 7.2 | 834.3 | 7.4 | 787.5 | 4.6 | 794.3 | 6.6 |
| 89 | 996.8 | 14.8 | 947.9 | 18.6 | 1009.0 | 16.2 | 948.2 | 15.2 | 985.9 | 16.2 | 976.4 | 15.6 | 965.5 | 15.8 | 979.4 | 17.0 | 976.1 | 17.8 | 997.0 | 14.4 | 939.7 | 17.2 | 974.7 | 16.2 |
| *Av* (11–89) | | 5.8 | | 4.8 | | 5.0 | | 5.6 | | 5.0 | | 5.0 | | 5.2 | | 4.6 | | 5.4 | | 6.2 | | 5.2 | | 5.2 |

**Table 4**
Significant differences between the $CDD_{10,20,30}$ values reaching the respective phenological stages in the different cultivars. $CDD_{10,20,30}$ values of the same BBCH (Lorenz et al., 1995) stage marked with the same letter did not differ significantly (according to the Duncan test ($P \leq 0.05$)). If no significant differences were observed, no notations were depicted.

| BBCH stage | Riesling | Rivaner | Elbling | Gewürz-traminer | Pinot blanc | Auxerrois | Sauvignon blanc | Pinot gris | Chardonnay | Merlot | Pinot noir |
|---|---|---|---|---|---|---|---|---|---|---|---|
| 01 | | | | | | | | | | | |
| 03 | | | | | | | | | | | |
| 05 | | | | | | | | | | | |
| 07 | | | | | | | | | | | |
| 09 | c | bc | ab | abc | abc | bc | bc | bc | a | c | bc |
| 11 | b | b | ab | b | b | b | b | b | a | b | b |
| 12 | | | | | | | | | | | |
| 13 | b | ab | ab | ab | ab | ab | ab | ab | a | ab | ab |
| 14 | b | ab | a | ab | ab | ab | b | ab | a | ab | ab |
| 15 | c | bc | a | bc | c | bc | c | c | ab | c | bc |
| 16 | bc | c | a | bc | c | bc | bc | bc | ab | bc | bc |
| 17 | cd | cd | a | bc | cd | cd | d | cd | ab | cd | c |
| 18 | cd | cd | a | bc | cd | cd | d | cd | ab | cd | bc |
| 19 | de | cde | a | bc | cde | cde | e | e | ab | cde | bcd |
| 53 | | | | | | | | | | | |
| 55 | | | | | | | | | | | |
| 57 | b | ab | ab | b | b | b | b | b | a | b | ab |
| 61 | b | ab | ab | ab | ab | ab | b | ab | a | ab | ab |
| 63 | ab | ab | ab | ab | ab | ab | b | ab | a | ab | ab |
| 65 | ab | ab | ab | ab | ab | b | b | ab | a | ab | ab |
| 68 | ab | ab | ab | ab | ab | ab | b | ab | a | ab | ab |
| 69 | ab | ab | ab | ab | ab | ab | b | ab | a | ab | ab |
| 71 | ab | ab | ab | ab | ab | b | b | ab | a | b | aba |
| 73 | ab | ab | ab | ab | a | ab | b | ab | a | ab | ab |
| 75 | abc | abc | abc | bc | abc | abc | c | abc | a | a | ab |
| 77 | abc | bcd | ab | abcd | ab | abc | abcd | ab | a | d | cd |
| 79 | ab | cde | a | ab | ab | abc | bcd | ab | ab | e | de |
| 81 | cd | a | bcd | bc | bcd | bcd | bcd | b | bcd | d | b |
| 83 | b | a | b | b | b | b | b | b | b | b | b |
| 85 | bc | a | bc | bc | bc | bc | bc | bc | b | c | b |
| 89 | | | | | | | | | | | |

2009) or Müller-Thurgau (Molitor et al., 2014a). If using a model for any of the 10 cultivars of investigation (besides Riesling), the calculated starting date might be corrected by the thermal-temporal difference between BBCH 09 in Riesling and the respective cultivars. Correction factors ($CDD_{10,20,30}$) can be derived from Table 3. However, it has to be kept in mind, that, besides Chardonnay, the other cultivars of investigation did not differ significantly from Riesling in case of the $CDD_{10,20,30}$ values at the date of BBCH 09. Hence, models for BBCH 09 for cultivars other than Riesling may also be directly used to calculate the starting date of UniPhen.

Generally, using a biological stage (here: budburst (BBCH 09) in Riesling) as the starting date of the temperature sum accumulation makes the model more robust than calendar-based models facing differences in the temperature conditions before budburst (influenced by the location and annual meteorological conditions).

Generally, on average for all cultivars, normalized standard deviations at 15 °C were lowest at stages around BBCH 09. Here, standard deviations corresponded on average to around 2 days, indicating the extremely high model precision in the pre-flowering period. During flowering (BBCH 61 – 69), in post-flowering stages (BBCH 71–79) as well as at veraison (BBCH 81), average normalized standard deviations corresponded in most stages to 4 to 6 days. Higher average normalized standard deviations were observed in stages 77 (beginning of bunch closure) and 79 (end of bunch closure). The explanation for this is (i) that the determination of these stages is highly influenced by the cluster structure, which is defined by the success of the flowering process, the water and nutrient supply, as well as the crop load (Molitor et al., 2014b) as well as (ii) the perception of e.g. bunch closure is more subjective than the perception of e.g. budburst or flowering (Verdugo-Vasquez et al., 2015). The highest deviations were observed for stage BBCH 89, which, for present observation data sets, was defined as the day of the year when 60° Oechsle were reached or exceeded for the first time in the respective years. These high deviations can be explained by (i) the interval of observations (7 days compared to 2–3 days for the other stages), (ii) annual differences in the crop load influencing the sugar accumulation (Santesteban and Royo, 2006) and (iii) the cumulative nature of the model accumulating potential systematic errors.

Interestingly, differences in average normalized standard deviations between the different cultivars were low (4.6 days in Pinot gris vs. 6.2 days in Merlot) indicating that UniPhen might be applied to all cultivars of investigation without distinct differences in model precision.

UniPhen allows for a classification of the relative precocity of all 11 cultivars under investigation in each of the 31 BBCH stages between 01 and 89 and may be extended to any other grape cultivar. As a major output of the present investigation, the sequence of the relative precocity of the different cultivars is not stable over the different stages of phenological development. As an example, Elbling is the first of all 11 cultivars to reach BBCH stages 14 to 19 while reaching BBCH 89 last. Consequently, the present investigations demonstrate that a general classification of grape cultivars in groups such as “early cultivars” or “late cultivars” are of limited information and should not be used herein. Instead, a classification of the cultivars’ relative precocity is only reasonable if related to a specific phenological stage. Furthermore, a general classification into “early” and “late” cultivars is highly questionable since under different climatic conditions, cultivars with completely different annual heat demands are traditionally cultivated (Fraga et al., 2016). For example, in the climatic conditions of the Luxembourgish winegrowing region, Riesling is the traditional cultivar with the latest ripening period, while in Mediterranean conditions, Riesling might be considered as an early ripening cultivar. However, we assume that the relative precocity of different cultivars to each other at the same stage does not change even under completely different climatic conditions, making UniPhen applicable in different climatic conditions and for a broad range of cultivars.

| BBCH stage | Riesling | Rivaner | Elbling | Gewürz-traminer | Pinot blanc | Auxerrois | Sauvignon blanc | Pinot gris | Chardonnay | Merlot | Pinot noir |
|---|---|---|---|---|---|---|---|---|---|---|---|
| 01 | -43 | -45 | -45 | -44 | -42 | -43 | -40 | -41 | -45 | -44 | -45 |
| 03 | -31 | -34 | -35 | -34 | -33 | -33 | -31 | -32 | -39 | -33 | -35 |
| 05 | -24 | -28 | -28 | -26 | -25 | -23 | -20 | -25 | -31 | -23 | -26 |
| 07 | -13 | -15 | -19 | -18 | -14 | -14 | -13 | -13 | -23 | -13 | -16 |
| 09 | 0 | -5 | -11 | -9 | -7 | -1 | -3 | -1 | -16 | 0 | -6 |
| 11 | 7 | 6 | -2 | 2 | 2 | 5 | 6 | 6 | -8 | 7 | 5 |
| 12 | 15 | 12 | 2 | 10 | 11 | 12 | 10 | 13 | 3 | 13 | 10 |
| 13 | 22 | 18 | 9 | 19 | 20 | 18 | 17 | 18 | 8 | 19 | 16 |
| 14 | 37 | 27 | 17 | 25 | 30 | 29 | 35 | 32 | 17 | 28 | 26 |
| 15 | 47 | 44 | 26 | 42 | 45 | 44 | 46 | 49 | 31 | 46 | 42 |
| 16 | 60 | 61 | 41 | 54 | 61 | 60 | 59 | 60 | 47 | 59 | 55 |
| 17 | 77 | 74 | 54 | 68 | 78 | 73 | 85 | 77 | 57 | 75 | 71 |
| 18 | 90 | 86 | 64 | 79 | 88 | 87 | 98 | 90 | 69 | 90 | 80 |
| 19 | 109 | 102 | 77 | 92 | 106 | 106 | 116 | 116 | 86 | 106 | 100 |
| 53 | 55 | 57 | 47 | 54 | 51 | 51 | 56 | 54 | 41 | 50 | 49 |
| 55 | 82 | 71 | 69 | 92 | 80 | 78 | 81 | 79 | 67 | 80 | 71 |
| 57 | 159 | 150 | 147 | 158 | 157 | 161 | 168 | 163 | 129 | 168 | 151 |
| 61 | 222 | 214 | 216 | 221 | 215 | 217 | 231 | 213 | 180 | 218 | 202 |
| 63 | 233 | 226 | 228 | 231 | 226 | 232 | 247 | 223 | 195 | 229 | 218 |
| 65 | 243 | 236 | 239 | 239 | 235 | 247 | 262 | 234 | 208 | 240 | 229 |
| 68 | 261 | 250 | 255 | 258 | 251 | 263 | 273 | 252 | 227 | 257 | 241 |
| 69 | 269 | 260 | 265 | 266 | 265 | 274 | 286 | 264 | 236 | 270 | 250 |
| 71 | 284 | 272 | 278 | 284 | 281 | 293 | 302 | 280 | 251 | 289 | 266 |
| 73 | 316 | 306 | 315 | 325 | 297 | 325 | 338 | 308 | 287 | 323 | 301 |
| 75 | 407 | 391 | 398 | 422 | 402 | 412 | 431 | 401 | 376 | 375 | 385 |
| 77 | 461 | 489 | 433 | 471 | 439 | 453 | 478 | 434 | 424 | 522 | 513 |
| 79 | 538 | 608 | 497 | 537 | 513 | 545 | 570 | 503 | 526 | 670 | 627 |
| 81 | 777 | 653 | 760 | 740 | 752 | 752 | 764 | 730 | 746 | 784 | 731 |
| 83 | 798 | 687 | 782 | 766 | 781 | 773 | 788 | 766 | 769 | 800 | 763 |
| 85 | 820 | 719 | 801 | 792 | 804 | 792 | 808 | 792 | 788 | 834 | 788 |
| 89 | 997 | 948 | 1009 | 948 | 986 | 976 | 966 | 979 | 976 | 997 | 940 |

**Fig. 2.** Heat map of the average $CDD_{10,20,30}$ values relative to BBCH 09 in Riesling until the respective BBCH stage was reached in the 11 cultivars of investigation. In each BBCH stage, the cultivar with the lowest $CDD_{10,20,30}$ value (=earliest development) is depicted in green and the cultivar with the highest $CDD_{10,20,30}$ value (=latest development) in red. Intermediate values are presented in graduated colours between green and red. (For interpretation of the references to colour in this figure legend, the reader is referred to the web version of this article.)

In most stages, significant differences between the cultivars were observed. The fact that at stage BBCH 89, cultivars did not differ significantly might be explained by the abovementioned effects of the interval of observation and the natural annual differences in the crop load.

Knowledge of the classification of relative precocity can be used in practical conditions, e.g. for the selection of cultivars. Information about the relative precocity of budburst (BBCH 09) might be important for cultivar selection in regions where late frost damages might constitute a serious threat for sustainable wine production, such as in many viticulture regions currently considered as “cool-climate” regions (Kartschall et al., 2015; Leolini et al., 2018; Madelin and Beltrando, 2005; Modedale et al., 2015; Molitor et al., 2014a; Orlandini et al., 2003; Poling, 2008; Sgubin et al., 2018). Here cultivars with early bud development and early bud burst might be avoided based on the information derived from the present model.

Another example for the potential application of the classification is the observed differences in the CDD reaching beginning of bunch closure (BBCH 77) – traditionally a moment for botryticide treatments (Molitor et al., 2018). Assuming a relatively constant fruit set and water-/nutrient supply, a classification of relative precocity at this stage might be used to time botryticide applications. Here cultivars might be classified into different groups of precocity (e.g. group 1: Elbling, Pinot blanc, Pinot gris, Chardonnay; group 2: Riesling, Gewürztraminer, Auxerrois, Sauvignon blanc; group 3: Rivaner, Merlot, Pinot noir (here: clone Freiburg L 13, other clones might be classified differently)) and applications might be timed according to the expected moment of reaching BBCH 77 in the specific groups.

Furthermore, the classification of relative precocity of the maturity period (BBCH 81–89) might be used for the selection of cultivars in climate change adaptation strategies. Since high temperatures in the maturity period negatively affect the fruitiness and aroma of grapes and wines (Duchene et al., 2010), cultivars with a later maturity period, i.e. grapes that usually ripen under cooler temperature conditions, might be selected based on the UniPhen classification to adapt to climate change and maintain the typicity of a specific region. However, such an adaption strategy needs to guarantee that the annual heat consumption of a specific region or location is sufficient to lead to adequate grape maturity. This information about the general suitability of cultivars for cultivation under specific climatic conditions might also be derived from the UniPhen model. The model opens the possibility of calculating the virtual dates of specific phenological stages to be reached based on the long-term observation of projection temperature datasets. In fact, cultivars, in which on average stage BBCH 89 (in present study defined as reaching 14.18° brix) is projected not to be reached, are not suitable for production of wines with protected designation of origin as defined in Luxembourg. Consequently, UniPhen might be used as a bioclimatic indicator providing information about the suitability of a region/location for a specific cultivar. Commonly used bioclimatic indicators in viticulture, such as the average growing season temperature according to Jones (2007), the Winkler index (Amerine and Winkler, 1944) or the heliothermic index according to Huglin (1978), operate with fixed calendar-based start and end dates and do not take into account the plant response to temperature (Caubel et al., 2015). Hence, such bioclimatic indicators do not perfectly reflect the real vegetation period of specific cultivars (Holzkämper et al., 2010). These limitations could be overcome when using UniPhen as a bioclimatic indicator.

UniPhen is generally open for any other grape cultivar. Additional, newly selected or crossed cultivars could be introduced to the UniPhen system based on observation data. In case additional observation data (from the same location) of at least one of the 11 cultivars mentioned in the present manuscript are absent, BBCH 09 in Riesling might be

simulated by one of the budburst models described above.

At present, the high-resolution observation data of 15 late ripening cultivars cultivated in the abovementioned observation vineyard in Remich are recorded and will be included in the next version of the model. Furthermore, UniPhen might be extended to other phenological stages than the stages covered by the BBCH scale or e.g. additional ° brix levels (provided that respective records for calibration are available).

Generally, it has to be kept in mind that the present model is based on observation data originating from one location, and further investigations and adaptation to other locations are required. Nevertheless, based on the results of leave-one-out cross- validation, we assume that the model should be applicable in other regions with comparable climatic conditions. In different climatic conditions, the model may need to be validated before being applied. The model allows the selection of different parameterization options, which can be useful when adapting the model to other regions. Generally, the model design is open for re-calibration based on local observation data.

## 5. Conclusions

The unified grape phenological model developed, UniPhen, enables a precise simulation of all 31 BBCH stages between the beginning of bud swell (01) and berries ripe for harvest (89) for 11 cultivars grown in the climatic conditions of the Luxembourgish grapegrowing region using a unified cumulative degree day approach with three temperature thresholds at 10 °C, 20 °C and 30 °C.

Investigations revealed that the sequence of the relative precocity of the different cultivars was not stable over the different stages of phenological development. As a consequence, a classification of cultivars' relative precocity is only reasonable if it relates to a specific phenological stage.

The model is open to be extended for other grape cultivars and re-calibration in different climatic conditions. UniPhen could be used as an indicator for the suitability of a location/region for the cultivation of specific cultivars overcoming the limitations of commonly used calendar-based bioclimatic indicators.

## Declaration of Competing Interest

The authors declare that they have no known competing financial interests or personal relationships that could have appeared to influence the work reported in this paper.

## Acknowledgements

The authors thank R. Mannes, M. Schultz & S. Fischer (IVV - Institut Viti-Vinicole, Remich, Luxembourg) for providing meteorological and grape maturity data sets, L. Auguin for language editing as well as M. Schultz, R. Mannes (IVV), N. Baron, R. Rausch, L. Vesque, B. Biewers & D. Dam (LIST – Luxembourg Institute of Science and Technology) for supporting the phenological assessments.

This work was partly funded by the Institut Viti-Vinicole (Remich/Luxembourg) in the framework of the research projects "TerroirFuture" and "VinoManAOP", as well as by the European Union in the framework of the research project "Clim4Vitis" (Horizon 2020 research and innovation programme; grant agreement No 810176). Helder Fraga thanks the FCT for CEECIND/00447/2017.

## References

Alleweldt, G., Hofäcker, W., 1975. Einfluss von Umweltfaktoren auf Austrieb, Blüte, Fruchtbarkeit und Triebwachstum bei der Rebe. Vitis 14, 103–115.

Amerine, M.A., Winkler, A.J., 1944. Composition and quality of musts and wines of California grapes. Hilgardia 15, 493–675.

Bonhomme, R., 2000. Review: bases and limits to using 'degree.day' units. Eur. J. Agron. 13, 1–10.

Caffarra, A., Eccel, E., 2010. Increasing the robustness of phenological models for Vitis vinifera cv. Chardonnay. Int. J. Biometeorol. 54, 255–267. https://doi.org/10.1007/s00484-009-0277-5.

Caubel, J., et al., 2015. Broadening the scope of ecoclimatic indicators to assess crop climate suitability according to ecophysiological, technical and quality criteria. Agric. For. Meteorol. 207, 94–106. https://doi.org/10.1016/j.agrformet.2015.02.005.

Cola, G., et al., 2014. Description and testing of a weather-based model for predicting phenology, canopy development and source-sink balance in Vitis vinifera L. cv. Barbera. Agric. For. Meteorol. 184, 117–136. https://doi.org/10.1016/j.agrformet.2013.09.008.

Duchene, E., Huard, F., Dumas, V., Schneider, C., Merdinoglu, D., 2010. The challenge of adapting grapevine varieties to climate change. Climate Res. 41, 193–204. https://doi.org/10.3354/cr00850.

Fraga, H., Pinto, J.G., Santos, J.A., 2019. Climate change projections for chilling and heat forcing conditions in European vineyards and olive orchards: a multi-model assessment. Climat. Change 152, 179–193. https://doi.org/10.1007/s10584-018-2337-5.

Fraga, H., et al., 2016. Statistical modelling of grapevine phenology in Portuguese wine regions: observed trends and climate change projections. J. Agric. Sci. 154, 795–811. https://doi.org/10.1017/S0021859615000933.

García de Cortázar-Atauri, I., Brisson, N., Gaudillere, J., 2009. Performance of several models for predicting budburst date of grapevine (*Vitis vinifera* L.). Int. J. Biometeorol. 53, 317–326. https://doi.org/10.1007/s00484-009-0217-4.

Gladstones, J., 1992. Viticulture and environment. Ed. Winetitles, Adelaide, 310 p.

Gladstones, J., 2011. Wine, Terroir and Climate Change. Wakefield press, Kent town SA, pp. 279.

Hannah, L., et al., 2013. . Climate change, wine, and conservation. Proc. Natl. Acad. Sci. U.S.A. 110, 6907–6912. https://doi.org/10.1073/pnas.1210127110.

Holzkämper, A., Calanca, P., Fuhrer, J., 2010. Evaluating climate suitability for agriculture based on agroclimatic indices. Editors In: Swayne, D., Yang, W., Voinov, A., Rizzoli, A., Filatova, T. (Eds.), 2010 International Congress on Environmental Modelling and Software Modelling for Environment's Sake. International Environmental Modelling and Software Society (iEMSs). Ottawa, Canada.

Hoppmann, D., 2010. Terroir. Wetter, Klima, Boden. Verlag Eugen Ulmer, Stuttgart.

Hoppmann, D., Berkelmann-Loehnertz, B., 2000. Prognosis of phenological stages of *Vitis vinifera* (cv. Riesling) for optimizing pest management. EPPO Bull. 30, 121–126.

Huglin, M.P., 1978. Nouveau mode d'évaluation des possibilités héliothermiques d'un milieu viticole. Comptes rendus des séances de l'Académie d'agriculture de France 64, 1117–1126.

Jones, G.V., 2007. In: Essick, E., Griffin, P., Keefer, B., Miller, S., Storchmann, K. (Eds.), Whitman College Economics Department, Walla Walla, WA Editors.

Jones, G.V., 2013. Winegrape phenology. Phenology: An Integrative Environmental Science. Springer, Dordrecht Heidelberg New York London, pp. 563–580.

Jones, G.V., Davis, R.E., 2000. Climate influences on grapevine phenology, grape composition, and wine production and quality for Bordeaux, France. Am. J. Enol. Vitic. 51, 249–261.

Jones, G.V., et al., 2005. . Changes in European winegrape phenology and relationships with climate. In: Proc. XIV GESCO Symposium. Geisenheim, Germany.

Kartschall, T., et al., 2015. Changes in phenology and frost risks in *Vitis vinifera* (cv Riesling) between 1901 and 2100. Meteorologische Zeitschrift 24, 189–200. https://doi.org/10.1127/metz/2015/0534.

Ladenbruch, P.A., Mickey, M.R., 1968. Estimation of error rates in discriminant analysis. Technometrics 10, 1–11.

Leolini, L., et al., 2018. Late spring frost impacts on future grapevine distribution in Europe. Field Crop Res. 222, 197–208. https://doi.org/10.1016/j.fcr.2017.11.018.

Lorenz, D.H., et al., 1995. Phenological growth stages of the grapevine, *Vitis vinifera* L. ssp. *vinifera*. Codes and descriptions according to the extended BBCH scale. Aust. J. Grape Wine Res. 1, 100–103.

Madelin, M., Beltrando, G., 2005. Spatial interpolation-based mapping of the spring frost hazard in the Champagne vineyards. Meteorol. Appl. 12, 51–56. https://doi.org/10.1017/S1350482705001568.

Mariani, L., Parisi, S., Cola, G., Failla, O., 2012. Climate change in Europe and effects on thermal resources for crops. Int. J. Biometeorol. 56, 1123. https://doi.org/10.1007/s00484-012-0528-8.

Modedale, J., Wilson, R.J., Maclean, I.M.D., 2015. Climate change and crop exposure to adverse weather: changes to frost risk and grapevine flowering conditions. PLoS ONE 10, e0141218. https://doi.org/10.1371/journal.pone.0141218.

Molitor, D., Baus, O., Hoffmann, L., Beyer, M., 2016. Meteorological conditions determine the thermal-temporal position of the annual Botrytis bunch rot epidemic on *Vitis vinifera* L. cv. Riesling grapes. Oeno One 50, 231–244. https://doi.org/10.20870/oeno-one.2016.50.4.36.

Molitor, D., et al., 2014a. Late frost damage risk for viticulture under future climate conditions: a case study for the Luxembourgish winegrowing region. Aust. J. Grape Wine Res. 20, 160–168. https://doi.org/10.1111/ajgw.12059.

Molitor, D. and Junk, J., 2019. Climate change is implicating a two-fold impact on air temperature increase in the ripening period under the conditions of the Luxembourgish grapegrowing region. Oeno One, 10.20870/oeno-one.2019.53.3.2329, accepted.

Molitor, D., Junk, J., Evers, D., Hoffmann, L., Beyer, M., 2014b. A high resolution cumulative degree day based model to simulate phenological development of grapevine. Am. J. Enol. Vitic. 65, 72–80. https://doi.org/10.5344/ajev.2013.13066.

Molitor, D., et al., 2018. Efficacy of fenhexamid treatments against *Botrytis cinerea* in grapevine as affected by time of application and meteorological conditions. Crop Protect. 110, 1–13. https://doi.org/10.1016/j.cropro.2018.03.007.

Molitor, D., Keller, M., 2016. Yield of Müller-Thurgau and Riesling grapevines is altered

by meteorological conditions in the current and previous growing seasons. Oeno One 50, 245–258. https://doi.org/10.20870/oeno-one.2016.50.4.1071.
Nendel, C., 2010. Grapevine bud break prediction for cool winter climates. Int J Biometeorol 54, 231–241. https://doi.org/10.1007/s00484-009-0274-8.
Oliveira, M.l., 1998. Calculation of budbreak and flowering base temperatures for *Vitis vinifera* cv. Touriga Francesa in the Douro region of Portugal. Am. J. Enol. Vitic. 49, 74–78.
Orlandini, S., Mancini, M., Maracchi, G. and Moriondo, M., 2003. Le gelate primaverili: metodo di valutazione del rischio per il vigneto, Vignevini, pp. 100–104.
Ortega-Farias, S., Riveros-Burgos, C., 2019. Modeling phenology of four grapevine cultivars (*Vitis vinifera* L.) in Mediterranean climate conditions. Sci. Hortic. 250, 38–44. https://doi.org/10.1016/j.scienta.2019.02.025.
Parker, A., de Cortazar-Atauri, I., Van Leeuwen, C., Chuine, I., 2011. General phenological model to characterise the timing of flowering and veraison of *Vitis vinifera* L. Aust. J. Grape Wine Res. 17, 206–216. https://doi.org/10.1111/j.1755-0238.2011.00140.x.
Parker, A., et al., 2013. Classification of varieties for their timing of flowering and veraison using a modelling approach: a case study for the grapevine species V*itis vinifera* L. Agric. For. Meteorol. 180, 249–264. https://doi.org/10.1016/j.agrformet.2013.06.005.
Parker, A., et al., 2020. Temperature-based grapevine sugar ripeness (GSR) modelling for a wide range of *Vitis vinifera* L. cultivars. Agric. For. Meteorol. 285-286, 107902. https://doi.org/10.1016/j.agrformet.2020.107902.
Peyer, E., Koblet, W., 1966. Der Einfluss der Temperatur und der Sonnenstunden auf den Blütezeitpunkt der Reben. Schweizer Zeitschrift für Obst- und Weinbau 10, 250–255.
Poling, E.B., 2008. Spring cold injury to winegrapes and protection strategies and methods. Hortscience 43, 1652–1662. https://doi.org/10.21273/hortsci.43.6.1652.
Santesteban, L.G., Royo, J.B., 2006. Water status, leaf area and fruit load influence on berry weight and sugar accumulation of cv. 'Tempranillo' under semiarid conditions. Sci. Hortic. 109, 60–65. https://doi.org/10.1016/j.scienta.2006.03.003.
Schultz, H.R., 1992. An empirical model for the simulation of leaf appearance and leaf-area development of primary shoots of several grapevine (*Vitis vinifera* L) canopy-systems. Sci. Hortic. 52, 179–200. https://doi.org/10.1016/0304-4238(92)90020-D.
Sgubin, G., et al., 2018. The risk of tardive frost damage in French vineyards in a changing climate. Agric. For. Meteorol. 250-251, 226–242. https://doi.org/10.1016/j.agrformet.2017.12.253.
Verdugo-Vasquez, N., et al., 2015. Spatial variability of phenology in two irrigated grapevine cultivar growing under semi-arid conditions. Precis. Agric. 17, 218–245. https://doi.org/10.1007/s11119-015-9418-5.
Verdugo-Vasquez, N., Panitrur-De la Fuente, C., Ortega-Farias, S., 2017. Model development to predict phenological scales of table grapes (cvs. Thompson, Crimson and Superior Seedless and Red Globe) using growing degree days. Oeno One 51, 277–288. https://doi.org/10.20870/oeno-one.2017.51.3.1833.
van Leeuwen, C., et al., 2008. Heat requirements for grapevine varieties is essential information to adapt plant material in a changing climate. In: Proceedings of the 7th International Terroir Congress, Changins, Switzerland (Agroscope Changins-Wädenswil: Switzerland), pp. 222–227.
Wang, E., Engel, T., 1998. Simulation of phenological development of wheat crops. Agric. Syst. 58, 1–24. https://doi.org/10.1016/S0308-521X(98)00028-6.
Webb, L., Whetton, P., Barlow, E., 2007. Modelled impact of future climate change on the phenology of winegrapes in Australia. Aust. J. Grape Wine Res. 13, 165–175. https://doi.org/10.1111/j.1755-0238.2007.tb00247.x.
Wolkovich, E.M., Burge, D.O., Walker, M.A., Nicolas, K.A., 2017. Phenological diversity provides opportunities for climate change adaptation in winegrapes. J. Ecol. 105, 905–912. https://doi.org/10.1111/1365-2745.12786.
Wolkovich, E.M., Garcia de Cortazar-Atauri, I., Morales-Castilla, I., Nicolas, K.A., Lacombe, T., 2018. From Pinot to Xinomavro in the world's future wine-growing regions. Nat. Clim. Chang. 8, 29–37. https://doi.org/10.1038/s41558-017-0016-6.
Yan, W., Hunt, L.A., 1999. An equation for modelling the temperature response of plants using only the cardinal temperatures. Ann. Bot. 84, 617. https://doi.org/10.1006/anbo.1999.0955. -614.
Zapata, D., Salazar-Gutierrez, M., Charves, B., Keller, M., Hoogenbbom, G., 2017. Predicting key phenological stages for 17 grapevine cultivars (*Vitis vinifera* L.). Am. J. Enol. Vitic. 68, 60–72. https://doi.org/10.5344/ajev.2016.15077.
Zapata, D., Salazar, M., Chaves, B., Keller, M., Hoogenboom, G., 2015. Estimation of the base temperature and growth phase duration in terms of thermal time for four grapevine cultivars. Int. J. Biometeorol. 59, 1771. https://doi.org/10.1007/s00484-015-0985-y.

applied sciences

MDPI

*Review*

# A Review of the Potential Climate Change Impacts and Adaptation Options for European Viticulture

**João A. Santos [1,*], Helder Fraga [1], Aureliano C. Malheiro [1], José Moutinho-Pereira [1], Lia-Tânia Dinis [1], Carlos Correia [1], Marco Moriondo [2], Luisa Leolini [3], Camilla Dibari [3], Sergi Costafreda-Aumedes [3], Thomas Kartschall [4], Christoph Menz [4], Daniel Molitor [5], Jürgen Junk [5], Marco Beyer [5] and Hans R. Schultz [6]**

1 Centre for the Research and Technology of Agro-environmental and Biological Sciences, CITAB, Universidade de Trás-os-Montes e Alto Douro, UTAD, 5000-801 Vila Real, Portugal; hfraga@utad.pt (H.F.); amalheir@utad.pt (A.C.M.); moutinho@utad.pt (J.M.-P.); liatdinis@utad.pt (L.-T.D.); correia@utad.pt (C.C.)
2 National Research Council of Italy, Institute of BioEconomy (CNR-IBE), 50019 Florence, Italy; marco.moriondo@cnr.it
3 Department of Agriculture, Food, Environment and Forestry, University of Florence, UniFi, 50144 Florence, Italy; luisa.leolini@unifi.it (L.L.); camilla.dibari@unifi.it (C.D.); sergi.costafredaaumedes@unifi.it (S.C.-A.)
4 Potsdam Institute for Climate Impact Research, PIK, 14473 Potsdam, Germany; thomas@pik-potsdam.de (T.K.); menz@pik-potsdam.de (C.M.)
5 Luxembourg Institute of Science and Technology (LIST), 4422 Belvaux, Luxembourg; daniel.molitor@list.lu (D.M.); juergen.junk@list.lu (J.J.); marco.beyer@list.lu (M.B.)
6 Department of General and Organic Viticulture, Hochschule Geisenheim University, 65366 Geisenheim, Germany; hans.reiner.schultz@hs-gm.de
* Correspondence: jsantos@utad.pt

Received: 31 March 2020; Accepted: 27 April 2020; Published: 29 April 2020


**Abstract:** Viticulture and winemaking are important socioeconomic sectors in many European regions. Climate plays a vital role in the terroir of a given wine region, as it strongly controls canopy microclimate, vine growth, vine physiology, yield, and berry composition, which together determine wine attributes and typicity. New challenges are, however, predicted to arise from climate change, as grapevine cultivation is deeply dependent on weather and climate conditions. Changes in viticultural suitability over the last decades, for viticulture in general or the use of specific varieties, have already been reported for many wine regions. Despite spatially heterogeneous impacts, climate change is anticipated to exacerbate these recent trends on suitability for wine production. These shifts may reshape the geographical distribution of wine regions, while wine typicity may also be threatened in most cases. Changing climates will thereby urge for the implementation of timely, suitable, and cost-effective adaptation strategies, which should also be thoroughly planned and tuned to local conditions for an effective risk reduction. Although the potential of the different adaptation options is not yet fully investigated, deserving further research activities, their adoption will be of utmost relevance to maintain the socioeconomic and environmental sustainability of the highly valued viticulture and winemaking sector in Europe.

**Keywords:** viticulture; wine production; climate change; adaptation; risk reduction

## 1. Introduction

A brief characterization of the global viticulture and winemaking sector is provided upfront to better understand its relevance in the world economy. As detailed in the latest report of the International Organization of Vine and Wine (OIV) [1], it is estimated that the world vineyards cover an area of approximately 7.449 million ha (2018). In this same year, Spain encompassed 13% of the world

vineyard area, closely followed by China (12%), France (11%), Italy (9%), and Turkey (6%). These five countries represent approximately one half of the global vineyard area. From the same report, it can be concluded that the time evolution of the world vineyard area underwent an overall downward trend over the last two decades, particularly in the period from 2003 to 2011. The weak recovery from 2012 to 2014 was then followed by a new decline thereafter. Stabilization of the vineyard area, or a slightly decreasing trend, is observed during the last five years in most of the countries where viticulture is a relevant sector, apart from the robust declines in Turkey and Iran. Nonetheless, some countries show a clear growth of the vineyard area, mainly China and India [1].

Following the same OIV report [1], and on the contrary to the world vineyard area, the global grape production experienced a noticeable upward trend over the last two decades, highlighting productivity gains. As also reported by the OIV [1], the estimated production quantity was of roughly 77.8 million tons ($10^3$ kg) in 2018, a record-breaking value, against 60–65 million tons at the beginning of the 21st century. Generally, grapes are produced in the form of wine grapes (57% of all grapes), table grapes (36%), or dried grapes (7%). The production of both table and dried grapes is prevalent in some countries that have no tradition in wine production, such as China (89.7% of all grape production), Turkey (96.8%), India (98.5%), Iran (100%), Uzbekistan (96.3%), Egypt (99.5%), and Brazil (53.5%). Conversely, the production of wine grapes is associated with countries where viticulture is largely devoted to wine production, such as Italy (86.5%), Spain (96%), France (99.6%), Argentina (93.7%), Australia (90.9%), Germany (99.6%), or Romania (93.1%), ranked in descending order in terms of production volume. The evolution of global table grape production, mostly generated by China, Turkey, India, Iran, Uzbekistan, Italy, and the USA (all of them with production over 1 million tons in 2018), has shown a consistent increase, whereas wine grape production has remained relatively stable [1]. No significant changes occurred for dried grapes. Hence, wine grapes are becoming gradually less prominent in the viticultural sector in terms of volume, but still represent the majority [1].

Concerning the winemaking sector, global wine production was 292 million hl in 2018, remaining relatively stable over the last two decades [1]. The four most important wine producers, ranked by their production in volume, are Italy (54.8 million hl), France (48.6), Spain (44.4), and the USA (23.9), with the first three being the most important global exporters. Wine consumption increased from 2000 to 2007, but remained nearly constant thereafter, with a current value of 246 million hl [1]. The five major wine consumers are the USA (13% of world wine consumption), France (11%), Italy (9%), Germany (8%), and China (8%) [1]. Although wine trade, in volume, has been stable since 2011, wine trade in monetary value has been growing continuously to reach a record-breaking value of approximately EUR 30,000 million in 2018 [1].

Geographically, grapevines are historically cultivated on six out of seven continents, between latitudes 4° and 51° in the Northern Hemisphere (NH) and between 6° and 45° in the Southern Hemisphere (SH), and across a large diversity of climates (oceanic, warm oceanic, transition temperate, continental, cold continental, Mediterranean, subtropical, attenuated tropical, arid, and hyperarid climates), but with the majority occurring in temperate climate regions [2]. The most important viticultural regions in the world are shown in Figure 1a, whereas the vineyard land cover in Europe is displayed in Figure 1b. Large areas in Europe, equatorward of the 51° N parallel, are devoted to viticulture. Many viticultural regions also underlay strict regulations concerning typicity and quality of the product, sometimes several centuries old [3], also, in some cases, with wine region delimitation systems (e.g., denominations or appellations of origin, among many others).

Along the previous lines, it is clear that viticulture is a key socioeconomic and cultural sector in many countries and regions worldwide, with a high economic impact in the network of all relevant industry branches of the supply and distribution chains. Besides the direct income from wine sales, which benefit the whole production chain (wine and subsidiary companies, their employees, viticulturists, and property owners), there are other indirect benefits provided, spreading from landscape and ecosystem services to tourism. Therefore, an assessment of the sustainability of viticulture under future conditions, both environmentally and economically, is of utmost importance.

This paper will treat the subject in seven sections. First, a brief description of the *terroir* concept, which is the interplay between soil, climate, and human activity, in many ways fundamental to wine production (Section 2), and the interplay between weather/climate and grapevines (Section 3) will be given. Second, the potential climate change impacts (Section 4) and the adaptation options (Section 5) on these interrelationships will be discussed on the basis of state-of-the-art scientific knowledge. Finally, some existing knowledge gaps and research challenges will be explored (Section 6), followed by the conclusions (Section 7).

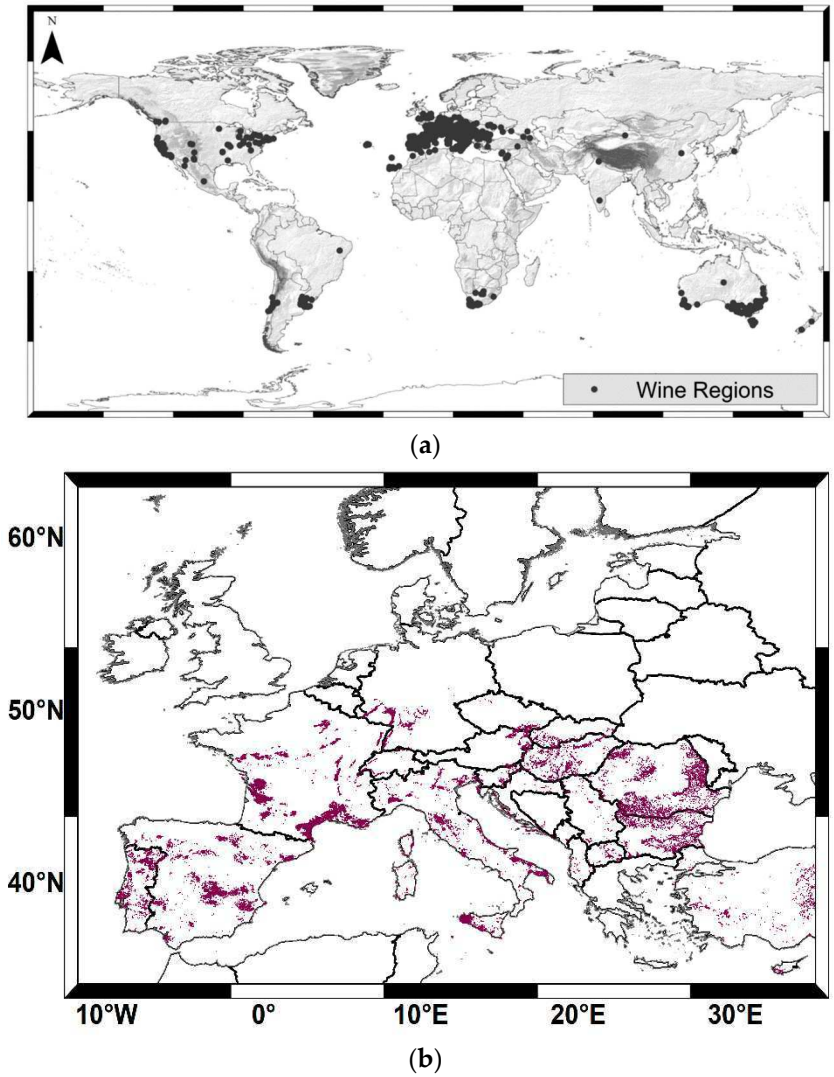


**Figure 1.** (**a**) World distribution of the viticultural regions (black circles) [4]. (**b**) Political map of Europe with the vineyard land cover (shading). Source: Copernicus CORINE Land Cover (CLC) 2018 (https://land.copernicus.eu/).

Taking into account the wide-ranging scope of the present review, an exhaustive compilation of all previous studies in the field is not feasible, not even of the most recent studies. The main goal is to provide an updated overview of this topic on the basis of the results of relevant and illustrative research, which may be useful not only for researchers and academics, but also for stakeholders and decision-makers. Although the focus is largely on European viticulture, most of the discussion can be easily extrapolated to other wine regions outside Europe that share similar environmental conditions.

## 2. Viticultural *Terroir*

Winemaking regions are characterised by their particular natural environment, such as climate, soil properties, and a human factor, deciding on the use of grapevine cultivars and viticultural practices. According to Carbonneau [5], the climatic characteristics of a given viticultural region are key factors in understanding its varietal suitability and wine types, as will be further discussed in Section 3. The soil properties of a given region or site also play a central role in viticulture, whereas soils are also prone to changes induced by climate evolution (see Section 4). Grapevine varieties and scion/rootstock combinations have different soil preferences that eventually determine the characteristics of the produced wine. In fact, soil physical and chemical properties heavily influence grapevine development and grape berry composition [6]. The importance of these local-scale pedoclimatic characteristics has been recognized in all winemaking regions, sometimes over centuries, as vine growers have continuously adapted local viticultural practices, to some extent empirically, to best suit their surrounding environmental conditions [7]. The soil–plant–atmosphere continuum largely determines the outcomes from a vineyard. Besides pedoclimatic conditions, biotic factors, such as the influence of pests and diseases; the role of functional biodiversity in the vineyard; and agro-management practices, namely, scion and rootstock choice, pruning, pinching, girdling, topping, or thinning, play a key role in grapevine growth, development, and berry quality [8].

On the basis of the aforesaid interactions, the concept of *terroir* has been widely adopted [3]. According to OIV (Resolution OIV/VITI 333/2010), "Terroir is a concept which refers to an area in which collective knowledge of the interactions between the identifiable physical and biological environment and applied viticultural and oenological practices develops, providing distinctive characteristics for the products originating from this area. Terroir includes specific soil, topography, climate, landscape characteristics and biodiversity features". As such, the terroir significantly affects grapevine development and berry composition and has been accepted as a key aspect in determining wine quality and typicity of a given region [9].

## 3. Atmospheric Influence on Grapevine Development

### 3.1. Grapevine Cycles Versus Weather and Climate

Grapevine development is associated with several stages of its vegetative and reproductive cycles. Under the conditions of many traditional viticultural regions (i.e., extratropical viticulture), the grapevine vegetative cycle extends over one full year, whereas its reproductive cycle lasts for two years. The reproductive cycle governs several important qualitative and quantitative properties, such as the number of grape clusters in the following year. The vegetative cycle encompasses two main sequential periods: dormancy period and growing season. The grapevine phenological development comprises several stages or phenophases (Figure 2). These stages of grapevine vegetative and reproductive cycles are largely controlled by atmospheric conditions [10].

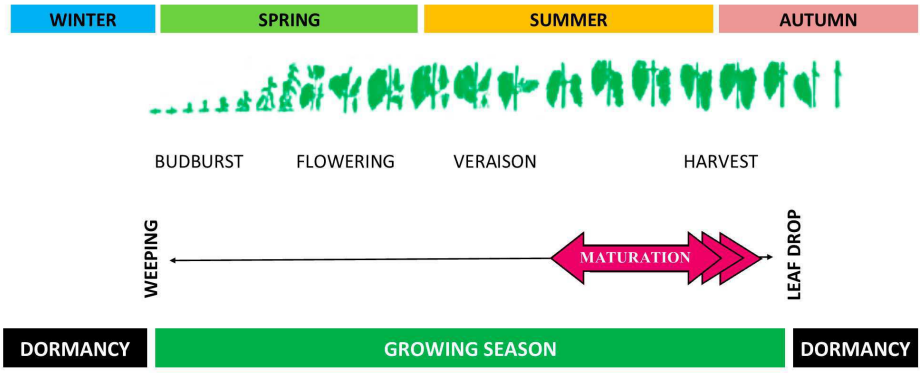


**Figure 2.** Vegetative cycle and main vine phenological stages.

The impact of atmospheric forcing on grapevine can be divided into two different time scales. On the long-term, climate, which corresponds to the statistical distribution of the different atmospheric variables over long-term periods (decades) at a given location [11], determines the bioclimatic envelope of that location and its viticultural suitability [3,12]. Macroclimates are determinant of the wine geography and the distribution of grapevine varieties, whereas mesoclimates and microclimates promote different terroir units, with diverse wine identity and diversity [13]. The wide range of climate-driven scales, as well as the spatial complexity and temporal dynamics in viticulture, have already been documented [14]. On the short-term, weather considerably governs the whole grapevine development process, as it requires suitable temperatures, radiation intensities, and duration, as well as specific levels of water availability throughout its growth cycle, ultimately influencing yield, biomass production, berry attributes, and wine structure and flavour [15,16]. Effectively, the evolution of weather conditions in a given location can be used to predict local/regional grapevine parameters, such as yield [17] or phenology [18].

### 3.2. The Role of Temperature

Among all atmospheric elements, air temperature is considered the most important in driving the growth and development of grapevines [19], in cases where water, radiation, and nutrient requirements of the plant are fulfilled [20,21]. From the climatological viewpoint, the distribution of traditional viticultural regions worldwide is mainly confined within a belt defined by the isotherms of average growing season temperatures (April–October, NH; October–April, SH) of 12–13 °C and 22–24 °C [12], underlining the key role played by temperature on viticultural suitability. Growing season temperatures below 12–13 °C commonly occur in regions with growing seasons too short for proper vine development, with typically low solar radiation levels and insufficient heat accumulation. On the other hand, growing season temperatures above 22–24 °C often lead to excessive heat stress on vines, which is also frequently associated with either severe water stress, in dry climates, or strong pest and disease pressures, in humid climates. These areas may also have difficulty in meeting the chilling requirements for the dormancy period, with resulting erratic bud break [12].

For the meteorological timescales, temperature conditions strongly control both grapevine physiology and berry composition during the preceding and the current growing season [22,23]. The inflorescence primordia differentiation starts around the bloom stage of the preceding year [24,25]. Warm and sunny conditions during this period promote the formation of inflorescence primordia, whereas cool and cloudy weather promotes the formation of tendrils [26,27]. Hence, the environmental conditions in the preceding year have a direct influence on the yield of the following season [28].

From leaf fall to the beginning of spring, grapevines are dormant and consist entirely of woody tissue, with little physiological activity [3]. This period encompasses two sub-periods that are controlled by endogenous and exogenous thermal factors needed for dormancy release. The first sub-period (endo-dormancy) is triggered by chilling accumulation (chill units) during autumn/winter, whereas the second sub-period (eco-dormancy) is driven by heat accumulation until bud break. Therefore, the winter chill is an important condition for grapevine growth development, as cold promotes bud dormancy [29,30], besides other processes such as day length shortening and ageing of the photosynthetic active parts of the plants. From late winter to early spring, the accumulation of daily mean temperatures above 7 to 10 °C generally promote dormancy break and the onset of the grapevine growing cycle [31].

During the growing season, grapevines undergo constant changes in terms of morphology and physiology. The length of the growing season for each variety is directly related to the growing season mean air temperature [32], though it may be additionally linked to soil moisture and crop management practices [33]. The length of the different phenological stages significantly differs not only according to each variety, but also to the thermal conditions in a given region for each specific year [34,35]. Despite relatively high resilience to abiotic stresses, extremely low temperatures during winter [36], negative temperatures (Celsius scale) around/after budburst [37–40], and hail events may severely damage the

developing buds, leaves, and inflorescences [41,42]. Cool conditions [38] or extreme heat [28,43,44] may also affect vine physiology and yield, though some grapevine varieties are more tolerant to extreme temperatures than others. Grapevines under severe heat stress may undergo a significant decrease in photosynthetic productivity, as well as suffer injures in other biochemical processes [45]. Extreme events during the veraison–maturity period, such as heatwaves, can significantly influence sugar accumulation [46] and may lead to a decrease in anthocyanin biosynthesis and content [47]. Secondary metabolites, more specifically phenolics, due to their contribution to colour, flavour, aroma, texture, astringency, and stabilization of wine, as well as antioxidant properties [48], are extremely important for fruit quality and wine production [49]. High temperatures may also lead to important losses, as they also influence the synthesis of volatile compounds, which strongly contribute to the sensory character of wines [50]. In autumn, the gradual shortening of the day length and decreasing of temperatures promote acclimation to freezing temperatures in winter. During this phase, the translocation of carbohydrates, amino acids, organic acids, and some minerals from leaves to perennial organs (trunk and roots) reaches its maximum [51]. This period, considered as a survival strategy, ordinarily coincides with the generalized leaf senescence, followed by leaf fall and the subsequent dormancy period.

### 3.3. The Role of Water

Precipitation is another key atmospheric variable in viticulture, as it has a large footprint on soil water balance, determining soil water availability for the plant and its corresponding water status. Water stress leads to a wide range of effects that are also dependent on the grapevine development stage [52]. For instance, moderate-to-high soil moisture during budburst and shoot/inflorescence development is critical for vine growth [53]. Water stress at this stage may lead to stunted shoot growth, as well as poor flower-clustering development and berry set [54]. However, excessive humidity during early development stages may also overstimulate growth, which may lead to excessively vigorous and dense canopies, thereby potentiating the risks of diseases. From flowering to berry ripening, severe water stress may lead to reduced leaf area, thus limiting photosynthesis, as well as promoting flower abortion and cluster abscission [55]. Nevertheless, dry weather during ripening is generally favourable to high-quality wine production [56–58]. Slower leaf development also promotes higher water use efficiency [59]. Conversely, excessive precipitation is commonly unfavourable to maturation [2], for instance due to sugar dilution [60] or to bunch rot [61]. Recent studies indicated that water deficit affects grape and wine composition [62,63]. Regulated deficit irrigation has been used to improve berry and wine quality [64], increasing the concentration of terpenes by modulating structural and regulatory genes involved in volatile organic compounds biosynthesis [62]. Water deficit early in the season, before veraison, also stimulated increased anthocyanins and phenolic concentrations [65]. Furthermore, the timing and intensity of water deficits influence the extent of changes in berry metabolism and in wine colour, aroma, and flavour by modifying berry size and/or the synthesis of berry compounds, with a positive contribution to the fruit and wine organoleptic properties. Indeed, a water-deficit treatment typically increases the skin to pulp ratio in the berries, when compared with well-watered grapevines [66], increasing the amount of skin tannins and anthocyanins. Colour differences may result from increased anthocyanin synthesis caused by water deficit during the fruit development [67].

### 3.4. The Role of Radiation

Solar radiation is also a crucial factor in viticulture. The synthesis and accumulation of sugar, phenolic, and many aromatic compounds during maturation are indeed favoured by high solar radiation levels [68]. Regions with relatively low solar radiation normally adjust the training systems and canopy density to maximize the sun-exposed leaf area. Although more exposed leaves generally favour photosynthesis and stomatal conductance, water demand also increases [69], and other problems may also arise, such as leaf and cluster sunburn. On the contrary, less exposed clusters result in lower berry temperatures, generally leading to lower sugar contents and lower anthocyanin concentrations [70].

Additionally, shading due to high canopy density may significantly decrease bud fertility [71], thus negatively affecting the yield potential in the subsequent season.

In the Mediterranean-type climatic regions, such as in Southern Europe, vineyards are already typically exposed to high radiation levels, high air temperatures, and soil water deficits, which can impact grapevine productivity. Under these circumstances, grapevine leaves often show temporary photoinhibition, chlorosis, and necrosis, thus leading to low intrinsic water use efficiency and excessive exposure of grape clusters [72]. Hence, low vigour tends to be connected to reduced berry weight, sugar content, and yields. Still, other organoleptic properties of berries, such as flavour and aroma attributes, are frequently inhibited by excessive solar radiance and severe dryness or, as in the case of tannins, may be exacerbated in concentration and/or altered in molecular structure. These conditions may lead to unbalanced wines, with undesirable high alcoholic content and low acidity [73], with low commercial value. However, other studies [74–76] showed that vineyards exposed to relatively high levels of sunlight, including UV-B radiation, produce berries of high quality for winemaking by inducing synthesis of polyphenols and monoterpenes as photo-protectors.

### 3.5. Agro-Climatic Indices and Viticultural Zoning

The aforementioned effects of climate and weather on grapevines have been described by several agro-climatic indices. They commonly provide closer relationships between the grapevine development and atmospheric conditions than individual atmospheric variables, such as monthly mean temperatures, radiation, or precipitation. These indices were developed to integrate the plant–atmosphere interactions, thus following the plant physiological development more closely. Further, they can be used to assess the suitability of a given region or site for viticulture, in general, or a specific variety in particular. Due to the strong link between temperature and grapevine development, the agro-climatic indices are frequently based on temperature, such as indices using simple growing degree-day concepts (temperature integration). As a classical example, Amerine and Winkler [31] developed the Winkler growing degree-day scale for a base temperature of 10 °C. Following a similar concept, after some modifications in the temperature summation during the growing season and including a coefficient for day length, the Huglin index [77] was later developed. Molitor et al. [78] applied a trapezoidal model approach to simulate grapevine phenology (UniPhen), on the basis of cumulative degree-days, using three threshold temperatures (10 °C—lower threshold; 20 °C—upper threshold; 30 °C—heat threshold). Other indices based on hourly temperature accumulation were more recently applied [30]. To put more emphasis on the temperature conditions during the ripening period, which may ultimately influence the wine style, the cool night index [2,79], based on the mean minimum temperature in September (NH), was proposed. The dryness index is another very common index in viticultural zoning [68,79], which is based on an estimation of the potential soil water balance. Hence, viticultural zoning using agro-climatic indices is common to assess the suitability of a given region for viticulture and wine production for specific grapevine varieties.

## 4. Potential Climate Change Impacts

### 4.1. Ongoing Climate Change

The above-mentioned close relationships between grapevine development and weather/climate make viticulture particularly vulnerable to climate change and susceptible to its detrimental impacts. Through the combination of (i) generally increasing air temperatures and (ii) shift of the ripening period toward earlier (usually warmer parts of the season), climate change has a two-fold impact from the recent-past warming, especially clear during the ripening period [80].

Historical temperature trends for the main viticultural regions worldwide show that the growing season mean temperatures increased by 1.3 °C between 1950–1999 and 1.7 °C from 1950 to 2004 [81]. Associated with increasing temperatures over the last few decades, alterations in the grapevine growth and physiological development have been documented [56,57,82–84]. Changing climates are thereby

influencing grapevine yield, as well as berry and wine quality [81,85]. In this regard, it was found that higher temperatures during the growing season promoted a decrease in the grape berry total acidity content [12,86], upward trends in sugar content or probable alcohol [87], and a decoupling between technological and phenolic maturity [83]. Earlier phenological timings and growing season shortening were observed in many viticultural regions [88–92]. These earlier phenological timings may lead to ripening during excessively warm conditions [93], with increased alcohol content, decreased acidity, and modifications in wine sensory profiles [94,95]. The 2019 ProWein Business Report (available at https://www.prowein.de/) presented the results of an industry survey, with the participation of more than 1700 enterprises, stating that the sensory profiles of wines have changed over the past decades. As such, climate change is also potentially threatening the wine typicity of traditional winemaking regions [80].

### 4.2. Climate Change Projections and Impacts on Grapevines

Climate change projections for the 21st century, based on global and regional climate models, are in general agreement with the observed trends over the past decades [96], leading to important impacts on viticulture. In some regions, climate change is supposed to be beneficial for viticulture, for instance due to higher fruit maturity and opening new areas for cultivation, whereas the impact might be detrimental in other regions by challenging the ability for adequate grape cultivation and wine production [12]. Alterations in the spatial patterns and temporal regimes of temperature and precipitation [97] may significantly modify current viticultural bioclimatic zones in Europe [98]. Climate change studies for Italy [99–102], France [82,103,104], Spain [105], Portugal [18,30,106], Germany [37,107,108], Greece [109], and Luxembourg [80,110,111], among others, hint at an increase in the growing season mean temperature.

In future scenarios, the current winemaking regions in southern Europe may undergo a decline in their viticultural suitability [112–115], mainly due to severe dryness [112]. These regions may indeed become excessively dry for high-quality winemaking [85] and, in some most extreme cases, will require intensive irrigation [112,116]. Regions such as Andalucía, La Mancha (Spain), Alentejo (Portugal), Sicily, Puglia, and Campania (Italy) will very likely suffer from severe water deficits [98]. It was also shown that increased summer dryness in southern Europe will lead to yield reduction, mostly due to the synergistic effect of warming and drying [98].

For some southern European winemaking regions, increased inter-annual variability and more frequent extremes are expected to intensify the irregularity of yields, with harmful impacts on the whole winemaking sector. Winemaking regions under extremely high temperatures may experience an increase in the risk of organoleptic degradation [94], excessively high alcohol contents [117], an acceleration in the degradation of organic acids [84], and an inhibition in the synthesis of anthocyanin [118], thus affecting grape colour and aroma [119–122]. In particular, the fruitiness, aroma [84], acidity, and relatively low alcohol content, characteristics of white wines in (former) cool climate wine regions, is expected to be negatively affected by high ripening temperatures [80]. Moreover, such high ripening temperatures are supposed to lead to higher concentrations of some specific phenols and an astringent wine taste [123]. Projected future increases in minimum temperatures during ripening, for example on the Iberian Peninsula [98], may also result in a decrease in wine quality. Higher respiratory rates at night associated with higher temperatures will consume more sugar, which is a key precursor for the biosynthesis of vital flavour compounds.

Future warmer climates may also have positive impacts for several traditional wine regions in Western and Central Europe, such as Burgundy, Champagne, Alsace, Loire Valley, Rheingau, and Mosel [95,114], as well as for potential new areas north- and eastwards of these traditional regions, although there are still many uncertainties owed to the complex interplay of different factors. As an example, a doubling of the areas suitable for viticulture in Austria by 2050s was projected on the basis of temperature evolution [124]. Hungarian southern winemaking regions are also expected to expand [125]. Furthermore, the expected warming in Central and Northern Europe will lead to longer

growing seasons and frost-free periods [126], which will reduce fall frost damage and favour potential wine quality [127].

The impact of climate change on spring frost risk has been discussed controversially in the scientific literature in recent years. Generally, spring frost occurs when budburst precedes the date of the last frost event in the spring of a given year. Under future climate conditions, both events are projected to occur earlier. Although some studies suggest that the last frost events will move to earlier dates at a faster rate than budburst and, hence, reduce spring frost risk in the future [39], other studies were inconsistent or predicted increased risks for spring frost damage [37,38,40,128,129], indicating a high degree of uncertainty [80].

Although winter, spring, and fall frosts may threaten the economic sustainability of viticulture in a specific region/location and, hence, warming is considered as mostly positive, the production of ice wines is jeopardized. Ice wines are traditional premium wines of many cool climate regions that are produced when grape berries are exposed in fall or early winter to a frost event of −7 °C, or below, and are pressed in the frozen status. In this case, water in the berries is in the form of ice crystals and the juice is then concentrated, leading to the production of these unique dessert wines. However, these conditions are expected to become increasingly rare in the future. This is mostly due to the combination of two effects: higher temperatures leading to earlier maturity, and the date of first relevant frost events (minimum temperature of −7 °C or below) being delayed, or such events not even occurring in the future. Hence, ripe grapes have to sustain a much longer period until the freezing event occurs and the risk of severe berry decay and complete yield loss will thus increase [130].

In a comprehensive modelling effort, where a process-based crop model was coupled with climate, soil, and terrain databases, taking into account physiological effects of water supply and $CO_2$ concentration, European grapevine yields, phenology, water, and nitrogen stresses, both for present (1980–2005) and future (2041–2070) climate scenarios (Representative Concentration Pathway (RCP), RCP4.5 and RCP8.5), were analysed [98]. For current climates, the simulated components (e.g., yield and phenology) were validated against multi-site observations. For the future climates, the projected changes suggested an extension of the climatic suitability for grapevine cultivation up north to the 55° N parallel, thus creating the necessary conditions for the emergence of new winemaking regions at higher latitudes in Europe. The main phenological stages (budburst, flowering, veraison, and maturation) are projected to undergo significant advancements (> 2 weeks earlier), with implications for phenophase lengths between these stages [98]. Increased dryness throughout Europe was also projected, but with severe water stress over several regions in southern Europe (e.g., southern Spain, Portugal, and Italy), locally reduced yield and leaf area. Future biomass changes may lead to modifications in nitrogen (N) demands. Under future climate conditions, vineyards in Southern Europe may experience a reduction in biomass growth, owing to severe water stress. This will result in a high propensity of N deficit in Northern/Central Europe, under warmer and moist conditions [98]. In this context, increased atmospheric $CO_2$ may partially offset the dryness effects, promoting yield and leaf area index increases in Central/Northern Europe.

The higher concentrations of $CO_2$ in the future are expected to have positive impacts on the grapevine development cycle and yield attributes [131–136], although many uncertainties remain. Experiments conducted in free air carbon dioxide enrichment (FACE) systems have shown significant impacts of elevated $CO_2$ on, for instance, several vegetative growth parameters, primary productivity, grapevine bud fertility, and yield potential [135,136]. Higher $CO_2$ concentrations may contribute to a decrease in plant transpiration rates, which may tend to compensate for increased soil evaporation [137], thus mitigating the evapotranspiration increase under future conditions [138].

Changes in UV-B radiation have been of concern in the past, due to alterations of the protective ozone layer. UV-B radiation has an impact on grape composition, with modifications in secondary metabolites, such as flavonoids, amino acids, and carotenoids [134]. Irrespective of a further future increase in UV-B radiation, the combination of high radiation levels and high temperatures, particularly

under severe water stress, is often responsible for sunburn damages in both leaves and berries [139,140], conditions that are anticipated to become more frequent in Southern Europe.

Crop protection may be another critical aspect of changing climates. It faces mostly two challenges: (i) pests and diseases from warmer regions may increasingly survive during warmer winters and (ii) the spectrum of existing pests and diseases may change. An example of a new challenge posed by an invasive species in viticulture is the spotted wing drosophila, a fruit fly that is native to Southeast Asia, but has been spreading to the USA and Europe since 2008. Whereas the spreading is a result of increasing globalization and not climate change, the survival and continuous spread into new areas of this species is due to increasingly mild winters [141]. Data from three decades on selected grape pests point to changes in the phenology of grape berry moths, shifts in distribution ranges of leafhoppers as vectors of grapevine diseases, and range expansion of grapevine mealybugs [142]. On the one hand, temperature increases resulting from climate change are likely to allow for more pest generations per growing season, however, at the same time, fruit maturity and thus harvest dates are expected earlier, limiting damage from late-season pest generations [143]. Climate change may also result in decreasing disease pressure and, consequently, a reduced necessity for the use of pesticides, as was demonstrated for powdery and downy mildew in the region of Burgundy [144]. However, at the global level, mildews are likely to remain the major phytosanitary threat [145].

Modifications in interannual variability and extremes of the meteorological conditions are showing a profound influence in the year-to-year variations in yields and wine quality [56,94]. Extreme weather events, such as heatwaves, extreme precipitation, droughts, hailstorms, and windstorms, among others, are more likely to occur in the future [146] and, as a result, may also have an important impact on future viticulture. Overall, climate change is expected to significantly change grapevine growth, development and yield, grape berry attributes, wine style and typicity, and, hence, the perception of the terroir of many traditional viticultural regions [2,80,147], thus requiring adaptation to warrant future sustainable viticulture. Despite the genetic diversity amongst grapevine varieties and clones within varieties, as well as the resulting plasticity in their adaptation to a wide range of climates [148], there are suitability limits that cannot be exceeded to maintain viticulture both environmentally and socioeconomically sustainable in a given region.

### *4.3. The Role of Soils under Changing Climates*

Within the complex interactions between soil, plant functioning, fruit quality, and an evolving climate, the role of soils, the changes associated with soils, and the impacts resulting from these changes onto the soil-plant-atmosphere-continuum have been the least studied [149]. However, soil temperature has increased, at least at a rate similar to air temperature, over the past more than 100 years [150], and this has also been shown for soils in a vineyard region [151]. In the latter study, summer (NH; June, July, August (JJA)) soil temperatures (50 cm depth) were about 6 °C warmer than autumn temperatures (September, October, November (SON)) over most of the last century until about 1980. After this, JJA temperatures increased much faster than SON temperatures and reached average values today around 4 °C higher than about 40 years ago and about 8 °C warmer than SON temperatures [151]. These temperature increases are much larger than those observed over the same period for air temperature, and there is a high propensity that this already has profound effects on microbial community characteristics and activity [152]. Soils store about 2500 billion tons of carbon—more carbon than the atmosphere (780 billion tons) and plants (560 billion tons) combined on the planet [152] and, depending on cultivation practices, part of the carbon may be either released or additional carbon may be sequestered by the soil. A change in temperature may also alter the potential emission of some greenhouse gases from the soil, but this strongly interacts with soil water content [153].

The temperature may play a potent role, because, depending on organic matter content; water holding capacity; pore size distribution; precipitation rates; and other climate variables, such as solar radiation, the temperature has a large effect on the mineralization rate [154,155]. A comparison of the

simulated rates of nitrogen mineralization during the growing season, for 30 year periods since 1961, showed increasing rates over the past 50 years, with substantial differences between soils [156,157]. This analysis suggested that modifications in temperature and water relations in some vineyard sites already had a substantial impact on the release of nitrogen, which might have increased the risk for bunch rot development on these sites. However, independent measurements to validate model simulations are lacking, and a recent study on warming effects on microbial communities in temperate vineyard soils, which would be involved in N mineralization, did not find substantial changes [158].

Soil temperature also has a direct effect on root and shoot hydraulics, which will affect the transpiration rate, which is so far under-rated in the quantification of possible climate change effects on plant water use. These increases in hydraulic conductance have been attributed to changes in membrane fluidity and permeability [159,160], or changes in water viscosity [161], but most likely are a combination of both [162]. For a vineyard situation, attempts have been made to estimate these currently hypothetical changes, and the results show substantial possible effects on transpiration [151].

## 5. Climate Change Adaptation Strategies

Suitable adaptation measures need to be applied by the winemaking sector to face climate change impacts, mainly by planning adequate strategies at regional/local scales [163–165], particularly in regions that will experience the most adverse impacts. Grapevine growers are becoming gradually more aware of the threats, whereas timely and strategic planning against its negative impacts may provide competitive advantages [166]. As such, it is up to the stakeholders and decision-makers to take action against climate change. Some adaptation measures in viticulture are discussed in the following subsections, although an exhaustive discussion is not envisioned. Even though changes in oenological practices may also have important adaptation potential [167], they are out of the scope of the present review. In general, the effectiveness of each measure strongly depends on the local situation and regional climate change signal. The overall approach should always be the adoption of a combination of local solutions to cope with a global problem.

### *5.1. Short-Term Adaptation Strategies*

Short-term adaptation measures can be considered as a primary protection strategy against climate change and are commonly focused on specific threats. Short-term adaptation strategies are hereby defined as vineyard interventions that can be applied within a grapevine growing season. These measures generally imply changes in management practices, and some of them are briefly outlined in the following sub-sections.

#### 5.1.1. Crop Cultural Measures

Short-term adaptation strategies may involve crop cultural practices and techniques [165]. There are multitudes of possibilities to delay ripening to move the decisive stages in maturity after veraison into the cooler part of the season. Among these, of note are changes in canopy geometry, reduction of the assimilation surface by leaf removal above the cluster-zone, reduction of canopy size to minimize water consumption, application of anti-transparent substances/materials to reduce both carbon assimilation and water consumption, use of shadow nets, and earlier harvest to achieve moderate sugar levels and adequate acidity [3,168]. Cluster-zone leaf removal, which nowadays represents a standard measure in many viticultural regions where bunch rot represents a major threat due to its strong phytosanitary effects [169,170], may be questionable in the future due to higher susceptibility towards sunburn damage.

#### 5.1.2. Protection against Extreme Heat and Sunburns

The negative impacts of extreme heat, water scarcity, and high irradiance in vineyards urge short-term adaptation strategies, such as the application of exogenous compounds that could maintain, or even improve, plant growth and development under these environmental stresses. Several sunscreen

materials that form an inert particle film upon the leaves, such as calcium carbonate ($CaCO_3$), kaolin ($Al_2Si_2O_5(OH)_4$), and potassium silicate ($K_2SiO_3$), or the use of shade nets, have been studied to increase canopy and fruit zone reflective capacity [171,172]. Currently, one of the most commonly used compounds in viticulture is kaolin, a white clay, which is chemically inert and has excellent reflective properties. Glenn et al. [173] were the first to test the effects of this mineral on apple productivity. More recently, several studies developed for grapevines grown under severe summer stress corroborated that the use of kaolin has a positive impact on leaf cooling, minimizing the scorching of leaves and clusters during the hottest summer days [139,140]. Additionally, structure and function of the photosynthetic machinery and water relations were significantly improved [140,174,175], in part as a response to altered hormonal relationships (abscisic acid (ABA) decreased; indoleacetic acid (IAA) increased) [176]. In terms of yield and quality attributes, it was also shown for cv. Touriga-Nacional that kaolin application improved the antioxidant capacity in berries, as well as the amounts of some secondary metabolites, such as total phenols, flavonoids, and anthocyanins [174,175]. In another study, it was found that these compounds, qualitatively associated with the increase of colour, flavour, aroma, texture, astringency, antioxidant capacity, and stabilization of wines, were synthesized in greater quantity due to a more favourable stimulus of biosynthetic pathways (especially the phenylpropanoid and flavonoid synthetic pathways) and associated gene expression [47,177].

#### 5.1.3. Irrigation

Records of grapevine irrigation date back to ancient times (2900 BC) [178], and is a common practice in many countries, especially in the "New World" (e.g., Australia, USA). Even in countries where grapevines are traditionally rain-fed (e.g., France, Spain, Portugal, or Germany), irrigation has increasingly been implemented and local guidelines have slowly been adapted for this practice. However, for the production of high-quality wines (e.g., Brunello di Montalcino in Italy or Port Wine in Portugal), the current regulation only permits "rescue" irrigation.

Irrigation is used to improve and standardize crop yield and quality, whenever rainfall is too low to meet the defined grapevine water requirements. The management of vineyard irrigation is based on deficit irrigation (DI) strategies (e.g., regulated deficit irrigation, sustained deficit irrigation, partial root drying) to take advantage of the relationship between grapevine water status and the yield/quality [179]. Taking into consideration these strategies, drip irrigation is generally implemented as the most efficient water saving method [180,181], although sprinkler and furrow irrigation systems are still being used [182]. The implementation of DI strategies can be used to enhance water savings, which is particularly needed in wine regions with greater water deficits [183]. Furthermore, these cultural practices may be maximized with automated and smart irrigation (with real-time control and optimisation) systems [184].

A common methodology for DI implementation consists of the selection of a defined percentage of the computed crop evapotranspiration [185]. However, soil and/or plant water status indicators and respective thresholds should be used, preventing a continuous decrease in root-zone water content. Although measurements of soil water content (or soil water potential) may roughly determine the amount and the timing of irrigation, strong under- or overestimations may occur because the real depth of the root system is not taken into account. If this is the case, direct plant water status indicators are particularly useful [186,187]. Among those indicators, stem and leaf water potential have been extensively used. More recently, other techniques, such as trunk diameter variations and sap flow measurements have been implemented, with the advantage of possible automation [188,189].

Using a deficit irrigation technique, no yield reduction was observed for Godello grapevines [190]. Improvements in quality attributes were also found using these strategies on other varieties [191–193]. Hence, a sustainable water use strategy together with available water resources can be quite advantageous and cost-effective for the growers [194]. Nonetheless, the assessment of the real benefits and costs (including terrain factors, water distribution systems, technological options, on-farm *versus* catchment or basin-scale water savings, and socio-economic conditions) for implementing

irrigation under future climates is critical for the adoption of these adaptation measures [184,195], particularly in Southern Europe, where water availability is predicted to diminish [10,112].

#### 5.1.4. Pest and Disease Control

Under future climate conditions, wine regions may struggle with increased risk of pests and diseases, in principle demanding more intense plant protection measures at times where environmental impacts from phytosanitary treatments need to be reduced [196]. A recent general simulation study on possible changes in the fitness status of insect pests as a function of latitude showed that fitness level will decrease close to the equator, but increase poleward of the 30° latitude parallels [197]. Data from three decades on grapevine pests point to changes in the phenology of grape berry moths, shifts in distribution ranges of leafhoppers as vectors of grapevine diseases, and range expansion of grapevine mealybugs [142]. Pest and disease control is a dynamic process that requires monitoring, continuous innovation, and adaptation, because pests and diseases adapt to their environment, as well as to the control actions taken by growers. Adaptation can either take place by technology transfer from regions where the pest is already successfully controlled or by novel pest management approaches, such as the application of various natural compounds, but research gaps still exist that are hindering their widespread use [198]. In some cases, climate change may also lead to lower disease pressure and, in such cases, awareness of the decreased need for disease control should be raised among growers as an adaptive measure. In any case, to derive adaptive measures, a deeper understanding of tri-trophic interactions in vineyards is needed [142].

#### 5.1.5. Soil Management

Soil management is an essential adaptation tool, critical for soil and plant protection, water fluxes, greenhouse gas emission (GHE) rates, and possible carbon storage. In terms of water and carbon conservation, tillage is no longer advised, particularly in shallow soils on steep terrain, as it may also negatively affect yield and quality [199,200]. Moreover, mechanical cultivation affects most soil microbes and their functioning (e.g., arbuscular mycorrhizal fungi) and promotes the mineralization of organic matter and soil erosion, which is one of the most important environmental problems aggravated by conventional agriculture. Eroded soils have low fertility and low water-holding capacity, which limits water use efficiency. The consequences of erosion are of major relevance, as climate change and extreme events may exacerbate erosion rates, and many vineyards in Europe are on slopes, which aggravates potential erosion. Higher yields are usually achieved when the soil is managed with herbicides. However, bare soil reduces water infiltration and does not protect against erosion [201]. In addition, problems of ground-water contamination; changes on soil structure; the significant increase of resistant weed populations; and, in some situations, residues in grapes and wine are a source of concern that encourages the adoption of more sustainable solutions. For all these reasons, other practices should be implemented in order to safeguard soil fertility and preserve non-renewable resources. The use of compost obtained from different materials, such as municipal solid waste, green waste and urban sludge, wood ash, leaves, pruned vine-shoots, winery sludge, grape stalks, and other biomass residues from the farm, can be a good option. The application of compost increases soil microbiome, organic matter content, soil porosity and soil structural stability, nutrient supply, and water retention capacity, also reducing soil erosion. However, when applying a compost, the nutrient input into the vineyard has to be considered, because, for instance, high nitrogen freights might cause nitrate leaching into groundwater and lead to excessive plant vigour, dense foliage in the cluster zone, and compact clusters, which are directly linked to a higher predisposition towards bunch rot [170,202,203]. Likewise, the use of synthetic (e.g., black polyethylene and geotextile) and organic mulches, including compost, bark, or straw, may have positive effects on soil water content [204] and yield under future warmer and drier conditions [205]. Mulches also moderate soil temperatures and suppress diseases and harmful pests.

In all vineyards, the soil should be covered by green vegetation (spontaneous or cultivated herbaceous cover crops), at least during the rainy season, and by dead material (as in the case of Mediterranean viticulture) or partial cover crops as in intermittent rainfall areas, during the dry part of the season. The species used as cover crops should be selected on the basis of the local pedoclimatic conditions. Under low water availability, these species should have minimal competition for water (e.g., with short vegetative cycle) and make a positive contribution to soil fertility, as some self-reseeding annual legume species are comparatively less competitive for water than grasses and can fix atmospheric nitrogen [206]. A mixture of different species and cultivars should be chosen, as it increases the likelihood of success under variable weather conditions, being also advantageous to soil properties. On the other hand, in conditions of high-vigour environments, grasses could be inserted into the mixture. Cover crops keep the soil protected against erosion; reduce soil compaction, water evaporation, and dust; increase water infiltration, organic carbon, and trafficability; provide habitats for beneficial insects, and prevent nitrate leaching, resulting in enhanced yield and quality [207], as long as competition for water and nutrients will not cause deficits for the crop [208]. Furthermore, cover crops enable tractor passages for crop protection, particularly in sloped vineyards during intense rainfall periods and are, hence, safeguarding yield. Thus, well-designed cover crop mixtures may benefit soil and water quality, as well as the adaptive capacity of grapevines to climate change, and may also act as an ecosystem service [209].

### *5.2. Long-Term Adaptation Strategies*

Long-term adaptation strategies are measures employed by growers to adapt to climate change throughout several growing seasons or before the planting of a vineyard. In effect, grapevine as a perennial crop remains economically productive for several generations. The adoption of some long-term adaptation measures may be crucial, although their application may also bring significant socio-economic impacts. Although significant changes in bioclimatic conditions are expected to occur in the future [113], the potential of the different adaptation strategies may still prevent dramatic changes in viticultural suitability [210]. Some examples of long-term adaptation strategies are provided in the following sub-sections.

#### 5.2.1. Changes in Training Systems

The joint effect of growing temperatures with abiotic and biotic stresses projected for the upcoming decades will require changes in the current/traditional training systems, which may also be undertaken by optimizing canopy management practices [211]. Changes in training systems may target the following objectives:

(i) Delay of the maturation period (see also Section 5.1.1). To avoid grapes ripening under high-temperature conditions, training systems that delay ripening may be beneficial under future climate conditions. Minimal pruning systems in their various forms (i.e., semi-minimal pruned hedge) can delay maturity and bunch rot formation [212].

(ii) Lower sugar accumulation. To achieve reduced sugar content of grapes and thus reduced alcohol content, the leaf area to fruit weight ratio can be manipulated. Higher crop load per unit leaf area may, however, cause undesired lowering of wine quality, whereas a reduction of leaf area to fruit weight ratio by limiting the canopy height may cause the opposite [168].

(iii) Reduced radiation in the cluster-zone. Modifications of canopy geometry, such as row orientation, will influence light interception and wind velocity, and may also provide high adaptive potential [213,214]. For example, higher canopies, as well as closer distances between rows, may increase shadowing effects and, hence, decrease sunburn risk. However, both changes might lead to conflicts of objectives, such as higher water consumption and potential earlier maturation (high canopies) concomitant to unfavourable microclimatic conditions in the cluster-zone, fostering

bunch rot (narrow rows) [215]. Vineyard orientation should be optimized whenever possible, as it may significantly change radiation interception [213,214,216].

(iv) Higher water use efficiency. Regions under extreme dryness should promote higher water use efficiency [183] by adopting training systems that promote shorter trunks, such as the Gobelet [211] or Guyot systems [3].

Changes in the training systems can also be combined with changes in planting density and/or in trunk height, as they are inter-dependent. In general, higher planting densities lead to enhanced root competition, lower vegetative growth, deeper root penetration, and larger available soil volume, which can be useful in temperate humid climates. If canopy geometry remains the same, higher density at similar row distances reduces water stress [14]. However, when row distance changes concomitant to density, water deficit may be exacerbated [14].

#### 5.2.2. Varietal/Clonal and Rootstock Selection

Because the suitability for the successful cultivation of different varieties is largely temperature dependent, long-term adaptation strategies may consist of changes in the varietal spectrum [12]. A recent study postulated dramatic changes in arable viticultural land under strong warming, showing that in situ varietal selection may provide important climate change adaptation potential under moderate climate change scenarios [217]. Cooler northern European winemaking regions may benefit from a wide range of varieties from southern Europe [114], whereas southern Europe will be limited to varieties well adapted to very dry and warm climates. Some heat-tolerant varieties, such as Cabernet Franc, Cabernet Sauvignon, Malbec, Merlot, Syrah, or Tempranillo, have already been identified [32]. Hence, grapevine breeding should be focused on the development of heat-tolerant vine varieties [106]. A framework for genetic breeding of new varieties that will be more adapted to future climates has already been proposed [218]. The selection of appropriate varieties might be guided by mid-term climate change projections and bioclimatic indices describing the thermal demand of specific cultivars, such as the Huglin heliothermic index [77] or the average growing season temperature [56]. However, it needs to be kept in mind that these indices describe the lower temperature threshold for a variety, whereas the upper threshold is mostly unknown. This has previously led to substantial misconceptions concerning the prediction of future suitability of grape-growing regions [113,210]. Therefore, preserving the existing biodiversity of autochthonous grapevine varieties is vital, as some varieties may thrive in future climates and may thereby open new adaptation opportunities [219,220].

Because most of the sensory properties and the fame of many terroir wines rely on specific varieties [12], their replacement with more resistant ones is challenging in viticulture [12], as immediate varietal changes may cause economic losses. Accordingly, to fully exploit the potential of varietal selection, the preference of retailers and consumers for specific varieties needs to be changed, for instance by marketing wine from better-adapted varieties under a specific climate change adaptation label. The clonal selection has also a very important adaptation potential, as different clones from a given variety are more resilient to future abiotic and biotic stresses, at the same time contributing to the maintenance of local or regional wine typicity.

Rootstocks can also confer plant resistance, particularly to soil-borne pests and pathogens, but they also differ with regards to their resistance to abiotic stress. Planting new vineyards on rootstocks with enhanced resistance towards the primary abiotic stresses, present in a particular region or predicted to become the dominant stresses, can become a key element in adaptation [221]. More adapted rootstocks will be beneficial to yield, quality, and other vine physiological parameters [222,223]. Many studies have been performed to assess rootstock effects under different soil water conditions [223–225]. Rootstocks may present the single most effective cultural strategy to find a long-term solution concerning water availability, without tapping into the public water supply in the form of irrigation. However, to achieve this, the genetic potential of *Vitis* germplasm needs to be further explored in order to enhance water use efficiency and maintain yield and quality [226].

Grafting *Vitis vinifera* scions to phylloxera-resistant American *Vitis* rootstocks is commonly used in (Western) European countries, where hybrids (or interspecific hybrids) are generally not yet accepted for "quality wine" production [227]. However, the use of hybrids has increased worldwide in recent years (e.g., Brazil, China, and the USA). Especially in the emerging grape growing regions in northern Europe, new vineyards are frequently planted with interspecific crossings, with reduced susceptibility towards fungal diseases (the so-called "Piwis"). Furthermore, the OIV has been developing and discussing some project resolutions regarding this subject. This plant material is considered to be particularly resistant to fungal diseases and severe climate conditions [228]. Thus, the use of resistant hybrids can be a possible option and a challenge for the wine sector, in terms of perception of producers and consumers and regulation adaptations [227].

#### 5.2.3. Vineyard Relocation

These measures comprise modifications in vineyard location, as some regions may become excessively warm and dry for sustainable viticulture [229]. Shifts to cooler sites, such as those located at higher latitudes [230], at higher elevations [231], at coastal zones, or in areas with overall lower solar radiation (such as poleward exposed sites), are long-term measures that should be envisioned when choosing new vineyard sites [232]. Nevertheless, the use of these strategies must be carefully evaluated by considering the relevant economic consequences [233].

## 6. Knowledge Gaps and Research Challenges

Although research on potential impacts of climate change on viticulture is already largely developed, when compared to other crops, some important knowledge gaps remain. The use of climate projection datasets linked to grapevine simulation models represents the most feasible approach for predicting plant behaviour and production in the future [98], which can be complemented by climate chamber experiments, among others, for model development, calibration, and validation. In this regard, more experiments carried out under similar conditions and measuring the same variables are needed for a better comparison between studies and quantification of effects. Nonetheless, the evaluation of climate change impacts on any cultivated crop is sensitive to uncertainties in the future climate projections, deriving from model parameterizations, sub-grid scale processes, model initializations, intrinsic biases, radiative forcing scenarios, and other sources. Natural variability of the climate system needs also be taken into account, increasing the level of uncertainty with increasing distance into the future. These uncertainties need to be more thoroughly incorporated in the climate change projections and impact assessments, using more comprehensive probabilistic and risk analyses. This information should also be better communicated to stakeholders and decision-makers, instead of providing only ensemble means or other central tendency measures, which can be misleading and may impede or misguide an effective adaptation. Furthermore, these projections are available on platforms that are frequently not user-friendly, with data formats, as well as temporal and spatial scales, not being suitable for knowledge transfer to decision-makers [234]. A good example of an easy-to-use interface that is focused on cereal crops is the NASA (National Aeronautics and Space Administration) Harvest Crop Monitor interface, using remote sensing data to forecast crop conditions (https://cropmonitor.org/index.php/data-and-tools/cmet/).

Although grapevine simulation models, usually process-based, are already able to satisfactorily reproduce different interactions between the soil–plant–atmosphere continuum at a very detailed level, further enhancements and integrations are undeniably necessary to improve model reliability. As an illustration, estimations of bud break occurrences are often based on forcing models, without considering the effect of chilling during dormancy. This shortcoming frequently leads to erratic estimations of bud break under warmer climates, with obvious implications throughout the simulation of the phenological cycle [235]. Although the isolated effects of $CO_2$ and temperature on the radiation use efficiency and transpiration have already been extensively reported, their opposite impact on evapotranspiration, and their combined effect in future warmer climates, are not fully understood

yet [235,236]. Furthermore, simulation models should incorporate the incidence level of pests and diseases [237] and the impact of nitrogen and water stress [238,239], which are expected to have more impact on plants in a climate change context. Modelling approaches that would be able to incorporate aspects of grape quality will play a key role in understanding changes in berry metabolites [86]. Thus far, only a few grapevine models are currently available, and a very limited number of varieties can be simulated. More models, and more versatile models, are needed in order to implement multi-model ensemble scenarios, thereby enhancing the robustness of the projections. For a broader assessment on the effects on different varieties, the incorporation of key variables describing varietal behaviour is also lacking thus far.

The need to describe the plant processes at a very detailed level, using a high number of inputs, may currently preclude the applicability of simulation models as decision support tools for farmers. However, models coupled with the use of new technologies (e.g., drones and automatic plant-based irrigation systems) may determine the most appropriate management practices in the future. New projects using IoT (Internet of Things) platforms will be an effective way to tackle these challenges. Despite many proposed measures to cope with climate change, their corresponding adaptive potential under a wide range of local conditions is not yet sufficiently investigated and precise. Additionally, it is not sufficiently clear how the interplay between socioeconomic and ecological factors will affect decision-making in adaptation [240].

## 7. Conclusions

Even though grapevines have an array of survival strategies, their development is strongly controlled by weather and climate, over a wide range of processes and timescales. Wine style and wine typicity of a given region, recognised by consumers, are strongly connected to local terroirs, thus exacerbating the vulnerability of the whole wine sector to climate change. Threats to viticultural suitability have already been reported for several winemaking regions worldwide. Some changes have already been noticed on different levels by the winemaking sector. The 2019 ProWein Business Report mentions that viticulturists are already experiencing significant changes in their vineyards and are already responding. Among the adaptations considered most urgent in many regions are changes in vineyard locations, grapevine varieties, and some cultivation practices to avoid stronger irregularity in production and prevent an increase in the market volatility. In general, climate change is perceived as an important risk for viticulture, threatening in some cases, or challenging in most cases, viticulture and the winemaking sector. The adoption of timely, cost-effective, and suitable adaptation strategies may significantly contribute to risk reduction, thereby decreasing the susceptibility of the sector and enhancing its resilience under a changing climate. Even though the potential of the different adaptation options in reducing detrimental impacts still comprises many uncertainties and demands further research, the implementation of a blend of effective measures in the vineyard, tuned to local terroirs and local climate change projections, will contribute to the future environmental and socio-economic sustainability of existing wine regions. For that purpose, the communication channels between science, stakeholders, and consumers should be improved to enhance capacity building and knowledge transfer to the wine sector and increase acceptance to necessary changes by the consumer.

**Author Contributions:** J.A.S contributed to the manuscript conception, J.A.S., H.F., A.C.M., J.M.-P., L.-T.D., C.C., M.M., L.L., C.D., S.C.-A., T.K., C.M., D.M., J.J., M.B., H.R.S. contributed to the bibliographic search, discussion, writing, and revision. All authors have read and agreed to the published version of the manuscript.

**Funding:** This study was funded by Clim4Vitis project—"Climate change impact mitigation for European viticulture: knowledge transfer for an integrated approach", funded by the European Union's Horizon 2020 Research and Innovation Programme, under grant agreement no. 810176; it was also supported by FCT—Portuguese Foundation for Science and Technology, under the project UIDB/04033/2020.

**Conflicts of Interest:** The authors declare no conflict of interest. The funders had no role in the design of the study; in the collection, analyses, or interpretation of data; in the writing of the manuscript; or in the decision to publish the results.

## References


1. OIV. *2019 Statistical Report on World Vitiviniculture*; International Organisation of Vine and Wine: Paris, France, 2019.
2. Tonietto, J. Les Macroclimats Viticoles Mondiaux et l'Influence du Mésoclimat sur la Typicité de la Syrah et du Muscat de Hambourg dans le sud de la France: Méthodologie de Caractérisation. Ph.D. Thesis, Ecole Nationale Supérieure Agronomique, Montpellier, France, 1999; 233p.
3. Magalhães, N. *Tratado de Viticultura: A Videira, a Vinha e o Terroir*; Esfera Poética: Lisboa, Portugal, 2015; p. 605.
4. Fraga, H.; Malheiro, A.C.; Moutinho-Pereira, J.; Santos, J.A. Future scenarios for viticultural zoning in Europe: Ensemble projections and uncertainties. *Int. J. Biometeorol.* **2013**, *57*, 909–925. [CrossRef] [PubMed]
5. Carbonneau, A. Ecophysiologie de la vigne et terroir. In *Terroir, Zonazione, Viticoltura. Trattato Internazionale*; Phytoline: Centreville, VA, USA, 2003; pp. 61–102.
6. Mackenzie, D.E.; Christy, A.G. The role of soil chemistry in wine grape quality and sustainable soil management in vineyards. *Water Sci. Technol.* **2005**, *51*, 27–37. [CrossRef] [PubMed]
7. Jones, G.V. Climate, grapes, and wine: Structure and suitability in a changing climate. *Acta Hortic.* **2012**, *931*, 19–28. [CrossRef]
8. Winkler, A.J. *General Viticulture*; University of California Press: Berkeley, CA, USA, 1974.
9. van Leeuwen, C.; Friant, P.; Choné, X.; Tregoat, O.; Koundouras, S.; Dubordieu, D. Influence of climate, soil, and cultivar on terroir. *Am. J. Enol. Vitic.* **2004**, *55*, 207–217.
10. Fraga, H.; Malheiro, A.C.; Moutinho-Pereira, J.; Santos, J.A. An overview of climate change impacts on European viticulture. *Food Energy Secur.* **2012**, *1*, 94–110. [CrossRef]
11. Peixoto, J.P.; Oort, A.H. *Physics of climate*; American Institute of Physics: New York, NY, USA, 1992; p. xxxix. 520p.
12. Schultz, H.R.; Jones, G.V. Climate induced historic and future changes in viticulture. *J. Wine Res.* **2010**, *21*, 137–145. [CrossRef]
13. White, M.A.; Whalen, P.; Jones, G.V. Land and wine. *Nat. Geosci.* **2009**, *2*, 82–84. [CrossRef]
14. Neethling, E.; Barbeau, G.; Coulon-Leroy, C.; Quenol, H. Spatial complexity and temporal dynamics in viticulture: A review of climate-driven scales. *Agric. For. Meteorol.* **2019**, 276. [CrossRef]
15. Makra, L.; Vitanyi, B.; Gal, A.; Mika, J.; Matyasovszky, I.; Hirsch, T. Wine quantity and quality variations in relation to climatic factors in the Tokaj (Hungary) winegrowing region. *Am. J. Enol. Vitic.* **2009**, *60*, 312–321.
16. Fraga, H.; Costa, R.; Moutinho-Pereira, J.; Correia, C.M.; Dinis, L.-T.; Gonçalves, I.; Silvestre, J.; Eiras-Dias, J.; Malheiro, A.C.; Santos, J.A. Modeling phenology, water status, and yield components of three portuguese grapevines using the STICS crop model. *Am. J. Enol. Vitic.* **2015**, *66*, 482–491. [CrossRef]
17. Fraga, H.; Santos, J.A. Daily prediction of seasonal grapevine production in the Douro wine region based on favourable meteorological conditions. *Aust. J. Grape Wine Res.* **2017**. [CrossRef]
18. Costa, R.; Fraga, H.; Fonseca, A.; de Cortazar-Atauri, I.G.; Val, M.C.; Carlos, C.; Reis, S.; Santos, J.A. Grapevine phenology of cv. Touriga Franca and Touriga Nacional in the Douro Wine Region: Modelling and climate change projections. *Agron. Basel* **2019**, *9*, 210. [CrossRef]
19. Fraga, H.; Pinto, J.G.; Santos, J.A. Climate change projections for chilling and heat forcing conditions in European vineyards and olive orchards: A multi-model assessment. *Clim. Chang.* **2019**, *152*, 179–193. [CrossRef]
20. Webb, L.; Whetton, P.; Barlow, E. Modelled impact of future climate change on the phenology of winegrapes in Australia. *Aust. J. Grape Wine Res.* **2007**, *13*, 165–175. [CrossRef]
21. Gladstones, J. *Wine, Terroir and Climate Change*; Wakefield Press: Kent Town, South Australia, 2011.
22. Due, G.; Morris, M.; Pattison, S.; Coombe, B.G. Modeling grapevine phenology against weather—Considerations based on a large data set. *Agric. For. Meteorol.* **1993**, *65*, 91–106. [CrossRef]
23. Coombe, B.G. Influence of temperature on composition and quality of grapes. *Acta Hort.* **1987**, *206*, 23–36. [CrossRef]
24. Alleweldt, G.; Ilter, E. Untersuchungen über die Beziehungen zwischen Blütenbildung und Triebwachstum bei Reben. *Vitis* **1969**, *8*, 286–313.
25. Morrison, J.C. Bud development in *Vitis vinifera* L. *Bot. Gaz.* **1991**, *152*, 304–315. [CrossRef]
26. Buttrose, M.S. Fruitfulness in grape-vines: The response of different cultivars to light, temperature and daylength. *Vitis* **1970**, *9*, 121–125.
27. Keller, M. *The Science of Grapevines. Anatomy and Physiology*, 2nd ed.; Elsevier Academic Press: London, UK, 2015.

28. Molitor, D.; Keller, M. Yield of Müller-Thurgau and Riesling grapevines is altered by meteorological conditions in the current and the previous growing seasons. *OENO One* **2016**, *50*, 245–258.
29. Kliewer, W.M.; Soleiman, A. Effect of chilling on budbreak in Thompson seedless and Carignane grapevines. *Am. J. Enol. Vitic.* **1972**, *23*, 31–34.
30. Santos, J.A.; Costa, R.; Fraga, H. Climate change impacts on thermal growing conditions of main fruit species in Portugal. *Clim. Chang.* **2017**, *140*, 273–286. [CrossRef]
31. Amerine, M.A.; Winkler, A.J. Composition and Quality of Musts and Wines of California Grapes. *Hilgardia* **1944**, *15*, 493–675. [CrossRef]
32. Jones, G.V. Climate and Terroir: Impacts of climate variability and change on wine. In *Fine Wine and Terroir—The Geoscience Perspective*; Macqueen, R.W., Meinert, L.D., Eds.; Geoscience Canada, Geological Association of Canada: Saint John, NL, Canada, 2006.
33. Webb, L.B.; Whetton, P.H.; Bhend, J.; Darbyshire, R.; Briggs, P.R.; Barlow, E.W.R. Earlier wine-grape ripening driven by climatic warming and drying and management practices. *Nat. Clim. Chang.* **2012**, *2*, 259–264. [CrossRef]
34. Mandelli, F.; Tonietto, J.; Hasenack, H.; Weber, E.J. Zoneamento Climático para a produção de uvas para vinhos de qualidade. In Proceedings of the Congersso Brasileiro de Agrometeorologia, Campinas, Brazil, 18–21 July 2005.
35. Fraga, H.; Amraoui, M.; Malheiro, A.C.; Moutinho-Pereira, J.; Eiras-Dias, J.; Silvestre, J.; Santos, J.A. Examining the relationship between the Enhanced Vegetation Index and grapevine phenology. *Eur. J. Remote Sens.* **2014**, *47*, 753–771. [CrossRef]
36. Hidalgo, L. *Tratado de Viticultura General*; Mundi-Prensa Libros: Madrid, Spain, 2002.
37. Kartschall, T.; Wodinski, M.; von Bloh, W.; Oesterle, H.; Rachimow, C.; Hoppmann, D. Changes in phenology and frost risks in *Vitis vinifera* (cv Riesling) between 1901 and 2100. *Meteorol. Z.* **2015**. [CrossRef]
38. Modedale, J.; Wilson, R.J.; Maclean, I.M.D. Climate change and crop exposure to adverse weather: Changes to frost risk and grapevine flowering conditions. *PLoS ONE* **2015**, *10*, e0141218.
39. Molitor, D.; Caffarra, A.; Sinigoj, P.; Pertot, I.; Hoffmann, L.; Junk, J. Late frost damage risk for viticulture under future climate conditions: A case study for the Luxembourgish winegrowing region. *Aust. J. Grape Wine Res.* **2014**, *20*, 160–168. [CrossRef]
40. Sgubin, G.; Swingedouw, D.; Dayon, G.; Garcia de Cortazar-Atauri, I.; Ollat, N.; Pagé, C.; Van Leeuwen, C. The risk of tardive frost damage in French vineyards in a changing climate. *Agric. For. Meteorol.* **2018**, *250–251*, 226–242. [CrossRef]
41. Branas, J. *Viticulture*; Dehan: Montpellier, France, 1974; p. 990.
42. Spellman, G. Wine, weather and climate. *Weather* **1999**, *54*, 230–239. [CrossRef]
43. Kliewer, W.M. Effect of high-temperatures during bloom-set period on fruit-set, ovule fertility, and berry growth of several grape cultivars. *Am. J. Enol. Vitic.* **1977**, *28*, 215–222.
44. White, M.A.; Diffenbaugh, N.S.; Jones, G.V.; Pal, J.S.; Giorgi, F. Extreme heat reduces and shifts United States premium wine production in the 21st century. *Proc. Natl. Acad. Sci. USA* **2006**, *103*, 11217–11222. [CrossRef] [PubMed]
45. Berry, J.; Bjorkman, O. Photosynthetic response and adaptation to temperature in higher-plants. *Annu. Rev. Plant Phys.* **1980**, *31*, 491–543. [CrossRef]
46. Greer, D.H.; Weedon, M.M. The impact of high temperatures on Vitis vinifera cv. Semi lion grapevine performance and berry ripening. *Front. Plant Sci.* **2013**, *4*. [CrossRef]
47. Conde, A.; Pimentel, D.; Neves, A.; Dinis, L.T.; Bernardo, S.; Correia, C.M.; Geros, H.; Moutinho-Pereira, J. Kaolin foliar application has a stimulatory effect on phenylpropanoid and flavonoid pathways in grape berries. *Front. Plant Sci.* **2016**, *7*. [CrossRef]
48. Teixeira, A.; Eiras-Dias, J.; Castellarin, S.D.; Geros, H. Berry Phenolics of Grapevine under Challenging Environments. *Int. J. Mol. Sci.* **2013**, *14*, 18711–18739. [CrossRef]
49. Gutierrez-Gamboa, G.; Perez-Alvarez, E.P.; Rubio-Breton, P.; Garde-Cerdan, T. Changes on grape volatile composition through elicitation with methyl jasmonate, chitosan, and a yeast extract in Tempranillo (Vitis vinifera L.) grapevines. *Sci. Hortic Amst.* **2019**, *244*, 257–262. [CrossRef]
50. Robinson, A.L.; Boss, P.K.; Solomon, P.S.; Trengove, R.D.; Heymann, H.; Ebeler, S.E. Origins of Grape and Wine Aroma. Part 1. Chemical Components and Viticultural Impacts. *Am. J. Enol. Vitic.* **2014**, *65*, 1–24. [CrossRef]

51. Field, S.K.; Smith, J.P.; Holzapfel, B.P.; Hardie, W.J.; Emery, R.J.N. Grapevine response to soil temperature: Xylem cytokinins and carbohydrate reserve mobilization from budbreak to anthesis. *Am. J. Enol. Vitic.* **2009**, *60*, 164–172.
52. Austin, M.E.; Bondari, K. A Study of Cultural and Environmental-Factors on the Yield of Vitis-Rotundifolia. *Sci. Hortic Amst.* **1988**, *34*, 219–227. [CrossRef]
53. Hardie, W.J.; Martin, S.R. Shoot growth on de-fruited grapevines: A physiological indicator for irrigation scheduling. *Aust. J. Grape Wine Res.* **2000**, *6*, 52–58. [CrossRef]
54. Hardie, W.J.; Considine, J.A. Response of grapes to water-deficit stress in particular stages of development. *Am. J. Enol. Vitic.* **1976**, *27*, 55–61.
55. During, H. ABA and water stress in grapevines. *Acta Hortic* **1986**, *179*, 413–420. [CrossRef]
56. Jones, G.V.; Davis, R.E. Using a synoptic climatological approach to understand climate-viticulture relationships. *Int. J. Clim.* **2000**, *20*, 813–837. [CrossRef]
57. Nemani, R.R.; White, M.A.; Cayan, D.R.; Jones, G.V.; Running, S.W.; Coughlan, J.C.; Peterson, D.L. Asymmetric warming over coastal California and its impact on the premium wine industry. *Clim. Res.* **2001**, *19*, 25–34. [CrossRef]
58. Ramos, M.C.; Jones, G.V.; Martinez-Casasnovas, J.A. Structure and trends in climate parameters affecting winegrape production in northeast Spain. *Clim. Res.* **2008**, *38*, 1–15. [CrossRef]
59. Porter, J.R.; Semenov, M.A. Crop responses to climatic variation. *Philos. Trans. R. Soc. Lond. Ser. B Biol. Sci.* **2005**, *360*, 2021–2035. [CrossRef]
60. Reynolds, A.G.; Naylor, A.P. Pinot-Noir and Riesling grapevines respond to water-stress duration and soil water-holding capacity. *Hortscience* **1994**, *29*, 1505–1510. [CrossRef]
61. Molitor, D.; Baus, O.; Hoffmann, L.; Beyer, M. Meteorological conditions determine the thermal-temporal position of the annual Botrytis bunch rot epidemic on *Vitis vinifera* L. cv. Riesling grapes. *OENO One* **2016**, *50*, 231–244. [CrossRef]
62. Savoi, S.; Wong, D.C.; Arapitsas, P.; Miculan, M.; Bucchetti, B.; Peterlunger, E.; Fait, A.; Mattivi, F.; Castellarin, S.D. Transcriptome and metabolite profiling reveals that prolonged drought modulates the phenylpropanoid and terpenoid pathway in white grapes (Vitis vinifera L.). *BMC Plant Biol.* **2016**, *16*, 67. [CrossRef]
63. Vilanova, M.; Fandino, M.; Frutos-Puerto, S.; Cancela, J.J. Assessment fertigation effects on chemical composition of Vitis vinifera L. cv. Albarino. *Food Chem.* **2019**, *278*, 636–643. [CrossRef] [PubMed]
64. Chapman, D.M.; Roby, G.; Ebeler, S.E.; Guinard, J.X.; Matthews, M.A. Sensory attributes of Cabernet Sauvignon wines made from vines with different water status. *Aust. J. Grape Wine Res.* **2005**, *11*, 339–347. [CrossRef]
65. Deluc, L.G.; Grimplet, J.; Wheatley, M.D.; Tillett, R.L.; Quilici, D.R.; Osborne, C.; Schooley, D.A.; Schlauch, K.A.; Cushman, J.C.; Cramer, G.R. Transcriptomic and metabolite analyses of Cabernet Sauvignon grape berry development. *BMC Genom.* **2007**, *8*, 429. [CrossRef] [PubMed]
66. Roby, G.; Harbertson, J.F.; Adams, D.A.; Matthews, M.A. Berry size and vine water deficits as factors in winegrape composition: Anthocyanins and tannins. *Aust. J. Grape Wine Res.* **2004**, *10*, 100–107. [CrossRef]
67. Castellarin, S.D.; Matthews, M.A.; Di Gaspero, G.; Gambetta, G.A. Water deficits accelerate ripening and induce changes in gene expression regulating flavonoid biosynthesis in grape berries. *Planta* **2007**, *227*, 101–112. [CrossRef]
68. Riou, C.; Carbonneau, A.; Becker, N.; Caló, A.; Costacurta, A.; Castro, R.; Pinto, P.A.; Carneiro, L.C.; Lopes, C.; Clímaco, P.; et al. *Le Determinisme Climatique de la Maturation du Raisin: Application au Zonage de la Teneur en Sucre dans la Communauté Européenne*; Office des Publications Officielles des Communautés Européennes: Luxembourg, 1994; p. 319.
69. Archer, E.; Strauss, H.C. The effect of vine spacing on some physiological aspects of Vitis vinifera L. (cv. Pinot noir). *S. Afr. J. Enol. Vitic.* **1990**, *11*, 49–58. [CrossRef]
70. Smart, R.E.; Robinson, J.B.; Due, G.R.; Brien, C.J. Canopy microclimate modification for the cultivar Shiraz.1. Definition of canopy microclimate. *Vitis* **1985**, *24*, 17–31.
71. Morgan, D.C.; Stanley, C.J.; Warrington, I.J. The effects of simulated daylight and shade-light on vegetative and reproductive growth in kiwifruit and grapevine. *J. Hortic Sci.* **1985**, *60*, 473–484. [CrossRef]

72. Moutinho-Pereira, J.M.; Correia, C.M.; Goncalves, B.M.; Bacelar, E.A.; Torres-Pereira, J.M. Leaf gas exchange and water relations of grapevines grown in three different conditions. *Photosynthetica* **2004**, *42*, 81–86. [CrossRef]
73. Jones, G.V.; White, M.A.; Cooper, O.R.; Storchmann, K.-H. Climate and wine: Quality issues in a warmer world. In Proceedings of the Vineyard Data Quantification Society's 10th OEonometrics Meeting, Dijon, France, May 2004.
74. Berli, F.; D'Angelo, J.; Cavagnaro, B.; Bottini, R.; Wuilloud, R.; Silva, M.F. Phenolic composition in grape (Vitis vinifera L. cv. Malbec) ripened with different solar UV-B radiation levels by capillary zone electrophoresis. *J. Agric. Food Chem.* **2008**, *56*, 2892–2898. [CrossRef]
75. Berli, F.J.; Fanzone, M.; Piccoli, P.; Bottini, R. Solar UV-B and ABA are involved in phenol metabolism of Vitis vinifera L. increasing biosynthesis of berry skin polyphenols. *J. Agric. Food Chem.* **2011**, *59*, 4874–4884. [CrossRef] [PubMed]
76. Carbonell-Bejerano, P.; Diago, M.P.; Martinez-Abaigar, J.; Martinez-Zapater, J.M.; Tardaguila, J.; Nunez-Olivera, E. Solar ultraviolet radiation is necessary to enhance grapevine fruit ripening transcriptional and phenolic responses. *BMC Plant Biol.* **2014**, 14. [CrossRef] [PubMed]
77. Huglin, P. *Nouveau Mode d'évaluation des Possibilités Héliothermiques d'un Milieu Viticole. Comptes Rendus de l'Académie d'Agriculture*; Académie d'agriculture de France: Paris, France, 1978.
78. Molitor, D.; Junk, J.; Evers, D.; Hoffmann, L.; Beyer, M. A high-resolution cumulative degree day-based model to simulate phenological development of grapevine. *Am. J. Enol. Vitic.* **2014**, *65*, 72–80. [CrossRef]
79. Tonietto, J.; Carbonneau, A. A multicriteria climatic classification system for grape-growing regions worldwide. *Agric. For. Meteorol.* **2004**, *124*, 81–97. [CrossRef]
80. Molitor, D.; Junk, J. Climate change is implicating a two-fold impact on air temperature increase in the ripening period under the conditions of the Luxembourgish grapegrowing region. *OENO One* **2019**, *53*, 409–422. [CrossRef]
81. Jones, G.V.; White, M.A.; Cooper, O.R.; Storchmann, K. Climate change and global wine quality. *Clim. Chang.* **2005**, *73*, 319–343. [CrossRef]
82. Duchene, E.; Schneider, C. Grapevine and climatic changes: A glance at the situation in Alsace. *Agron. Sustain. Dev.* **2005**, *25*, 93–99. [CrossRef]
83. Petrie, P.R.; Sadras, V.O. Advancement of grapevine maturity in Australia between 1993 and 2006: Putative causes, magnitude of trends and viticultural consequences. *Aust. J. Grape Wine Res.* **2008**, *14*, 33–45. [CrossRef]
84. Duchene, E.; Huard, F.; Dumas, V.; Schneider, C.; Merdinoglu, D. The challenge of adapting grapevine varieties to climate change. *Clim. Res.* **2010**, *41*, 193–204. [CrossRef]
85. Kenny, G.J.; Harrison, P.A. The effects of climate variability and change on grape suitability in Europe. *J. Wine Res.* **1992**, *3*, 163–183. [CrossRef]
86. Leolini, L.; Moriondo, M.; Romboli, Y.; Gardiman, M.; Costafreda-Aumedes, S.; de Cortazar-Atauri, I.G.; Bindi, M.; Granchi, L.; Brilli, L. Modelling sugar and acid content in Sangiovese grapes under future climates: An Italian case study. *Clim. Res.* **2019**, *78*, 211–224. [CrossRef]
87. Jones, G.V.; Davis, R.E. Climate influences on grapevine phenology, grape composition, and wine production and quality for Bordeaux, France. *Am. J. Enol. Vitic.* **2000**, *51*, 249–261.
88. Bock, A.; Sparks, T.; Estrella, N.; Menzel, A. Changes in the phenology and composition of wine from Franconia, Germany. *Clim. Res.* **2011**, *50*, 69–81. [CrossRef]
89. Chuine, I.; Yiou, P.; Viovy, N.; Seguin, B.; Daux, V.; Ladurie, E.L. Historical phenology: Grape ripening as a past climate indicator. *Nature* **2004**, *432*, 289–290. [CrossRef]
90. Marta, A.; Grifoni, D.; Mancini, M.; Storchi, P.; Zipoli, G.; Orlandini, S. Analysis of the relationships between climate variability and grapevine phenology in the Nobile di Montepulciano wine production area. *J. Agric. Sci.* **2010**, *148*, 657–666. [CrossRef]
91. Daux, V.; Garcia de Cortazar-Atauri, I.; Yiou, P.; Chuine, I.; Garnier, E.; Le Roy Ladurie, E.; Mestre, O.; Tardaguila, J. An open-database of Grape Harvest dates for climate research: Data description and quality assessment. *Clim. Past Discuss.* **2011**, *7*, 3823–3858. [CrossRef]
92. Webb, L.B.; Whetton, P.H.; Barlow, E.W.R. Observed trends in winegrape maturity in Australia. *Glob. Chang. Biol.* **2011**, *17*, 2707–2719. [CrossRef]

93. Webb, L.B.; Whetton, P.H.; Barlow, E.W.R. Modelling the relationship between climate, winegrape price and winegrape quality in Australia. *Clim. Res.* **2008**, *36*, 89–98. [CrossRef]
94. Orduna, R.M. Climate change associated effects on grape and wine quality and production. *Food Res. Int.* **2010**, *43*, 1844–1855. [CrossRef]
95. Neethling, E.; Barbeau, G.; Bonnefoy, C.; Quenol, H. Change in climate and berry composition for grapevine varieties cultivated in the Loire Valley. *Clim. Res.* **2012**, *53*, 89–101. [CrossRef]
96. IPCC. *Climate Change 2014: Synthesis Report. Contribution of Working Groups I, II and III to the Fifth Assessment Report of the Intergovernmental Panel on Climate Change*; Pachauri, R.K., Meyer, L.A., Eds.; IPCC: Geneva, Switzerland, 2014; p. 151.
97. Meehl, G.A.; Stocker, T.F.; Collins, W.D.; Friedlingstein, P.; Gaye, A.T.; Gregory, J.M.; Kitoh, A.; Knutti, R.; Murphy, J.M.; Noda, A.; et al. Global Climate Projections. In *Climate Change 2007: The Physical Science Basis. Contribution of Working Group I to the Fourth Assessment Report of the Intergovernmental Panel on Climate Change*; Solomon, S., Qin, D., Manning, M., Chen, Z., Marquis, M., Averyt, K.B., Tignor, M., Miller, H.L., Eds.; Cambridge University Press: Cambridge, UK; New York, NY, USA, 2007; pp. 747–845.
98. Fraga, H.; García de Cortázar Atauri, I.; Malheiro, A.C.; Santos, J.A. Modelling climate change impacts on viticultural yield, phenology and stress conditions in Europe. *Glob. Chang. Biol.* **2016**, *22*, 3774–3788. [CrossRef] [PubMed]
99. Teslić, N.; Vujadinović, M.; Ruml, M.; Antolini, G.; Vuković, A.; Parpinello, G.P.; Ricci, A.; Versari, A. Climatic shifts in high quality wine production areas, Emilia Romagna, Italy, 1961–2015. *Clim. Res.* **2017**, *73*, 195–206. [CrossRef]
100. Eccel, E.; Zollo, A.L.; Mercogliano, P.; Zorer, R. Simulations of quantitative shift in bio-climatic indices in the viticultural areas of Trentino (Italian Alps) by an open source R package. *Comput. Electron. Agric.* **2016**, *127*, 92–100. [CrossRef]
101. Bonfante, A.; Alfieri, S.M.; Albrizio, R.; Basile, A.; De Mascellis, R.; Gambuti, A.; Giorio, P.; Langella, G.; Manna, P.; Monaco, E.; et al. Evaluation of the effects of future climate change on grape quality through a physically based model application: A case study for the Aglianico grapevine in Campania region, Italy. *Agric. Syst.* **2017**, *152*, 100–109. [CrossRef]
102. Bonfante, A.; Monaco, E.; Langella, G.; Mercogliano, P.; Bucchignani, E.; Manna, P.; Terribile, F. A dynamic viticultural zoning to explore the resilience of terroir concept under climate change. *Sci. Total Environ.* **2018**, *624*, 294–308. [CrossRef]
103. Duchene, E. How can grapevine genetics contribute to the adaptation to climate change? *OENO One* **2016**, *50*. [CrossRef]
104. García de Cortázar-Atauri, I.; Duchêne, E.; Destrac-Irvine, A.; Barbeau, G.; de Rességuier, L.; Lacombe, T.; Parker, A.K.; Saurin, N.; van Leeuwen, C. Grapevine phenology in France: From past observations to future evolutions in the context of climate change. *OENO One* **2017**, *51*. [CrossRef]
105. Ramos, M.C. Projection of phenology response to climate change in rainfed vineyards in north-east Spain. *Agric. For. Meteorol.* **2017**, *247*, 104–115. [CrossRef]
106. Santos, J.A.; Costa, R.; Fraga, H. New insights into thermal growing conditions of Portuguese grapevine varieties under changing climates. *Theor. Appl. Climatol.* **2018**. [CrossRef]
107. Neumann, P.A.; Matzarakis, A. Estimation of wine characteristics using a modified Heliothermal Index in Baden-Wurttemberg, SW Germany. *Int. J. Biometeorol.* **2014**, *58*, 407–415. [CrossRef]
108. Neumann, P.A.; Matzarakis, A. Viticulture in southwest Germany under climate change conditions. *Clim. Res.* **2011**, *47*, 161–169. [CrossRef]
109. Lazoglou, G.; Anagnostopoulou, C.; Koundouras, S. Climate change projections for Greek viticulture as simulated by a regional climate model. *Theor. Appl. Climatol.* **2017**. [CrossRef]
110. Junk, J.; Goergen, K.; Krein, A. Future heat waves in different European capitals based on climate change indicators. *Int. J. Environ. Res. Public Health* **2019**, *19*, 3959. [CrossRef] [PubMed]
111. Goergen, K.; Beersma, L.; Hoffmann, L.; Junk, J. ENSEMBLES-based assessment of regional climate effects in Luxembourg and their impact on vegetation. *Clim. Chang.* **2013**, *119*, 761–773. [CrossRef]
112. Fraga, H.; García de Cortázar Atauri, I.; Santos, J.A. Viticultural irrigation demands under climate change scenarios in Portugal. *Agric. Water Manag.* **2018**, *196*, 66–74. [CrossRef]

113. Hannah, L.; Roehrdanz, P.R.; Ikegami, M.; Shepard, A.V.; Shaw, M.R.; Tabor, G.; Zhi, L.; Marquet, P.A.; Hijmans, R.J. Climate change, wine, and conservation. *Proc. Natl. Acad. Sci. USA* **2013**, *110*, 6907–6912. [CrossRef] [PubMed]
114. Stock, M.; Gerstengarbe, F.W.; Kartschall, T.; Werner, P.C. Reliability of climate change impact assessments for viticulture. In Proceedings of the VII International Symposium on Grapevine Physiology and Biotechnology, Davis, CA, USA, 31 Augest 2005; Volume 689, pp. 29–39.
115. Toth, J.P.; Vegvari, Z. Future of winegrape growing regions in Europe. *Aust. J. Grape Wine Res.* **2016**, *22*, 64–72. [CrossRef]
116. Koundouras, S.; Van Leeuwen, C.; Seguin, G.; Glories, Y. Influence of water status on vine vegetative growth, berry ripening and wine characteristics in mediterranean zone (example of Nemea, Greece, variety Saint-George, 1997). *J. Int. Des. Sci. Vigne Vin.* **1999**, *33*, 149–160. [CrossRef]
117. Jackson, D.I.; Lombard, P.B. Environmental and management practices affecting grape composition and wine quality—A review. *Am. J. Enol. Vitic.* **1993**, *44*, 409–430.
118. Buttrose, M.S.; Hale, C.R.; Kliewer, W.M. Effect of temperature on composition of Cabernet Sauvignon berries. *Am. J. Enol. Vitic.* **1971**, *22*, 71–75.
119. Chalmers, Y.; Downey, M.; Krstic, M.; Loveys, B.; Dry, P.R. Influence of sustained deficit irrigation on colour parameters of Cabernet Sauvignon and Shiraz microscale wine fermentations. *Aust. J. Grape Wine Res.* **2010**, *16*, 301–313. [CrossRef]
120. Downey, M.O.; Dokoozlian, N.K.; Krstic, M.P. Cultural practice and environmental impacts on the flavonoid composition of grapes and wine: A review of recent research. *Am. J. Enol. Vitic.* **2006**, *57*, 257–268.
121. Bureau, S.M.; Razungles, A.J.; Baumes, R.L. The aroma of Muscat of Frontignan grapes: Effect of the light environment of vine or bunch on volatiles and glycoconjugates. *J. Sci. Food Agric.* **2000**, *80*, 2012–2020. [CrossRef]
122. Trought, M.C.T.; Parker, A.; Van Leeuwen, C. Can a change in vineyard practice mitigate warming due to climate change? *Acta Hortic* **2015**, 397–402. [CrossRef]
123. Brandt, M.; Scheidweiler, M.; Rauhut, D.; Patz, C.D.; Will, F.; Zorn, H.; Stoll, M. The influence of temperature and solar radiation on phenols in berry skin and maturity parameters of *Vitis vinifera* L. cv. Riesling. *OENO One* **2018**, *2*, 287–302. [CrossRef]
124. Eitzinger, J.; Kubu, G.; Formayer, H.; Gerersdorfer, T. Climatic wine growing potential under future climate scenarious in Austria. *Sustain. Dev. Bioclim. Rev. Conf. Proc.* **2009**, 146–147. Available online: http://www.startclim.at/fileadmin/user_upload/reports/StCl08_fin.pdf (accessed on 21 April 2020).
125. Gaal, M.; Moriondo, M.; Bindi, M. Modelling the impact of climate change on the Hungarian wine regions using random forest. *Appl. Ecol. Environ. Res.* **2012**, *10*, 121–140. [CrossRef]
126. Bertin, R.I. Plant phenology and distribution in relation to recent climate change. *J. Torrey Bot. Soc.* **2009**, *135*, 126–146. [CrossRef]
127. Ashenfelter, O.; Storchmann, K. Measuring the Economic Effect of Global Warming on Viticulture Using Auction, Retail, and Wholesale Prices. *Rev. Ind. Organ.* **2010**, *37*, 51–64. [CrossRef]
128. Kotremba, C.; Tintrup, G.; Trapp, M. Spätfrostgefährdung des Weinbaugebietes Pfalz—eine klimatologische und reliefbasierte Betrachtung. In *Deutsches Weinbau Jahrbuch*; Schultz, H.R., Stoll, M., Eds.; Eugen Ulmer KG: Stuttgart, Germany, 2014.
129. Leolini, L.; Moriondo, M.; Fila, G.; Costafreda-Aumedes, S.; Ferrise, R.; Bindi, M. Late spring frost impacts on future grapevine distribution in Europe. *Field Crop. Res.* **2018**, *222*, 197–208. [CrossRef]
130. Molitor, D.; Junk, J. Keine Chance mehr für Eiswein? *Die Winz. Z.* **2019**, *11*, 33–34.
131. Bindi, M.; Fibbi, L.; Gozzini, B.; Orlandini, S.; Miglietta, F. Modelling the impact of future climate scenarios on yield and yield variability of grapevine. *Clim. Res.* **1996**, *7*, 213–224. [CrossRef]
132. Moutinho-Pereira, J.; Goncalves, B.; Bacelar, E.; Cunha, J.B.; Coutinho, J.; Correia, C.M. Effects of elevated CO2 on grapevine (Vitis vinifera L.): Physiological and yield attributes. *Vitis* **2009**, *48*, 159–165.
133. Edwards, E.J.; Unwin, D.; Kilmister, R.; Treeby, M. Multi-seasonal effects of warming and elevated CO 2 on the physiology, growth and production of mature, field grown, Shiraz grapevines. *OENO One* **2017**, *51*. [CrossRef]
134. Schultz, H. Climate change and viticulture: A European perspective on climatology, carbon dioxide and UV-B effects. *Aust. J. Grape Wine Res.* **2000**, *6*, 2–12. [CrossRef]

135. Wohlfahrt, Y.; Smith, J.P.; Tittmann, S.; Honermeier, B.; Stoll, M. Primary productivity and physiological responses of Vitis vinifera L. cvs. under Free Air Carbon dioxide Enrichment (FACE). *Eur. J. Agron.* **2018**, *101*, 149–162. [CrossRef]
136. Wohlfahrt, Y.; Collins, C.; Stoll, M. Grapevine bud fertility under conditions of elevated carbon dioxide. *OENO One* **2019**, *53*. [CrossRef]
137. Rabbinge, R.; Vanlatesteijn, H.C.; Goudriaan, J. Assessing the greenhouse-effect in agriculture. *Ciba Found. Symp.* **1993**, *175*, 62–79.
138. Wramneby, A.; Smith, B.; Samuelsson, P. Hot spots of vegetation-climate feedbacks under future greenhouse forcing in Europe. *J. Geophys. Res. Atmos.* **2010**, *115*, D21119. [CrossRef]
139. Dinis, L.T.; Ferreira, H.; Pinto, G.; Bernardo, S.; Correia, C.M.; Moutinho-Pereira, J. Kaolin-based, foliar reflective film protects photosystem II structure and function in grapevine leaves exposed to heat and high solar radiation. *Photosynthetica* **2016**, *54*, 47–55. [CrossRef]
140. Dinis, L.T.; Malheiro, A.C.; Luzio, A.; Fraga, H.; Ferreira, H.; Goncalves, I.; Pinto, G.; Correia, C.M.; Moutinho-Pereira, J. Improvement of grapevine physiology and yield under summer stress by kaolin-foliar application: Water relations, photosynthesis and oxidative damage. *Photosynthetica* **2018**, *56*, 641–651. [CrossRef]
141. Langille, A.B.; Arteca, E.M.; Newman, J.A. The impacts of climate change on the abundance and distribution of the Spotted Wing Drosophila (Drosophila suzukii) in the United States and Canada. *PeerJ* **2017**, *5*. [CrossRef] [PubMed]
142. Reineke, A.; Thiery, D. Grapevine insect pests and their natural enemies in the age of global warming. *J. Pest Sci.* **2016**, *89*, 313–328. [CrossRef]
143. Caffarra, A.; Rinaldi, M.; Eccel, E.; Rossi, V.; Pertot, I. Modelling the impact of climate change on the interaction between grapevine and its pests and pathogens: European grapevine moth and powdery mildew. *Agric. Ecosyst. Environ.* **2012**, *148*, 89–101. [CrossRef]
144. Zito, S.; Caffarra, A.; Richard, Y.; Castel, T.; Bois, B. Climate change and vine protection: The case of mildews management in Burgundy. *E3s Web Conf.* **2018**, *50*, 01006. [CrossRef]
145. Bois, B.; Zito, S.; Calonnec, A. Climate vs grapevine pests and diseases worldwide: The first results of a global survey. *OENO One* **2017**, *51*, 133–139. [CrossRef]
146. IPCC. *Climate Change 2013: The Physical Science Basis. Summary for Policymakers. Working Group I Contribution to the IPCC Fifth Assessment Report*; IPCC: Geneva, Switzerland, 2013.
147. Ollat, N.; Touzard, J.M.; van Leeuwen, C. Climate Change Impacts and Adaptations: New Challenges for the Wine Industry. *J. Wine Econ.* **2016**, *11*, 139–149. [CrossRef]
148. This, P.; Lacombe, T.; Thomas, M.R. Historical origins and genetic diversity of wine grapes. *Trends Genet.* **2006**, *22*, 511–519. [CrossRef]
149. Paustian, K.; Lehmann, J.; Ogle, S.; Reay, D.; Robertson, G.P.; Smith, P. Climate-smart soils. *Nature* **2016**, *532*, 49–57. [CrossRef]
150. Böhme, M.; Böttcher, F. Bodentemperaturen im Klimawandel: Auswertungen der Messreihe der Sälularstation Potsdam. *Klimastatusbericht Des. Dtsch. Wetterd.* **2011**, *1*, 85–90.
151. Schultz, H.R. The soil as an important part in the interaction with plant functioning and fruit quality under climate change—An integrated view on a moving target. In Proceedings of the OENOVITI, International Symposium, Athens, Greece, 12–14 May 2019; p. 4.
152. Lal, R. Managing Soils and Ecosystems for Mitigating Anthropogenic Carbon Emissions and Advancing Global Food Security. *Bioscience* **2010**, *60*, 708–721. [CrossRef]
153. Oertel, C.; Matschullat, J.; Zurba, K.; Zimmermann, F.; Erasmi, S. Greenhouse gas emissions from soils A review. *Chem. Erde-Geochem.* **2016**, *76*, 327–352. [CrossRef]
154. Schaller, L.; Jagoutz, H.; Berthold, G.; Emde, K.; Löhnertz, O.; Hoppmann, D. *Bewirtschaftungssystem und Nitratbildung in Rebflächen. Teil 1: Grundlage für die Erarbeitung eines Simulationsmodells*; Geisenheim University: Geisenheim, Germany, 1994.
155. Schaller, L.; Jagoutz, H.; Berthold, G.; Emde, K.; Löhnertz, O.; Hoppmann, D. *Bewirtschaftungssystem und Nitratbildung in Rebflächen. Teil 2: Parameterschätzung und Umsetzung zu einem Düngeberatungsmodell*; Geisenheim University: Geisenheim, Germany, 1994.
156. Schultz, H.R. Global Climate Change, Sustainability, and Some Challenges for Grape and Wine Production. *J. Wine Econ.* **2016**, *11*, 181–200. [CrossRef]

157. Schultz, H.R.; Hofmann, M. The ups and downs of environmental impact on grapevines: Future challenges in temperate viticulture. In *Grapevine in a Changing Environment: A Molecular and Ecophysiological Perspective*; Géros, H., Chaves, M.M., Gil, H.M., Delrot, S., Eds.; John Wiley & Sons Ltd. Publishers: London, UK, 2016; Volume 1, pp. 18–37.
158. Corneo, P.E.; Pellegrini, A.; Cappellin, L.; Gessler, C.; Pertot, I. Moderate Warming in Microcosm Experiment Does Not Affect Microbial Communities in Temperate Vineyard Soils. *Microb. Ecol.* **2014**, *67*, 659–670. [CrossRef] [PubMed]
159. Ameglio, T.; Morizet, J.; Cruiziat, P.; Martignac, M. The Effects of Root Temperature on Water Flux, Potential and Root Resistance in Sunflower. *Agronomie* **1990**, *10*, 331–340. [CrossRef]
160. Carvajal, M.; Cooke, D.T.; Clarkson, D.T. Plasma membrane fluidity and hydraulic conductance in wheat roots: Interactions between root temperature and nitrate or phosphate deprivation. *Plant Cell Environ.* **1996**, *19*, 1110–1114. [CrossRef]
161. Hertel, A.; Steudle, E. The function of water channels in Chara: The temperature dependence of water and solute flows provides evidence for composite membrane transport and for a slippage of small organic solutes across water channels. *Planta* **1997**, *202*, 324–335. [CrossRef]
162. Cochard, H.; Martin, R.; Gross, P.; Bogeat-Triboulot, M.B. Temperature effects on hydraulic conductance and water relations of Quercus robur L. *J. Exp. Bot.* **2000**, *51*, 1255–1259. [CrossRef]
163. Metzger, M.J.; Rounsevell, M.D.A. A need for planned adaptation to climate change in the wine industry PERSPECTIVE. *Environ. Res. Lett.* **2011**, *6*. [CrossRef]
164. Neethling, E.; Petitjean, T.; Quénol, H.; Barbeau, G. Assessing local climate vulnerability and winegrowers' adaptive processes in the context of climate change. *Mitig. Adapt. Strateg. Glob. Chang.* **2016**. [CrossRef]
165. van Leeuwen, C.; Darriet, P. The Impact of Climate Change on Viticulture and Wine Quality. *J. Wine Econ.* **2016**, *11*, 150–167. [CrossRef]
166. Battaglini, A.; Barbeau, G.; Bindi, M.; Badeck, F.W. European winegrowers' perceptions of climate change impact and options for adaptation. *Reg. Environ. Chang.* **2009**, *9*, 61–73. [CrossRef]
167. Lobell, D.B.; Field, C.B.; Cahill, K.N.; Bonfils, C. Impacts of future climate change on California perennial crop yields: Model projections with climate and crop uncertainties. *Agric. For. Meteorol.* **2006**, *141*, 208–218. [CrossRef]
168. Stoll, M.; Bischoff-Schaefer, M.; Lafontaine, M.; Tittmann, S.; Henschke, J. Impact of various leaf area modifications on berry maturation in *Vitis vinifera* L. cv. Riesling. *Acta Hortic* **2013**, *978*, 293–299. [CrossRef]
169. Hed, B.; Ngugi, H.K.; Travis, J.W. Short- and long-term effects of leaf removal and gibberellin on Chardonnay grapes in the Lake Erie region. *Am. J. Enol. Vitic.* **2014**, *66*, 22–29. [CrossRef]
170. Molitor, D.; Behr, M.; Fischer, S.; Hoffmann, L.; Evers, D. Timing of cluster-zone leaf removal and its impact on canopy morphology, cluster structure and bunch rot susceptibility of grapes. *J. Int. Des. Sci. Vigne Vin.* **2011**, *45*, 149–159. [CrossRef]
171. Basile, B.; Caccavello, G.; Giaccone, M.; Forlani, M. Effects of early shading and defoliation on bunch compactness, yield components, and berry composition of aglianico grapevines under warm climate conditions. *Am. J. Enol. Vitic.* **2015**, *66*, 234–243. [CrossRef]
172. Bedrech, S.A.; Farag, S.G. Usage of some sunscreens to protect the Thompson Seedless and Crimson Seedless grapevines growing in hot. *Nat. Sci.* **2015**, *13*, 35–41.
173. Glenn, D.M.; Erez, A.; Puterka, G.J.; Gundrum, P. Particle films affect carbon assimilation and yield in 'Empire' Apple. *J. Am. Soc. Hortic Sci.* **2003**, *128*, 356–362. [CrossRef]
174. Dinis, L.T.; Bernardo, S.; Conde, A.; Pimentel, D.; Ferreira, H.; Felix, L.; Geros, H.; Correia, C.M.; Moutinho-Pereira, J. Kaolin exogenous application boosts antioxidant capacity and phenolic content in berries and leaves of grapevine under summer stress. *J. Plant Physiol.* **2016**, *191*, 45–53. [CrossRef]
175. Bernardo, S.; Dinis, L.T.; Luzio, A.; Pinto, G.; Meijon, M.; Valledor, L.; Conde, A.; Geros, H.; Correia, C.M.; Moutinho-Pereira, J. Kaolin particle film application lowers oxidative damage and DNA methylation on grapevine (Vitis vinifera L.). *Environ. Exp. Bot.* **2017**, *139*, 39–47. [CrossRef]
176. Dinis, L.T.; Bernardo, S.; Luzio, A.; Pinto, G.; Meijon, M.; Pinto-Marijuan, M.; Cotado, A.; Correia, C.; Moutinho-Pereira, J. Kaolin modulates ABA and IAA dynamics and physiology of grapevine under Mediterranean summer stress. *J. Plant Physiol.* **2018**, *220*, 181–192. [CrossRef] [PubMed]

177. Conde, A.; Neves, A.; Breia, R.; Pimentel, D.; Dinis, L.T.; Bernardo, S.; Correia, C.M.; Cunha, A.; Geros, H.; Moutinho-Pereira, J. Kaolin particle film application stimulates photoassimilate synthesis and modifies the primary metabolome of grape leaves. *J. Plant Physiol.* **2018**, *223*, 47–56. [CrossRef] [PubMed]
178. Mole, W. *Gods, Men and Wine*; Wine & Food Society: London, UK, 1966; p. 516.
179. Ferreira, M.I.; Silvestre, J.; Conceicao, N.; Malheiro, A.C. Crop and stress coefficients in rainfed and deficit irrigation vineyards using sap flow techniques. *Irrig. Sci.* **2012**, *30*, 433–447. [CrossRef]
180. Peacock, W.L.; Rolston, D.E.; Aljibury, F.K.; Rauschkolb, R.S. Evaluating drip, flood, and sprinkler irrigation of wine grapes. *Am. J. Enol. Vitic.* **1977**, *28*, 193–195.
181. Sauer, T.; Havlík, P.; Schneider, U.A.; Schmid, E.; Kindermann, G.; Obersteiner, M. Agriculture and resource availability in a changing world: The role of irrigation. *Water Resour. Res.* **2010**, *46*. [CrossRef]
182. Goldammer, T. *Grape Grower's Handbook—A Guide to Viticulture for Wine Production*; APEX Publishers: Centreville, VA, USA, 2015; p. 713.
183. Flexas, J.; Galmes, J.; Galle, A.; Gulias, J.; Pou, A.; Ribas-Carbo, M.; Tomas, M.; Medrano, H. Improving water use efficiency in grapevines: Potential physiological targets for biotechnological improvement. *Aust. J. Grape Wine Res.* **2010**, *16*, 106–121. [CrossRef]
184. Koech, R.; Langat, P. Improving irrigation water use efficiency: A review of advances, challenges and opportunities in the Australian context. *Water* **2018**, *10*, 1771. [CrossRef]
185. Allen, R.G.; Pereira, L.S.; Raes, D.; Smith, M. *Crop Evapotranspiration: Guidelines for Computing Crop Water Requirements*; FAO: Rome, Italy, 1998; Volume 56.
186. Blanco-Cipollone, F.; Lourenco, S.; Silvestre, J.; Conceicao, N.; Monino, M.J.; Vivas, A.; Ferreira, M.I. Plant water status indicators for irrigation scheduling associated with iso- and anisohydric behavior: Vine and plum trees. *Horticulturae* **2017**, *3*, 47. [CrossRef]
187. Fernandez, J.E. Plant-based methods for irrigation scheduling of woody crops. *Horticulturae* **2017**, *3*, 35. [CrossRef]
188. Malheiro, A.C.; Goncalves, I.N.; Fernandes-Silva, A.A.; Silvestre, J.C.; Conceicao, N.S.; Paco, T.A.; Ferreira, M.I. Relationships between relative transpiration of grapevines and plant and soil water status in Portugal's Douro Wine Region. In Proceedings of the Xxviii International Horticultural Congress on Science and Horticulture for People (Ihc2010): International Symposium on Climwater 2010: Horticultural Use of Water in a Changing Climate, Lisbon, Portugal, 22–27 August 2010; Volume 922, pp. 261–267.
189. Montoro, A.; Fereres, E.; Lopez-Urrea, R.; Manas, F.; Lopez-Fuster, P. Sensitivity of trunk diameter fluctuations in Vitis vinifera L. Tempranillo and Cabernet Sauvignon cultivars. *Am. J. Enol. Vitic.* **2012**, *63*, 85–93. [CrossRef]
190. Miras-Avalos, J.M.; Fandino, M.; Trigo-Cordoba, E.; Martinez, E.M.; Moutinho-Pereira, J.; Correia, C.M.; Dinis, L.T.; Rey, B.J.; Malheiro, A.C.; Cancela, J.J. Effects of surface and subsurface drip irrigation on physiology and yield of 'Godello' grapevines grown in Galicia, NW Spain. *Cienc. Tec. Vitivinic.* **2017**, *32*, 42–52. [CrossRef]
191. Bindon, K.; Dry, P.; Loveys, B. Influence of partial rootzone drying on the composition and accumulation of anthocyanins in grape berries (Vitis vinifera cv. Cabernet Sauvignon). *Aust. J. Grape Wine Res.* **2008**, *14*, 91–103. [CrossRef]
192. Du, T.S.; Kang, S.Z.; Zhang, J.H.; Li, F.S.; Yan, B.Y. Water use efficiency and fruit quality of table grape under alternate partial root-zone drip irrigation. *Agric. Water Manag.* **2008**, *95*, 659–668. [CrossRef]
193. Poni, S.; Bernizzoni, F.; Civardi, S. Response of "Sangiovese"' grapevines to partial root-zone drying: Gas-exchange, growth and grape composition. *Sci. Hortic Amst.* **2007**, *114*, 96–103. [CrossRef]
194. Garcia, J.G.; Martinez-Cutillas, A.; Romero, P. Financial analysis of wine grape production using regulated deficit irrigation and partial-root zone drying strategies. *Irrig. Sci.* **2012**, *30*, 179–188. [CrossRef]
195. Harmanny, K.S.; Malek, Z. Adaptations in irrigated agriculture in the Mediterranean region: An overview and spatial analysis of implemented strategies. *Reg. Environ. Chang.* **2019**, *19*, 1401–1416. [CrossRef]
196. Butt, T.M.; Copping, L.G. Fungal biological control agents. *Pestic. Outlook* **2000**, *11*, 186–191. [CrossRef]
197. Deutsch, C.A.; Tewksbury, J.J.; Tigchelaar, M.; Battisti, D.S.; Merrill, S.C.; Huey, R.B.; Naylor, R.L. Increase in crop losses to insect pests in a warming climate. *Science* **2018**, *361*, 916–919. [CrossRef]
198. Dam, D.; Molitor, D.; Beyer, M. Natural compounds for controlling Drosophila suzukii. A review. *Agron. Sustain. Dev.* **2019**, *39*. [CrossRef]

199. Bahar, E.; Yasasin, A.S. The yield and berry quality under different soil tillage and clusters thinning treatments in grape (Vitis vinifera L.) cv. Cabernet-Sauvignon. *Afr. J. Agric. Res.* **2010**, *5*, 2986–2993.
200. Gomez, J.A.; Gema Guzman, M.; Giraldez, J.V.; Fereres, E. The influence of cover crops and tillage on water and sediment yield, and on nutrient, and organic matter losses in an olive orchard on a sandy loam soil. *Soil Tillage Res.* **2009**, *106*, 137–144. [CrossRef]
201. Gomez, J.A.; Giraldez, J.V.; Pastor, M.; Fereres, E. Effects of tillage method on soil physical properties, infiltration and yield in an olive orchard. *Soil Tillage Res.* **1999**, *52*, 167–175. [CrossRef]
202. Molitor, D.; Baron, N.; Sauerwein, T.; André, C.M.; Kicherer, A.; Döring, J.; Stoll, M.; Beyer, M.; Hoffmann, L.; Evers, D. Postponing first shoot topping reduces grape cluster compactness and delays bunch rot epidemic. *Am. J. Enol. Vitic.* **2015**, *66*, 164–176. [CrossRef]
203. Tello, J.; Ibanez, J. What do we know about grapevine bunch compactness? A state-of-the-art review. *Aust. J. Grape Wine Res.* **2017**. [CrossRef]
204. Judit, G.; Gabor, Z.; Adam, D.; Tamas, V.; Gyorgy, B. Comparison of three soil management methods in the Tokaj wine region. *Mitt Klosterneubg.* **2011**, *61*, 187–195.
205. Fraga, H.; Santos, J.A. Vineyard mulching as a climate change adaptation measure: Future simulations for Alentejo, Portugal. *Agric. Syst.* **2018**, *164*, 107–115. [CrossRef]
206. Uliarte, E.M.; Schultz, H.R.; Frings, C.; Pfister, M.; Parera, C.A.; del Monte, R.F. Seasonal dynamics of CO2 balance and water consumption of C-3 and C-4-type cover crops compared to bare soil in a suitability study for their use in vineyards in Germany and Argentina. *Agric. For. Meteorol.* **2013**, *181*, 1–16. [CrossRef]
207. Xi, Z.M.; Zhang, Z.W.; Cheng, Y.F.; Li, H. The effect of vineyard cover crop on main monomeric phenols of grape berry and wine in Vitis viniferal L. cv. Cabernet Sauvignon. *Agric. Sci. China* **2010**, *9*, 440–448. [CrossRef]
208. Unger, P.W.; Vigil, M.F. Cover crop effects on soil water relationships. *J. Soil Water Conserv.* **1998**, *53*, 200–207.
209. Garcia, L.; Celette, F.; Gary, C.; Ripoche, A.; Valdes-Gomez, H.; Metay, A. Management of service crops for the provision of ecosystem services in vineyards: A review. *Agric. Ecosyst. Environ.* **2018**, *251*, 158–170. [CrossRef]
210. Van Leeuwen, C.; Schultz, H.R.; de Cortazar-Atauri, I.G.; Duchene, E.; Ollat, N.; Bios, B.; Goutouly, J.-P.; Quenol, H.; Touzard, J.-M.; Malheiro, A.C.; et al. Why climate change will not dramatically decrease viticultural suitability in main wine-producing areas by 2015. *Proc. Natl. Acad. Sci. USA* **2013**, *110*, E3051–E3052. [CrossRef] [PubMed]
211. Pieri, P.; Gaudillere, J.P. Sensitivity to training system parameters and soil surface albedo of solar radiation intercepted by vine rows. *Vitis* **2003**, *42*, 77–82.
212. Molitor, D.; Schultz, M.; Mannes, R.; Pallez-Barthel, M.; Hoffmann, L.; Beyer, M. Semi-minimal pruned hedge: A potential climate change adaptation strategy in viticulture. *Agronomy* **2019**, *9*, 173. [CrossRef]
213. Grifoni, D.; Carreras, G.; Zipoli, G.; Sabatini, F.; Dalla Marta, A.; Orlandini, S. Row orientation effect on UV-B, UV-A and PAR solar irradiation components in vineyards at Tuscany, Italy. *Int. J. Biometeorol.* **2008**, *52*, 755–763. [CrossRef]
214. Intrieri, C.; Poni, S.; Rebucci, B.; Magnanini, E. *Row Orientation Effects on Whole-Canopy Gas Exchange of Potted and Field-Grown Grapevines*; JKI: Siebeldingen, Germany, 1998; Volume 37.
215. Smart, R.; Robinson, M. *Sunlight into Wine. A Handbook for Winegrape Canopy Management*; Winetitles: Adelaide, Australia, 1991.
216. Friedel, M.; Stoll, M.; Patz, C.D.; Will, F.; Dietrich, H. Impact of light exposure on fruit composition of white 'Riesling' grape berries (*Vitis vinifera* L.). *Vitis* **2015**, *54*, 107–116.
217. Morales-Castilla, I.; García de Cortázar-Atauri, I.; Cook, B.I.; Lacombe, T.; Parker, A.; van Leeuwen, C.; Nicholas, K.A.; Wolkovich, E.M. Diversity buffers winegrowing regions from climate change losses. *Proc. Natl. Acad. Sci. USA* **2020**. [CrossRef]
218. Duchene, E.; Butterlin, G.; Dumas, V.; Merdinoglu, D. Towards the adaptation of grapevine varieties to climate change: QTLs and candidate genes for developmental stages. *Appl. Genet.* **2012**, *124*, 623–635. [CrossRef]
219. Wolkovich, E.M.; de Cortazar-Atauri, I.G.; Morales-Castilla, I.; Nicholas, K.A.; Lacombe, T. From Pinot to Xinomavro in the world's future wine-growing regions. *Nat. Clim. Chang.* **2018**, *8*, 29–37. [CrossRef]
220. Tello, J.; Cordero-Bueso, G.; Aporta, I.; Cabellos, J.M.; Arroyo, T. Genetic diversity in commercial wineries: Effects of the farming system and vinification management on wine yeasts. *J. Appl. Microbiol.* **2012**, *112*, 302–315. [CrossRef]

221. Ollat, N.; Bordenave, L.; Tandonnet, J.P.; Boursiquot, J.M.; Marguerit, E. Grapevine rootstocks: Origins and perspectives. *Acta Hortic.* **2016**, 11–22. [CrossRef]
222. Hedberg, P.R.; Mcleod, R.; Cullis, B.; Freeman, B.M. Effect of rootstock on the production, grape and wine quality of Shiraz vines in the Murrumbidgee irrigation area. *Aust. J. Exp. Agric.* **1986**, *26*, 511–516. [CrossRef]
223. Pavlousek, P. Evaluation of drought tolerance of new grapevine rootstock hybrids. *J. Environ. Biol. Acad. Environ. Biol. India* **2011**, *32*, 543–549.
224. Harbertson, J.F.; Keller, M. Rootstock effects on deficit-irrigated winegrapes in a dry climate: Grape and wine composition. *Am. J. Enol. Vitic.* **2012**, *63*, 40–48. [CrossRef]
225. Ozden, M.; Vardin, H.; Simsek, M.; Karaaslan, M. Effects of rootstocks and irrigation levels on grape quality of Vitis vinifera L. cv. Shiraz. *Afr. J. Biotechnol.* **2010**, *9*, 3801–3807.
226. Koundouras, S.; Tsialtas, I.T.; Zioziou, E.; Nikolaou, N. Rootstock effects on the adaptive strategies of grapevine (Vitis vinifera L. cv. Cabernet-Sauvignon) under contrasting water status: Leaf physiological and structural responses. *Agric. Ecosyst. Environ.* **2008**, *128*, 86–96. [CrossRef]
227. EC. C.R. Establishing a Common Organisation of Agricultural Markets and on Specific Provisions for Certain Agricultural Products (Single CMO Regulation). 2009. Available online: https://eur-lex.europa.eu/eli/reg/2009/491/oj (accessed on 21 April 2020).
228. Lloreda, M.D. Use of hybrids in viticulture. A challenge for the OIV. *OENO One* **2018**, *52*, 231–234. [CrossRef]
229. Moriondo, M.; Jones, G.V.; Bois, B.; Dibari, C.; Ferrise, R.; Trombi, G.; Bindi, M. Projected shifts of wine regions in response to climate change. *Clim. Chang.* **2013**, *119*, 825–839. [CrossRef]
230. Karvonen, J.I. Northern european viticulture compared to Central European high altitude viticulture: Annual growth cycle of grapevines in the years 2012–2013. *Int. J. Wine Res.* **2014**, *6*, 1–7. [CrossRef]
231. Egarter Vigl, L.; Schmid, A.; Moser, F.; Balotti, A.; Gartner, E.; Hatz, H.; Quendler, S.; Ventura, S.; Raifer, B. Upward shifts in elevation—A winning strategy for mountain viticulture in the context of climate change? In Proceedings of the XIIth International Terroir Congress, Zaragoza, Spain, 18–22 June 2018.
232. Moriondo, M.; Bindi, M.; Fagarazzi, C.; Ferrise, R.; Trombi, G. Framework for high-resolution climate change impact assessment on grapevines at a regional scale. *Reg. Environ.. Chang.* **2011**, *11*, 553–567. [CrossRef]
233. Zhu, X.Q.; Moriondo, M.; van Ierland, E.C.; Trombi, G.; Bindi, M. A model-based assessment of adaptation options for Chianti wine production in Tuscany (Italy) under climate change. *Reg. Environ. Chang.* **2016**, *16*, 85–96. [CrossRef]
234. Dunn, M.R.; Lindesay, J.A.; Howden, M. Spatial and temporal scales of future climate information for climate change adaptation in viticulture: A case study of User needs in the Australian winegrape sector. *Aust. J. Grape Wine Res.* **2015**, *21*, 226–239. [CrossRef]
235. Moriondo, M.; Ferrise, R.; Trombi, G.; Brilli, L.; Dibari, C.; Bindi, M. Modelling olive trees and grapevines in a changing climate. *Environ. Model. Softw.* **2015**, *72*, 387–401. [CrossRef]
236. Bindi, M.; Fibbi, L.; Miglietta, F. Free Air CO2 Enrichment (FACE) of grapevine (Vitis vinifera L.): II. Growth and quality of grape and wine in response to elevated CO2 concentrations. *Eur. J. Agron.* **2001**, *14*, 145–155. [CrossRef]
237. Caubel, J.; Launay, M.; Garcia de Cortazar-Atauri, I.; Ripoche, D.; Huard, F.; Buis, S.; Brisson, N. A new integrated approach to assess the impacts of climate change on grapevine fungal diseases: The coupled MILA-STICS model. *J. Int. Sci. Vigne Vin.* **2014**, *48*, 45–54.
238. Nendel, C.; Kersebaum, K.C. A simple model approach to simulate nitrogen dynamics in vineyard soils. *Ecol. Model.* **2004**, *177*, 1–15. [CrossRef]
239. Valdes-Gomez, H.; Celette, F.; de Cortazar-Atauri, I.G.; Jara-Rojas, F.; Ortega-Farias, S.; Gary, C. Modelling soil water content and grapevine growth and development with the Stics Crop-Soil Model under two different water management strategies. *J. Int. Des. Sci. Vigne Vin.* **2009**, *43*, 13–28. [CrossRef]
240. Lereboullet, A.L.; Beltrando, G.; Bardsley, D.K. Socio-ecological adaptation to climate change: A comparative case study from the Mediterranean wine industry in France and Australia. *Agric. Ecosyst. Environ.* **2013**, *164*, 273–285. [CrossRef]


applied sciences

MDPI

*Article*

# What Is the Impact of Heatwaves on European Viticulture? A Modelling Assessment

**Helder Fraga [1,*], Daniel Molitor [2], Luisa Leolini [3] and João A. Santos [1,*]**

[1] Centre for the Research and Technology of Agro-Environmental and Biological Sciences, CITAB, Universidade de Trás-os-Montes e Alto Douro, UTAD, 5000-801 Vila Real, Portugal

[2] Luxembourg Institute of Science and Technology (LIST), Environmental Research and Innovation (ERIN) Department, 41, rue du Brill, L-4422 Belvaux, Luxembourg; daniel.molitor@list.lu

[3] Department of Agriculture, Food, Environment and Forestry (DAGRI), University of Florence, Piazzale delle Cascine 18, 50144 Florence, Italy; luisa.leolini@unifi.it

* Correspondence: hfraga@utad.pt (H.F.); jsantos@utad.pt (J.A.S.)

Received: 7 April 2020; Accepted: 24 April 2020; Published: 26 April 2020

**Abstract:** Extreme heat events or heatwaves can be particularly harmful to grapevines, posing a major challenge to winegrowers in Europe. The present study is focused on the application of the crop model STICS to assess the potential impacts of heatwaves over some of the most renowned winemaking regions in Europe. For this purpose, STICS was applied to grapevines, using high-resolution weather, soil and terrain datasets from 1986 to 2015. To assess the impact of heatwaves, the weather dataset was artificially modified, generating periods with anomalously high temperatures (+5 °C), at specific onset dates and with specific episode durations (from five to nine days). The model was then run with this modified weather dataset, and the results were compared to the original unmodified runs. The results show that heatwaves can have a very strong impact on grapevine yields. However, these impacts strongly depend on the onset dates and duration of the heatwaves. The highest negative impacts may result in a decrease in the yield by up to −35% in some regions. The results show that regions with a peak vulnerability on 1 August will be more negatively impacted than other regions. Furthermore, the geographical representation of yield reduction hints at a latitudinal gradient in the heatwave impact, indicating stronger reductions in the cooler regions of Central Europe than in the warmer regions of Southern Europe. Despite some uncertainties inherent to the current modelling assessment, the present study highlights the negative impacts of heatwaves on viticultural yields in Europe, which is critical information for stakeholders within the winemaking sector for planning suitable adaptation measures.

**Keywords:** heatwaves; viticulture; vineyards; Europe; climate change; yield; pinot noir

## 1. Introduction

Most of the renowned wine regions in Europe (Figure 1) are characterized by warm temperate climates, namely Mediterranean, oceanic or humid continental [1]. These regions are expected to have pronounced climate change impacts, particularly due to extreme events, such as droughts and extreme heat [2]. Hence, it becomes clear that viticulture is exposed and vulnerable to the change in climatic conditions [3,4], particularly in Southern Europe [5]. Given these threats and their impacts on the vulnerability of grapevine in a warmer world, it is imperative to understand how climate change and extreme events can influence this economically valuable crop in Europe.

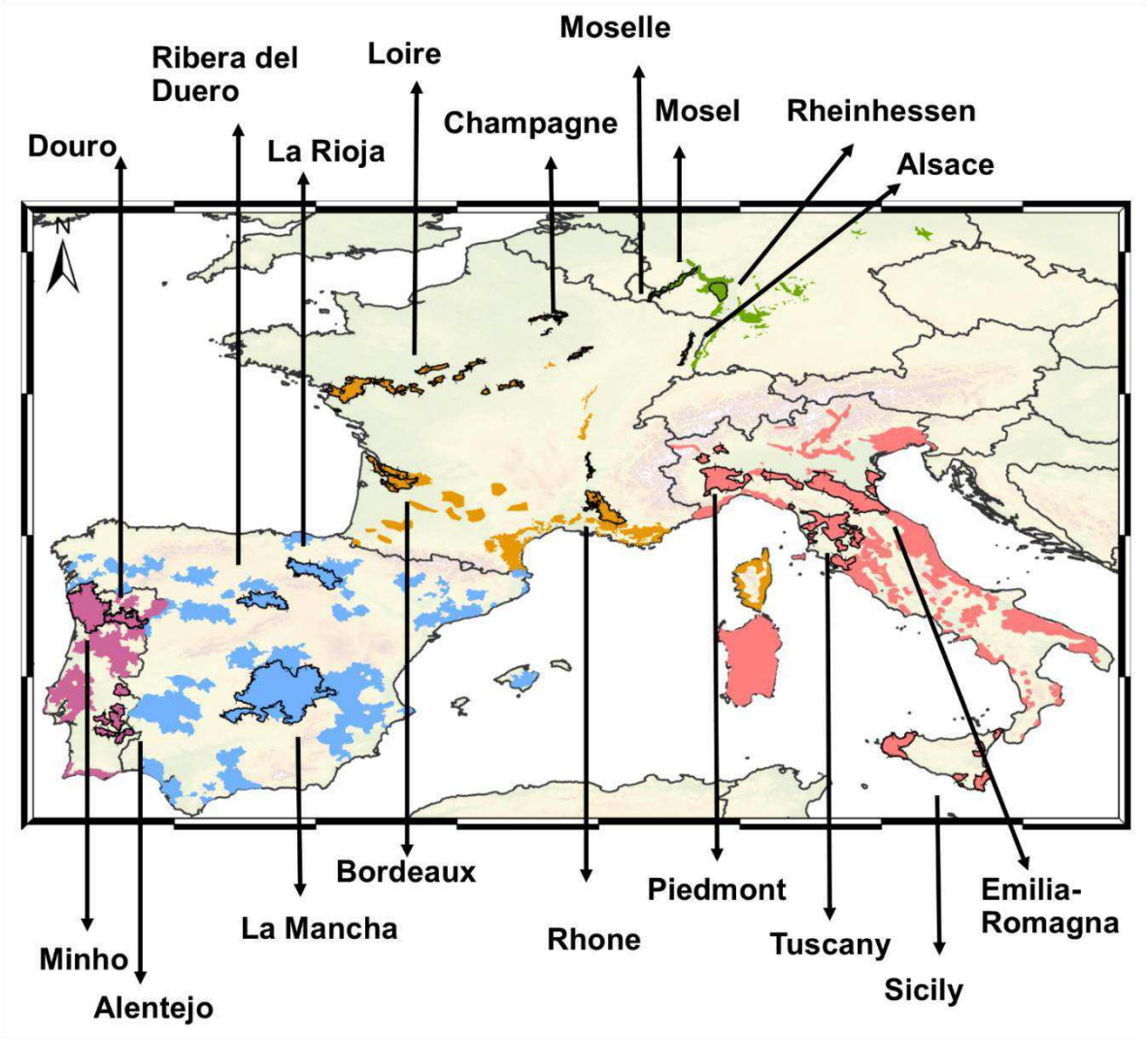


**Figure 1.** Selected wine regions in Europe (18), highlighted by a black line contour, and their corresponding designations. Other wine regions are also outlined, with different color shadings for different countries.

Temperature is a key factor affecting plant growth and development rates [6]. For grapevines, air temperature is considered to be a fundamental factor controlling the main physiological processes, phenological timings and overall productivity and quality [7]. Although other atmospheric variables, such as precipitation, humidity and solar radiation, also play an important role in grapevine development, temperature is considered to be the main factor. In effect, grapevine physiology and fruit metabolism/composition are highly influenced by the thermal conditions during the growing season [8]. For adequate grapevine growth, phenological development and yield attributes [9], there are indeed optimum temperature ranges and thermal thresholds, establishing both lower and upper limits, which are, however, variety-dependent. One of the most well-known climatic requirements of the grapevine is the 10 °C base temperature for heat accumulation, which is needed for the onset of its vegetative cycle [10–15]. Over the last decades, most research was aimed at the lower thermal limits for heat accumulation, which has traditionally been a major concern for winegrowers. Nonetheless, the effect of high temperatures on grape physiology is likely to become more important in the future, due to global warming [15]. Hence, a better analysis of the upper thermal limits for grape development and physiology is of foremost relevance.

It is known that if air temperature exceeds a given upper threshold (e.g., 35 °C) at certain critical periods of grapevine development, negative impacts on grapevine should be expected [16]. In effect, extreme heat can be particularly harmful to grapevines. Grapevines growing under severe heat stress

experience a significant decline in productivity, e.g., due to limitations in photosynthesis [17], as well as injures under other physiological processes [18]. As an example, a study carried out by Matsui et al. [19] concluded that the exposure of Thompson Seedless and Napa Gamay to 40 °C for six consecutive days reduced berry size, as well as sugar accumulation, and delayed ripening. Other studies, for other grapevine varieties exposed to severe heat, showed similar results [20,21]. Furthermore, several physiological processes, such as photosynthesis, are either severely reduced or inhibited at high temperatures (~35 °C), mostly owing to stomatal closure [16,22,23].

The World Meteorological Organization (WMO) defines a heatwave as a weather extreme episode with "5 or more consecutive days of prolonged heat in which the daily maximum temperature is higher than the average maximum temperature by 5 °C or more". Due to climate change, extreme weather events are projected to increase in frequency, duration and intensity [24]. Combined with the increase in mean temperature projected to occur in the future, heatwaves can indeed be seen as a major challenge that winegrowers will have to deal with in the upcoming decades. As an illustration, the 2003 heatwave in Europe highlighted the potential impact of heatwaves on viticulture [25], particularly during harvest [26]. This record-breaking heatwave in Europe may be seen as a demonstrative extreme event that is expected to occur more frequently under enhanced atmospheric greenhouse gas concentrations and anthropogenic radiative forcing [26,27]. More recently, in 2019, there were three consecutive heatwave events in Europe (in June, July and August), with temperatures reaching 44 °C in some regions during June. Given the risk that heatwaves pose to viticulture and winemaking, a better assessment of the effects of these events on this sector is thereby of the utmost importance.

Crop models can be a valuable tool in assessing the impact of heatwaves on viticulture [28]. These models mechanistically simulate plant development while incorporating weather, soil properties, plant data and management decisions [29]. The simulation of crop parameters, such as yields, under different pedoclimatic conditions, and abiotic stresses, are main outcomes from these models. One of their strongest advantages is the fact that they have already been applied and validated with field measurements, thus reducing the need to provide extensive experimental trials, when properly calibrated and validated. Hence, coupling dynamic (process-based) crop models with high-resolution climate, soil and plant data allows reliable yield simulations over a wide region to be produced. Despite the aforementioned advantages of these models, to our knowledge, their application to understanding the impact of heatwaves on viticulture has not been conducted yet [30].

The present study aims at analyzing the impacts of heatwaves on European viticulture, particularly on grapevine yield. As such, the objectives of the present study are fourfold: (1) to simulate recent-past yields over several main European winemaking regions, using a state-of-the-art crop model for simulating grapevines, forced by observed climate conditions over a past baseline period (control runs); (2) to carry out a sensitivity analysis to heatwaves, applying synthetic heatwave disturbances (heatwave runs); (3) to compute the regional yield differences between control and heatwave runs; and (4) to discuss potential adaptation measures to be implemented by viticulturists and winemakers, to cope with upcoming heatwaves in the near future.

## 2. Materials and Methods

### *2.1. Vineyard Locations*

The study sites were selected by considering some of the main winegrowing regions in Europe. These regions were selected based on their importance for the current viticultural sector, though not exhaustively. While many other regions in Europe can be considered to be top winemaking regions, they are out of the focus of the current study. The following regions were considered herein (from west to east; Figure 1): Minho, Douro and Alentejo (Portugal); Ribera del Duero, La Rioja and La Mancha (Spain); Bordeaux, Loire Valley, Champagne, Rhone and Alsace (France); Moselle (Luxembourg); Mosel and Rheinhessen (Germany); Piedmont, Tuscany, Sicily and Emilia-Romagna (Italy). All these winemaking regions present temperate climate characteristics [1], despite local and regional specificities. Regarding the annual mean temperatures, these regions typically range from

10 to 17 °C (Table 1), being the coldest regions in the Mosel/Moselle area, in both Germany and Luxembourg, closely followed by Champagne (Northern France), while the warmest is Alentejo (Southern Portugal), followed by Sicily (Southern Italy) and La Mancha (inner Southern Spain). Regarding annual precipitation totals, it roughly varies from 400 to 1000 mm, with Piedmont (Northwestern Italy), Minho (Northwestern Portugal) and Emilia-Romagna (Northern Italy) being the wettest regions, whereas Ribera del Duero (inner Northern Spain), La Mancha and Sicily are the driest regions.

**Table 1.** Targeted winemaking regions (18 in total), with country and region designation, along with their centroid longitude and latitude, and area-means of annual mean temperature (T) and precipitation sum (P), calculated from the E-OBS dataset, version 19.0e, over the baseline period of 1986–2015. The three highest and lowest values are highlighted in bold.

| COUNTRY | REGION | LON (°) | LAT (°) | T (°C) | P (mm) |
|---|---|---|---|---|---|
| **France** | Alsace | 7.38 | 48.20 | 10.6 | 605 |
| | Bordeaux | 0.55 | 44.50 | 13.2 | 807 |
| | Champagne | 4.00 | 49.16 | **10.5** | 664 |
| | Loire Valley | 0.13 | 47.12 | 12.3 | 684 |
| | Rhone | 4.83 | 44.06 | **14.7** | 733 |
| **Germany** | Mosel | 6.87 | 49.28 | **10.4** | 766 |
| | Rheinhessen | 8.13 | 49.92 | 10.6 | 579 |
| **Italy** | Emilia-Romagna | 10.93 | 44.50 | 13.1 | **840** |
| | Piedmont | 8.67 | 44.66 | 13.3 | **988** |
| | Sicily | 13.99 | 37.64 | **15.9** | 482 |
| | Tuscany | 11.77 | 43.08 | 13.6 | 723 |
| **Luxembourg** | Moselle | 6.35 | 49.55 | **10.3** | 743 |
| **Portugal** | Alentejo | −7.56 | 38.38 | **17.2** | 562 |
| | Douro | −7.55 | 41.17 | 13.3 | 830 |
| | Minho | −8.41 | 41.82 | 14.1 | **956** |
| **Spain** | La Mancha | −2.69 | 39.65 | 14.2 | **455** |
| | La Rioja | −2.40 | 41.57 | 11.5 | 523 |
| | Ribera del Duero | −4.36 | 41.63 | 12.3 | **423** |

### *2.2. Crop Model Description*

The STICS (*Simulateur mulTIdisciplinaire pour les Cultures Standard*) crop model, version 121, was used herein to simulate grapevine yields [31]. This model is currently one of the few crop models that incorporates the necessary parameterizations for perennial crops and, more specifically, for grapevine simulations [32–34]. In a study by Fraga et al. [35], the STICS model was used to simulate yield, phenology and abiotic (water) stress conditions throughout Europe, showing a high agreement with observational data [35,36]. Subsequently, this model was used in assessing the potential impacts of climate change on viticulture and the effectiveness of different adaptation strategies, like irrigation or mulching [37,38]. The current study follows the same guidelines and parameterizations as in Fraga, et al. [35].

Regarding the model runs, the model operates on a daily time-step, simulating grapevine growth driven by daily weather data. Grapevine budburst is simulated by using the BRIN model [39], whereas flowering and veraison are simulated by using growing degree-days, with a base temperature of 10 °C. To simulate biomass growth, nitrogen and carbon reserves are considered, also taking into account competition between vegetative and generative organs. $CO_2$ effects on plant physiology and radiation use efficiency are also simulated [31]. Fruit growth is described by the dynamics of dry-matter accumulation and water content [40]. Temperature thresholds (i.e., frost and heat shock) are also taken into consideration for growth and development, which is critical for the objectives of the present study.

### *2.3. Input Data*

The model requires a large range of input data, such as daily weather data, typical soil properties, topographic features, varietal characteristics and crop management information. The required daily variables comprise daily maximum air temperature (Tmax), daily minimum air temperature (Tmin), daily accumulation of solar radiation (Rad), daily precipitation total (Prec), daily mean wind speed (Wspeed), daily mean relative humidity (Rh) and $CO_2$ level. These data were obtained from two different observational sources. Tmax, Tmin and Prec were obtained from the E-OBS dataset, version 19e [41], whilst Rad, WSpeed and Rh were retrieved from the ERA5 dataset [42]. These two datasets have been widely used and validated by many previous studies. Data were extracted at 0.1° latitude–longitude regular grids (spatial resolution of approximately 10 km) for the baseline period of 1986–2015.

Soil data, like soil texture and pH, were obtained from the Harmonized World Soil Database HWSD and [43], available from two layers (depths 0–30 cm and 30–100 cm). Some soil properties for STICS were estimated by using pedotransfer functions [44], such as soil albedo, runoff, soil permeability, field capacity, wilting point and bulk density. Additionally, some soil properties were set as standard, following Brisson, et al. [31]: initial soil water content (set at field capacity); maximum unimpeded root depth (200 cm), initial root density (0.05 $cm \cdot cm^{-3}$) and soil organic N content (6% of dry soil). Terrain data, such as slope degree and orientation, were obtained from the GTOPO30 digital elevation model and using GIS techniques (https://lta.cr.usgs.gov/GTOPO30).

For a large-scale comprehensive modelling approach throughout Europe, some assumptions were made concerning cultivated varieties and cultural practices. As it will not be possible to analyze all the specific varieties grown at each location, which would also impede a comparative analysis among regions, a standard variety was considered for all locations. The selected variety was cv. Pinot noir, due to its early-to-intermediate ripening and moderate yields, being suitable for a large number of viticultural regions [45]. Pinot noir is currently the 10th most planted variety and the 7th fastest-expanding variety in the world [46]. Since it is grown in vineyards throughout Europe, from the warmer countries in Southern Europe to the cooler Central–Northern European wine regions [46], it was chosen herein. Furthermore, this variety was already validated in a previous study [35].

Cultural practices were kept invariant in the model runs, and crop interventions were set to a minimum (i.e., topping, thinning and leaf removal were not considered in the model). The default trellis system was Cordon, and vine density was set to 4000 vines ha-1, a reasonable value considering most commercial vineyards in Europe [47]. The technological harvest date was determined once the berry water content reached a maximum of 77%, corresponding to a probable alcohol level of 12.5 (%*v*/*v*) [40].

### *2.4. Model Runs*

The STICS model was initialized by using the abovementioned input variables. Two types of model runs were performed: control-runs vs. heatwave-runs. The control-run is based on observed conditions, using the observational unmodified weather data. Conversely, for the heatwave-runs, the observed weather conditions were modified, generating heatwave pulses at specific periods of the year and with specific durations (synthetic heatwave disturbances). Therefore, for each year, a heatwave pulse was added to the temperature time series by increasing the daily maximum temperature by 5 ºC with respect to the climatological maximum (following the WMO definition). This change in daily maximum temperature also impacts daily mean temperature. Regarding the onsets of the heatwaves, they were generated with a 15-day leap period, starting on July and ending in September: 1 and 15 July; 1 and 15 August; and 1 and 15 September. Therefore, the most vulnerable period of grapevine exposition to heatwaves is covered. The heatwave then lasted for a period ranging from 5 to 9 days (heatwave length/duration). Only one heatwave per year was considered. During the heatwave, the daily precipitation was set to 0 mm, which is typical during a heatwave. A comprehensive chart of these synthetic heatwaves is shown in Figure 2.

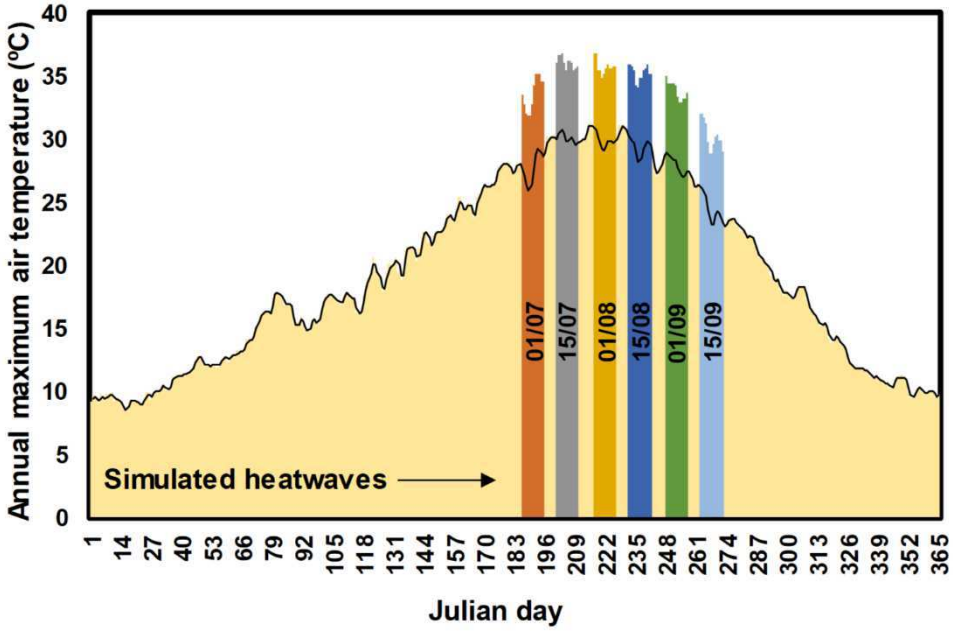


**Figure 2.** Illustrative representation of the synthetic heatwave disturbances/pulses during a calendar year, outlining their onset (dates within color bars), duration (color bar width) and intensity (color bar top). The observed temperature time series are represented by the background shaded graph, while the synthetic temperature time series of the heatwave disturbances are indicated at the top of each color bar.

STICS performance under the recent-past conditions has previously been evaluated and revealed good agreement with field data [35]. Thus, the remaining model parameterization followed the previous study [35]. Hence, model runs were carried out for each of the 18 regions, year (30 years; 1986–2015) and type of run (control vs. heatwave), corresponding to a total of 6480 simulations. In order to evaluate the potential impacts of heatwaves on grapevine yields, the heatwave-runs and the control-runs where compared. More specifically, the relative differences (%) in their corresponding yields were analyzed, thus disregarding absolute values and restraining the effects of some uncertainties in the STICS simulations. Nonetheless, it is important to state that the STICS model already showed a high agreement with statistical yields over Europe [35].

## 3. Results

Figure 3 shows the impacts of heatwaves on grapevine yields for each of the selected winemaking regions in Europe. Overall (Figure 3), for all regions, the occurrence of heatwaves will lead to a decrease in yields, with its magnitude increasing along with the heatwave duration. The main differences between these impacts are the maximum yield decrease and the corresponding dates of occurrence of the heatwave vulnerability (heatwave peak, henceforth). Starting with the westernmost regions, for Portugal (Figure 3a–c), all regions reveal a heatwave peak between 1 and 15 July. The region with the strongest decrease in Portugal is Minho, with −15% (five heatwave days) to −29% (nine heatwave days). Conversely, in the Portuguese region of Alentejo, the impacts will not be so pronounced (−12% to −17%). For Spain (Figure 3d–f), La Mancha also shows a peak between 1 and 15 July, while for Ribera del Duero and La Rioja, this peak is expected to occur slightly later, between 15 July and 1 August. Regarding the potential impacts on yield, they will be very similar across these three Spanish wine regions, ranging from −12% to −25%. For the French winemaking regions (Figure 3g–k), the strongest impacts will occur in the Loire Valley and Alsace, reaching −30%, while Rhone will be the region with the lowest negative impacts, with −25%. All regions will tend to show the heatwave peak for 15 July, except in Champagne, which will occur on 1 August. Owing to their geographical proximity, the Luxembourgish region of Moselle (Figure 3l) and the German region of Mosel (Figure 3m) show very similar impacts. Both regions show peak dates around 1

August and impacts from −15% to 30%. Similar results can be observed for Rheinhessen, also due to their fairly identical climatic conditions (Figure 3n). For the Italian regions (Figure 3o–r), the impacts vary from −15% and −27%. All regions will tend to have their peak dates from the 1 July to 15 July. It is worth noting that Emilia-Romagna (Figure 3q) depicts a comparatively narrow curve, which is very concentrated around the peak date.

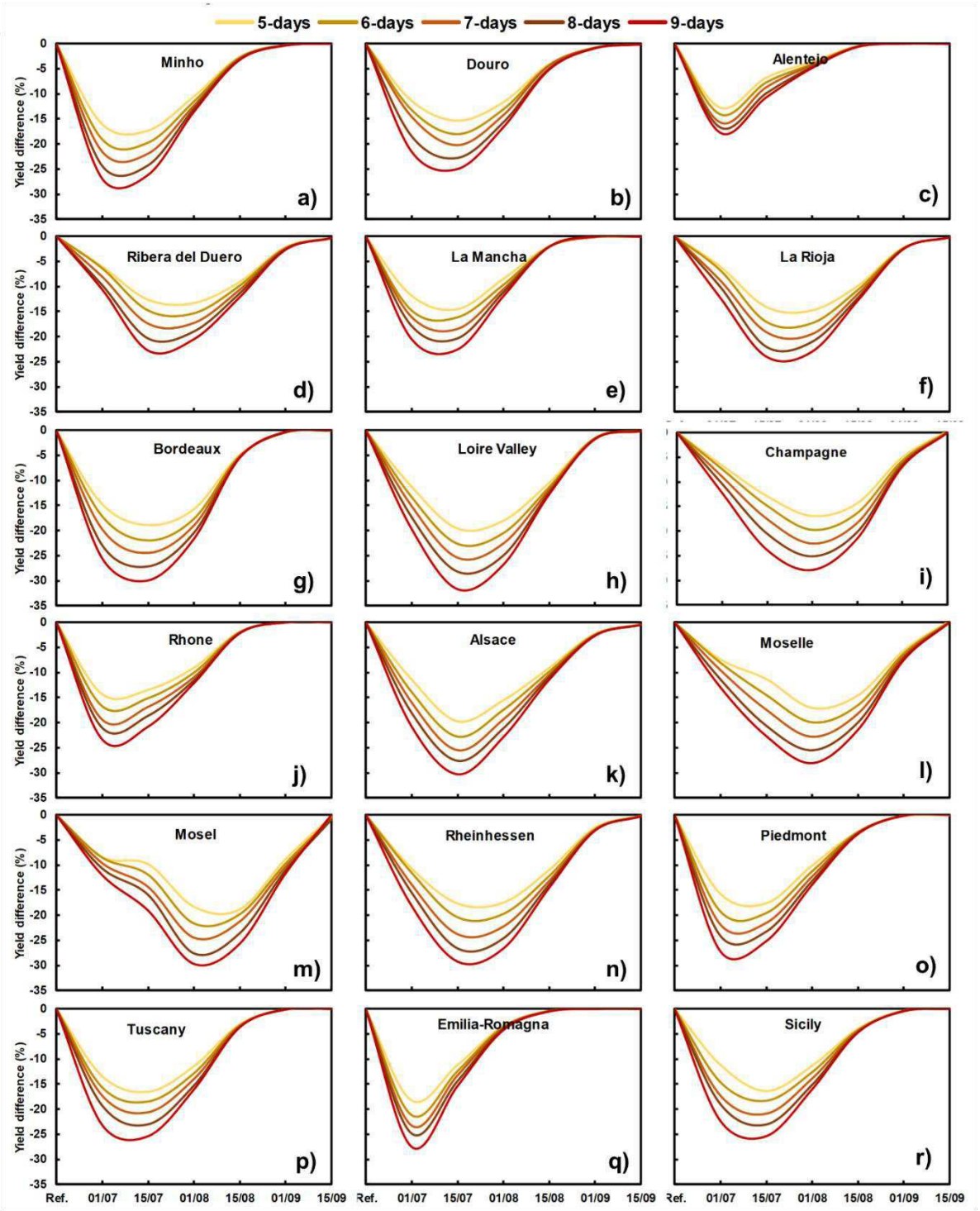


**Figure 3.** Yield relative difference (in %) between normal years and years with heatwaves, with a duration from five to nine days, in (**a**) Minho, (**b**) Douro, (**c**) Alentejo, (**d**) Ribera del Duero, (**e**) La Mancha, (**f**) La Rioja, (**g**) Bordeaux, (**h**) Loire Valley, (**i**) Champagne, (**j**) Rhone, (**k**) Alsace, (**l**) Moselle, (**m**) Mosel, (**n**) Rheinhessen, (**o**) Piedmont, (**p**) Tuscany, (**q**) Emilia-Romagna and (**r**) Sicily, depending on to the date of onset of the heatwave.

Figure 4 shows a comparison of the peak dates over the 18 selected winemaking regions in Europe. The heatwave peak dates occur before 1 August (inclusively) for all regions. Minho (Portugal), Alentejo (Portugal), Rhone (France), Piedmont and Emilia-Romagna (Italy) reveal stronger heatwaves earlier in the year than other regions. Conversely, La Rioja (Spain), Champagne (France), Moselle (Luxembourg) and Mosel (Germany) will experience stronger impacts when heatwaves occur later (1 August). It should be noted that the regions where the strongest impacts of the heatwaves tend to occur earlier/later are also the regions with the highest/lowest annual mean temperatures (warmer/cooler climates).

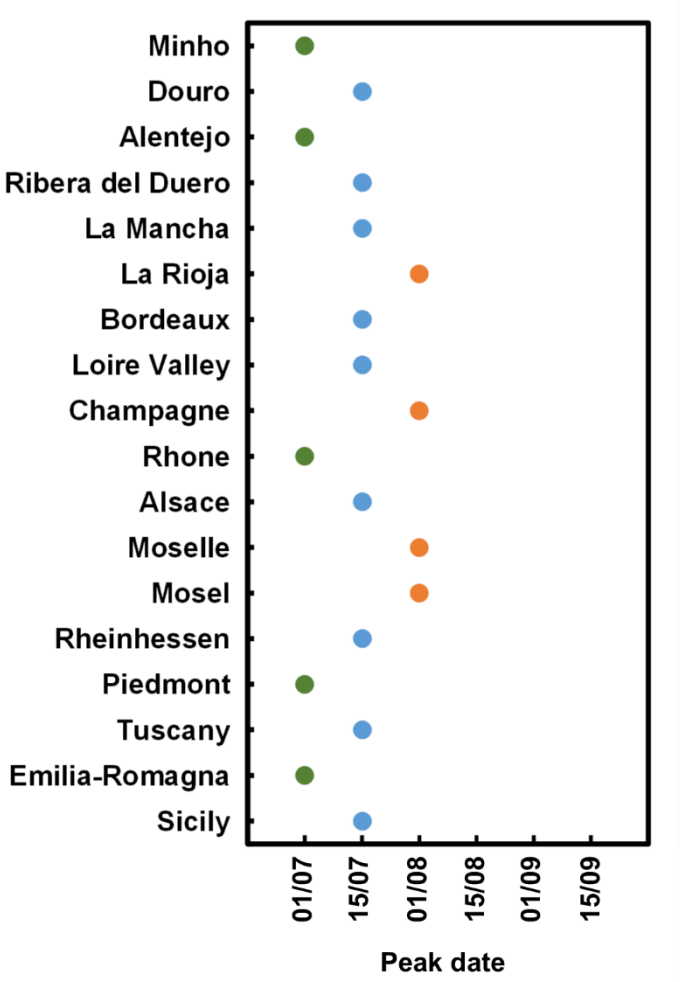


**Figure 4.** Comparison of the heatwave peak dates over the 18 selected winemaking regions in Europe. Different peak dates are represented by different colors.

Figure 5 provides a comparison across all regions of the highest and lowest decrease in yields at each peak date. This assessment was based on the heatwave peak date for each region. The results suggest that the most affected regions are the Loire Valley, Alsace and Bordeaux. These regions will undergo yield decreases from −30%/−35% (nine days of heatwaves) to −20% (five days of heatwaves). On the other hand, the least affected region is Alentejo, being the highest decrease of −20%. Figure 6 shows the average yield difference at each peak date for all the regions combined. Results show that the regions where the peak date occurs later (1 August) are more negatively affected than the regions where this peak occurs earlier.

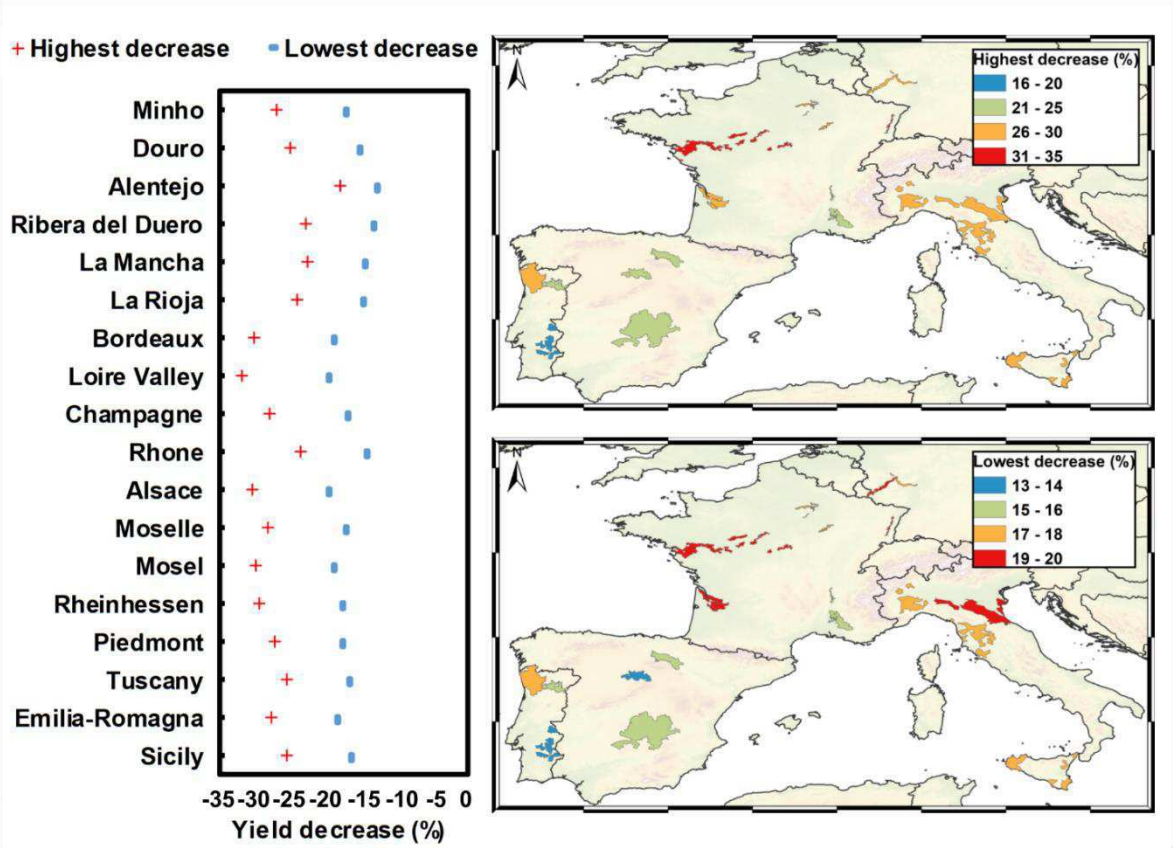


**Figure 5.** Left panel: highest and lowest yield decrease due to heatwaves for each winemaking region at the peak date. Right panel: geographical representation of the highest and lowest decrease in yields over Europe at the peak date.

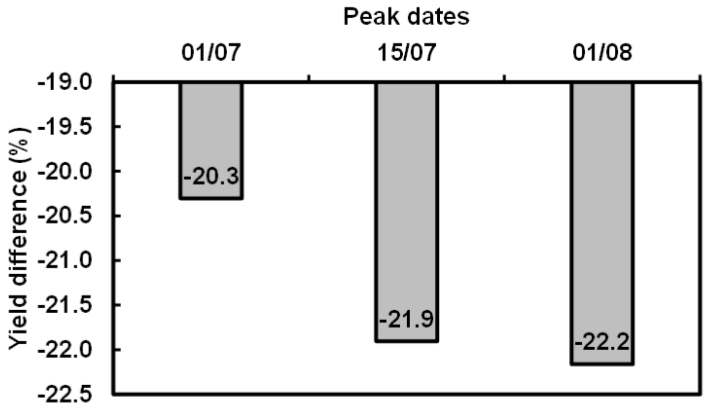


**Figure 6.** Average relative yield differences (%) for all the regions at each peak date.

## 4. Discussion and Conclusions

The results show that heatwaves can have a very strong impact on grapevine yields. These impacts strongly depend on the onset dates and duration of the heatwaves. The highest negative impacts may result in a decrease in the yield by up to −35% in some regions (Figure 5, left panel). The descending-order ranking of the frequency of occurrence of the heatwave peak dates is 15 July, 1 July and 1 August (Figure 4). The results have shown that regions that have their peak date on 1 August will be more negatively impacted than other regions (Figure 6). The impacts of heatwaves before and after these dates resulted in much less yield reduction (Figure 3). Heatwaves in September show a very low impact in many regions. While being true that heatwaves at this specific period may not be very common, this pattern may be modified by climate change.

This reduction in yields is explained by the detrimental effects of extremely high temperatures on grapevine physiology. Several studies have documented these effects [23,48–51]. As an example, Molitor and Keller [52] showed for the Luxembourgish Moselle region that post-bloom maximum temperatures (especially over the first three weeks after bloom) are negatively correlated with annual yield. This might be explained by the fact that cell division and cell expansion are reduced under heat conditions and, as a result, berries remain smaller [52]. Kliewer [53] demonstrated that temperatures above 32.5 °C between bloom and 12 to 18 days thereafter reduced berry size compared to 25 °C.

The geographical representation of yield reduction hints at a latitudinal gradient in the heatwave impact (Figure 5, right panel). In fact, regions at lower latitudes seem to show slightly lower negative impacts than regions at higher latitudes. This may be partially explained by the fact that vineyards in Southern Europe are most adapted to higher temperatures than regions in Central Europe. Furthermore, productivity in Southern European countries, such as Spain and Portugal, is already typically low [54], when compared to Central Europe, and this productivity difference could partially explain the lower decrease. Under Southern European conditions, the highest yield reductions were observed when a heatwave occurs in July, while this was verified in early August for the northern cooler regions. This might be explained by the later annual phenological cycle under cooler conditions, i.e., it is assumed that the temporal shift in phenology might be the reason for the temporal shift of maximum yield reduction.

Some limitations of the present study can be mentioned. In effect, there are uncertainties inherent to this kind of modelling assessment. The first limitation is tied to the crop model. Although STICS has previously shown a high agreement with observed conditions, the model may not satisfactorily incorporate critical plant processes to assess the full impact of heatwaves. As an example, the model does not include a module to address berry and leaf sunburn, which is a common consequence of heatwaves. Another limitation of the current study is that it does not take into account multiple heatwaves in a single year, i.e., only one heatwave per year was considered. The uncertainty related to the future scenarios should also be mentioned. Increased atmospheric $CO_2$ concentration partially offsets the dryness effects, promoting yield and leaf area index increases in Central/Northern Europe. Moreover, the current study simulations are based on a modification of a single climatic variable (air temperature), whereas several other atmospheric variables can also play a key role during a heatwave, such as air humidity, radiation fluxes, wind and pressure, amongst others. Another aspect is related to the occurrence or not of precipitation in the days before the heatwave, as it may also impact the results.

Furthermore, there is still some uncertainty related to the effect of high temperatures that are not completely understood [30]. As an example, in some studies with reduced stomatal conductance owed to extreme heat exposure, grapevines recovered within a few days [16,19,20]. Furthermore, some varieties are more heat-tolerant than others [55,56], and several acclimatization processes have been identified for extreme temperatures [25,49,57]. In the present study, a single variety (cv. Pinot noir) was used in the modelling approach. Nevertheless, in reality, vineyards in Europe are composed of many rootstocks, cultivars and botanical clones that eventually determine yields, e.g., see [58].

Given these results, and to the projected increase in heatwave occurrence and intensity under future climate conditions, adequate and timely planning of suitable adaptation measures needs to be adopted by the winemaking sector. One of the main adaptation measures is the selection and cultivation of variety-clone-rootstock combinations more resilient to the projected heat and water stress conditions [45]. Additionally, training systems that promote higher water-use efficiency should be envisioned, such as the Gobelet [59]. In general, all measures that promote higher water-use efficiency may be seen as adequate adaptation measures against the negative impact of heatwaves [60–62]. The present study may be considered to be a first approach to modelling heatwave impact on grapevines. Although these findings highlight the detrimental impact that heatwaves may bring to the European winegrowers, further research should be envisioned to evaluate and improve these modelling assessments, so as to provide more accurate information regarding the effects of extreme events on viticulture.

## 5. Conclusions

The present study highlights the negative impacts that heatwaves may have on the main viticultural regions in Europe. This information, is critical for stakeholders and decision-makers within the European winemaking sector, as it allows them to timely plan suitable adaptation measures that may ensure the future sustainability of this important socioeconomic sector.

**Author Contributions:** Conceptualization, H.F.; methodology, H.F.; software, H.F.; validation, H.F., D.M., L.L. and J.A.S.; formal analysis, H.F., D.M., L.L. and J.A.S.; investigation, H.F.; resources, H.F.; data curation, H.F. writing—original draft preparation, H.F.; writing—review and editing, H.F., D.M., L.L. and J.A.S.; visualization, H.F., D.M., L.L. and J.A.S.; supervision, H.F.; project administration, H.F.; funding acquisition, H.F. All authors have read and agreed to the published version of the manuscript.

**Funding:** This research was funded by FCT—Portuguese Foundation for Science and Technology contract CEECIND/00447/2017 and Project COA/CAC/0030/2019.

**Acknowledgments:** Helder Fraga thanks the FCT—Portuguese Foundation for Science and Technology for contract CEECIND/00447/2017. This study was carried out under the CoaClimateRisk FCT Project (COA/CAC/0030/2019). This work was also supported by National Funds by FCT under the project UIDB/04033/2020. We also thank the Clim4Vitis project, "Climate change impact mitigation for European viticulture: knowledge transfer for an integrated approach", funded by European Union's Horizon 2020 Research and Innovation Programme, under grant agreement n° 810176.

**Conflicts of Interest:** The authors declare no conflict of interest.

## References

1. Kottek, M.; Grieser, J.; Beck, C.; Rudolf, B.; Rubel, F. World map of the Koppen-Geiger climate classification updated. *Meteorol. Z.* **2006**, *15*, 259–263, doi:10.1127/0941-2948/2006/0130.
2. Giorgi, F. Climate change hot-spots. *Geophys. Res. Lett.* **2006**, *33*, doi:10.1029/2006gl025734.
3. Baldocchi, D.; Wong, S. Accumulated winter chill is decreasing in the fruit growing regions of California. *Clim. Chang.* **2008**, *87*, S153–S166, doi:10.1007/s10584-007-9367-8.
4. Luedeling, E.; Girvetz, E.H.; Semenov, M.A.; Brown, P.H. Climate Change Affects Winter Chill for Temperate Fruit and Nut Trees. *PLoS ONE* **2011**, *6*, doi:10.1371/journal.pone.0020155.
5. Atkinson, C.J.; Brennan, R.M.; Jones, H.G. Declining chilling and its impact on temperate perennial crops. *Environ. Exp. Bot.* **2013**, *91*, 48–62, doi:10.1016/j.envexpbot.2013.02.004.
6. Gladstones, J. *Wine, Terroir and Climate Change*; Wakefield Press: Adelaide, Australia, 2011.
7. Keller, M. *The Science of Grapevines: Anatomy and Physiology*; Elsevier, Inc.: New York, NY, US, 2010; p. 400.
8. Coombe, B.G. Influence of temperature on composition and quality of grapes. *Acta Hort.* **1987**, *206*, 23–36.
9. Schwartz, M.D.; Hanes, J.M. Continental-scale phenology: warming and chilling. *Int. J. Clim.* **2010**, *30*, 1595–1598, doi:10.1002/joc.2014.
10. Winkler, A.J. *General Viticulture*; University of California Press: Berkeley, CA, USA, 1974.
11. Bonhomme, R. Review: Bases and limits to using 'degree.day' units. *Eur. J. Agron.* **2000**, *2000*, 1–10.
12. Mariani, L.; Parisi, S.; Cola, G.; Failla, O. Climate change in Europe and effects on thermal resources for crops. *Int. J. Biometeorol.* **2012**, doi:10.1007/s00484-012-0528-8.
13. Wang, E.; Engel, T. Simulation of phenological development of wheat crops. *Agric. Syst.* **1998**, *58*, 1–24.
14. Yan, W.; Hunt, L.A. An equation for modelling the temperature response of plants using only the cardinal temperatures. *Ann. Bot.* **1999**, *84*, 617–614.
15. Molitor, D.; Junk, J.; Evers, D.; Hoffmann, L.; Beyer, M. A high resolution cumulative degree day based model to simulate phenological development of grapevine. *Am. J. Enol. Vitic.* **2014**, *65*, 72–80.
16. Ferrini, F.; Mattii, G.B.; Nicese, F.P. Effect of Temperature on Key Physiological Responses of Grapevine Leaf. *Am. J. Enol. Vitic.* **1995**, *46*, 375.
17. Moutinho-Pereira, J.M.; Correia, C.M.; Goncalves, B.M.; Bacelar, E.A.; Torres-Pereira, J.M. Leaf gas exchange and water relations of grapevines grown in three different conditions. *Photosynthetica* **2004**, *42*, 81–86.
18. Berry, J.; Bjorkman, O. Photosynthetic Response and Adaptation to Temperature in Higher-Plants. *Annu. Rev. Plant Physiol. Plant Mol. Biol.* **1980**, *31*, 491–543, doi:10.1146/annurev.pp.31.060180.002423.

19. Matsui, S.; Ryugo, K.; Kliewer, W.M. Lowered berry quality due to heat stress at the early ripening stage of berry growth in a seeded grapevine, Vitis vinifera L. *Research Bulletin of the Faculty of Agriculture-Gifu University*, **1991**.
20. Sepúlveda, G.; Kliewer, W.M. Stomatal Response of Three Grapevine Cultivars (<em>Vitis vinifera</em> L.) to High Temperature. *Am. J. Enol. Vitic.* **1986**, *37*, 44.
21. Kliewer, W.M. Influence of Temperature, Solar Radiation and Nitrogen on Coloration and Composition of Emperor Grapes. *Am. J. Enol. Vitic.* **1977**, *28*, 96.
22. Schultz, H.R. Extension of a Farquhar model for limitations of leaf photosynthesis induced by light environment, phenology and leaf age in grapevines Vitis vinifera L. cvv. White Riesling and Zinfandel). *Funct. Plant Biol.* **2003**, *30*, 673–687.
23. Greer, D.H.; Weston, C. Heat stress affects flowering, berry growth, sugar accumulation and photosynthesis of Vitis vinifera cv. Semillon grapevines grown in a controlled environment. *Funct. Plant Biol.* **2010**, *37*, 206–214, doi:10.1071/fp09209.
24. Ingvordsen, C.H.; Lyngkjaer, M.F.; Peltonen-Sainio, P.; Mikkelsen, T.N.; Stockmarr, A.; Jorgensen, R.B. How a 10-day heatwave impacts barley grain yield when superimposed onto future levels of temperature and CO2 as single and combined factors. *Agric. Ecosyst. Environ.* **2018**, *259*, 45–52, doi:10.1016/j.agee.2018.01.025.
25. Grace, W.J.; Sadras, V.O.; Hayman, P.T. Modelling heatwaves in viticultural regions of southeastern Australia. *Aust. Meteorol. Oceanogr. J.* **2009**, *58*, 249–262, doi:10.22499/2.5804.004.
26. Menzel, A. A 500 year pheno-climatological view on the 2003 heatwave in Europe assessed by grape harvest dates. *Meteorol. Z.* **2005**, *14*, 75–77, doi:10.1127/0941-2948/2005/0014-0075.
27. Beniston, M. The 2003 heat wave in Europe: A shape of things to come? An analysis based on Swiss climatological data and model simulations. *Geophys Res Lett* **2004**, *31*, doi:10.1029/2003gl018857.
28. Costa, R.; Fraga, H.; Fonseca, A.; de Cortazar-Atauri, I.G.; Val, M.C.; Carlos, C.; Reis, S.; Santos, J.A. Grapevine Phenology of cv. Touriga Franca and Touriga Nacional in the Douro Wine Region: Modelling and Climate Change Projections. *Agron. Basel* **2019**, *9*, doi:10.3390/agronomy9040210.
29. Moriondo, M.; Ferrise, R.; Trombi, G.; Brilli, L.; Dibari, C.; Bindi, M. Modelling olive trees and grapevines in a changing climate. *Environ. Model. Softw.* **2015**, *72*, 387–401, doi:10.1016/j.envsoft.2014.12.016.
30. Leolini, L.; Bregaglio, S.; Moriondo, M.; Ramos, M.C.; Bindi, M.; Ginaldi, F. A model library to simulate grapevine growth and development: software implementation, sensitivity analysis and field level application. *Eur. J. Agron.* **2018**, *99*, 92–105, doi:10.1016/j.eja.2018.06.006.
31. Brisson, N.; Launay, M.; Mary, B.; Beaudoin, N. *Conceptual Basis, Formalisations and Parameterization of the STICS Crop Model*; Editions Quae: Versailles, France, 2008; p. 297.
32. García de Cortazar-Atauri, I. Adaptation du modèle STICS à la vigne (Vitis vinifera L.). Utilisation dans le cadre d'une étude d'impact du changement climatique à l'échelle de la France. *Phd Thesismontpelliersupagro.* **2006**.
33. Fraga, H.; Costa, R.; Moutinho-Pereira, J.; Correia, C.M.; Dinis, L.-T.; Gonçalves, I.; Silvestre, J.; Eiras-Dias, J.; Malheiro, A.C.; Santos, J.A. Modeling Phenology, Water Status, and Yield Components of Three Portuguese Grapevines Using the STICS Crop Model. *Am. J. Enol. Vitic.* **2015**, *66*, 482–491, doi:10.5344/ajev.2015.15031.
34. Valdes-Gomez, H.; Celette, F.; García de Cortazar-Atauri, I.; Jara-Rojas, F.; Ortega-Farias, S.; Gary, C. Modelling Soil Water Content and Grapevine Growth and Development with the Stics Crop-Soil Model under Two Different Water Management Strategies. *J. Int. Des Sci. De La Vigne Et Du Vin* **2009**, *43*, 13–28.
35. Fraga, H.; García de Cortázar Atauri, I.; Malheiro, A.C.; Santos, J.A. Modelling climate change impacts on viticultural yield, phenology and stress conditions in Europe. *Glob. Chang. Biol.* **2016**, *22*, 3774–3788, doi:10.1111/gcb.13382.
36. Fraga, H.; Santos, J.A.; Moutinho-Pereira, J.; Carlos, C.; Silvestre, J.; Eiras-Dias, J.; Mota, T.; Malheiro, A.C. Statistical modelling of grapevine phenology in Portuguese wine regions: observed trends and climate change projections. *J. Agric. Sci.* **2015**, *FirstView*, 1-17, doi:doi:10.1017/S0021859615000933.
37. Fraga, H.; Santos, J.A. Vineyard mulching as a climate change adaptation measure: Future simulations for Alentejo, Portugal. *Agric. Syst.* **2018**, *164*, 107–115, doi:10.1016/j.agsy.2018.04.006.
38. Fraga, H.; García de Cortázar Atauri, I.; Santos, J.A. Viticultural irrigation demands under climate change scenarios in Portugal. *Agric. Water Manag.* **2018**, *196*, 66–74, doi:10.1016/j.agwat.2017.10.023.

39. García de Cortazar-Atauri, I.; Brisson, N.; Gaudillere, J.P. Performance of several models for predicting budburst date of grapevine (Vitis vinifera L.). *Int. J. Biometeorol.* **2009**, *53*, 317–326, doi:10.1007/s00484-009-0217-4.
40. García de Cortazar-Atauri, I.; Brisson, N.; Ollat, N.; Jacquet, O.; Payan, J.C. Asynchronous dynamics of grapevine (Vitis vinifera) maturation: experimental study for a modelling approach. *J. Int. Des Sci. De La Vigne Et Du Vin* **2009**, *43*, 83–97.
41. Cornes, R.C.; van der Schrier, G.; van den Besselaar, E.J.M.; Jones, P.D. An Ensemble Version of the E-OBS Temperature and Precipitation Data Sets. *J. Geophys. Res. Atmos.* **2018**, *123*, 9391–9409, doi:10.1029/2017JD028200.
42. C3S. ERA5: Fifth generation of ECMWF atmospheric reanalysis of the global climate. Copernicus Climate Change Service Climate Data Store (CDS). 2017. Available online: https://climate.copernicus.eu/climate-data-store (accessed on 1 February 2020).
43. FAO/IIASA/ISRIC/ISSCAS/JRC. *Harmonized World Soil Database (version 1.2);* FAO: Rome, Italy; IIASA: Laxenburg, Austria, 2012.
44. Bouma, J. Using Soil Survey Data for Quantitative Land Evaluation. In *Advances in Soil Science*; Stewart, B.A., Ed.; Springer US: New York, NY, US, 1989; Volume 9, pp. 177–213.
45. Jones, G.V. *Climate and Terroir: Impacts of Climate Variability and Change on Wine in Fine Wine and Terroir - The Geoscience Perspective*; Macqueen, R.W., Meinert, L.D., Eds.; Geoscience Canada, Geological Association of Canada: St. John's, NL, Canada, 2006.
46. Anderson, K.; Aryal, N.R. *Which Winegrape Varieties are Grown Where? A Global Empirical Picture*; University of Adelaide Press: Adelaide, Australia, 2013; 700p.
47. Jackson, R.S. *Wine Science: Principles and Applications;* Elsevier Science, Amsterdam, The Netherlands, 2008; 776p.
48. White, M.A.; Diffenbaugh, N.S.; Jones, G.V.; Pal, J.S.; Giorgi, F. Extreme heat reduces and shifts United States premium wine production in the 21st century. *Proc. Natl. Acad. Sci. USA* **2006**, *103*, 11217–11222, doi:10.1073/pnas.0603230103.
49. Carvalho, L.C.; Coito, J.L.; Colaco, S.; Sangiogo, M.; Amancio, S. Heat stress in grapevine: the pros and cons of acclimation. *Plant Cell Environ.* **2015**, *38*, 777–789, doi:10.1111/pce.12445.
50. Greer, D.H.; Weedon, M.M.; Weston, C. Reductions in biomass accumulation, photosynthesis in situ and net carbon balance are the costs of protecting Vitis vinifera 'Semillon' grapevines from heat stress with shade covering. *Aob Plants* **2011**, *2011*, plr023, doi:10.1093/aobpla/plr023.
51. Webb, L.; Watt, A.; Hill, T.; Whiting, J.; Wigg, F.; Dunn, G.; Needs, S.; Barlow, E.W.R. *Extreme heat: managing grapevine response. Documenting regional and inter-regional variation of viticultural impact and management input relating to the 2009 heatwave in South-Eastern Australia. GWRDC and University of Melbourne: Melbourne.*; University of Melbourne: Melbourne, Australia, 2009.
52. Molitor, D.; Keller, M. Yield of Müller-Thurgau and Riesling grapevines is altered by meteorological conditions in the current and the previous growing seasons. *Oeno One* **2016**, *50*, 245–258.
53. Kliewer, W.M. Effect of High-Temperatures during Bloom-Set Period on Fruit-Set, Ovule Fertility, and Berry Growth of Several Grape Cultivars. *Am. J. Enol. Vitic.* **1977**, *28*, 215–222.
54. OIV. *2019 Statistical Report on World Vitiviniculture*; International Organisation of Vine and Wine: Paris, France, 2019.
55. Schaffer, B.; Andersen, P.C. *Handbook of Environmental Physiology of Fruit Crops. Volume 1. Temperature Crops;* CRC Press: Boca Raton, FL, USA, 1994; 358p.
56. Moutinho-Pereira, J.; Magalhães, N.; Gonçalves, B.; Bacelar, E.; Brito, M.; Correia, C. Gas exchange and water relations of three Vitis vinifera L. cultivars growing under Mediterranean climate. *Photosynthetica* **2007**, *45*, 202–207, doi:10.1007/s11099-007-0033-1.
57. Wang, L.J.; Li, S.H. Thermotolerance and related antioxidant enzyme activities induced by heat acclimation and salicylic acid in grape (Vitis vinifera L.) leaves. *Plant Growth Regul.* **2006**, *48*, 137–144, doi:10.1007/s10725-005-6146-2.
58. Renouf, V.; Tregoat, O.; Roby, J.P.; Van Leeuwen, C. Soils, Rootstocks and Grapevine Varieties in Prestigious Bordeaux Vineyards and Their Impact on Yield and Quality. *J. Int. Des Sci. De La Vigne Et Du Vin* **2010**, *44*, 127–134.
59. Van Leeuwen, C.; Darriet, P. The Impact of Climate Change on Viticulture and Wine Quality. *J. Wine Econ.* **2016**, *11*, 150–167, doi:10.1017/jwe.2015.21.

60. Chaves, M.M.; Santos, T.P.; Souza, C.R.; Ortuno, M.F.; Rodrigues, M.L.; Lopes, C.M.; Maroco, J.P.; Pereira, J.S. Deficit irrigation in grapevine improves water-use efficiency while controlling vigour and production quality. *Ann. Appl. Biol.* **2007**, *150*, 237–252, doi:10.1111/j.1744-7348.2006.00123.x.
61. Fraga, H.; Atauri, I.G.D.; Malheiro, A.C.; Moutinho-Pereira, J.; Santos, J.A. Viticulture in Portugal: A review of recent trends and climate change projections. *Oeno One* **2017**, *51*, 61–69, doi:10.20870/oeno-one.2016.0.0.1621.
62. Fraga, H.; Santos, J.A. Daily prediction of seasonal grapevine production in the Douro wine region based on favourable meteorological conditions. *Aust. J. Grape Wine Res.* **2017**, *23*, 296–304, doi:10.1111/ajgw.12278.

applied sciences

MDPI

*Article*

# Phenological Model Intercomparison for Estimating Grapevine Budbreak Date (*Vitis vinifera* L.) in Europe

**Luisa Leolini [1,*], Sergi Costafreda-Aumedes [1], João A. Santos [2], Christoph Menz [3], Helder Fraga [2], Daniel Molitor [4], Paolo Merante [5], Jürgen Junk [4], Thomas Kartschall [3], Agnès Destrac-Irvine [6], Cornelis van Leeuwen [6], Aureliano C. Malheiro [2], José Eiras-Dias [7], José Silvestre [7], Camilla Dibari [1], Marco Bindi [1] and Marco Moriondo [8]**

1 Department of Agriculture, Food, Environment and Forestry, DAGRI, University of Florence, UNIFI, 50144 Florence, Italy; sergi.costafredaaumedes@unifi.it (S.C.-A.); camilla.dibari@unifi.it (C.D.); marco.bindi@unifi.it (M.B.)
2 Centre for the Research and Technology of Agro-Environmental Sciences, CITAB, Universidade de Trás-os-Montes e Alto Douro, UTAD, 5000-801 Vila Real, Portugal; jsantos@utad.pt (J.A.S.); hfraga@utad.pt (H.F.); amalheir@utad.pt (A.C.M.)
3 Potsdam Institute for Climate Impact Research, PIK, 14473 Potsdam, Germany; menz@pik-potsdam.de (C.M.); thomas@pik-potsdam.de (T.K.)
4 Luxembourg Institute of Science and Technology, LIST, 4422 Luxembourg, Luxembourg; daniel.molitor@list.lu (D.M.); juergen.junk@list.lu (J.J.)
5 Georg-August-Universität Göttingen, 37073 Göttingen, Germany; paolo.merante@uni-goettingen.de
6 EGFV, Bordeaux Sciences Agro, INRAE, University of Bordeaux, F-33882 Villenave d'Ornon, France; agnes.destrac-irvine@inra.fr (A.D.-I.); vanleeuwen@agro-bordeaux.fr (C.v.L.)
7 Instituto Nacional de Investigação Agrária e Veterinária, INIAV, Estação Vitivinícola Nacional, Quinta da Almoínha, 2565-191 Dois Portos, Portugal; eiras.dias@iniav.pt (J.E.-D.); jose.silvestre@iniav.pt (J.S.)
8 Institute of Bioeconomy, National Research Council, CNR-IBE, 50019 Florence, Italy; marco.moriondo@cnr.it
* Correspondence: luisa.leolini@unifi.it; Tel.: +39-055-2755742

Received: 16 April 2020; Accepted: 22 May 2020; Published: 29 May 2020


**Abstract:** Budbreak date in grapevine is strictly dependent on temperature, and the correct simulation of its occurrence is of great interest since it may have major consequences on the final yield and quality. In this study, we evaluated the reliability for budbreak simulation of two modeling approaches, the chilling-forcing (CF), which describes the entire dormancy period (endo- and eco-dormancy) and the forcing approach (F), which only describes the eco-dormancy. For this, we selected six phenological models that apply CF and F in different ways, which were tested on budbreak simulation of eight grapevine varieties cultivated at different latitudes in Europe. Although none of the compared models showed a clear supremacy over the others, models based on CF showed a generally higher estimation accuracy than F where fixed starting dates were adopted. In the latter models, the accurate simulation of budbreak was dependent on the selection of the starting date for forcing accumulation that changes according to the latitude, whereas CF models were independent. Indeed, distinct thermal requirements were found for the grapevine varieties cultivated in Northern and Southern Europe. This implies the need to improve modeling of the dormancy period to avoid under- or over-estimations of budbreak date under different environmental conditions.

**Keywords:** chilling-forcing models; dormancy; forcing models; phenology

## 1. Introduction

Grapevine phenological phases have a profound influence on the final grape and wine quality [1–3]. In particular, changes in the current climate conditions are strongly affecting the occurrence of the developmental stages and length of the grapevine growing cycle in the most renowned wine areas [4,5].

Several authors have reported the increasing temperature trend across the most traditional wine areas of the Mediterranean basin during the last decades. For example, Tomasi et al. [6] showed a 2.3 °C-temperature increase over the grape growing season in Veneto region (Italy) during the period 1964-2009, while van Leeuwen et al. [7] evidenced a 2.0 °C increase from 1951 to 2016 in the Bordeaux wine production area. Moreover, Ramos et al. [8] observed an overall warming from 1.0 to 2.2 °C during the grape growing season in north-eastern Spain. These changes are expected to greatly influence grapevine varietal suitability across the European region [9–12].

Since grapevine phenology is mainly temperature-driven [4], the current warming is affecting the phenological stages and shifting the annual growing cycle [13–16]. Among the most important developmental phases, budbreak represents the starting point of vegetative growth. A temperature increase can have a dual effect on this phase (anticipating or delaying its occurrence), with strong consequences on the following reproductive stages. Indeed, a shift in budbreak may determine poor shoot growth together with fewer clusters and an inhomogeneous grape development [17,18].

Under increasing temperature, a delay in budbreak phase can be determined by insufficient chilling during the dormancy period [19]. Indeed, the bud vegetative growth is limited by a first sub-period induced by physiological conditions (endo-dormancy), and then by a second sub-period in which bud opening is affected by the environmental conditions (eco-dormancy [17,20]). In this context, some studies showed that dormancy release is regulated by bud exposure period to temperatures between 0 to 10 °C [19,21], until fulfilment of the chilling requirement, and a subsequent period of temperatures (from 0 to 25 °C), until the reaching of the forcing requirement [22].

Budbreak occurrence being strongly influenced by the dormancy period, several studies attempted the implementation of phenological models for improving the prediction of this developmental stage [23–28]. Phenological models can be classified in two main categories: forcing and chilling-forcing models. Forcing models are simply based on the forcing unit accumulation, starting, in general, from a fixed date in the year. These models only focus on the description of the eco-dormancy period assuming that the chilling unit accumulation requirement was previously fulfilled and the endo-dormancy period had concluded. Instead, chilling-forcing models can explain both the endo- and eco-dormancy periods by taking into consideration the chilling unit and the forcing accumulation with respect to specific temperature thresholds [24,29,30].

Hence, the selection of one of these two categories for an accurate budbreak simulation often gave rise to a wide debate [29,30]. Chilling-forcing models can take into account the influences of temperature on the entire dormancy period, evidencing not only the shortening effect of warmer temperatures during eco-dormancy but also a possible delay of budbreak caused by a failed chilling requirement [13,31]. However, the limited improvement in the performances of these models and the easier implementation provided by forcing models, focus on the issue about the most suitable modeling approach for budbreak estimation. In modeling studies, the choice of phenological model plays an important role in the use of crop simulation models and in determining potential risk of late spring frost events. In crop simulation models, phenology defines the plant growing cycle with important consequences on future biomass partitioning [32]. In this context, an accurate estimation of budbreak stage may avoid randomly selecting a starting point for vegetative biomass accumulation and over- or under-detection of late spring frost events under different climate scenarios [31,33].

Thus, the phenological intercomparison may be useful to highlight the performances of different models in simulating budbreak [29,30]. In order to take into account the influences of the grapevine precocity cycle and the effects of environmental conditions on budbreak estimation, model intercomparison experiments should consider multiple grapevine varieties and study sites. Indeed, grapevine varieties are characterized by various thermal requirements and focusing on a specific variety

does not allow the range of different physiological responses derived from the impact of temperature on dormancy period to be highlighted [30]. In addition, the use of a single date as a starting point for the chilling and forcing accumulation [29] does not allow the influence of temperature on the beginning of endo- or eco-dormancy periods to be appreciated, especially when the model intercomparison is performed with phenological data of grapevine varieties collected in different environments.

The objective of this study is to evaluate the performances of six phenological models (BRIN tested using hourly and daily temperature) at reproducing the budbreak date of eight grapevine varieties collected at different latitudes in Europe. In order to consider the influences of temperature during the dormancy period on model representations, two starting dates were set during chilling-forcing and forcing models' simulation, respectively. The analysis of budbreak date estimation is thus addressed to obtain responses of grapevine varieties' behavior under different environments.

## 2. Materials and Methods

### *2.1. Observations*

The phenological data were collected from 15 experimental vineyards in three European countries (France, Luxembourg and Portugal, see Figure 1 and Table 1). The weather data (i.e., daily maximum and minimum air temperature, °C) were freely available from weather services. More specifically, for France, the land-based daily weather data were collected by the National Centers for Environmental Information and then archived at NOAA (https://www.ncdc.noaa.gov/ [34]) and from a weather station near the VitAdapt project [35]. Hourly temperatures, rainfall, wind speed and reference evapotranspiration were recorded and stored in Climatik, a database managed by INRA, US 1116 Agroclim research station, 84914 Avignon, France (https://intranet.inra.fr/climatik_v2; limited access). For Luxembourg, the weather data were collected by the Administration des Services Techniques de l'Agriculture at the Institut Viti-Vinicole (https://agriculture.public.lu/) while the weather data for Portugal derived from the Instituto Nacional de Investigação Agrária e Veterinária (INIAV http://www.iniav.pt/) and the Associação para o Desenvolvimento da Viticultura Duriense (ADVID https://www.advid.pt/). The weather data were obtained from the closest and more representative stations for the vineyard weather conditions (Figure 1 and Table 1).

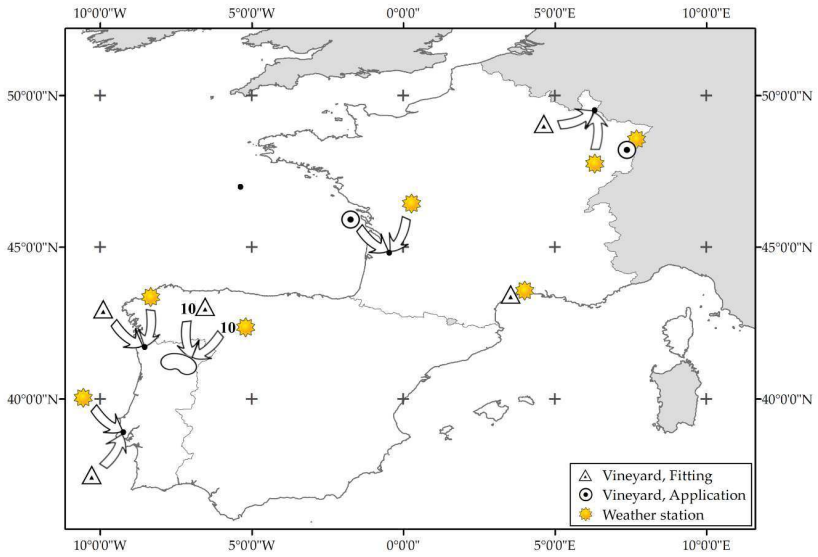


**Figure 1.** Map of the vineyards and weather stations situated in three European countries (Luxembourg, France and Portugal). The vineyards are displayed with triangles and points in relation to the use of phenological data for model fitting or application. The arrows indicate that both vineyards and weather stations are located in the same site. 10 weather stations and 10 vineyards are situated in Douro valley (Portugal).

**Table 1.** Observed weather (daily maximum and minimum air temperature, °C) and budbreak data of eight grapevine varieties used for model fitting, validation and application in different locations across Europe. The geographical positions of all weather stations and vineyards are identified with the latitude (Lat) and longitude (Long) coordinates (degrees).

| Variety × Site | | | Weather Data | | | Budbreak Data | | | |
|---|---|---|---|---|---|---|---|---|---|
| Procedure | Variety | Country | Weather Station | | Period | Vineyard | | Period | Cases |
| | | | Lat | Long | Years | Lat | Long | Years | Number |
| Fitting & Validation | Cabernet Sauvignon | France | 43.58 | 3.96 | 1950–2017 | 43.33 | 3.56 | 1951–2012 | 39 |
| | | Luxembourg | 49.50 | 6.35 | 2016–2018 | 49.50 | 6.35 | 2017–2018 | 2 |
| | Chardonnay | France | 43.58 | 3.96 | 1950–2017 | 43.33 | 3.56 | 1951–2012 | 33 |
| | | Luxembourg | 49.50 | 6.35 | 2010–2018 | 49.50 | 6.35 | 2011–2018 | 8 |
| | Gewürztraminer | Luxembourg | 49.50 | 6.35 | 1970–2018 | 49.50 | 6.35 | 1972–2018 | 50 |
| | Grenache | France | 43.58 | 3.96 | 1950–2017 | 43.33 | 3.56 | 1951–2012 | 41 |
| | Pinot Gris | Luxembourg | 49.50 | 6.35 | 1970–2018 | 49.50 | 6.35 | 1971–2018 | 51 |
| | Riesling | Luxembourg | 49.50 | 6.35 | 1970–2018 | 49.50 | 6.35 | 1971–2018 | 50 |
| | Touriga Franca | Portugal | 39.04 | −9.18 | 1994–2014 | 39.04 | −9.18 | 1995–2014 | 20 |
| | | | 41.81 | −8.41 | 2004–2009 | 41.81 | −8.41 | 2005–2009 | 5 |
| | | | 41.25 | −7.11 | 2013–2018 | 41.25 | −7.11 | 2014–2018 | 5 |
| | | | 41.19 | −7.54 | 2013–2018 | 41.19 | −7.54 | 2014–2018 | 5 |
| | | | 41.04 | −7.04 | 2013–2017 | 41.04 | −7.04 | 2014–2017 | 4 |
| | | | 41.17 | −7.56 | 2013–2017 | 41.17 | −7.56 | 2014–2017 | 4 |
| | | | 41.15 | −7.62 | 2013–2018 | 41.15 | −7.62 | 2014–2018 | 5 |
| | | | 41.17 | −7.55 | 2014–2018 | 41.17 | −7.55 | 2015–2018 | 4 |
| | Touriga Nacional | Luxembourg | 49.50 | 6.35 | 2016–2018 | 49.50 | 6.35 | 2017–2018 | 2 |
| | | Portugal | 39.04 | −9.18 | 1989–2014 | 39.04 | −9.18 | 1990–2014 | 19 |
| | | | 41.81 | −8.41 | 2004–2009 | 41.81 | −8.41 | 2005–2009 | 5 |
| | | | 41.21 | −7.43 | 2013–2018 | 41.21 | −7.43 | 2014–2018 | 5 |
| | | | 41.24 | −7.76 | 2014–2017 | 41.24 | −7.76 | 2015–2017 | 3 |
| | | | 41.22 | −7.54 | 2013–2018 | 41.22 | −7.54 | 2014–2018 | 5 |
| | | | 41.15 | −7.76 | 2015–2018 | 41.15 | −7.76 | 2016–2018 | 3 |
| Application | Cabernet Sauvignon | France | 44.79 | −0.58 | 2012–2019 | 44.79 | −0.58 | 2013–2019 | 7 |
| | Chardonnay | France | 48.55 | 7.64 | 1950–2017 | 48.22 | 7.35 | 1976–1990 | 15 |
| | Gewürztraminer | France | 48.55 | 7.64 | 1950–2017 | 48.22 | 7.35 | 2006–2009 | 4 |
| | Grenache | France | 48.55 | 7.64 | 1950–2017 | 48.22 | 7.35 | 1976–1990 | 13 |
| | Pinot Gris | France | 48.55 | 7.64 | 1950–2017 | 48.22 | 7.35 | 1976–1990 | 15 |
| | Riesling | France | 48.55 | 7.64 | 1950–2017 | 48.22 | 7.35 | 2006–2009 | 4 |
| | Touriga Franca | France | 44.79 | −0.58 | 2012–2019 | 44.79 | −0.58 | 2013–2019 | 7 |
| | Touriga Nacional | France | 44.79 | −0.58 | 2012–2019 | 44.79 | −0.58 | 2013–2019 | 7 |

The phenological data were collected for eight grapevine varieties (Cabernet Sauvignon, Chardonnay, Gewürztraminer, Grenache, Pinot Gris, Riesling, Touriga Franca and Touriga Nacional). For France, these data were retrieved from PERPHECLIM platform (https://www6.inrae.fr/projet-accaf-perpheclim_eng/The-PERPHECLIM-project [36]) and VitAdapt project [35]. For Luxembourg, the data were obtained from the Administration des Services Techniques de l'Agriculture at the Institut Viti-Vinicole. Finally, the data for the Lisbon wine region (Portugal) were obtained from the national ampelographic collection at the INIAV, located in Dois Portos. The data for the Douro wine region were collected by the associates from ADVID. Most of these grapevine varieties are for high-quality wine production derived from the world's benchmark regions and can be grouped on the basis of average growing season temperatures and ripening potential [37]. The phenological observations were collected by different research institutions and farmers at budbreak date which typically corresponded to BBCH 09 [38], except for Cabernet Sauvignon, Touriga Franca and Touriga Nacional collected in France (Bordeaux site; BBCH 07). We assumed that the distance between BBCH 07 and 09 is covered in 2 days as reported in [27].

### 2.2. Phenological Models

In total, we tested 6 models for estimating the budbreak date, divided into forcing (F) and chilling-forcing (CF) models. We used Growing Degree Days (GDD; [39]), WANG [40] and UNIFORC [24] for F models and BRIN [29] (Hourly and Daily approach), UNICHILL and UNIFIED [24] for CF models.

#### 2.2.1. GDD

The GDD model [39] is an F model that describes the eco-dormancy period based on accumulation of the daily average temperature ($T_{avg}$; °C) above a specific threshold ($T_b$; °C). The GDD accumulation ($Forc_{GDD}$) starts at a fixed date of the year ($t_0$) and is accumulated until the GDD requirement is satisfied at budbreak date (*Bud*; Equation (1)).

$$Forc_{GDD} = \sum_{t_0}^{Bud} (T_{avg} - T_b), \tag{1}$$

#### 2.2.2. WANG

The WANG model [40] is a temperature response function used, in this study, to describe the eco-dormancy period from a fixed date of the year ($t_0$) and not to calculate the chilling unit accumulation as reported for other similar functions [30]. The temperature function ($Forc_{WANG}$) allows the phenological development of grapevine to be evaluated using a non-linear approach based on three cardinal temperatures: $T_{opt}$ (optimum temperature, °C), $T_{\max}$ (maximum temperature, °C) and $T_{\min}$ (minimum temperature, °C; Equations (2a) and (2b)).

$$Forc_{WANG} = \sum_{t_0}^{Bud} Max\left[\left(\frac{2 \cdot \left(T_{avg} - T_{\min}\right)^{\alpha} \cdot \left(T_{opt} - T_{\min}\right)^{\alpha} - \left(T_{avg} - T_{\min}\right)^{2\alpha}}{\left(T_{opt} - T_{\min}\right)^{2\alpha}}\right), 0\right], \tag{2a}$$

$$\text{with } \alpha = \frac{\ln(2)}{\ln\left(\frac{T_{\max} - T_{\min}}{T_{opt} - T_{\min}}\right)}, \tag{2b}$$

where $T_{avg}$ is the daily average temperature (°C) and *Bud* is the budbreak date.

#### 2.2.3. UNIFORC

The UNIFORC model [24] is an F model based on a sigmoid curve for calculating the forcing unit accumulation ($Forc_{UNIFORC}$) from a fixed day of the year ($t_0$) until budbreak occurrence (*Bud*; Equation (3)):

$$Forc_{UNIFORC} = \sum_{t_0}^{Bud} \frac{1}{1 + e^{d \cdot (T_{avg} - e)}}, \tag{3}$$

where $T_{avg}$ is daily average temperature (°C), while $d$ and $e$ ($d < 0$ and $e > 0$) are empirical parameters of the function.

#### 2.2.4. BRIN

The BRIN model [29] is a CF model based on the Bidabe's Cold Action Model [41,42] in which the endo-dormancy period is evaluated through the accumulation of chilling units ($Chill_{BRIN}$; Equation (4)). The eco-dormancy period is based on forcing unit accumulation ($Forc_{BRIN}$) calculated with the Richardson equation [23]. The $Forc_{BRIN}$ is computed using both a daily (Equation (5)) and hourly (Equations (6a) and (6b)) temperature accumulation approach.

$$Chill_{BRIN} = \sum_{t_0}^{C_{endo}} (Q_{10c}^{\frac{-T_x(n)}{10}} + Q_{10c}^{\frac{-T_n(n)}{10}}), \tag{4}$$

$$Forc_{BRINDaily} = \sum_{C_{endo}}^{Bud} Richardson_{Daily}(n), \tag{5}$$

$$Forc_{BRINHourly} = \sum_{C_{endo}}^{Bud} Richardson_{Hourly}(n) \quad (6a)$$

$$Richardson = Max(Min(T_{avg} - T_l, T_h - T_l), 0), \quad (6b)$$

where $t_0$ is the simulation starting date, $T_{avg}$ is daily average temperature (°C), $C_{endo}$ is the date at which the chilling requirement is satisfied, $Bud$ is budbreak date, $Q_{10c}$ is the geometric progression rate of the thermal dormancy response, $T_n$ and $T_x$ are daily minimum and maximum temperatures (°C), respectively. $Richardson_{Daily}$ and $Richardson_{Hourly}$ are daily and hourly Richardson equations used for representing the eco-dormancy period [29]. The Richardson equations are limited by two cardinal temperatures: a lower ($T_l$, °C) and an upper limit temperature ($T_h$, °C).

#### 2.2.5. UNICHILL

The UNICHILL model [24] is a CF two-phase sequential model constituted by two functions describing chilling accumulation ($Chill_{UNICHILL}$) during endo-dormancy (Equation (7)) and forcing unit accumulation ($Forc_{UNICHILL}$) during eco-dormancy period (Equation (8)). After chilling requirement is satisfied at a specific date ($C_{endo}$), the forcing units start accumulating until the forcing requirement is reached, leading to the occurrence of the budbreak phase ($Bud$). The two functions are defined as followed:

$$Chill_{UNICHILL} = \sum_{t_0}^{C_{endo}} \frac{1}{1 + e^{a(T_{avg}-c)^2 + b(T_{avg}-c)}}, \quad (7)$$

$$Forc_{UNICHILL} = \sum_{C_{endo}}^{Bud} \frac{1}{1 + e^{d(T_{avg}-e)}}, \quad (8)$$

where $t_0$ is the simulation starting date, $T_{avg}$ is daily average temperature (°C) and $a$, $b$, $c$, $d$ and $e$ are empirical parameters of the function.

#### 2.2.6. UNIFIED

The UNIFIED model [24] is a CF overlapping model based on the same equations for chilling and forcing unit accumulation used in the UNICHILL model. However, UNIFIED model includes the effect of chilling units on forcing accumulation through implementation of the exponential decrease curve (Equation (9)) in which $ForcReq_{UNIFIED}$ (Fcrit) is the critical amount of forcing and $Chill_{UNIFIED}$ is the total amount of chilling at day $t_d$. The budbreak date is estimated when both chilling and forcing requirements are satisfied:

$$ForcReq_{UNIFIED} = we^{-zChill_{UNIFIED}(t_d)}, \quad (9)$$

where $w$ and $z$ are empirical parameters of the function.

### 2.3. Model Fitting and Validation

#### 2.3.1. Outliers Removal

The model fitting, validation and application were performed after removing outliers from the observed dataset. This procedure consists in the identification of possible anomalies by comparing the observed and simulated results obtained by a preliminary models' fitting against the original datasets for each variety. The outliers were identified by using the Tukey method [43], based on the non-parametric measure of the statistical dispersion of a given distribution quantified using the interquartile range (IQR). For each model and starting date, the outliers represent the values in which the difference between the observed and simulated budbreak Days of Year (DOYs) are outside the whiskers of the distribution (below Q1 − 1.5 IQR or above Q3 + 1.5 IQR values). An outlier of a specific variety is removed from the dataset when it is observed in at least 4 combinations (models x starting

date). The percentage of outliers removed from the fitting, validation and application datasets is: 4.17% (Cabernet Sauvignon), 5.36% (Chardonnay), 1.85% (Gewurztraminer and Riesling), 3.70% (Grenache), 1.52% (Pinot Gris), 10% (Touriga Franca and Nacional). These values were generally observed after extreme weather conditions (e.g., frosts of 1956, 1963 in France) or due to other influences (e.g., agronomic practices or errors in data collection) which cannot be reproduced during model simulation.

#### 2.3.2. Parameters' Range and Starting Date

The parameters' range of variation in the 6 phenological models was defined according to the literature [29,30,44–46]. For the GDD model, the fitted parameter was $T_b$ which ranges from 0 to 10 °C. In this study, 0 °C was considered the limit temperature for bud growth while 10 °C was the maximum base temperature adopted for describing the eco-dormancy period as found in other studies [19,22,29,44]. For the WANG model, this function being generally used for wheat simulation [47], the parameter range of the cardinal temperatures was established considering the values obtained by other similar functions (Fbeta) implemented for simulating budbreak date in grapevine [30]. Thus, $T_{\min}$ and $T_{\max}$ were set at 0 and 45 °C respectively, while $T_{opt}$ ranged in a ±30% of the value reported in Fila et al. [30]. For UNIFORC model, the $d$ and $e$ parameter values varied in a ±30% interval with respect to the average value reported for different grapevine varieties (Glera, Cabernet Sauvignon, Chardonnay and Merlot [46]). For both daily and hourly approaches of BRIN model, the $Q_{10}$ parameter range was defined in a ±30% interval of the value estimated for several grapevine varieties [29]. Moreover, the lower limit temperature ($T_l$) was fitted in the range 0–10 °C, as reported for GDD model while the upper limit temperature ($T_h$) for post dormancy was fixed at 25 °C as indicated in Garcia de Cortazar-Atauri et al. [29]. For the UNICHILL model, the parameters $a$, $b$, $c$, $d$ and $e$ were in a range of ±30% of the overall minimum and maximum value reported by Fila [46] for Glera, Cabernet Sauvignon, Chardonnay and Merlot varieties (field calibration). However, in the specific case of Cabernet Sauvignon and Chardonnay, the parameter range of $a$, $b$, $c$, $d$ and $e$ varied in ±30% interval with respect to the parameter values found for these varieties. Similarly, the range adopted for $a$, $b$, $c$, $d$ and $e$ parameters in UNIFIED model was identified by considering ±30% of the minimum and maximum values reported by Fila et al. [46] (field calibration). Based on the same study, the parameters $w$ and $z$ were fixed by considering the average values reported for field calibration of Sangiovese and Montepulciano.

Concerning the use of fixed starting dates $t_0$ during model simulation, we set the 1st of January [30] and 1st of March [27] of the current year for the F models and the 1st September [24] and 1st of August [29] of the previous year for the CF models.

#### 2.3.3. Model Fitting, Validation and Application

The methodology used for model fitting, validation and application is displayed in Figure 2. After outliers removal (Section 2.3.1), the first step was to randomly split the observed data (budbreak DOY per year) into 10 random subsamples (RS) in which 60% of the observed data was used for model fitting whereas the remaining 40% was retained for validation. Once the 10 random subsamples were prepared, the model fitting was performed for any combination of varieties, models and starting dates using the Phenological Modeling Platform (PMP) software (version 5.5) [48] and setting the parameter ranges as described in Section 2.3.2. The best fitting for any combination was found by exploring the range of each parameter through the Metropolis-Hastings algorithm [49–51] of PMP. Each fitted model was validated on the remaining 40% of the data and then applied on the validation datasets of the other subsamples by using the R software environment (version 3.5.0) [52]. Thus, the parameter set of each model combination (model x variety x starting date), which provided the highest-performance (HP) during fitting and validation procedures, was selected. Moreover, the average parameter sets (AV) derived from all fitted subsamples was also tested on the entire distribution of validation datasets. Finally, the HP and AV parameter sets were applied to the independent datasets of other study sites to evaluate the behavior of different parameterizations under different environmental conditions.

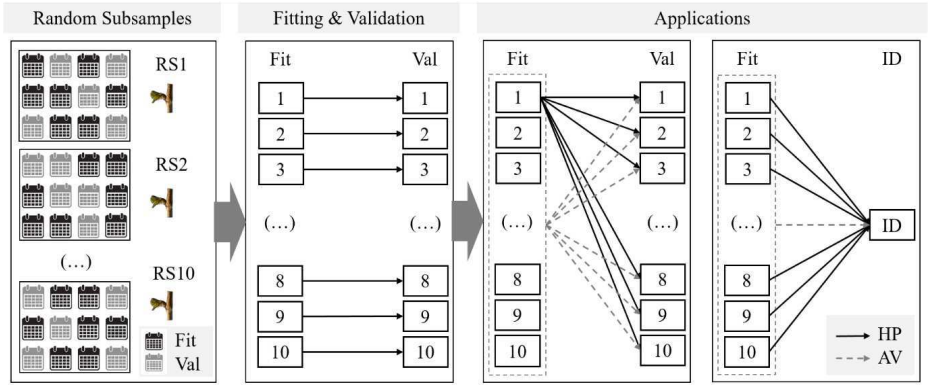


**Figure 2.** Workflow of the methodology adopted in this study. Random subsamples = Random distribution of the phenological observed data in subsample; Fitting and Validation = Model fitting on the selected 60% of the observed data and model validation on the remaining 40%; Applications = Model application on all validation and independent datasets. Fit = model fitting; Val = model validation; HP = highest-performance models; AV = average models; RS(n) = random subsamples; ID = independent datasets.

### *2.4. Statistical Analysis*

The statistical indices used for evaluating the phenological model performances during fitting, validation and application were: R-squared ($R^2$, Equation (10), [53]); Akaike information criterion (AIC, Equation 11, [54]); Root Mean Squared Error (RMSE, Equation (12), [55]) and modeling efficiency coefficient (EF, Equation (13), [56]), each defined as follows:

$$R^2 = 1 - \frac{\sum\limits_i (O_i - P_i)^2}{\sum\limits_i (O_i - \overline{O})^2}, \tag{10}$$

$$AIC = 2k - 2\ln(\hat{L}), \tag{11}$$

$$RMSE = \left[\sum_{i=1}^{n} \frac{(P_i - O_i)^2}{n}\right]^{0.5}, \tag{12}$$

$$EF = 1 - \frac{\sum\limits_{i=1}^{n} (P_i - O_i)^2}{\sum\limits_{i=1}^{n} \left(O_i - \overline{O}\right)^2}, \tag{13}$$

where $O_i$ is the observed value, $\overline{O}$ is the average of the observed values, $P_i$ is the predicted value, $n$ is the number of observations, $k$ is the number of parameters in the model, and $\hat{L}$ is the maximized value of the likelihood function of the predicted model.

Finally, the minimum, 10% quantile, median, mean, 90% quantile and maximum values of the statistics were extracted for describing the simulation results on all validation datasets.

## 3. Results

### *3.1. Overall Model Behavior in Fitting and Validation*

The results of the phenological model intercomparison were described comparing the performances of the different modeling approaches (e.g., F vs. CF) and starting dates (1st January/March vs. 1st September/August) during model fitting and validation. Initially, the model fitting and validation results evidenced higher average performances for CF (Fit, $R^2$ = 0.74; AIC = 150.42; RMSE = 4.22, Val,

$R^2$ = 0.61; AIC = 111.64; RMSE = 5.79) compared to F models (Fit, $R^2$ = 0.61; AIC = 160.62; RMSE = 5.51; Val, $R^2$ = 0.59; AIC = 112.01; RMSE = 6.10). Among all models (Figure 3 and Table S1), the highest performances were achieved by UNIFIED model (Fit, $R^2$ = 0.77; AIC = 147.60; RMSE = 3.96; Val, $R^2$ = 0.64; AIC = 110.74; RMSE = 5.42), while the lowest were obtained by the WANG model (Fit, $R^2$ = 0.61; AIC = 161.15; RMSE = 5.60) and GDD model (Val, $R^2$ = 0.58; AIC = 112.59; RMSE = 6.25). Moreover, higher performances were found for those models in which the starting date was fixed at 1st September in CF models (Fit, $R^2$ = 0.74; AIC = 150.24; RMSE = 4.21; Val, $R^2$ = 0.61; AIC = 111.59; RMSE = 5.75) and at 1st January in F models (Fit, $R^2$ = 0.66; AIC = 159.20; RMSE = 5.53; Val, $R^2$ = 0.63; AIC = 111.10; RMSE = 6.15). Finally, concerning grapevine varieties, Chardonnay was best fitted by the models (Fit, $R^2$ = 0.90; AIC = 138.66; RMSE = 4.90; Val, $R^2$ = 0.89; AIC = 101.54; RMSE = 5.97), while the poorest results were obtained for Touriga Nacional (Fit, $R^2$ = 0.42; AIC = 147.09; RMSE = 6.23; Val, $R^2$ = 0.31; AIC = 105.40; RMSE = 7.74) and Touriga Franca in terms of AIC values (Fit = 180.19; Val = 127.35).

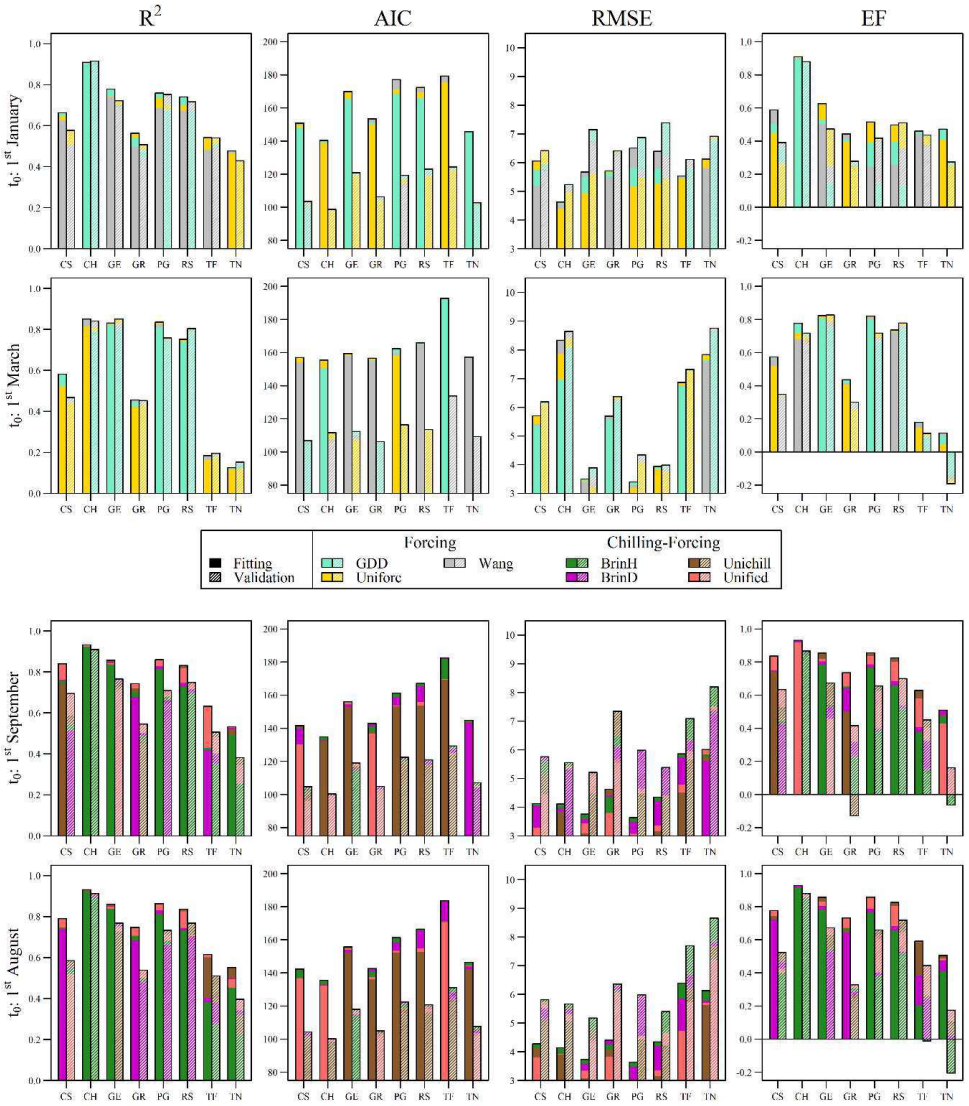


**Figure 3.** Statistical performances ($R^2$, AIC, RMSE, EF) of all combinations of the six phenological models, eight grapevine varieties and different starting dates during fitting and validation. The results of forcing (F) and chilling-forcing (CF) models (different bar colours) are displayed at the top and bottom of the figure, respectively. The two bars identify the model fitting (no bar texture) and validation (line bar texture). CS = Cabernet Sauvignon, CH = Chardonnay, GE = Gewürztraminer, GR = Grenache, PG = Pinot Gris, RS = Riesling, TF = Touriga Franca, TN = Touriga Nacional.

### 3.2. HP versus AV

In order to compare the results of different models' parameterizations, we selected the highest performance parameter set (HP, Table 2) from the 10 fitting and validation subsamples for each combination of model, starting date and variety. We then selected the average parameter set (AV, Table 3) from the 10 fitting subsamples for each combination model, starting date and variety. On these bases, Figures S1–S7 show the performances ($R^2$ and AIC) of the model fitting and validation (symbols) and the applications of the different parameterizations on all validation subsamples (boxplot) obtained by considering all grapevine varieties and starting dates. In detail, the selected parameter sets with highest performances (HP; filled symbols with different shapes according to the starting dates) were the result of the highest rank value of $R^2$ and AIC and the minimum discrepancy between fitting (red) and validation (blue) models. By contrast, the AV parameter sets (boxplots in shadow area) were the application of the average parameterization obtained for all subsamples. Despite that similar performances for HP and AV parameter sets were evidenced in Figures S1–S7, higher discrepancy was found in the behavior of CF and F models. In Figures S1–S4 (CF models), no differences were observed when different starting dates were set during model fitting and application. On the other hand, high discrepancy was found in model performances when different starting dates were adopted in Figures S5–S7 (F models). This trend is also evidenced by the correlations between observed and simulated DOYs in Figure 4, Figures S8 and S9. The results of model fitting showed accurate performances for all selected HP, with more discrepancy between starting dates of F models (yellow and green correlations) compared to those used in CF models (blue and red correlations). The values of $R^2$ also highlighted the higher performances obtained with some varieties compared to others (Chardonnay vs. Touriga Nacional).

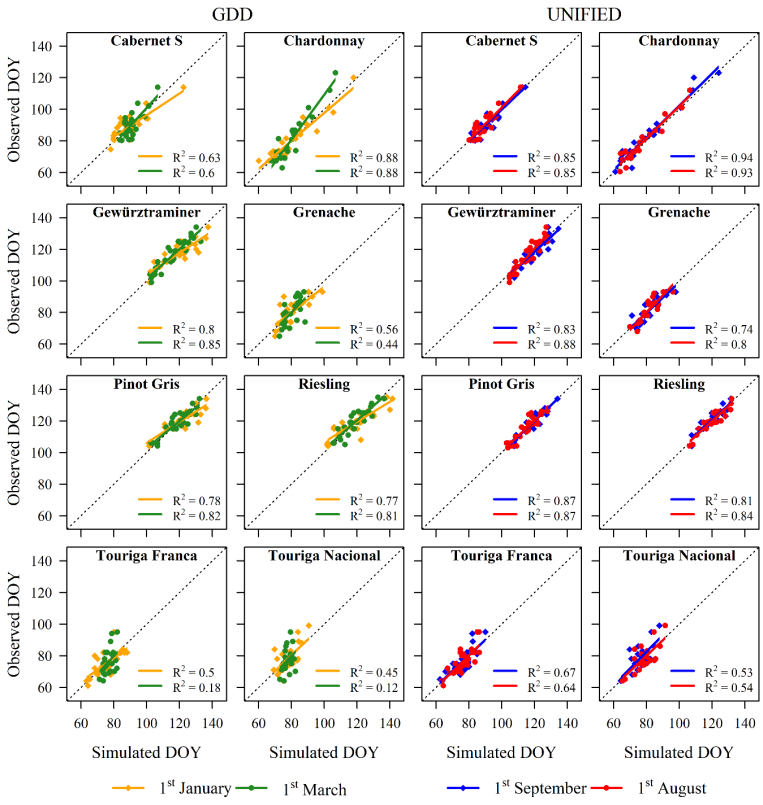


**Figure 4.** Correlations between observed and simulated budbreak Days of Year (DOY) of the GDD and UNIFIED models. The results were obtained for all grapevine varieties and starting dates using the HP parameter set.

**Table 2.** HP (highest-performance) parameter sets for each combination of models, grapevine varieties and starting dates. $C_{crit}$ = critical amount of chilling and $F_{crit}$ = critical amount of forcing.

| | | GDD | | WANG | | | | UNIFORC/UNICHILL/UNIFIED | | | | | | | | BRIN h/BRIN d | | | | |
|---|---|---|---|---|---|---|---|---|---|---|---|---|---|---|---|---|---|---|---|---|
| **Variety** | $t_0$ | $F_{crit}$ | $T_b$ | $F_{crit}$ | $T_{opt}$ | $T_{min}$ | $T_{max}$ | $C_{crit}$ | $F_{crit}$ | a | b | c | d | e | w | z | $C_{crit}$ | $F_{crit}$ | $Q_{10c}$ | $T_l$ | $T_h$ |
| Cabernet Sauvignon | 1 | 763.47 | 0 | 67.32 | 18.15 | 0 | 45 | - | 16.39 | - | - | - | −0.21 | 16.47 | - | - | 190.14 | 6636.2 | 1.54 | 5.07 | 25 |
| | −121 | | | | | | | 142.36 | 26.54 | 0.15 | −23.61 | −20.41 | −0.19 | 11.80 | - | - | 184.86 | 295.3 | 1.54 | 4.45 | |
| | | | | | | | | 151.14 | 20.62 | 1.31 | −31.06 | −1.45 | −0.20 | 12.44 | −0.00025 | 21.05 | | | | | |
| | 60 | 286.89 | 1.18 | 19.49 | 23.96 | 0 | 45 | - | 7.74 | - | - | - | −0.21 | 16.45 | - | - | 217.53 | 6597.1 | 1.52 | 5.07 | 25 |
| | −152 | | | | | | | 178.96 | 23.19 | 0.16 | −15.33 | −24.24 | −0.25 | 11.83 | - | - | 206.55 | 272.1 | 1.59 | 4.84 | |
| | | | | | | | | 175.24 | 20.40 | 0.91 | −26.60 | −1.63 | −0.14 | 14.69 | −0.00025 | 21.05 | | | | | |
| Chardonnay | 1 | 432.23 | 2.34 | 14.63 | 30.42 | 0 | 45 | - | 8.58 | - | - | - | −0.21 | 18.46 | - | - | 148.48 | 5194.0 | 1.54 | 5.86 | 25 |
| | −121 | | | | | | | 132.02 | 17.55 | 0.72 | −29.03 | −17.19 | −0.24 | 12.56 | - | - | 148.34 | 238.3 | 1.54 | 4.99 | |
| | | | | | | | | 123.96 | 19.71 | 0.85 | −32.05 | −2.20 | −0.28 | 11.79 | −0.00025 | 21.05 | | | | | |
| | 60 | 49.18 | 7.21 | 4.00 | 31.26 | 0 | 45 | - | 1.33 | - | - | - | −0.30 | 18.36 | - | - | 173.38 | 5276.9 | 1.54 | 5.81 | 25 |
| | −152 | | | | | | | 165.85 | 19.05 | 0.46 | −19.82 | −13.84 | −0.24 | 11.93 | - | - | 172.90 | 211.9 | 1.54 | 5.44 | |
| | | | | | | | | 172.71 | 19.63 | 1.19 | −34.66 | 0.22 | −0.25 | 10.46 | −0.00025 | 21.05 | | | | | |
| Grenache | 1 | 645.68 | 0 | 47.27 | 21.91 | 0 | 45 | - | 13.40 | - | - | - | −0.21 | 16.48 | - | - | 177.23 | 3769.3 | 1.67 | 6.63 | 25 |
| | −121 | | | | | | | 156.67 | 8.05 | 0.61 | −20.19 | −11.39 | −0.19 | 16.94 | - | - | 158.40 | 312.9 | 1.55 | 4.02 | |
| | | | | | | | | 157.54 | 20.94 | 0.55 | −30.18 | −10.31 | −0.26 | 9.98 | −0.00025 | 21.05 | | | | | |
| | 60 | 85.11 | 5.99 | 5.17 | 30.40 | 0 | 45 | - | 4.17 | - | - | - | −0.21 | 16.49 | - | - | 215.25 | 5029.4 | 1.53 | 5.27 | 25 |
| | −152 | | | | | | | 186.21 | 4.73 | 0.79 | −26.99 | −7.35 | −0.18 | 21.33 | - | - | 210.27 | 319.2 | 1.54 | 2.80 | |
| | | | | | | | | 186.89 | 20.41 | 1.04 | −30.11 | −1.81 | −0.28 | 9.72 | −0.00025 | 21.05 | | | | | |
| Gewürrtztraminer | 1 | 137.17 | 7.10 | 12.11 | 31.26 | 0 | 45 | - | 9.37 | - | - | - | −0.21 | 18.50 | - | - | 283.90 | 3961.1 | 1.53 | 6.19 | 25 |
| | −121 | | | | | | | 186.01 | 17.05 | 0.17 | −32.51 | −12.74 | −0.35 | 10.79 | - | - | 280.72 | 181.3 | 1.54 | 5.39 | |
| | | | | | | | | 172.62 | 20.42 | 1.18 | −34.32 | −10.15 | −0.23 | 11.48 | −0.00025 | 21.05 | | | | | |
| | 60 | 255.89 | 3.61 | 9.17 | 31.26 | 0 | 45 | - | 8.43 | - | - | - | −0.23 | 16.45 | - | - | 312.24 | 4159.1 | 1.53 | 5.98 | 25 |
| | −152 | | | | | | | 161.74 | 12.51 | 1.62 | −34.01 | −6.44 | −0.33 | 12.71 | - | - | 311.34 | 182.5 | 1.54 | 5.36 | |
| | | | | | | | | 214.68 | 20.29 | 0.50 | −31.89 | −10.95 | −0.28 | 10.28 | −0.00025 | 21.05 | | | | | |
| Pinot Gris | 1 | 122.16 | 7.39 | 12.15 | 31.26 | 0 | 45 | - | 9.63 | - | - | - | −0.21 | 18.49 | - | - | 285.01 | 4633.1 | 1.53 | 5.22 | 25 |
| | −121 | | | | | | | 183.87 | 14.70 | 0.56 | −23.01 | −19.53 | −0.25 | 12.67 | - | - | 284.32 | 225.9 | 1.55 | 4.11 | |
| | | | | | | | | 183.25 | 20.45 | 0.95 | −30.94 | −10.68 | −0.28 | 10.26 | −0.00025 | 21.05 | | | | | |
| | 60 | 250.48 | 3.91 | 9.36 | 31.23 | 0 | 45 | - | 9.44 | - | - | - | −0.21 | 16.54 | - | - | 314.40 | 6374.7 | 1.53 | 3.52 | 25 |
| | −152 | | | | | | | 174.41 | 12.60 | 1.13 | −25.39 | −8.01 | −0.33 | 12.02 | - | - | 314.75 | 218.9 | 1.54 | 4.29 | |
| | | | | | | | | 211.57 | 20.26 | 0.36 | −11.66 | −7.14 | −0.28 | 10.31 | −0.00025 | 21.05 | | | | | |
| Riesling | 1 | 156.14 | 6.74 | 12.60 | 31.26 | 0 | 45 | - | 9.90 | - | - | - | −0.21 | 18.46 | - | - | 267.03 | 4980.8 | 1.53 | 5.44 | 25 |
| | −121 | | | | | | | 150.99 | 5.33 | 1.39 | −27.15 | −5.31 | −0.18 | 21.68 | - | - | 280.95 | 208.2 | 1.56 | 4.93 | |
| | | | | | | | | 173.34 | 20.47 | 1.09 | −28.42 | −10.79 | −0.21 | 11.23 | −0.00025 | 21.05 | | | | | |
| | 60 | 279.34 | 3.46 | 11.80 | 30.29 | 0 | 45 | - | 10.14 | - | - | - | −0.22 | 16.45 | - | - | 297.05 | 5022.2 | 1.53 | 5.41 | 25 |
| | −152 | | | | | | | 168.39 | 10.63 | 1.08 | −23.72 | −7.63 | −0.29 | 13.89 | - | - | 313.12 | 221.8 | 1.53 | 4.68 | |
| | | | | | | | | 163.61 | 20.58 | 1.00 | −19.62 | −5.65 | −0.26 | 10.30 | −0.00025 | 21.05 | | | | | |
| Touriga Franca | 1 | 743.93 | 0 | 36.53 | 26.70 | 0 | 45 | - | 16.61 | - | - | - | −0.21 | 16.45 | - | - | 158.30 | 7933.9 | 1.53 | 4.80 | 25 |
| | −121 | | | | | | | 142.03 | 24.35 | 0.83 | −21.47 | −1.62 | −0.32 | 10.79 | - | - | 144.69 | 493.9 | 1.52 | 2.89 | |
| | | | | | | | | 141.22 | 20.61 | 0.42 | −14.45 | −10.02 | −0.27 | 12.24 | −0.00025 | 21.05 | | | | | |
| | 60 | 149.08 | 2.86 | 7.61 | 28.57 | 0 | 45 | - | 4.84 | - | - | - | −0.21 | 16.45 | - | - | 180.41 | 6998.5 | 1.52 | 5.79 | 25 |
| | −152 | | | | | | | 171.91 | 24.24 | 0.33 | −18.24 | −25.30 | −0.23 | 11.70 | - | - | 183.23 | 293.1 | 1.52 | 5.28 | |
| | | | | | | | | 159.86 | 20.53 | 0.38 | −13.35 | −5.10 | −0.19 | 14.67 | −0.00025 | 21.05 | | | | | |
| Touriga Nacional | 1 | 688.00 | 1.06 | 35.57 | 26.38 | 0 | 45 | - | 16.11 | - | - | - | −0.21 | 16.46 | - | - | 133.81 | 13,660.2 | 1.59 | 2.15 | 25 |
| | −121 | | | | | | | 117.39 | 21.11 | 0.19 | −22.31 | −18.25 | −0.21 | 15.44 | - | - | 123.57 | 774.2 | 1.54 | 0.92 | |
| | | | | | | | | 124.23 | 19.76 | 0.47 | −27.59 | −0.002 | −0.14 | 17.19 | −0.00025 | 21.05 | | | | | |
| | 60 | 199.94 | 0.80 | 8.19 | 28.71 | 0 | 45 | - | 5.20 | - | - | - | −0.21 | 16.45 | - | - | 165.37 | 12,985.3 | 1.57 | 2.40 | 25 |
| | −152 | | | | | | | 148.45 | 20.97 | 0.61 | −22.96 | −6.80 | −0.21 | 15.47 | - | - | 144.19 | 823.9 | 1.55 | 0.42 | |
| | | | | | | | | 150.90 | 20.54 | 0.26 | −8.36 | −0.72 | −0.14 | 17.87 | −0.00025 | 21.05 | | | | | |

**Table 3.** AV (average) parameter sets for each combination of models, grapevine varieties and starting dates. $C_{crit}$ = critical amount of chilling and $F_{crit}$ = critical amount of forcing.

| | | GDD | | WANG | | | | UNIFORC/UNICHILL/UNIFIED | | | | | | | | BRIN h/BRIN d | | | | |
|---|---|---|---|---|---|---|---|---|---|---|---|---|---|---|---|---|---|---|---|---|
| **Variety** | $t_0$ | $F_{crit}$ | $T_b$ | $F_{crit}$ | $T_{opt}$ | $T_{min}$ | $T_{max}$ | $C_{crit}$ | $F_{crit}$ | a | b | c | d | e | w | z | $C_{crit}$ | $F_{crit}$ | $Q_{10c}$ | $T_l$ | $T_h$ |
| Cabernet Sauvignon | 1 | 765.16 | 0 | 68.54 | 17.99 | 0 | 45 | - | 16.42 | - | - | - | −0.21 | 16.45 | - | - | 182.31 | 11,075.3 | 1.54 | 2.07 | 25 |
| | −121 | | | | | | | 145.70 | 24.79 | 0.18 | −20.62 | −20.10 | −0.19 | 11.91 | - | - | 177.95 | 508.7 | 1.55 | 1.49 | |
| | | | | | | | | 152.62 | 20.60 | 0.94 | −23.60 | −2.86 | −0.22 | 12.08 | -0.00025 | 21.05 | | | | | |
| | 60 | 225.25 | 3.16 | 11.83 | 28.64 | 0 | 45 | - | 7.31 | - | - | - | −0.21 | 16.46 | - | - | 196.01 | 11,942.8 | 1.56 | 1.91 | 25 |
| | −152 | | | | | | | 176.29 | 25.03 | 0.18 | −21.03 | −18.95 | −0.19 | 11.89 | - | - | 193.98 | 496.5 | 1.61 | 1.80 | |
| | | | | | | | | 180.78 | 20.59 | 0.87 | −27.91 | −4.13 | −0.19 | 12.69 | -0.00025 | 21.05 | | | | | |
| Chardonnay | 1 | 527.48 | 0.91 | 22.21 | 28.11 | 0 | 45 | - | 11.02 | - | - | - | −0.22 | 16.91 | - | - | 150.00 | 6316.0 | 1.61 | 4.97 | 25 |
| | −121 | | | | | | | 127.15 | 14.36 | 0.57 | −22.95 | −14.48 | −0.25 | 14.42 | - | - | 167.46 | 254.1 | 1.54 | 4.63 | |
| | | | | | | | | 130.52 | 20.32 | 0.88 | −24.70 | −2.52 | −0.27 | 11.40 | -0.00025 | 21.05 | | | | | |
| | 60 | 47.34 | 7.24 | 4.10 | 21.26 | 0 | 45 | - | 1.50 | - | - | - | −0.30 | 18.30 | - | - | 171.33 | 5931.7 | 1.61 | 5.35 | 25 |
| | −152 | | | | | | | 160.41 | 17.18 | 0.65 | −27.13 | −13.07 | −0.25 | 13.11 | - | - | 184.56 | 266.4 | 1.55 | 4.44 | |
| | | | | | | | | 163.81 | 20.45 | 0.85 | −28.65 | −3.25 | −0.26 | 11.35 | -0.00025 | 21.05 | | | | | |
| Grenache | 1 | 653.93 | 0 | 54.66 | 19.74 | 0 | 45 | - | 13.61 | - | - | - | −0.21 | 16.50 | - | - | 184.09 | 6316.6 | 1.58 | 4.31 | 25 |
| | −121 | | | | | | | 126.06 | 8.07 | 1.04 | −26.44 | −8.24 | −0.26 | 16.68 | - | - | 172.80 | 286.7 | 1.66 | 3.87 | |
| | | | | | | | | 151.30 | 20.59 | 0.78 | −24.27 | −5.82 | −0.24 | 10.49 | -0.00025 | 21.05 | | | | | |
| | 60 | 113.43 | 4.85 | 6.61 | 29.66 | 0 | 45 | - | 3.96 | - | - | - | −0.23 | 17.10 | - | - | 182.40 | 8882.5 | 1.67 | 2.97 | 25 |
| | −152 | | | | | | | 150.54 | 10.30 | 0.90 | −28.01 | −10.48 | −0.24 | 16.05 | - | - | 198.81 | 324.5 | 1.60 | 3.11 | |
| | | | | | | | | 173.87 | 20.58 | 0.80 | −25.81 | −5.45 | −0.24 | 11.04 | -0.00025 | 21.05 | | | | | |
| Gewürrtztraminer | 1 | 178.85 | 6.24 | 11.97 | 31.26 | 0 | 45 | - | 8.95 | - | - | - | −0.23 | 18.17 | - | - | 251.39 | 5324.3 | 1.71 | 5.01 | 25 |
| | −121 | | | | | | | 154.79 | 13.62 | 0.88 | −28.20 | −14.15 | −0.26 | 14.32 | - | - | 264.22 | 228.9 | 1.60 | 4.53 | |
| | | | | | | | | 149.42 | 20.26 | 0.89 | −23.75 | −8.10 | −0.25 | 11.17 | -0.00025 | 21.05 | | | | | |
| | 60 | 314.55 | 2.55 | 12.43 | 29.91 | 0 | 45 | - | 9.12 | - | - | - | −0.22 | 16.46 | - | - | 280.20 | 5274.6 | 1.66 | 5.05 | 25 |
| | −152 | | | | | | | 157.90 | 12.92 | 0.93 | −26.85 | −13.41 | −0.25 | 14.65 | - | - | 291.30 | 232.9 | 1.62 | 4.44 | |
| | | | | | | | | 176.90 | 20.45 | 0.71 | −25.17 | −8.95 | −0.26 | 10.95 | −0.00025 | 21.05 | | | | | |
| Pinot Gris | 1 | 126.62 | 7.39 | 12.26 | 31.26 | 0 | 45 | - | 7.61 | - | - | - | −0.25 | 18.35 | - | - | 271.42 | 6580.6 | 1.56 | 3.75 | 25 |
| | −121 | | | | | | | 169.54 | 14.04 | 0.89 | −27.31 | −13.36 | −0.23 | 14.11 | - | - | 269.51 | 287.7 | 1.59 | 3.29 | |
| | | | | | | | | 173.20 | 20.38 | 0.69 | −22.47 | −9.57 | −0.25 | 10.82 | −0.00025 | 21.05 | | | | | |
| | 60 | 359.67 | 1.77 | 15.09 | 28.93 | 0 | 45 | - | 9.48 | - | - | - | −0.21 | 16.47 | - | - | 292.53 | 6507.2 | 1.61 | 3.86 | 25 |
| | −152 | | | | | | | 188.72 | 14.01 | 0.85 | −25.77 | −12.46 | −0.24 | 14.19 | - | - | 299.62 | 290.8 | 1.57 | 3.24 | |
| | | | | | | | | 184.87 | 20.47 | 0.77 | −21.17 | −8.63 | −0.27 | 10.65 | −0.00025 | 21.05 | | | | | |
| Riesling | 1 | 156.13 | 6.78 | 12.43 | 31.26 | 0 | 45 | - | 8.51 | - | - | - | −0.23 | 18.47 | - | - | 267.92 | 6755.6 | 1.65 | 3.75 | 25 |
| | −121 | | | | | | | 167.21 | 13.93 | 0.94 | −25.59 | −11.82 | −0.24 | 14.39 | - | - | 270.05 | 317.7 | 1.63 | 2.84 | |
| | | | | | | | | 166.51 | 20.56 | 0.95 | −24.12 | −8.63 | −0.26 | 10.92 | −0.00025 | 21.05 | | | | | |
| | 60 | 416.44 | 0.93 | 16.95 | 28.35 | 0 | 45 | - | 9.76 | - | - | - | −0.21 | 16.65 | - | - | 294.27 | 6967.0 | 1.66 | 3.58 | 25 |
| | −152 | | | | | | | 176.49 | 13.62 | 0.99 | −27.07 | −12.29 | −0.27 | 13.61 | - | - | 296.64 | 297.4 | 1.66 | 3.20 | |
| | | | | | | | | 174.36 | 20.30 | 1.03 | −25.01 | −7.57 | −0.26 | 10.71 | −0.00025 | 21.05 | | | | | |
| Touriga Franca | 1 | 759.41 | 0.07 | 36.55 | 26.40 | 0 | 45 | - | 15.97 | - | - | - | −0.21 | 16.87 | - | - | 154.21 | 8897.4 | 1.54 | 4.39 | 25 |
| | −121 | | | | | | | 137.46 | 19.81 | 0.69 | −22.91 | −8.82 | −0.24 | 14.33 | - | - | 149.90 | 363.8 | 1.57 | 4.42 | |
| | | | | | | | | 137.41 | 20.48 | 0.73 | −23.67 | −6.05 | −0.23 | 13.26 | −0.00025 | 21.05 | | | | | |
| | 60 | 143.12 | 3.71 | 7.49 | 28.97 | 0 | 45 | - | 4.96 | - | - | - | −0.21 | 16.46 | - | - | 178.92 | 8466.3 | 1.54 | 4.63 | 25 |
| | −152 | | | | | | | 148.81 | 24.27 | 0.63 | −25.76 | −11.79 | −0.22 | 14.28 | - | - | 178.72 | 387.1 | 1.56 | 4.20 | |
| | | | | | | | | 165.50 | 20.42 | 0.64 | −22.47 | −5.83 | −0.21 | 13.90 | −0.00025 | 21.05 | | | | | |
| Touriga Nacional | 1 | 710.02 | 0.77 | 37.39 | 26.29 | 0 | 45 | - | 16.73 | - | - | - | −0.21 | 16.49 | - | - | 106.82 | 15,757.2 | 1.81 | 2.14 | 25 |
| | −121 | | | | | | | 108.60 | 19.98 | 0.59 | −23.76 | −7.24 | −0.22 | 15.56 | - | - | 118.99 | 694.1 | 1.58 | 1.98 | |
| | | | | | | | | 108.85 | 20.33 | 0.72 | −24.30 | −2.98 | −0.16 | 16.91 | −0.00025 | 21.05 | | | | | |
| | 60 | 176.18 | 1.89 | 9.42 | 26.87 | 0 | 45 | - | 4.86 | - | - | - | −0.21 | 16.66 | - | - | 134.59 | 16,289.3 | 1.71 | 1.86 | 25 |
| | −152 | | | | | | | 123.73 | 20.27 | 0.62 | −23.51 | −12.11 | −0.22 | 15.53 | - | - | 140.60 | 691.0 | 1.65 | 1.92 | |
| | | | | | | | | 139.52 | 20.67 | 0.82 | −25.39 | −3.31 | −0.16 | 16.66 | −0.00025 | 21.05 | | | | | |

A deeper analysis of the model validation showed that the normalized difference between HP and AV, (HP-AV/HP)*100, was higher in CF ($R^2$ = 11.99%, AIC = 3.36%, RMSE = 22.20%) compared to F models ($R^2$ = 5.73%, AIC = 1.51%, RMSE = 8.16%). Among CF models, UNICHILL model showed the lowest difference between HP and AV in terms of $R^2$ and AIC ($R^2$ = 6.20%, AIC = 2.70%), while it evidenced the highest difference in terms of RMSE (40.02%). Considering F models, WANG showed the highest difference ($R^2$ = 7.07%, AIC = 2.25%, RMSE = 9.38%) and UNIFORC, the lowest ($R^2$ = 4.21%, AIC = 0.84%, RMSE = 7.13%). Following the same trend, the starting dates 1st September and 1st August ($R^2$ = 3.89%, AIC = 0.86%, RMSE = 15.62%) showed bigger differences compared to 1st January and 1st March ($R^2$ = 2.96%, AIC = 0.72%, RMSE = 7.62%). In particular, 1st September showed a lower difference in terms of AIC and RMSE (AIC = 0.86%, RMSE = 13.53%) compared to 1st August in CF models while 1st January showed the highest difference in F models ($R^2$ = 2.88%, AIC = 0.65%, RMSE = 7.23%). Finally, regarding grapevine varieties, the highest difference was found for Touriga Nacional ($R^2$ = 23.96%, RMSE = 24.20%) while the lowest was shown by Chardonnay in terms of $R^2$ (1.89%) and by Touriga Franca in terms of AIC and RMSE (1.10% and 9.55%, respectively).

### *3.3. Model Applications on Other Independent Datasets*

The statistical performances of the phenological models, applied on the respective independent datasets, are reported in Figure 5 and Figures S10–S16 while the comparison between CF and F models during fitting and applications is shown in Figure 6 and Figure S17. In general, higher performances were found for CF compared to F models during fitting and applications (Figure 5), except for those varieties characterized by few observed data in the model application (Gewürztraminer, Riesling; Figure 6 and Figure S17).

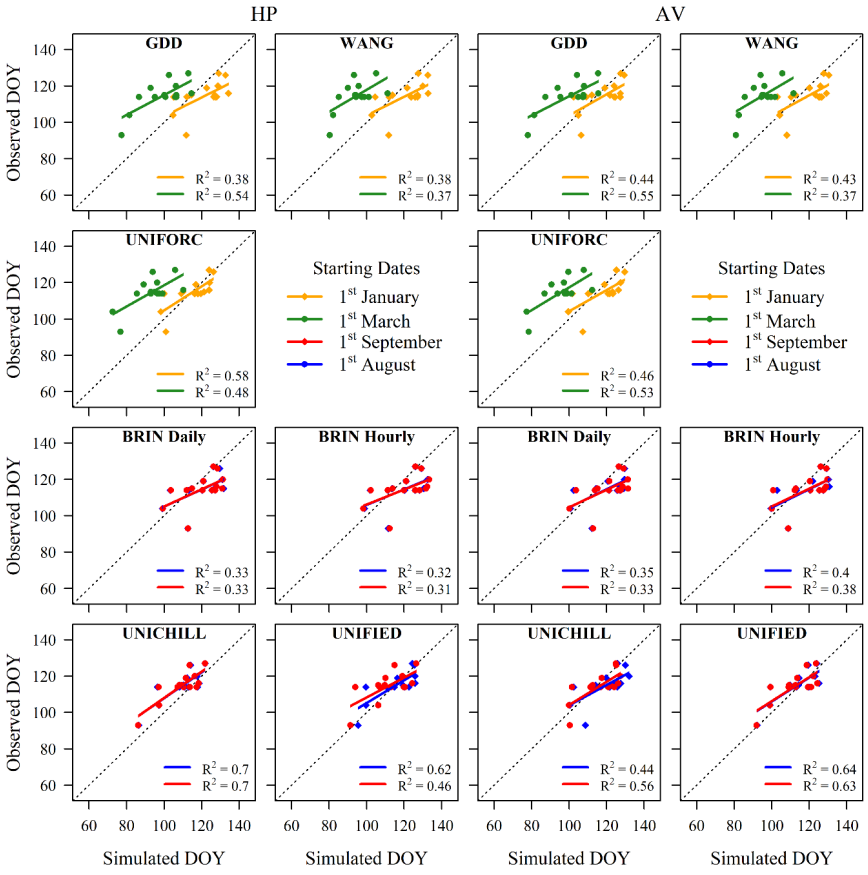


**Figure 5.** Highest-performance (HP) and average (AV) parameters' set applied on the independent datasets by considering all phenological models and starting dates. The example of Chardonnay variety.

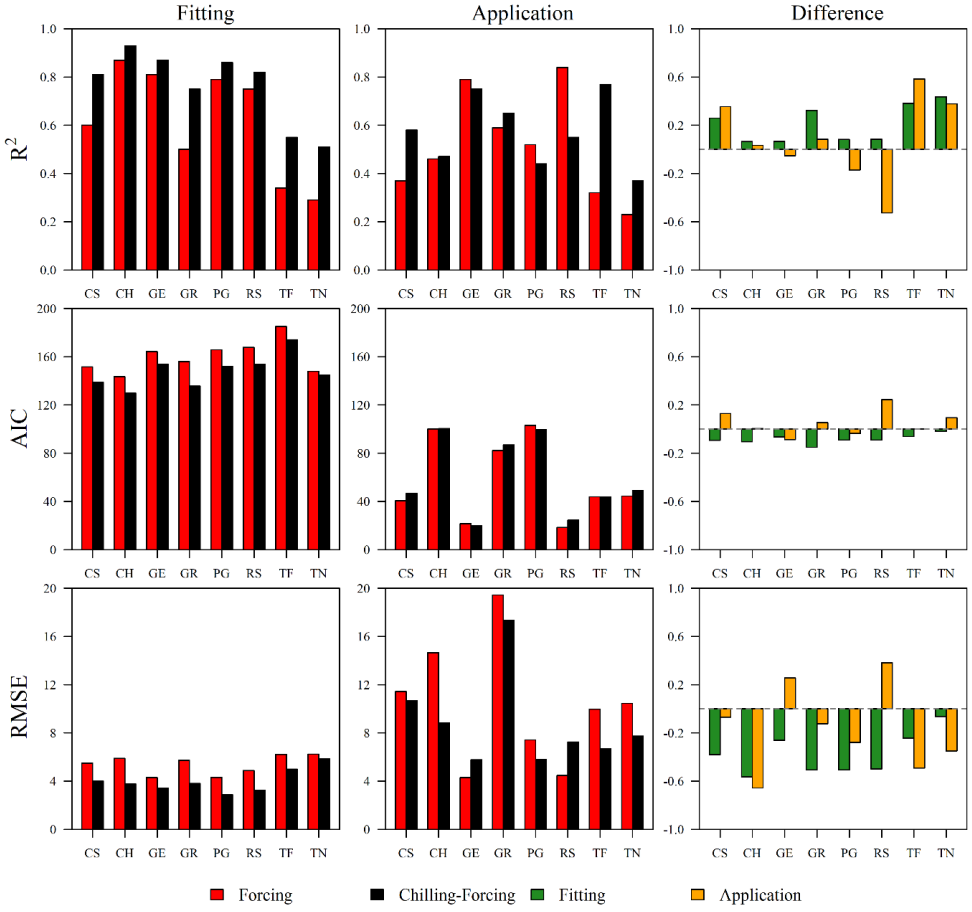


**Figure 6.** Statistical results ($R^2$, AIC and RMSE) of the comparison between CF (black bars) and F (red bars) approaches in model fitting and application for all grapevine varieties using HP parameter set. The differences between CF and F models (CF-F) in both fitting and applications are displayed using green and yellow bars, respectively. CS = Cabernet Sauvignon, CH = Chardonnay, GE = Gewürztraminer, GR = Grenache, PG = Pinot Gris, RS = Riesling, TF = Touriga Franca, TN = Touriga Nacional.

In particular, the model application showed similar performances for both HP ($R^2$ = 0.55, AIC = 57.97, RMSE = 9.41) and AV ($R^2$ = 0.54, AIC = 58.37, RMSE = 9.26) parameter sets. However, this difference slightly increased when CF ($R^2$ = 0.56, AIC = 59.05, RMSE = 8.75) and F models ($R^2$ = 0.52, AIC = 57.01, RMSE = 10.01) were compared without distinguishing between HP and AV parameterizations. Therefore, CF models showed better results in terms of $R^2$ (+8%) and RMSE (−15%) compared to F models while lower results of AIC value were obtained for CF compared to F models (+3.44%). A detailed analysis revealed that the CF models with highest performances ($R^2$ and AIC) were UNICHILL ($R^2$ = 0.64, AIC = 56.74) and UNIFIED ($R^2$ = 0.58, AIC = 56.61) models, while, in F models, the better results were provided by UNIFORC ($R^2$ = 0.54, AIC = 55.98). However, in terms of RMSE, highest performances were found for BRIN hourly (8.37, CF) and GDD (9.67, F). Concerning the starting dates, similar results were found when the 1st September ($R^2$ = 0.58, AIC = 58.92, RMSE = 8.55) and 1st of August ($R^2$ = 0.57, AIC = 59.17, RMSE = 8.95) were analyzed, with the 1st September showing better performance ($R^2$ = +1.83%, AIC = -0.44% and RMSE = -4.68%). Instead, higher differences were found when the 1st January ($R^2$ = 0.55, AIC = 60.47, RMSE = 7.74) and 1st of March ($R^2$ = 0.49, AIC = 52.57, RMSE = 12.47) were compared, evidencing the most relevant performances for 1st January ($R^2$ = +10.83% and RMSE = −61.23%, with the exception of AIC = +14.15%).

Moreover, the behavior of grapevine varieties in response to specific climate conditions was noticed during model application. The higher performances of CF compared to F, as well the relevant

differences between starting dates when F models were used, may be explained by the influence of temperatures on the dormancy period. The end of the first phase of dormancy (endo-dormancy) in CF models was generally simulated between the end of December (e.g., Touriga Nacional: DOY 356 for $t_0$ = −121 and −152, respectively) and end of February (e.g., Riesling: DOY 56 and 57 for $t_0$ = −121 and −152, respectively). More specifically, the period of endo-dormancy fulfilment was similarly reached regardless of starting date (1st September/August), allowing the next forcing unit accumulation during the eco-dormancy period to be correctly satisfied (differences in days from 0 to 3 days). The analysis further highlighted that the endo-dormancy release occurs later at northern than at southern latitudes and this is consistent with results obtained using F approach. These demonstrate that a late starting date (1st of March) for forcing unit accumulation is more suitable for budbreak simulation of varieties collected in Northern Europe (e.g., Gewürztraminer, Riesling and Pinot Gris), whose endo-dormancy release is simulated by CF late in the season (54 DOY on average). Conversely, an early starting date (1 January) provided the best results in simulating budbreak for grapevine varieties collected in Southern Europe (e.g., Touriga Franca and Nacional, Cabernet Sauvignon, Grenache and Chardonnay), which are characterized by an early end of endo-dormancy as simulated by CF models (13 DOY on average).

## 4. Discussion

This study compares the performance of six phenological models in simulating the budbreak date of eight grapevine varieties across different European sites. We found that the model performances characterized by a Chilling-Forcing approach were generally higher compared to those obtained for Forcing approach when different starting dates were set (Figure 6 and Figure S17).

Although model intercomparison studies on the estimation of budbreak date in grapevine have already been conducted by other authors [15,29,30], this study focused on evaluation of the models' reliability to reproduce budbreak in different environmental conditions, by considering the impact of temperature during the chilling and forcing accumulation period. In contrast to other works [27,30,57,58], this model intercomparison considers the use of a long-term series of observed phenology, which include grapevine varieties with different precocity levels collected at various latitudes in three European countries (France, Luxembourg and Portugal, Figure 1 and Table 1). The extensive observed dataset coupled to the methodology applied in this study allowed to evaluate the influence of study site-temperature variability on the grapevine development. Moreover, the cross-validation scheme adopted in this model intercomparison experiment provided an exhaustive analysis of the bias and variance of the CF and F models while the comparison between two different types of parameterization (HP or AV) pointed out the issue to select a specific parameter set for model applications (Results section, Figure 5). This in-depth investigation of model fitting, validation and application was particularly useful for evaluating the influence of temperature during the dormancy period. In this context, the different model responses during budbreak predictions are related to the physiological requirements needed for dormancy fulfilment of the grapevine varieties. Differently from the CF models, which describe the entire dormancy period (endo- and eco-dormancy), the F models only describe the eco-dormancy period through forcing units accumulation, under the assumption that the chilling requirement was already satisfied [24]. Although the debate on which model type provides the highest reliability is still open [29,30], our analysis shows that CF models, considering the influences of winter and spring temperatures on the accumulation of chilling and forcing units, may avoid the under- or over-estimation at the beginning of eco-dormancy, which occur when F models are set on fixed dates. In this study, we estimated a longer endo-dormancy for the vines from the Northern European sites (e.g., Gewürztraminer), which occurs later than the endo-dormancy of vines from the Southern European sites (e.g., Touriga Nacional), irrespective of the precocity level of the different varieties. In other terms, grapevine varieties such as Gewürztraminer (early budbreak) and Riesling (late budbreak) collected in Northern Europe showed a late endo-dormancy release (higher chilling requirement) with respect to Chardonnay (early budbreak) and Cabernet Sauvignon (late budbreak)

mainly collected in Southern Europe (lower chilling requirement). Although this trend was examined in this study only from a modeling point of view without any physiological evidence on the dormancy period, our results suggested that plants cultivated at different latitudes might show distinct dormancy period lengths. The higher accuracy of CF compared to F models is likely linked to the ability of these models to estimate the endo-dormancy release and to better account for the effect of temperature in this phase, avoiding the use of a fixed a priori value for the beginning of the eco-dormancy period as in F models [27,29]. Indeed, the goodness of F models is shown to significantly increase when the starting date is optimized against observed experimental data [30,45], demonstrating that the beginning of eco-dormancy period is dependent to the origin of the observed dataset and, thus, on the fulfilment of specific physiological requirements that change in relation to the climate conditions of the different environments. In fact, although no relevant differences were found for budbreak date estimation of grapevine varieties using CF models set on 1st of September/August starting dates, the discrepancy of the F model simulations was evident when 1st of January/March dates were used. Higher accuracy of F models to predict the budbreak date of grapevine varieties collected in Northern European countries was observed using the 1st of March starting date as also confirmed by [27], while the 1st January seems to be a more suitable starting date for representing budbreak date of the grapevine varieties from Southern Europe (Figures S5–S7). In this case, a compromise between both starting dates may be represented by the beginning of February [59]. However, the adoption of different starting dates in F models highlights the role of temperature on bud growth and the need to satisfy specific dormancy requirements for varieties cultivated at different latitudes before budbreak occurrence. These results were supported by the work of Reis-Pereira et al. [60] on the grapevine flowering stage. The authors pointed out that the selection of a priori value for the starting of thermal unit accumulation in F models may lead to an under- or over-estimation of the flowering phase, demonstrating the importance of a correct evaluation of the previous phenological stage in respect to the subsequent one. These findings were also observed in relation to the flowering stage of other species such as olive tree e.g., [61]). In this context, we infer that the dormancy period of grapevine may play a relevant role for predicting budbreak date especially under future scenarios. Indeed, more accurate estimations of budbreak date using CF models are provided when the endo-dormancy release is calibrated against observed data of perennial crops. This behavior is particularly evident under warmer temperatures (after 2050) where CF without endo-dormancy calibration and F models showed poor performances of phenology prediction [62]. The accurate identification of the endo-dormancy release avoids selecting a fixed a priori date, especially when this may have strong consequences on the estimation of budbreak date (as in F models).

The impact of warmer temperatures after the endo-dormancy release showed higher effect on the budbreak phase compared to the influence of temperatures during chilling accumulation, as reported by Martinez-Lüscher et al. [63] in a two-year ad hoc experiment with different grapevine varieties and temperature regimes. However, the starting date for thermal unit accumulation depends on the physiological features of the grapevine variety and their interaction with the environment. Indeed, we found that the effect of temperature during the last part of winter and beginning of spring was also evident when models were tested on external sites (independent datasets, Figure 5). Although most of the models showed satisfactory results during application ($R^2$ and AIC), the average error (RMSE) between observed and simulated data was relatively high (from 4 to 19 days). This situation was exacerbated in F models where the reliability in simulating budbreak is dependent to the use of a specific starting date (1st of January/1st of March) and thus the original observed dataset. The discrepancy between the two starting dates raises the question of which initial date to choose for forcing unit accumulation when simulations are conducted on a European scale [31,64].

The implications of this study are particularly relevant for growers especially when considering the impact of climate change. Our study, in line with a large part of literature, confirmed that chill units accumulations, the amount of which varies according to variety and location, is required for exiting from endo-dormancy phase. In a warmer climate, as expected in the future, this amount may not fully satisfy, leading to developmental issues during the growing season as outlined in the introduction of this paper. Some authors already highlighted that, on a global scale, wine areas may shift to match their specific climate niches in case of no adaptation [11,65], while new varietal selections and breeding programmes are needed for improving the adaptability of the grapevine varieties and maintaining the high quality production [12,59,66]. In this context, our parameterizations may be used as metric, in combination with climate simulations under future scenarios, to highlight which regions and varieties are expected to be most exposed to the risk of budbreak failure. Accordingly, the use of alternative varieties, better adapted to the expected future climate, may be proposed or the direction of specific breeding programmes can be indicated to develop varieties with a lower chill units requirement as requested in a warmer climate. Moreover, we should also take into account that, besides thermal requirements, dormancy phase may be influenced by the photoperiod [67]. Since each grapevine variety requires critical thresholds of day length for the onset of dormancy [68,69], this regulating factor should be considered when CF models are adopted for simulations at different latitudes. As such, comprehensive datasets of phenological observations and ad hoc experiments for evaluating the influence of more factors on dormancy [30,46,69] may be useful to take into account for improving model reliability under future climate scenarios and different environments [31,64,70].

## 5. Conclusions

This model intercomparison evidenced the different performance of the phenological models in reproducing the budbreak date of eight grapevine varieties collected in different European regions. The reliability of two main phenological modeling approaches (CF and F) was evaluated considering different starting dates (1st January/March or 1st September/August) and the selection methodologies of the parameter set (HP and AV) for model application. The results showed, in general, higher performances of CF compared to F models where fixed starting dates were adopted, even if neither modeling approach highlighted a clear supremacy over the other. For this reason, CF and F models' behavior should be further investigated through ad hoc experiments for evaluating the role of dormancy on budbreak occurrence. Indeed, the findings of our model simulations evidenced distinct thermal requirements for grapevine varieties cultivated at different latitudes (i.e., Northern Europe vs. Southern Europe). The use of different starting dates highlighted that, unlike CF models, the accurate estimation of budbreak in F models is affected by the selection of a starting date for beginning of the eco-dormancy period. This implies that, if this phase is not accurately defined, F models may lead to over- or under-estimations of the budbreak date under different environmental conditions. In this context, comprehensive phenological datasets (e.g., grapevine phenological data collected at different latitudes) are needed to thoroughly investigate the effect of temperature variability on dormancy period and budbreak estimation. Finally, it is proposed the development and implementation of improved phenological models, which consider the effect of other climate (e.g., radiation) and soil (e.g., soil temperature) variables as well as some regulating factors of the endo-dormancy phase (e.g., day length).

**Supplementary Materials:** The following are available online at http://www.mdpi.com/2076-3417/10/11/3800/s1. Figure S1: $R^2$ and AIC values of the BRIN Daily model obtained for all fitted and average models, grapevine varieties and starting dates. The symbols (points and triangles) show the model results at two starting dates (in this example $t_0$ = −121 and −152 DOY), while the two colours represent fitting (red) and validation (blue) procedure, respectively. The filled symbols constitute the $R^2$ and AIC values of the models obtained by the selected HP parameter sets, while the dashed (fitting) and dotted (validation) lines depict the average $R^2$ and AIC values for both starting dates (in this example orange line = −121 DOY and green line = −152 DOY). The boxplots represent the $R^2$ and AIC values distribution for HP (orange and light blue: HP model application on all validation subsamples for $t_0$ = −121 and $t_0$ = −152 DOY, respectively) and AV (boxplot in the shaded area, orange and light blue: AV application on all validation subsamples for t0 = −121 and t0 = −152 DOY, respectively). The outliers represent all values out of the 1.5*InterQuartile Range (IQR) of the boxplot. Figure S2: $R^2$ and AIC values of the BRIN Hourly model obtained for all fitted and average models, grapevine varieties and starting dates. The symbols (points and triangles) show the model results at two starting dates (in this example $t_0$ = −121 and −152 DOY), while the two colours represent fitting (red) and validation (blue) procedure, respectively. The filled symbols constitute the $R^2$ and AIC values of the models obtained by the selected HP parameter sets, while the dashed (fitting) and dotted (validation) lines depict the average $R^2$ and AIC values for both starting dates (in this example orange line = -121 DOY and green line = -152 DOY). The boxplots represent the $R^2$ and AIC values distribution for HP (orange and light blue: HP model application on all validation subsamples for $t_0$ = −121 and $t_0$ = -152 DOY, respectively) and AV (boxplot in the shaded area, orange and light blue: AV application on all validation subsamples for $t_0$ = -121 and $t_0$ = −152 DOY, respectively). The outliers represent all values out of the 1.5*InterQuartile Range (IQR) of the boxplot. Figure S3: $R^2$ and AIC values of the UNICHILL model obtained for all fitted and average models, grapevine varieties and starting dates. The symbols (points and triangles) show the model results at two starting dates (in this example $t_0$ = −121 and −152 DOY), while the two colours represent fitting (red) and validation (blue) procedure, respectively. The filled symbols constitute the $R^2$ and AIC values of the models obtained by the selected HP parameter sets, while the dashed (fitting) and dotted (validation) lines depict the average $R^2$ and AIC values for both starting dates (in this example orange line = −121 DOY and green line = −152 DOY). The boxplots represent the $R^2$ and AIC values distribution for HP (orange and light blue: HP model application on all validation subsamples for $t_0$ = −121 and $t_0$ = −152 DOY, respectively) and AV (boxplot in the shaded area, orange and light blue: AV application on all validation subsamples for $t_0$ = −121 and $t_0$ = −152 DOY, respectively). The outliers represent all values out of the 1.5*InterQuartile Range (IQR) of the boxplot. Figure S4: $R^2$ and AIC values of the UNIFIED model obtained for all fitted and average models, grapevine varieties and starting dates. The symbols (points and triangles) show the model results at two starting dates (in this example $t_0$ = −121 and −152 DOY), while the two colours represent fitting (red) and validation (blue) procedure, respectively. The filled symbols constitute the $R^2$ and AIC values of the models obtained by the selected HP parameter sets, while the dashed (fitting) and dotted (validation) lines depict the average $R^2$ and AIC values for both starting dates (in this example orange line = −121 DOY and green line = −152 DOY). The boxplots represent the $R^2$ and AIC values distribution for HP (orange and light blue: HP model application on all validation subsamples for $t_0$ = −121 and $t_0$ = −152 DOY, respectively) and AV (boxplot in the shaded area, orange and light blue: AV application on all validation subsamples for $t_0$ = −121 and $t_0$ = -152 DOY, respectively). The outliers represent all values out of the 1.5*InterQuartile Range (IQR) of the boxplot. Figure S5: $R^2$ and AIC values of the UNIFORC model obtained for all fitted and average models, grapevine varieties and starting dates. The symbols (points and triangles) show the model results at two starting dates (in this example $t_0$ = 1 and 60 DOY), while the two colours represent fitting (red) and validation (blue) procedure, respectively. The filled symbols constitute the $R^2$ and AIC values of the models obtained by the selected HP parameter sets, while the dashed (fitting) and dotted (validation) lines depict the average $R^2$ and AIC values for both starting dates (in this example orange line = 1 DOY and green line = 60 DOY). The boxplots represent the $R^2$ and AIC values distribution for HP (orange and light blue: HP model application on all validation subsamples for $t_0$ = 1 and $t_0$ = 60 DOY, respectively) and AV (boxplot in the shaded area, orange and light blue: AV application on all validation subsamples for $t_0$ = 1 and $t_0$ = 60 DOY, respectively). The outliers represent all values out of the 1.5*InterQuartile Range (IQR) of the boxplot. Figure S6: $R^2$ and AIC values of the GDD model obtained for all fitted and average models, grapevine varieties and starting dates. The symbols (points and triangles) show the model results at two starting dates (in this example $t_0$ = 1 and 60 DOY), while the two colours represent fitting (red) and validation (blue) procedure, respectively. The filled symbols constitute the $R^2$ and AIC values of the models obtained by the selected HP parameter sets, while the dashed (fitting) and dotted (validation) lines depict the average $R^2$ and AIC values for both starting dates (in this example orange line = 1 DOY and green line = 60 DOY). The boxplots represent the $R^2$ and AIC values distribution for HP (orange and light blue: HP model application on all validation subsamples for $t_0$ = 1 and $t_0$ = 60 DOY, respectively) and AV (boxplot in the shaded area, orange and light blue: AV application on all validation subsamples for $t_0$ = 1 and $t_0$ = 60 DOY, respectively). The outliers represent all values out of the 1.5*InterQuartile Range (IQR) of the boxplot. Figure S7: $R^2$ and AIC values of the WANG model obtained for all fitted and average models, grapevine varieties and starting dates. The symbols (points and triangles) show the model results at two starting dates (in this example $t_0$ = 1 and 60 DOY), while the two colours represent fitting (red) and validation (blue) procedure, respectively. The filled symbols constitute the $R^2$ and AIC values of the models obtained by the selected HP parameter sets, while the dashed (fitting) and dotted (validation) lines depict the average $R^2$ and

AIC values for both starting dates (in this example orange line = 1 DOY and green line = 60 DOY). The boxplots represent the $R^2$ and AIC values distribution for HP (orange and light blue: HP model application on all validation subsamples for $t_0$ = 1 and $t_0$ = 60 DOY, respectively) and AV (boxplot in the shaded area, orange and light blue: AV application on all validation subsamples for $t_0$ = 1 and $t_0$ = 60 DOY, respectively). The outliers represent all values out of the 1.5*InterQuartile Range (IQR) of the boxplot. Figure S8: Correlations between observed and simulated budbreak Days of Year (DOY) of the UNIFORC and UNICHILL models. The results were obtained for all grapevine varieties and starting dates using the HP parameter set. Figure S9: Correlations between observed and simulated budbreak Days of Year (DOY) of the WANG and BRIN Daily models. The results were obtained for all grapevine varieties and starting dates using the HP parameter set. Figure S10: Highest-Performance (HP) and average (AV) parameters' set applied on the independent datasets by considering all phenological models and starting dates. The example of Cabernet sauvignon variety. Figure S11: Highest-Performance (HP) and average (AV) parameters' set applied on the independent datasets by considering all phenological models and starting dates. The example of Gewürztraminer variety. Figure S12: Highest-Performance (HP) and average (AV) parameters' set applied on the independent datasets by considering all phenological models and starting dates. The example of Grenache variety. Figure S13: Highest-Performance (HP) and average (AV) parameters' set applied on the independent datasets by considering all phenological models and starting dates. The example of Pinot Gris variety. Figure S14: Highest-Performance (HP) and average (AV) parameters' set applied on the independent datasets by considering all phenological models and starting dates. The example of Riesling variety. Figure S15: Highest-Performance (HP) and average (AV) parameters' set applied on the independent datasets by considering all phenological models and starting dates. The example of Touriga Franca variety. Figure S16: Highest-Performance (HP) and average (AV) parameters' set applied on the independent datasets by considering all phenological models and starting dates. The example of Touriga Nacional variety. Figure S17: Statistical results ($R^2$, AIC and RMSE) of the comparison between CF (black bars) and F (red bars) models in model fitting and application for all grapevine varieties using AV parameters' set. The differences between CF and F models in model fitting and applications were displayed using green and yellow bars, respectively. CS = Cabernet Sauvignon, CH = Chardonnay, GE = Gewürztraminer, GR = Grenache, PG = Pinot Gris, RS = Riesling, TF = Touriga Franca, TN = Touriga Nacional. Table S1: Statistical indices (RMSE, EF, $R^2$, AIC) obtained for all models, varieties and starting dates after model fitting and validation on all subsamples.

**Author Contributions:** Conceptualization, L.L., S.C.-A., J.A.S. and M.M.; methodology, L.L., S.C.-A., C.M., M.M., H.F., C.v.L., P.M.; data provision, D.M., J.J., A.D.-I., C.v.L., J.A.S., J.E.-D. and J.S.; writing—original draft preparation, L.L. and S.C.-A.; writing—review and editing, L.L., S.C.-A., J.A.S., C.M., H.F., D.M., P.M., J.J., T.K., A.D.-I., C.v.L., A.C.M., C.D., M.B. and M.M.; supervision, M.M.; funding acquisition, M.B. All authors have read and agreed to the published version of the manuscript.

**Funding:** This research was funded by the European Union's Horizon 2020 Research and Innovation Programme, under the Clim4Vitis project: "Climate change impact mitigation for European viticulture: knowledge transfer for an integrated approach", grant agreement no. 810176. It was also supported by FCT-Portuguese Foundation for Science and Technology, under the project UIDB/04033/2020 and the French National Research Agency (ANR) in the frame of the Investments for the Future Program, within the cluster of excellence COTE (ANR-10-LABX-45).

**Acknowledgments:** We wish to acknowledge the Clim4Vitis project "Climate change impact mitigation for European viticulture: knowledge transfer for an integrated approach", funded by European Union's Horizon 2020 Research and Innovation Program, under grant agreement no. 810176 that supported this study. H.F. thanks the FCT for contract CEECIND/00447/2017 and project COA/CAC/0030/2019.

**Conflicts of Interest:** The authors declare no conflict of interest.

## References

1. Mullins, M.G.; Bouquet, A.; Williams, L.E. *Biology of the Grapevine*; Cambridge University Press: Cambridge, UK, 1992.
2. Van Leeuwen, C.; Seguin, G. The concept of terroir in viticulture. *J. Wine Res.* **2006**, *17*, 1–10. [CrossRef]
3. Jones, G.V. Winegrape phenology. In *Phenology: An Integrative Environmental Science*; Schwartz, M.D., Ed.; Springer: Dordrecht, The Nederlands, 2013; pp. 563–584.
4. Jones, G.V.; Davis, R.E. Climate influences on grapevine phenology, grape composition, and wine production and quality for Bordeaux, France. *Am. J. Enol. Vitic.* **2000**, *51*, 249–261.
5. Menzel, A. A 500 year pheno-climatological view on the 2003 heatwave in Europe assessed by grape harvest dates. *Meteorol. Zeitschrift* **2005**, *14*, 75–77.
6. Tomasi, D.; Jones, G.V.; Giust, M.; Lovat, L.; Gaiotti, F. Grapevine Phenology and Climate Change: Relationships and Trends in the Veneto Region of Italy for 1964-2009. *Am. J. Enol. Vitic.* **2011**, *62*, 329–339.
7. Van Leeuwen, C.; Destrac-Irvine, A.; Dubernet, M.; Duchêne, E.; Gowdy, M.; Marguerit, E.; Pieri, P.; Parker, A.; de Rességuier, L.; Ollat, N. An Update on the Impact of Climate Change in Viticulture and Potential Adaptations. *Agronomy* **2019**, *9*, 514. [CrossRef]

8. Ramos, M.C.; Jones, G.V.; Martínez-Casasnovas, J.A. Structure and trends in climate parameters affecting winegrape production in northeast Spain. *Clim. Res.* **2008**, *38*, 1–15. [CrossRef]
9. Moriondo, M.; Bindi, M.; Fagarazzi, C.; Ferrise, R.; Trombi, G. Framework for high-resolution climate change impact assessment on grapevines at a regional scale. *Reg. Environ. Chang.* **2011**, *11*, 553–567.
10. Gaál, M.; Moriondo, M.; Bindi, M. Modelling the impact of climate change on the Hungarian wine regions using Random Forest. *Appl. Ecol. Environ. Res.* **2012**, *10*, 121–140.
11. Moriondo, M.; Jones, G.V.; Bois, B.; Dibari, C.; Ferrise, R.; Trombi, G.; Bindi, M. Projected shifts of wine regions in response to climate change. *Clim. Change* **2013**, *119*, 825–839. [CrossRef]
12. Wolkovich, E.M.; García de Cortázar-Atauri, I.; Morales-Castilla, I.; Nicholas, K.A.; Lacombe, T. From Pinot to Xinomavro in the world's future wine-growing regions. *Nat. Clim. Chang.* **2018**, *8*, 29–37. [CrossRef]
13. Fraga, H.; Pinto, J.G.; Santos, J.A. Climate change projections for chilling and heat forcing conditions in European vineyards and olive orchards: A multi-model assessment. *Clim. Chang.* **2019**, *152*, 179–193. [CrossRef]
14. Malheiro, A.C.; Campos, R.; Fraga, H.; Eiras-Dias, J.; Silvestre, J.; Santos, J.A. Winegrape phenology and temperature relationships in the Lisbon wine region, Portugal. *J. Int. Sci. Vigne Vin* **2013**, *47*, 287–299.
15. Costa, R.; Fraga, H.; Fonseca, A.; De Cortázar-Atauri, I.G.; Val, M.C.; Carlos, C.; Reis, S.; Santos, J.A. Grapevine phenology of cv. Touriga Franca and Touriga Nacional in the Douro wine region: Modelling and climate change projections. *Agronomy* **2019**, *9*, 1–20.
16. Molitor, D.; Junk, J. Climate change is implicating a two-fold impact on air temperature increase in the ripening period under the conditions of the Luxembourgish grapegrowing region. *OENO One* **2019**, *53*, 409–422. [CrossRef]
17. Shulman, Y.; Nir, G.; Fanberstein, L.; Lavee, S. The effect of cyanamide on the release from dormancy of grapevine buds. *Sci. Hortic. (Amsterdam)* **1983**, *19*, 97–104.
18. Wicks, A.S.; Johnson, J.O.; Bracho, E.; Jensen, F.L.; Neja, R.A.; Lider, L.A.; Weaver, R.J. Induction of early and more uniform budbreak in *Vitis vinifera* L. cvs. Perlette, Thompson Seedless, and Flame Seedless. In Proceedings of the Bud Dormancy in Grapevine: Potential and Practical Uses of Hydrogen Cyanamide on Grapevine, Fresno, CA, USA, 20 August 1984; Weaver, R.J., Ed.; University of California: Fresno, CA, USA, 1984; pp. 48–58.
19. Dokoozlian, N.K. Chilling temperature and duration interact on the budbreak of "Perlette" grapevine cuttings. *HortScience* **1999**, *34*, 1054–1056. [CrossRef]
20. Sarvas, R. Investigations on the annual cycle of development of forest trees. Autumn dormancy and winter dormancy. *Commun. Inst. For. Fenn.* **1974**, *84*, 1–101.
21. Pouget, R. Considérations Générales sur le rythme végétatif et la dormance des bourgeons de la Vigne. *Vitis* **1972**, *217*, 198–217.
22. Pouget, R. Nouvelle conception du seuil de croissance chez la vigne. *Vitis* **1968**, *7*, 201–205.
23. Richardson, E.A.; Seeley, S.D.; Walker, D.R.; Walker, D.I. A model for estimating the completion of rest for "Redhaven" and "Elberta" peach trees. *Hortic. Sci.* **1974**, *9*, 331–332.
24. Chuine, I. A unified model for budburst of trees. *J. Theor. Biol.* **2000**, *207*, 337–347. [CrossRef] [PubMed]
25. Cesaraccio, C.; Spano, D.; Snyder, R.L.; Duce, P. Chilling and forcing model to predict bud-burst of crop and forest species. *Agric. For. Meteorol.* **2004**, *126*, 1–13. [CrossRef]
26. Garcia de Cortazar-Atauri, I.; Brisson, N.; Seguin, B.; Gaudillere, J.; Baculat, E. Simulation of budbreak date for vine. The bring model. Some application in climate change study. In Proceedings of the XIV International GESCO Viticulture Congress, Geisenheim, Germany, 23–27 August 2005; pp. 485–490.
27. Nendel, C. Grapevine bud break prediction for cool winter climates. *Int. J. Biometeorol.* **2010**, *54*, 231–241. [CrossRef]
28. Caffarra, A.; Eccel, E. Projecting the impacts of climate change on the phenology of grapevine in a mountain area. *Aust. J. Grape Wine Res.* **2011**, *17*, 52–61. [CrossRef]
29. García de Cortázar-Atauri, I.; Brisson, N.; Gaudillere, J.P. Performance of several models for predicting budburst date of grapevine (*Vitis vinifera* L.). *Int. J. Biometeorol.* **2009**, *53*, 317–326. [CrossRef]
30. Fila, G.; Gardiman, M.; Belvini, P.; Meggio, F.; Pitacco, A. A comparison of different modelling solutions for studying grapevine phenology under present and future climate scenarios. *Agric. For. Meteorol.* **2014**, *195–196*, 192–205. [CrossRef]

31. Leolini, L.; Moriondo, M.; Fila, G.; Costafreda-Aumedes, S.; Ferrise, R.; Bindi, M. Late spring frost impacts on future grapevine distribution in Europe. *Field Crops Res.* **2018**, *222*, 197–208. [CrossRef]
32. Moriondo, M.; Ferrise, R.; Trombi, G.; Brilli, L.; Dibari, C.; Bindi, M. Environmental Modelling & Software Modelling olive trees and grapevines in a changing climate *. *Environ. Model. Softw.* **2015**, *72*, 387–401.
33. Molitor, D.; Junk, J.; Evers, D.; Hoffmann, L.; Beyer, M. A high-resolution cumulative degree day-based model to simulate phenological development of grapevine. *Am. J. Enol. Vitic.* **2014**, *65*, 72–80. [CrossRef]
34. Menne, M.J.; Durre, I.; Vose, R.S.; Gleason, B.E.; Houston, T.G. An overview of the global historical climatology network-daily database. *J. Atmos. Ocean. Technol.* **2012**, *29*, 897–910. [CrossRef]
35. Destrac-Irvine, A.; van Leeuwen, C. VitAdapt: An experimental program to study the behavior of a wide range of Vitis vinifera varieties in a context of climate change in the Bordeaux vineyards. In Proceedings of the Sustainable Grape and Wine Production in the Context of Climate Change. ClimWine 2016 International Symposium, Bordeaux, France, 10–13 April 2016.
36. Garcia de Cortazar-Atauri, I.; Audergon, J.M.; Delzon, S.; Anger, C.; Duchêne, E.; Bonhomme, M.; Legave, J.M.; Chuine, I.; Raynal, H.; Davi, H.; et al. PERPHECLIM ACCAF Project-perennial fruit crops and forest phenology evolution facing climatic changes. In Proceedings of the XVI International Sumposium on Apricot Breeding and Culture and XV Chinese National Symposium on Plum and Apricot, Shenyang, China, 29 June–3 July 2015.
37. Jones, G.V. Climate and Terroir: Impacts of Climate Variability and Change on Wine. In *Fine Wine and Terroir-the Geoscience Perspective*; Meinert, L.D., Ed.; Geological Association of Canada: St. John's, NL, Canada, 2006; p. 247.
38. Eichhorn, V.K.W.; Lorenz, D.H. Phänologische Entwicklungsstadien der Rebe [Phenological development stages of the grapevine]. *Nachr. Dtsch. Pflanzenschutzd.* **1977**, *29*, 119–120.
39. Amerine, M.A.; Winkler, A.J. Composition and Quality of Musts and Wines of California Grapes. *Hilgardia* **1944**, *15*, 493–675. [CrossRef]
40. Wang, E.; Engel, T. Simulation of phenological development of wheat crops. *Agric. Syst.* **1998**, *58*, 1–24. [CrossRef]
41. Bidabe, B. Contrôle de l'époque de floraison du pommier par une nouvelle conception de l'action de températures. *C. R. Séances L'Acad. D'Agric. Fr.* **1963**, *49*, 934–945.
42. Bidabe, B. *L'action Des Températures Sur L'évolution Des Bourgeons de L'entrée en Dormance à la Floraison*; Congrès Pomologique: Paris, France, 1965.
43. Tukey, J.W. Box-and-whisker plots. In *Exploratory Data Analysis*; Addison-Wesley: Reading, MA, USA, 1977; pp. 39–43. ISBN 978-0201076165.
44. Shellie, K.C. Viticultural performance of red and white wine grape cultivars in southwestern Idaho. *Horttechnology* **2007**, *17*, 595–603. [CrossRef]
45. Parker, A.K.; Garcia de Cortazar-Atauri, I.; Van Leeuwen, C.; Chuine, I. General phenological model to characterise the timing of flowering and veraison of *Vitis vinifera* L. *Aust. J. Grape Wine Res.* **2011**, *17*, 206–216. [CrossRef]
46. Fila, G. Mathematical Models for the Analysis of the Spatio-Temporal Variability of Vine Phenology [Modelli Matematici per L'analisi Della Variabilità Spazio-Temporale Della Fenologia Della Vite]. Ph.D. Thesis, University of Padua, Padua, Italy, 2012.
47. Streck, N.A.; Weiss, A.; Xue, Q.; Stephen Baenziger, P. Improving predictions of developmental stages in winter wheat: A modified Wang and Engel model. *Agric. For. Meteorol.* **2003**, *115*, 139–150. [CrossRef]
48. Chuine, I.; Garcia de Cortazar-Atauri, I.; Kramer, K.; Hänninen, H. Plant development models. In *Phenology: An Integrative Environmental Science*; Schwartz, M.D., Ed.; Springer: Dordrecht, The Nederlands, 2013; pp. 275–293. ISBN 9789400769250.
49. Hastings, W.K. Monte carlo sampling methods using Markov chains and their applications. *Biometrika* **1970**, *57*, 97–109. [CrossRef]
50. Kirkpatrick, S.; Gelatt, C.D.; Vecchi, M.P. Optimization by simulated annealing. *Science* **1983**, *220*, 671–680. [CrossRef] [PubMed]
51. Metropolis, N.; Rosenbluth, A.W.; Rosenbluth, M.N.; Teller, A.H.; Teller, E. Equation of state calculations by fast computing machines. *J. Chem. Phys.* **1953**, *21*, 1087–1093.
52. R Development Core Team. *R: A Language and Environment for Statistical Computing*; Version 3.5.1; R Foundation for Statisrical Computing: Vienna, Austria, 2018; ISBN 3900051070.

53. Wright, S. Correlation and causation. *J. Agric. Res.* **1921**, *20*, 557–585.
54. Akaike, H. Information Theory and an Extension of the Maximum Likelihood Principle. In Proceedings of the Second International Symposium on Information Theory, Tsahkadsor, Armenia, 2–8 September 1973; Petrov, B.N., Caski, F., Eds.; Akademiai Kiado: Budapest, Hungary, 1973; pp. 267–281.
55. Kenney, J.F. Root mean square. In *Mathematics of Statistics*; Chapman & Hall, LTD.: Princeton, NJ, USA, 1962; pp. 59–60.
56. Nash, J.E.; Sutcliffe, J.V. River flow forecasting through conceptual models part I—A discussion of principles. *J. Hydrol.* **1970**, *10*, 282–290.
57. Cola, G.; Failla, O.; Maghradze, D.; Megrelidze, L.; Mariani, L. Grapevine phenology and climate change in Georgia. *Int. J. Biometeorol.* **2017**, *61*, 761–773. [CrossRef] [PubMed]
58. Fila, G.; Di, B.; Gardiman, M.; Storchi, P.; Tomasi, D.; Silvestroni, O.; Pitacco, A. Calibration and validation of grapevine budburst models using growth-room experiments as data source. *Agric. For. Meteorol.* **2012**, *160*, 69–79. [CrossRef]
59. Duchêne, E.; Huard, F.; Dumas, V.; Schneider, C.; Merdinoglu, D. The challenge of adapting grapevine varieties to climate change. *Clim. Res.* **2010**, *41*, 193–204. [CrossRef]
60. Reis Pereira, M.; Ribeiro, H.; Abreu, I.; Eiras-Dias, J.; Mota, T.; Cunha, M. Predicting the flowering date of Portuguese grapevine varieties using temperature-based phenological models: A multi-site approach. *J. Agric. Sci.* **2018**, *156*, 865–876. [CrossRef]
61. Moriondo, M.; Orlandini, S.; Nuntiis, P.D.; Mandrioli, P. Effect of agrometeorological parameters on the phenology of pollen emission and production of olive trees (*Olea europea* L. *Aerobiologia* **2001**, *17*, 225–232.
62. Chuine, I.; Bonhomme, M.; Legave, J.M.; García de Cortázar-Atauri, I.; Charrier, G.; Lacointe, A.; Améglio, T. Can phenological models predict tree phenology accurately in the future? The unrevealed hurdle of endodormancy break. *Glob. Chang. Biol.* **2016**, *22*, 3444–3460.
63. Martínez-Lüscher, J.; Kizildeniz, T.; Vučetić, V.; Dai, Z.; Luedeling, E.; van Leeuwen, C.; Gomès, E.; Pascual, I.; Irigoyen, J.J.; Morales, F.; et al. Sensitivity of Grapevine Phenology to Water Availability, Temperature and CO2 Concentration. *Front. Environ. Sci.* **2016**, *4*, 48. [CrossRef]
64. Fraga, H.; García de Cortázar Atauri, I.; Malheiro, A.C.; Santos, J.A. Modelling climate change impacts on viticultural yield, phenology and stress conditions in Europe. *Glob. Chang. Biol.* **2016**, *22*, 3774–3788. [CrossRef] [PubMed]
65. Hannah, L.; Roehrdanz, P.R.; Ikegami, M.; Shepard, A.V.; Shaw, M.R.; Tabor, G.; Zhi, L.; Marquet, P.A.; Hijmans, R.J. Climate change, wine, and conservation. *Proc. Natl. Acad. Sci. USA* **2013**, *110*, 6907–6912. [PubMed]
66. Fraga, H.; Santos, J.A.; Malheiro, A.C.; Oliveira, A.A.; Moutinho-Pereira, J.; Jones, G.V. Climatic suitability of Portuguese grapevine varieties and climate change adaptation. *Int. J. Climatol.* **2016**, *36*, 1–12.
67. Camargo-Alvarez, H.; Salazar-Gutiérrez, M.; Keller, M.; Hoogenboom, G. Modeling the effect of temperature on bud dormancy of grapevines. *Agric. For. Meteorol.* **2020**, *280*, 107782. [CrossRef]
68. Fennell, A.; Mathiason, K.; Luby, J. Genetic segregation for indicators of photoperiod control of dormancy induction in vitis species. *Acta Hortic.* **2005**, *689*, 533–540. [CrossRef]
69. Rubio, S.; Dantas, D.; Bressan-Smith, R.; Pérez, F.J. Relationship Between Endodormancy and Cold Hardiness in Grapevine Buds. *J. Plant Growth Regul.* **2016**, *35*, 266–275. [CrossRef]
70. Leolini, L.; Moriondo, M.; Romboli, Y.; Gardiman, M.; Costafreda-Aumedes, S.; Costafreda-Aumedes, S.; Bindi, M.; Granchi, L.; Brilli, L. Modelling sugar and acid content in Sangiovese grapes under future climates: An Italian case study. *Clim. Res.* **2019**, *78*, 211–224.



LUXEMBOURG
INSTITUTE OF SCIENCE
AND TECHNOLOGY
LIST